Mechanical Properties and Wear Performance of Bainitic Steels

Nong Jin
B.S., Tsinghua University, Beijing, China, 1986
M.S., Central Iron & Steel Research Institute, Beijing, China, 1989

A dissertation submitted to the faculty of the
Oregon Graduate Institute of Science & Technology
in partial fulfillment of the
requirements for the degree of
Doctor of Philosophy
in
Materials Science and Engineering

July 1995

The dissertation "Mechanical Properties and Wear Performance of Bainite Steels" by Nong Jin has been examined and approved by the following Examination Committee:

Paul Clayton, Thesis Advisor
Professor

Roger K. Steele
Association of American Railroads

David G. Atteridge
Professor

Milton Scholl
Assistant Professor

ACKNOWLEDGEMENTS

First of all, I would like to express my gratitude to my thesis advisor Dr. Paul Clayton for his guidance, help and encouragement. Next, I would like to express my thanks to my thesis committee members Dr. Roger Steele, Dr. David Atteridge and Dr. Milton Scholl for examining my thesis.

The program was funded primarily by the Association of American Railroads with Dr. Steele as technical monitor. Supplemental funding was received from the Federal Railroad Administration with W. R. Paxton as technical monitor assisted by Dr. O. Oringer of the Volpe National Transportation Systems Center.

I am grateful to Dr. Devanathan Ramaswamy for his help with my project initiation. I thank Lu Fang, Jun Ding, Xihong Wang, Daya Singh, Xiaoyan Su, Don McMerchie, Hua Li, Mengnie Li, Rajesh Dighde and Vivek A. Dikshit with whom I had very valuable discussions and from whom I received a lot of help. I also appreciate the help and support of Dale Christensen and all the technicians in the Department of Materials Science and Engineering.

Thanks to my parents, brother and sister for their continuous support. Finally, I would like to express my deep gratitude to my wife Limin, for her persistent encouragement, understanding and support through the course of my pursuing a Ph.D. and career success at OGI.

Dedicated to my wife

Table of Contents

LIST OF TABLES

LIST OF FIGURES

Mechanical Properties and Wear Performance of Bainitic Steels

ABSTRACT

As a potential candidate for a rail steel, bainitic steels have been studied for several years. Previous research conducted at OGI showed that high wear resistance was achieved in a low carbon (0.04%C) granular bainitic steel. A strong influence of microstructural features on the wear behavior highlighted the need to consider microstructure as well as mechanical properties in evaluating the wear behavior of a steel. This work was initiated to further investigate the wear performance of bainitic steels and establish structure/property relationships over a wider range of compositions.

Six Mo-B alloys were designed by varying additions of carbon, manganese, chromium, and nickel to provide a matrix of steels to investigate. Microstructural characterization was carried out by means of optical microscopy, SEM and TEM. The deterioration performance was investigated in two aspects: wear and deformation. Both wear and deformation tests were conducted in an Amsler machine under rolling/sliding conditions. The mechanical properties of the steels were investigated using tensile testing and Charpy impact testing. For comparison, a pearlitic rail steel and an austenitic manganese steel were also investigated in terms of wear and deformation resistance under rolling/sliding conditions.

The microstructural characterization revealed that granular bainite or carbide-free bainite was obtained in the Mo-B steels in the hot rolled conditions (except the as-received J2 that exhibited lower bainite) and with subsequent heat treatments with air-cooling or water quenching. A faster cooling rate produced more lath ferrite and reduced massive ferrite. The improved wear resistance was mainly associated with an increase of lath ferrite in the microstructure.

It was found that carbon played a significant role in determining microstructure, mechanical properties and wear performance. As carbon content increased, more lath ferrite in bainite was produced, which gave rise to an increased strength and improved wear performance. A decrease in wear rate with an increase in cooling rate was attributed to the microstructural changes and the improved mechanical properties. Carbide-free bainite with high strength and high deformation resistance was beneficial to improving wear resistance. This study confirmed that the wear resistance of the bainitic steels was comparable to high hardness pearlitic rail steels. The steel of 0.26%C could even compete with an austenitic manganese steel in terms of wear and deformation resistance.

INTRODUCTION

Since the advent of railways, rail materials have been challenged by the rising speed and weight of traffic. The first material used for rails was wrought iron. However, around 1850 heavier locomotives twisted and crushed wrought iron rails in Great Britain so that the development of new rails was essential. After over 57 years, accompanied by controversy and debate, suitable steel rails were developed and 100 lb/yd rails with 45 ft in length were produced by 1914.[1]

In modern railways, rail steel failures take place as a result of wear, deformation and fatigue. Accompanied by attempts to increase the strength of rails, improving resistance to wear, deformation and fatigue has been a big issue in the course of modern rail steel development. Tremendous work has been done by means of in-track testing,[2,3] simulated field experiments[4-8] and laboratory research.[9-32]

Commercial rail steels with high strength and wear resistance possess pearlitic structures. It has been shown that fine structure and small interlamellar spacing are very beneficial to improving the wear resistance. However, it seems that the reduction of the interlamellar spacing is approaching the extreme.[33] Research on other types of microstructure has been conducted. Because it generally provides a good combination of strength and toughness, bainite is considered a potential candidate for a rail steel. Unfortunately, the early studies manifested the inferior wear performance of bainitic steels with respect to pearlitic steels.[11,12,25,34,35] However, a study by Clayton *et al.*[36] revealed that under dry sliding conditions, the wear resistance of bainite could be comparable to pearlite.

A systematic study encouraged by this result was conducted under rolling/sliding conditions by Devanathan.[37] In that study, a low carbon steel (0.04%C) of granular bainite exhibited a comparable wear resistance to pearlite. In addition, the relationship between wear rate and contact pressure suggested that the wear resistance of bainite might be better than pearlite at high contact pressures above 1220 MPa. It was also suggested that bainite could be comparable to pearlite under very severe wear conditions.[23] Nonetheless, conflicting results still exist in recent studies. The superior wear performance of pearlitic steels to bainitic steels were also shown in the studies by Garnham and Beynon[23] and Clayton and Devanathan.[21]

Reviewing these studies, it has been found that the microstructures varied considerably although they were all termed bainite. The early studies lacked a thorough microstructural characterization and the research was not systematic in terms of microstructure, chemical composition and mechanical properties. The microstructure of bainite is very complicated; there are many other types besides upper and lower bainite.[38] The complexity of bainite is in part brought about by the complication and confusion in naming bainitic structures. Some nomenclatures have been developed to differentiate various types of bainite,[39-42] but none is successful in covering all variations in bainite.

It appears that the conflicting results of bainite wear resistance could be partly attributed to the complexity of the bainitic structures. Different types of bainite may exhibit different wear performance. Therefore, a deliberate characterization of the bainitic structure is essential.

The studies by Clayton *et al.*[36] and Devanathan[37] indicate a potential for bainitic steels as a wear resistant material in railroad applications. From the metallurgical perspective, the potential is associated with non-classical bainite and low carbon content in the steels. Following those studies, the current work was to further investigate the wear performance of bainitic steels in association with chemical composition, microstructure and mechanical properties. The objective of this study is to develop a high strength, high wear resistant bainitic steel which is also tough, weldable and fatigue resistant.

The work was conducted on experimental bainitic steels which provide a matrix of a wide range of carbon contents (0.03% – 0.25%) and other elements such as Mn, Cr and Ni (0 – 4%). The wear testing was carried out in an Amsler machine under rolling/sliding conditions which can produce the wear mode occurring in in-service rails.[19] The mechanical properties were investigated and their effects on wear resistance were analyzed. Weldability was also evaluated to provide the overall performance of the steels and shed some light for future work. For comparison, the wear performance of a pearlitic rail steel and a Hadfields austenitic manganese steel was tested.

CHAPTER 1

LITERATURE REVIEW AND PROJECT OUTLINE

1.1. BAINITE TRANSFORMATION

1.1.1 Definition of Bainite

Classically, bainite is defined as an austenite transformation product that forms in a temperature range bounded above by the end of the pearlite transformation region and below by the martensite start temperature, M_s.[38] However, the terminology defining the transformation products formed in this temperature range is still in disagreement and even somewhat confusing since the structural morphology has been found to vary considerably with materials and thermal conditions. Much discussion about the correct definition of bainite has been made in the context of transformation mechanisms based on crystallography, kinetics or surface relief.

The most common and familiar types of bainite are upper bainite and lower bainite. Upper bainite forms at the upper part of the bainitic transformation temperature range and typically comprises an aggregate of ferrite laths and carbide precipitates lying along the lath boundaries. The ferrite laths usually form in parallel groups to yield plate-shape regions, often described as sheaves,[43] with a low angle misorientation between the laths. Lower bainite forms at relatively lower temperatures. In this structure, ferrite is plate-like[44] and carbides precipitate in the bainitic ferrite at an angle of 55 to 60° to the long axis of the lath.

Since not all bainitic structures can be simply categorized into either upper or lower bainite, new nomenclature has been developed to differentiate types of bainite. Ohmori *et al.*[39] proposed a set of terms for low-carbon steels:

(a) **Bainite I (BI)**, carbide-free bainitic ferrite forming between 600°C and 500°C, consists of bundles of ferrite laths with untransformed austenite between them; the untransformed austenite can transform to martensite during subsequent quenching.

(b) **Bainite II (BII)** is a structure made up of ferritic laths with a cementite layer between them, similar to the classical upper bainite. In an isothermal transformation, it forms between 500°C and 450°C, whereas in continuous cooling, it forms after the BI reaction at intermediate cooling rates.

(c) **Bainite III (BIII)** forms between 500°C and the M_s in an isothermal transformation or on continuous cooling near the critical cooling rate, above which bainite transformation does not occur. The morphology of this bainite is similar to the classical lower bainite, but its crystallographic structure is almost the same as that of upper bainite. Based on the ferrite morphology and habit plane investigated in their study, Ohmori *et al.* argued that both BII and BIII should be classified as upper bainite.

Granular bainite, a term often used to describe a certain type of bainite, generally consists of ferrite and martensite-austenite constituents and was early reported in detail by Habraken and Economopoulos.[40] They used the terms "massive" or "granular" structures to depict a structure consisting of coarse plates and particles with an almost entirely granular aspect. The latter, delineating the prior austenite grain boundaries, was identified to consist of austenite and martensite and has been verified by many investigators since then.[45-47] The term "granular bainite" was accepted gradually later, and the regions consisting of martensite and austenite are now called a M-A (martensite-austenite) island or a M-A constituent. The coarse plates were later interpreted as sheaves of bainitic ferrite with very thin regions of austenite between the sub-units.[48] It was also reported that the ferrite could be polygonal, massive or acicular depending on the type and quantity of the alloying addition.[46] Granular bainite has been observed in low and medium alloy steels.[43] It is often produced by continuous cooling,[40,43] but isothermally produced granular bainite has also been reported.[49]

In some steels (e.g. silicon-containing steels), separate ferrite subunits divided by films of carbon-enriched retained austenite are produced without carbide precipitation. This kind of structure is referred to as **carbide-free bainite**. It is also described as consisting of packets of heavily dislocated ferritic laths with an interlath martensite-retained austenite (MA) phase rich in carbon.[36] However, some investigators used this term for structures where there is simply no carbide.[47]

Bramfitt and Speer[41] proposed a general definition for bainite transformation in an attempt to describe the full range of bainitic microstructures observed so far. In their terminology system, the principal bainite morphologies fall into three categories, $\mathbf{B_1}$, $\mathbf{B_2}$ or $\mathbf{B_3}$, depending on whether the acicular ferrite is found in association with (a) intralath precipitates, (b) interlath particles/films, or (c) discrete regions of retained parent phase (or secondary transformation product), respectively. Bramfitt and Speer's nomenclature describes general classes of bainite microstructure as follows:

(a) class 1 bainite ($\mathbf{B_1}$) incorporates an intralath(plate) constituent;
(b) class 2 bainite ($\mathbf{B_2}$) incorporates an interlath(plate) particle or film constituent; and
(c) class 3 bainite ($\mathbf{B_3}$) incorporates discrete regions of a retained parent phase (or secondary transformation product) constituent.

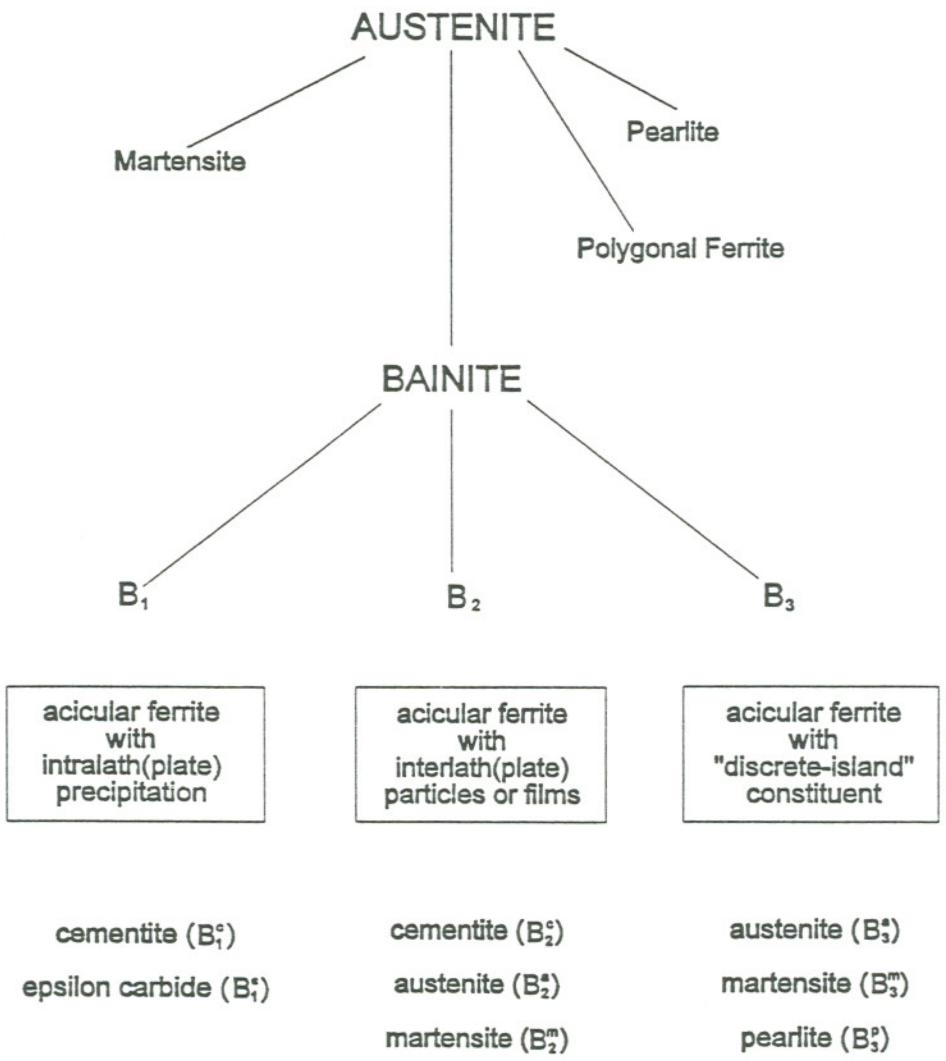

Figure 1.1 Proposed morphological system for bainite by Bramfitt and Speer.[41]

This proposed morphological classification system for bainite, illustrated in Figure 1.1, implies that a predominantly lath or plate morphology is essential to the classification of a microstructure as bainite. Consequently, a structure with an allotriomorphic or polygonal ferrite would not belong to bainite, nor would granular bainite.

The aim of developing these nomenclatures is to give an accurate description of bainitic structures. Unfortunately, none of them are completely successful. Some bainite nomenclatures are listed and commented on in Table 1.1.[50]

In the identification of bainitic structures, there are some other problems as well. The morphological similarity between Widmanstätten ferrite, bainite and martensite does make it very difficult to identify them unambiguously. It is also a problem to distinguish between lower bainite and auto-tempered martensite using optical or even electron microscopy unless more than one crystallographic variant of cementite is present in the latter structure. Furthermore, there is difficulty in differentiating between martensitic laths and bainitic laths if no carbides are present, although some work has been done on this aspect.[51,52] Consequently, the structure-property relationships of bainite to be found in the literature may not be entirely descriptive of "real" bainite because of the complexity and ambiguity of the structural classification and identification.

Table 1.1 Comparison of Classification Schemes for Bainite[50]

Description of Microstructure	Nomenclature		Comment
	Ohmori *et al.*[39]	Bramfitt and Speer[41]	
Acicular ferrite with interlath austenite	Bainite I	Class II, B_2^a	Araki *et al.*[42] identify acicular ferrite without carbide precipitates (α-B)
Acicular ferrite with interlath carbide	Bainite II	Class II, B_2^c	Classical upper bainite
Acicular ferrite with intralath carbide	Bainite III	Class I, B_1^c	Classical lower bainite*
Above forms of acicular ferrite mixed with separate regions of retained austenite and/or secondary transformation products, for example, pearlite or martensite	—	Class III (for example) B_3^a = with retained austenite B_3^m = with martensite $B_3^{a,m}$ = with retained austenite and martensite	Should include various types of low-carbon HSLA steel, and also low alloy creep resistant steels with granular bainite microstructure

* Note that the study by Ohmori *et al.* designated a lath morphology and ferrite crystallography of upper bainitic ferrite rather than that characteristic of high-carbon lower bainite.

1.1.2. Mechanism of Bainite Reaction

Similar to the definition of bainite, controversies remain in clarifying the mechanism. On one hand, bainite resembles martensite in acicular morphology, similar crystallographic, and surface relief effects. On the other hand, the reaction kinetics are those of nucleation and growth transformation except for the incomplete transformation phenomenon. The debates have been concentrated on the transformation by diffusional or diffusionless process. The diffusional viewpoint is that the lattice rearrangement is accomplished by long-range diffusion of substitutional atoms, whereas the diffusionless mechanism is that the lattice rearrangement is carried out in a shear mode like the martensite transformation.

Since bainite is an aggregate of ferrite and carbide, it was proposed that bainite forms from austenite by cooperative growth of the two phases.[53,54] The degree of cooperation in the growth process distinguishes bainite from pearlite.[54] For lower bainite, the plates lengthen at a rate controlled by diffusion of carbon in austenite ahead of an advancing ferrite interface.[55] Carbides precipitate from ferrite at a slight distance behind the interface since the carbon content in ferrite exceeds that for equilibrium with carbides. Thickening of the plates is accomplished by cooperative growth of ferrite at a rate controlled by diffusion of carbon through ferrite.[56] As an alternative diffusional mode, Aaronson[57] described bainitic growth as being non-cooperative and proposed that the two phases grow alternately rather than mutually, although the interface between one product phase and the parent phase does provide a favorable site for nucleation of the other phase.

The surface relief effect, generally taken as evidence for a diffusionless mechanism, was explained by a so-called ledge theory of growth by Kinsman and Aaronson.[57-59] They suggested that the plate-shape of ferrite develops because of a substantial barrier to growth at one orientation of the interface where the austenite and ferrite lattices match sufficiently well to form a semi-coherent interface. This interface is immobile in a direction normal to itself, but is able to advance in this direction by the formation and migration of ledges across it. The advance rate is controlled by long range diffusion.

With the similarities between bainite and martensite, bainite was believed to form initially as supersaturated ferrite by a lattice shearing process.[60-64] Vilella *et al.*[65] postulated that the transformation involved an abrupt formation of supersaturated ferrite plates along certain crystallographic planes of austenite; the ferrite then rejected carbon, leading to the formation of carbide particles. Klier and Lyman[66] proposed that prior to the transformation to bainite, austenite was compositionally unstable, and thus separated into two regions, carbon-rich and carbon-depleted. The carbon-depleted region transformed to supersaturated bainite of the same composition by a "martensite-like" lattice rearrangement, which then rapidly decomposed further by precipitating iron carbides.

The displacive transformation of bainite was expected to be paced by the diffusion of carbon in austenite. However, the measured bainite growth rate with a hot-stage microscope was 100 to 1000 times lower than that permitted by carbon diffusion[55] in alloy steels. This discrepancy was interpreted by Hehemann[55] in terms of a subunit nucleation rate. Based on the observation that an upper bainite needle consists of sub-structural units, it was suggested that if the subunits grow rapidly (though not necessarily at martensitic velocities), the measured growth rate may refer to the rate of subunit nucleation rather than the rate at which a unique interface advances under diffusion control. By a discontinuous growth process,[67-69] each bainite needle appears to develop by the sympathetic nucleation of subunits which grow to only a limited extent. In lower bainite, plates generally exhibit one straight edge and thicken from the other side only. The subunit direction change was attributed to the periodic carbide precipitation by interrupting the advance of the sub-structural units.[55,70]

The mechanisms of carbide precipitation were summarized by Christian and Edmonds.[71] A possible mechanism proposed earlier was that carbon must diffuse out of ferrite laths into the surrounding austenite to produce sufficient driving force for upper bainite growth. The growth rate is thus limited by diffusion. In lower bainite, carbide precipitation is accomplished by the relief of a full supersaturation in carbon out of the originally formed bainitic ferrite; the growth rate of a plate may be initially very fast but decrease to almost zero rapidly until the precipitation releases more free energy to drive the process. A more recently proposed mechanism is that the initially transformed regions are supersaturated with carbon in both upper and lower bainite. For upper bainite, individual regions are assumed to reach a limiting size very rapidly, and the apparent finite growth of a sheaf is caused by the isothermal nucleation of subsequent laths or subunits. Precipitation of carbides occurs by the diffusion of excess carbon into the surrounding austenite at the place where the subunit of a bainite needle stops growing. However, no carbide precipitation occurs if the austenite is very stable, for example, in silicon steels. At temperatures in the lower bainitic range, the increased driving force and lower mobility of the carbon result in the in-situ carbide precipitation in the bainitic ferrite.

Few investigations have been found in the literature regarding the mechanism of bainite transformation during continuous cooling while numerous studies have been made on upper and lower bainite under isothermal treatment conditions. The mechanism of granular bainite transformation was proposed by some investigators.[40,45,47] It is believed that fluctuation or dehomogenization in carbon concentration occurs in parent austenite[40,47] as in a classical bainite reaction. The bainite nucleates in the carbon-depleted region similar to the formation of massive martensite in carbon-free ferrous alloys[40] whereas the carbon-enriched austenite transforms to twinned martensite.[47] Based on carbon diffusion and the mechanism of carbide formation, Biss and Cryderman[45] proposed that the formation of M-A constituents from the carbon-enriched austenite depends on cooling rate. At low cooling rates, since there is enough time for carbon to diffuse in the austenite area, the austenite carbon content is not high enough to produce carbides, therefore, the austenite transforms to M-A constituent during cooling. If the cooling rate is high enough, carbon does not have enough time to diffuse in austenite. A very high carbon concentration area, formed at the interface between bainitic ferrite and the residual austenite on the austenite side, provides a nucleation site for carbide precipitation. Atom probe analysis indicates that no redistribution of substitutional elements occurs in the parent austenite.[72,73]

1.1.3. Orientation Relationships in Bainitic Steels

In upper bainite, it is generally believed that the long direction of the laths follows $\langle 111\rangle_\alpha$. There is no general agreement for the habit plane; $\{111\}_\gamma$, $\{223\}_\gamma$, $\{569\}_\gamma$ have been reported.[74-76] For lower bainite, the relative orientation between the bainitic ferrite and the parent austenite reported[77] is always close to K-S and N-W relationships, i.e.,

$$(011)_\alpha \,//\, (111)_\gamma$$
$$[11\bar{1}]_\alpha \,//\, [10\bar{1}]_\gamma$$

for the Kurdyumov-Sachs relationship and

$$(011)_\alpha \,//\, (111)_\gamma$$
$$[0\bar{1}1]_\alpha \,//\, [10\bar{1}]_\gamma$$

for the Nishiyama-Wassermann relationship.

In upper bainite, the carbides precipitating between bainitic ferrite laths are almost always cementite.[55,77] No carbides have been found inside ferrite. In lower bainite, carbides are distributed within ferrite in lines at an angle of about 60° to the longest axis of the ferrite platelet. In addition to cementite, ε-carbide is found within the lower bainitic ferrite,[55,67,76,78-80] but it is not able to precipitate if the dislocation density is high in steels containing up to 0.20 wt-%C.[81] κ-carbide may form in high-carbon steels[82,83] and η-carbide (Fe_2C) was reported to form in lower bainite of a high-silicon cast iron.[84,85] The carbide type is somewhat dependent on dislocation density in the bainitic ferrite. It should be noted that the precipitation of carbides could also occur between lower bainitic ferrite platelets, but this has received little attention. The interplate cementite comes from the decomposition of residual austenite between the bainitic ferrite platelets.

Shackleton and Kelly[44,86] reported that the most frequently observed orientation relationship between cementite and bainitic ferrite is the Bagaryatski relationship, i.e.

$$\{001\}_\theta \; // \; \{211\}_\alpha$$
$$\langle 100\rangle_\theta \; // \; \langle 0\bar{1}1\rangle_\alpha$$

The next frequent relationship is

$$\{001\}_\theta \; // \; \{\bar{2}\bar{1}5\}_\alpha$$
$$\langle 100\rangle_\theta \text{ within } 2.6^\circ \text{ of } \langle 3\bar{1}1\rangle_\alpha$$
$$\langle 010\rangle_\theta \text{ within } 2.6^\circ \text{ of } \langle 131\rangle_\alpha$$

1.2. MECHANICAL PROPERTIES OF BAINITIC STEELS

1.2.1. General Concepts

Mechanical properties of a steel, in principle, may be related to the morphological features of bainitic structures, for example, to the width of individual laths with low misorientations between them, to colony size (e.g. a packet or sheaf of laths) defined by high angle boundaries, and to the distribution and size of carbide precipitates.

Early studies[87-96] related the colony (or packet) size, D to strength and toughness, and got the expressions of the type

$$\sigma = K + k_y D^{-1/2}$$

and

$$T_c = K' - k_y' D^{-1/2}$$

where σ is the flow stress and T_c the impact transition temperature, the k_y and k_y' are parameters similar to those in the Hall-Petch equation, K and K′ are material constants. K includes a number of strengthening components and can be expressed by[97]

$$K = \sigma_0 + \sigma_{ss} + X$$

where σ_0 is a lattice friction stress, and σ_{ss} is a result of solid solution strengthening. The contribution factor X is more complicated and the greatest term arising from other strengthening factors, such as lath width, dislocation density and precipitation strengthening. The degree of strengthening attributable to each factor varies with the material.

1.2.2. Strength Properties

Four major factors are considered to contribute to the strength of bainitic steels:

1) a term relating to colony (packet) and lath size;
2) a term due to dislocation substructure within the laths;
3) a term in relation to solid solution hardening from substitutional elements, such as Si, Mn, Ni, etc., but additionally interstitial hardening from C and N; and
4) a term arising from the dispersion hardening effect of the carbide particles.

1.2.2.1. Colony/lath strengthening

Although the early work has shown that strength has a close relation with $D^{-1/2}$, where D is generally packet size, other work suggests that lath dimension can be correlated to the strength. For example, for a low carbon (0.05%C) steel, Brozzo *et al.*[98] showed a clear relationship between lath width and strength in terms of $K_y l^{-1}$ proposed by Langford and Cohen[99], but a weak one between colony size and strength. The generic relationship can be expressed by[100]

$$\sigma=\sigma_0+\sigma_{ss_s}+\sigma_{ss_i}+k_y''l^{-1}$$

where l is the average lath width, σ_{ss_s} and σ_{ss_i} are the contributions from solid solution strengthening due to substitutional and interstitial elements, respectively. It appears that for ultra-low carbon steels, the lath size has a more important influence on strength; whereas for conventional quenched and tempered steels, which consist of mixtures of bainite/martensite, a colony size appears to provide a better explanation of the changes in flow strength than lath size.

However, the validity of describing the effect of microstructure on strength becomes dubious because of the ambiguous use of the generic term "bainite" (which was sometimes used for both Widmanstätten ferrite and upper bainite). For this reason, a new concept was introduced in terms of active slip. It is assumed that strength is controlled by the active slip that can occur. It has been reported that 75% of all possible slip systems are oriented at 55° to the lath axis in bainite; the remainder lie parallel to the lath axis.[100] While slipping across the lath suggests that flow stress can be controlled by lath width, it was also proposed that the lath length may also contribute to strength.[101] Naylor[101] showed that slip band length is a function of both lath and packet dimensions and introduced a geometric factor M. The strength was then given as

$$\sigma=\sigma_0+\sigma_{ss}+\sigma_{cem}+k_Y M^{-1}$$

where M relates the average slip band length to both lath dimension and packet size, given by the expression

$$M=\frac{2}{\pi}\{l\cdot l n tan[0.5 arccos(\frac{1}{D})+0.25\pi]+0.5\pi D-D arcos(\frac{1}{D})\}$$

where l is the lath width and D the diameter of a packet.

Bhadeshia,[102] however, rationalized that the austenite grain size or packet size (which is dependent on the former) does not have any significant effect on strength. This is because the carbides and the films of retained austenite make greater contributions to strengthening for most bainitic steels. Also, the insensitivity of proof stress to grain size was presumably attributed partly to the gradual yielding behavior of bainitic steels,[103] for which there is no sharp yielding point in the uniaxial tensile curves.

1.2.2.2. Dislocation strengthening

The dislocation density in bainitic ferrite is higher than that of ferrite with polygonal or Widmanstätten morphology. For this reason, the dislocation configuration developed in bainite may make a significant contribution to the strength of a steel. It has been reported that the dislocation density in bainitic ferrite is of the order of 10^9 to 10^{10} cm^{-2}.[104,105] Yang[104] estimated that a density of 10^{10} cm^{-2} may cause an increase of 145MPa in strength. Whiteman[97] proposed a contribution of dislocations to strength in the form

$$\sigma_d = \alpha\mu b\rho^{1/2}$$

where σ_d is the strength contributed by dislocations, α a constant, μ the Young's modulus, **b** the Burgers vector, and ρ the dislocation density. The dislocation density increases with decreasing transformation temperature, which leads to an increase in strength. Some investigators[106,107] suggested that part of the dislocation structure in bainite may be inherited from the prior austenite.

1.2.2.3. Solution strengthening

Although the solid solution strengthening effect of carbon is not expected to be significant due to its low solubility in ferrite, a supersaturation of carbon in ferrite[72,108-110] has been shown to make a contribution to strength.[98] It was reported that about 0.01%C could be retained in bainitic ferrite. Brozzo *et al.*[98] proposed that the strength arising from the interstitial elements carbon and nitrogen can be calculated with the equation

$$\sigma_{ss_i}\ (MPa) = 1900\,(C+N)^{1/2}$$

where C and N are the concentration of carbon and nitrogen, respectively, in weight percent. If the carbon content in ferrite is 0.01% as reported,[72,108-110] a roughly estimated strength arising from solid solution strengthening would be 150 to 200 MPa, equivalent to that from a dislocation strengthening mechanism. It has been suggested that the pinning of interstitial element atoms to dislocations makes a significant contribution to strength.[100]

The solid solution strengthening of substitutional elements has been well documented,[111] showing that Mo, Si, P, Mn, Ni and Cu are effective strengtheners. The strengthening effect, in general, comes from the difference in atomic size of the elements from that of iron; the greater the difference, the stronger the effect. In addition, the differences in the elastic behavior of solute and solvent atoms are also important in determining the overall strengthening. For industrial steels, however, gaining solid solution strengthening is often not a major reason for using alloying elements; the alloying elements are often added to the steels for other reasons, for example, Mn to combine with sulphur, Mo to promote hardenability, and Ni to increase toughness.

As a matter of fact, many alloying elements are capable of lowering the bainitic transformation temperature and thereby increasing the strength of steels. An empirical equation of tensile strength, proposed by Pickering[91] for bainitic steels with respect to steel compositions with a carbon range of 0.05 to 0.20%, is as follows:

$$\sigma_u = 15.4[16+125C+15(Mn+Cr)+12Mo+6W+8Ni+4Cu+25(V+Ti)]$$

where σ_u is the tensile strength in MPa and the alloying elements are in weight percent.

1.2.2.4. Carbide strengthening

In upper bainite, carbides do not appear to increase strength through dispersion strengthening since they are coarse and distributed at lath boundaries. However, they may influence the ability of lath boundaries to impede dislocation motion, thereby confining slip within the laths and thus raising the lath size contribution to strength.[100] In lower bainite, carbides are distributed within the bainitic ferrite platelets and therefore take a direct dispersion strengthening effect; this effect is enhanced as the transformation temperature decreases.[112,113] The strengthening effect of carbides was also interpreted[114] by the Ashby-Orowan relationship

$$\sigma_{cem}=An_e\ln(\frac{B}{n_e})$$

where n_e is the number of effective carbides per unit area (i.e. carbides not at the lath boundaries) and A and B are material constants.

1.2.3. Toughness

Fractographic analysis, an important approach to understanding toughness, reveals the nature of cracking and associates toughness with microstructural characteristics which are in turn related to chemical composition, heat treatment and processing procedure.

The emphasis hereinafter is put on the relationships between toughness properties and microstructure. Of interest are the effects of structural size, carbide distribution, retained austenite, alloying elements and thermal and/or thermomechanical treatments on toughness.

1.2.3.1. Structural refinement

It is generally believed that "effective grain size" has an effect on toughness, but the concept of the "effective grain size" may be referred to as prior austenite grain size, packet size in bainite and martensite, or even lath size.

Several studies[92,115-117] showed that in upper bainite, the controlling factor for fracture is prior austenite grain size. Pickering reported that the ductile-brittle transition temperature is proportional to the prior austenite grain size D.[92] However, a relationship of the transition temperature being proportional to $-D^{-1/2}$ was also reported.[50]

The effect of bainite packet size on toughness has been shown in many investigations.[90,91,95,98,117-123] In most studies, a relationship between transition temperature and structural characteristic size has been reported in the form

$$T_{tr}(°C) \propto -\log(d^{-\frac{1}{2}})$$

where d is fracture facet size or bainite packet size.

When comparing upper bainite with lower bainite of the same strength, Tetelman and McEvily[124] pointed out that the impact properties of tempered lower bainite are far superior to those of untempered upper bainite. In upper bainite, the cleavage facets traverse several bainite grains and the "effective grain size" for fracture is the prior austenite grain size. In lower bainite, the cleavage planes in the bainitic ferrite are not aligned so the effective size for quasi-cleavage fracture is the ferrite needle (sheaf) size.

As the sheaf size is smaller by one to two orders of magnitude than the prior austenite grain size, the transition temperature of the lower bainite is much lower than that of upper bainite at the same strength level.

As far as the relationships between the prior austenite grain size and the substructure of the products transformed from the austenite are concerned, a study of Kamada[118] showed that the coarsening of austenite grain size does not necessarily bring about the coarsening of bainitic subunits. However, other studies[88,90,113,125] indicated that the substructure can be associated with the prior austenite grain size.

Although disagreements exist about the controlling factor of toughness in terms of microstructural size, the general trend is that a finer structure results in a higher toughness. This concept has been applied to the high-strength low-alloy (HSLA) steels, to which thermomechanical treatments have been used to improve toughness while maintaining high strengths.[126,127] Double heat treatment is another approach developed to gain higher toughness.[128,129] One example of a double treatment is illustrated in Figure 1.2.[126]

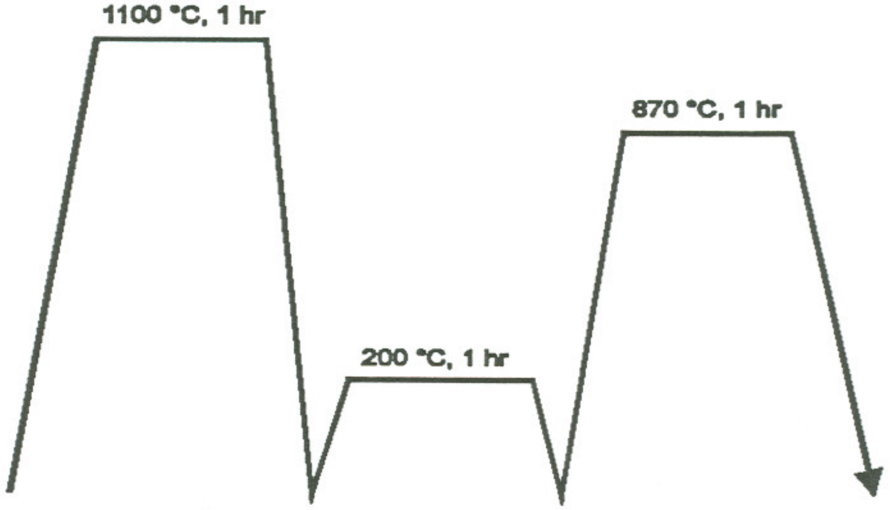

Figure 1.2 Double treatment for grain refinement

In industry, there have been two methods of raising toughness with respect to structural refinement: first, processing the steel to achieve a fine austenite grain size, and second, promoting a sufficient subdivision of the parent austenite to produce a small packet size.

1.2.3.2. Effect of carbides

The size, distribution and shape of carbides are other factors which influence the toughness of bainite.[118] In upper bainite, the carbides lying along lath boundaries may promote brittleness by lowering γ_m, the work done near the tip of a cleavage crack. In tempered lower bainite, the carbides, more uniformly distributed in ferrite, raise γ_m by interfering with cleavage cracks and promoting tearing.[115] The increase in γ_m also contributes to the superior toughness of tempered lower bainite compared to upper bainite at the same strength level.

Coarse carbides are considered to be detrimental to toughness.[115,118,130] In an A553B pressure-vessel steel, it was found that the carbide size distribution is the most important single microstructural feature that controls cleavage feature.[130] The coarsest carbides existing in the steel appeared to be the most deleterious to toughness. The carbides formed from the decomposition of interlath retained austenite in a bainitic microstructure also caused a fall in toughness.[131] Similar results have been found in the medium carbon steels consisting of lath-martensite structure with films of retained austenite surrounding the laths[132] and the decrease in toughness is termed tempered martensite embrittlement since it occurs on tempering near 350°C. The detrimental effects of carbides have been attributed to carbides providing either crack nucleation sites[133-136] and/or easy crack paths.[129,133,137] It has also been postulated that carbides obstruct the dislocation motion and thus enhance the stress concentration at the carbide/matrix interface, thereby giving rise to brittle fracture.[138]

A fine distribution of carbides, however, may be beneficial to toughness. Irvine and Pickering[115] reported that the presence of carbides may provide an obstacle to the fracture path and thereby improve impact properties.

1.2.3.3. Effect of retained austenite

The effect of retained austenite on toughness has been investigated by many workers. The second-phase austenite regions (in duplex structures) were intended originally to enhance the fracture toughness of high alloy steels.[139-142] The beneficial effect of retained austenite was later found in the steels with lath martensite,[129,143-147] and in the bainitic steels.[131,148] This effect was associated with the thermal and mechanical stability of the retained austenite, rather than its amount.[148,149] It is generally considered that the retained austenite can be stabilized by carbon enrichment. Carbon-enriched thin films of retained austenite between laths were found to be stable and therefore beneficial to toughness while unstable retained austenite is detrimental to toughness. Decomposition of retained austenite during tempering results in tempered martensite embrittlement (TME).[128,129,132,137] Bhadeshia and Edmonds[131] found that in the bainitic steels they investigated, retained austenite in blocky form is thermally and mechanically unstable and therefore detrimental to toughness. They proposed that a ratio of volume fraction of the film/blocky morphology greater than 0.9 would result in the best toughness and strength combination.

The means by which the beneficial effects of retained austenite on toughness can be achieved are summarized as follows:[129]

1. crack branching, resulting in a more tortuous crack propagation and a consequent increase in energy expended;
2. crack blunting, as a result of plastic flow in austenite resulting in a decrease in stress concentration requiring higher applied stresses for unstable fracture;
3. transformation induced plasticity (TRIP), the transformation of retained austenite to martensite under stress/strain relieves stress concentrations ahead of a crack in the plastic zone. However, some investigators[131,148,150] have reported that the transformation from austenite to martensite may cause a drop in toughness because the twinned martensite formed in transformation is deleterious to toughness.

The effect of retained austenite on ductility has been addressed by Sakuma *et al.*[151] They found that an improved ductility could be achieved by strain induced transformation of austenite to martensite without variation in strength.

1.2.3.4. Effect of alloying elements

1) Carbon

Like its effect on strength, carbon also influences the toughness of steels considerably. In general, toughness is deteriorated by increasing carbon content. Over a wide range of carbon content (0.1% – 0.8%), an increase in carbon content raises the impact transition temperature and reduces the absorbed energy.[152] Also, the transition temperature range is widened and the upper shelf energy decreased. For high carbon steels (0.7% – 1.0%C), small variations in carbon content can influence the fracture toughness significantly.[153] Lowering carbon content increases fracture toughness. This relationship was associated with the presence of retained austenite. Increasing carbon content resulted in an increase in retained austenite, which subsequently transformed to twinned martensite, and thereby deteriorated the toughness. In bainitic steels with 0.14% – 0.28% C, the deteriorating effect of carbon was attributed to the formation of carbides.[118]

2) Manganese

In low-carbon steels, manganese can substantially reduce the transition temperature in impact test specimens. With increasing Mn, the transition temperature decreases and the upper shelf energy increases.[154] Manganese content up to 2% improved the toughness in Fe-4Cr-C steels by increasing the amounts of retained austenite.[129] In high Cr steels (8% – 12%Cr), 1%Mn, added to obtain stable austenite films, produced a favorable lath martensite structure with interlath films of retained austenite. Consequently, a good combination of strength and toughness was achieved.[126] However, in niobium-manganese and vanadium-manganese steels, an addition of Mn greater than 2% deteriorates toughness by increasing the impact transition temperature of bainitic structures.[155] In an extra-low carbon (0.003%) Fe-Mn steel, Roberts[88] found that the impact transition temperature is insensitive to manganese content (0.01% – 9.60% Mn). No reason for the insensitivity was given in the study, but it is noted that the carbon content is extremely low. This probably suggests that for higher carbon steels, Mn may influence the toughness by affecting the formation of microstructure (for example, retained austenite), whereas no second phase was formed in almost pure-iron steels.

3) Chromium

Chromium is generally used to increase hardenability, and its effect on toughness has not been well documented. Roe and Bramfitt[156] pointed out that chromium raises the transition temperature slightly in plain carbon steels if below 0.90%.[156] However, Dieter[157] suggested that Cr has little effect on transition temperature. Medium carbon, straight chromium steels suffer tempered martensite embrittlement.[156] It has also been reported that Cr deteriorates toughness through the promotion of substructural twinning in martensite at high C levels.[143,158] In Mo-Cr steels with fully martensitic structures,[159] the Charpy impact energy dropped from around 54 J with approximately 9.0% Cr to 42 J with 12% Cr.

4) Nickel

Nickel generally improves toughness properties. An improved toughness with an addition of 5% Ni was attributed to its effect of increasing the amount of stable retained austenite.[129] Callender[160] found that the toughness of bainitic steels was improved by the addition of Ni up to 3%. He pointed out that this is an effect of nickel by itself, rather than a result of its interacting with other elements and/or microstructural changes.

5) Boron

The mechanical properties of boron-containing steels, where boron is generally used to increase the hardenability, have been extensively studied. The detrimental effect of boron on toughness was found in both fully hardened steels[161] and non-fully hardened steels.[162] Maitrepierre *et al.*[161] reported that in the fully martensitic steels, toughness decreased with an increase in boron content. They suggested that this is an intrinsic effect of boron. Some investigators[163] simply attributed the decrease in toughness to the increase in strength through the enhanced hardenability by boron. Some others[164,165] suggest that the undissolved borocarbides and grain boundary borocarbides provide the sites for crack initiation and thereby reduce the toughness of steels. For Fe-Cr-Mo steels with a martensitic microstructure,[166] boron impaired room temperature impact toughness and resulted in the temper embrittlement due to the formation of more or less continuous cementite at the martensitic lath boundaries.

However, a beneficial effect of boron on toughness was reported for quenched and tempered steels.[161] A tempered martensitic structure exhibited much better toughness than untempered bainitic structures and mixed structure of martensite and bainite. The martensitic structure was achieved through the increased hardenability achieved by boron addition. Roe and Bramfitt[156] point out that the beneficial effect of boron applies only to quenched and tempered steels and that boron reduces the toughness of as-rolled, as-annealed and as-normalized steels.

6) Niobium

Niobium is a microalloying element which is often used to refine grain size. In this aspect, Nb causes two effects, a solid solution drag effect and strain induced precipitation. In the Fe-Cr-Mn steels with Nb addition,[167] niobium refined the microstructure but no precipitates were found at the prior austenite grain boundaries. 0.02%Nb addition resulted in an increase in tensile ductility and Charpy toughness in the steels. In Fe-1.5Mn-0.06C steels, 0.05%Nb changed the microstructure from ferrite/bainite to acicular ferrite/martensite[168] and the impact energy at 20°C was 15 joules lower in the Nb bearing steel than in the Nb-free steel. Roe and Bramfitt[156] reported that the Nb effect on impact toughness is influenced by the hot-rolling-finishing temperature. Below 925°C, Nb improves toughness by refining the ferrite grain size; above 925°C, it may deteriorate toughness. However, a detrimental effect of Nb was found in a steel with a finishing temperature of 800°C.[168]

7) Silicon

Silicon, used in amounts of 0.15% – 0.30% to deoxidize steels, generally lowers the ductile-to-brittle fracture transition temperature and raises upper shelf energy.[156]

However, in bainitic steels, over 1%Si has been used to impede or depress carbide precipitation and thereby improve toughness due to the absence of carbides, as in silicon steels.[169]

1.3. WEAR BEHAVIOR OF STEELS

1.3.1. General Concepts

The term *tribology* was introduced in 1966 and defined as "the science and technology of interacting surfaces in relative motion".[170] *Wear*, according to the Webster's New World Dictionary,[171] is defined as the gradual impairment, loss, or diminution from use, friction, etc. Mechanical wear is caused by disintegration of interacting machine components as the result of over-stressing of the material in the immediate vicinity of the surface.[172] In a wearing system, many features contribute to the system wear characteristics. First, it is necessary to define the general shape of the contacting bodies. The relationship between the bodies determines the degree of conformity and thus the stress system. Secondly, it is necessary to define the applied load and the associated friction forces. In a lubricated system, a film of lubricant can be produced due to the interaction between speed and load. The presence of foreign particles in the lubricant may cause serious damage to one or both of the interacting surfaces.

Wear takes many forms. Barwell[172] categorizes wear into four main types: adhesive wear, abrasive wear, surface fatigue, and corrosion. However, corrosion is generally regarded as an independent damage mode and not included in wear.

Adhesive Wear is characterized by the interaction of asperities, causing metal to be transferred from one surface to another. A particular severe form of this kind of wear is known as scuffing. A feature of scuffing is a marked tendency for material to be removed from the hotter surface and deposited on the cooler surface.

Abrasive Wear may be defined as damage to a surface by a harder material. The hard material may be introduced between two rubbing surfaces from outside, or formed *in situ* by oxidation and other chemical processes, or the material forming the second surface. Resistance to abrasive wear is often related to the hardness of a material but many studies have shown that hardness is not always an indicator for wear resistance. Some steels are more resistant than others, irrespective of hardness. The type of the microstructure of a steel definitely influences abrasive wear resistance.

Surface Fatigue is caused by the repeated intense loading of a counterformal contact area. Cracking is initiated a little way below the surface where the maximum shear stress occurs due to the distribution of Hertzian stress. The crack subsequently propagates to the surface, leading to a piece of metal detached and a pit. Hence surface fatigue is also called a "pitting failure".

1.3.2. Damage of Rails

The damage of railroad tracks is known to be caused by plastic deformation, rolling contact fatigue (RCF), corrugations, wear and internal fatigue.[173] A failure of rail is often a result of the combination or interaction of these factors.

1.3.2.1. Plastic deformation

Rails almost invariably suffer from plastic deformation due to the rolling/sliding contact between rail and wheels. The deformation, driven by the high normal and tangential stresses acting between wheels and rails, is accumulated by each successive pass of a wheel over the rail, which causes a small increment in the plastic strains and results in the so-called incremental plastic flow or "ratchetting". The degree to which the deformation occurs varies with situation. On heavy haul lines, deformation is particularly severe and rails may collapse by ratchetting under high wheel loads. On high speed lines, a thin layer of material formed near the surface is sheared relative to the bulk material, but it does not generally cause any serious problems.[173] It is believed that the plastic deformation near the surface may contribute to both sliding wear and the initiation of contact fatigue cracking.[174]

1.3.2.2. Corrugation

Corrugation is surface damage in which periodical ripples are produced. These ripples are parallel to each other and perpendicular to the moving direction of the component. Although there are no consensus theories for the mechanism of corrugation,[175,176] it is generally conceded that corrugation is a direct result of periodic stick-slip (i.e. rolling-sliding) process of some wheel-rail contact patch, such a process being consistent with observed rail corrugation surface striations.[177] Corrugation can be divided into two categories: long wavelength and short wavelength. The long wavelength, 150 to more than 600 mm, is generally related to heavy haul corrugations, whereas short wavelength, i.e. 25 to 100 mm, is typical of the transit and passenger service corrugations. Heavy haul corrugations exhibit plastic deformation, severe cold working and in some cases fatigue cracks and lateral flow.[178] Transit-passenger corrugations show the surface effects of wheel stick-slip and severe heating.

1.3.2.3. Rolling contact fatigue

Pits may be formed on the surface of rolling elements by a fatigue process. Generally speaking, the phenomenon, which is termed *rolling contact fatigue*, is characterized by the sudden removal of surface material. A process of rolling contact fatigue involves three phases: pre-conditioning of the material prior to cracking, crack initiation, and crack propagation.

In the pre-conditioning period, deformation takes place due to normal pressure and combined rolling/sliding action. The deformation results in a pileup of material ahead of the contacting area. Subsequently, fatigue cracks initiate due to the plastic deformation. Suh[179,180] proposed a mechanism of near-surface plastic deformation. According to this mechanism, plastic flow nucleates voids and microcracks at defects just below the surface. As the deformation continues, the microcracks grow and join up. Finally, a wear flake is formed at the surface or a fatigue crack is initiated. The microcracks may propagate by a low cycle fatigue mechanism, driven by the cyclic plastic strains; alternatively, the failure process may be of ductile shear caused by the progressive shear deformation of the surface layer.

Dikshit *et al.*[181] investigated the rolling contact fatigue of a head-hardened rail. They found that cracks initiated on the surface of a rail in the early stage of its service life as a result of the formation of a white etching layer. The white etching layer was formed at the surface of rail and cracks propagated through the layer.

White etching layers have been frequently found in service rails. Dikshit[182] proposed that the white layers are of a martensitic structure because of their hardness. Newcomb and Stobbs[183] presumed that the white layer was of fully martensitic structure in a BS 11 rail. However, a question arises whether austenitization of the rail head could occur at 1% slip in the real situation because neither enough heat nor pressure could be generated for such an occurrence. Therefore, an alternative explanation is that the layer has a ferrite structure with dislocations supersaturated by carbon transfer from carbides during the high frequency pulsed shear fatigue of the rail surface. In various machining processes with similar white etching layers, Griffiths[184] points out that the white etching layers could have different structures and be formed by different mechanisms even though they have similar hardness and appearance. They could be formed by high temperatures, surface reactions, plastic deformation or some combination of these events. Although the nature of the layers has not yet been fully understood, the hardness of such layers was reported to be around 900 HV to 1000 HV.[185,186]

1.3.3. Laboratory Investigations

1.3.3.1. Abrasive wear behavior of bainitic steels

There have been many investigations of the abrasive wear behavior of bainite compared with other microstructures in steels. Those studies have revealed that a bainitic structure exhibits good wear performance.

The wear resistance of lower bainite was found to be higher than tempered martensite at the same hardness level.[187,188] Krushchov and Babichev[188] reported that bainitic structures exhibited superior wear resistance to annealed structures of the same hardness. Serpik and Kantor pointed out that lower bainite is a structural component of steels with maximum abrasion resistance.[189] They also proposed that wear resistance increases in the structural sequence from spheroidite to pearlite and from tempered martensite to bainite,[190] which was later confirmed by other investigators.[191-193]

In a study of Kar[194] on medium carbon low alloy steels with different microstructures, lower bainite exhibited better abrasive wear resistance in a 3%Ni steel over the whole tempering temperature range. However, the wear rates of a steel without Ni were almost identical for different microstructures and hardness over the same range of tempering temperatures.

The presence of retained austenite is believed to enhance the wear resistance in bainitic structures.[191,194] It was claimed that lower bainite contains three to four times the amount of retained austenite present in martensite structures.[191] Hurricks[195] has suggested that the degree of cohesion between austenite and carbides is greater than that between martensite and carbides, thereby enhancing wear resistance. Zum Gahr[196,197] attributes the beneficial effect of retained austenite to (i) the presence of ductile austenite films around ferritic laths, which tend to impede microcrack formation and growth associated with abrasion, (ii) the increase in work hardening rate with strain because of the austenite to martensite transformation and (iii) the surface compressive stresses arising from the transformation of austenite during wear.

In three-body abrasive wear, it was reported[198] that when a steel was used as a grinding media, its wear resistance increased as the worn surface hardness increased for the microstructures of bainite, pearlite, spheroidite and tempered martensite. At the same hardness level, the bainitic structure was less wear resistant than the tempered martensite. This differs from the results given above for two body abrasive wear conditions.

1.3.3.2. Wear behavior under rolling/sliding conditions

The investigation of wear behavior of steels under rolling/sliding conditions arises from the wear of wheel and rail steels in railroads service. The rolling/sliding wear in wheel and rail steels was classified into three regimes developed in laboratory tests:[18] Type I, Type II, and Type III. In Type I, very pronounced large thin metallic flakes are formed at the surface of the specimens, accompanied by oxidation. Type II wear, more severe than type I, often exhibits ripples without large flakes. The much smaller wear particles are produced predominantly in the troughs of the ripples. The type III wear, equivalent to the severe wear classification of Archard and Hirst,[199] shows extremely rough surface compared with both type I and II wear. Large particles are torn away from the surface and plowing tracks are very evident.

In railroad applications, low carbon bainitic steels have been successfully used as the nose in a crossing because of a good resistance to impact wear or "batter".[23] Under rolling/sliding conditions, early studies[11,12,25,34,35] showed that bainitic steels are less wear resistant than conventional pearlitic steels. The results, obtained by Heller and Schweitzer,[34] showed that 0.07%C and 0.3%C bainitic steel rails wore faster than conventional pearlitic steel rails at the same hardness level in service tests. Masumoto *et al.*[25] evaluated an as-rolled 0.33%C bainitic steel in a laboratory test and reached the same conclusion. Their study indicated that the bainitic steel wore even faster than a tempered martensitic steel. Unfortunately, no reasons for the poor wear performance of bainite were discussed in their studies. Ichinose *et al.*[35] obtained similar results for hot-rolled 0.3%C bainitic steels. They found that at the same hardness level, the wear resistance of a microstructure in an order from the best to the worst is pearlite, tempered martensite and bainite. They attributed the differences in wear resistance to the distribution, shape, and size of carbides in the microstructures. They proposed that the carbides distributed minutely at the surface layer by rolling contact are important to improve wear resistance.

Kalousek *et al.*[11] used a 0.72%C Cr-Mo steel of different microstructure and hardness to investigate wear performance. They found that the wear resistance of pearlite is better than that of bainite and that bainite is better than tempered martensite. In their study, the superior wear performance of pearlite was attributed to the very pronounced work hardening near the wear surface. Such work hardening was related to the morphology of carbides: the lamellar cementite in pearlite gives rise to the best wear resistance because the carbides reinforce the ferrite in pearlite effectively, thereby improve wear resistance. The spheroidal carbides in the tempered martensite results in the worst wear resistance because shear stresses in the ferrite are not transferred to the cementite, which then does not deform. Since the carbide morphology in bainite is intermediate between that of pearlite and tempered martensite, an intermediate wear performance is achieved.

Although many studies showed that bainitic steels did not exhibit good wear resistance, an investigation of Clayton *et al.*[36] indicated that under dry sliding conditions, wear resistance of bainitic steels are comparable to that of high hardness (>260 HV30) pearlitic steels and much better than that of low hardness (140 - 220 HV30) pearlitic steels. Systematic studies under rolling/sliding conditions have been conducted in recent years. A study[21] of a commercial chromium-molybdenum rail steel demonstrated that at a hardness of 39 HRC, a pearlite structure showed much better wear resistance than upper bainite. The superior wear resistance of the pearlitic steel was attributed to the resistance to deformation and/or fracture in the type III[18] wear process.

Garnham and Beynon[23] evaluated three bainitic steels (0.04%C – 0.52%C) and a pearlitic steel under rolling-sliding conditions with slip/roll ratios from 1.5 to 10% and contact pressures from 500 to 1800 MPa. The wear resistance of the pearlitic steels, found to be superior to the lower carbon bainitic steels, was attributed to a microstructural modification, i.e. the alignment of microstructure near the wear surface. Pearlitic steels, capable of considerable microstructural modification under rolling-sliding conditions, lead to a superior wear resistance. Once the microstructural realignment breaks down, the wear behavior of pearlitic steels with respect to bainitic steels is more likely to depend on their bulk hardness. The bainitic steels exhibited a wear resistance comparable to that of pearlitic steels at contact pressures above 1300 MPa. This comparability was associated with the realignment break-down. The wear resistance of the bainitic steels was found to be dependent on the volume fraction of hard phases, carbide and martensite-austenite phase.

Devanathan and Clayton[16] investigated three bainitic steels with carbon contents of 0.04%, 0.1% and 0.54%, respectively, under rolling/sliding conditions. They found that the 0.04%C steel with a granular bainitic structure and a hardness of 29HRC, appeared to have comparable wear resistance to a conventional pearlitic eutectoid rail steel with a hardness of 33 HRC. Two possible explanations were proposed for such a performance. First, the 0.04%C bainitic steel, with a higher work hardening rate than the pearlitic steels, achieves higher surface hardness as a result of plastic deformation. The effect of work hardening was also found in a study of Liu *et al.*[200] Some investigations suggested that the wear resistance could be better correlated with surface hardness rather than bulk hardness.[201-204] Second, the resistance of the bainitic steel to the type III wear is influenced by strain resistance. The reduction in area of the 0.04%C bainitic steel of almost four times that of a pearlitic steel reflects a superior ability of the former to sustain strain, which was assumed to enhance wear resistance.

Their study also showed that wear resistance increases with a decrease in carbon content due to the respective microstructural changes.[37] The 0.04%C and 0.1%C steels both consist of granular bainite with the latter containing more M-A islands. It was postulated that the M-A islands lead to a deterioration in wear resistance since the interface between the matrix and an island is weak for cracks to initiate. Hence, the wear resistance of the 0.1%C steel was decreased by the greater number of M-A islands. For the 0.52%C steel, a banded structure consisting of upper bainite and twinned martensite was believed to contribute to the lowest wear resistance since cracking occurred along the interfaces between the bands and at the prior austenite grain boundary precipitates.

The same study also showed that the wear rate of pearlitic steels increases parabolically with contact pressure, whereas that of bainitic steels linearly. It was, therefore, suggested that the bainitic steels might be more wear resistant than pearlite steels at higher contact pressures.

1.3.3.3. Effects of alloying elements

Clayton *et al.*[36] conducted a systematic investigation of the wear behavior of a series of low-carbon (0.1% – 0.3% C) bainitic steels under dry sliding conditions. The results showed that in a hardness range 230-300 HV30, the wear resistance of bainitic steels was comparable to that of higher carbon pearlitic steels. They found that the wear rate could be associated with the contents of the steels in the following form:

$$\mathtt{wear\ rate}\ (mm^3/cm) \propto (C+Cr+\frac{Mn}{33})\ wt\%$$

This equation suggests that Cr is an important element with respect to wear resistance. The reason for the effect of Cr on wear resistance was not clear, but it was assumed to be brought about by a combined improvement in strength, ductility and toughness. It was concluded that Cr is an important alloying element in producing a tough, wear resistant bainitic steel. For the steels with microstructures of martensite, and ferrite and pearlite, carbon, silicon and chromium were found important elements to improve wear resistance.[205]

1.3.4. Summary

Some investigations have revealed that pearlitic steels exhibit better wear resistance than bainitic steels of the same hardness under rolling sliding conditions. Other studies, however, have indicated that bainitic steels are comparable to pearlitic steels and could even be better if the contact pressure is high enough. It should be noted that the test conditions were quite different in those studies and that the microstructures could also vary significantly although they are all bainitic. Upper and lower bainites are the two most common and well understood microstructures. They can form through isothermal transformation in medium and high carbon steels. Nonetheless, the bainitic structures which form on continuous cooling are more complex and an accurate definition has not yet been reached.

The conclusion that pearlite is better than bainite in wear resistance was challenged by Clayton and Devanathan on the grounds that the previous studies had lacked systematic investigation with respect to test conditions, chemical composition and other mechanical properties. Furthermore, the characterization of the steels had not been sufficiently detailed. The study made by Devanathan and Clayton[16] revealed a promising potential of an extra low carbon steel (0.04%C), which possessed a granular bainitic structure, with respect to wear resistance under rolling-sliding conditions. The results were quite encouraging in that granular bainite exhibited a comparable wear resistance to pearlite and indicated that better wear resistance might be achieved at higher contact pressures than 1220 MPa. A similar result, that wear resistance of bainite is comparable with that of pearlite, was also obtained by Garnham and Beynon[23] at high contact pressures and large slide/roll ratios.

The insufficient description of microstructural characterization in some studies brings out questions as to what type of bainite was investigated and what affects the wear performance in that type of bainite. Thorough microstructural characterization was carried out in some other investigations. But it is still difficult to reach a general conclusion that pearlite is better than bainite in wear resistance or that bainite is comparable to pearlite because testing parameters, such as slide/roll ratio and contact pressure, were quite different in various studies and because the type of bainite may also be different in those studies.

Consequently, a systematic study is still necessary to investigate the wear behavior of bainitic steels, which should involve a thorough characterization of the microstructure of steels and consistent test conditions. The purpose of the current study is to continue to evaluate the wear resistance of bainitic steels and to try to reveal the factors which may control or influence the wear performance of bainite. Effects of alloying elements, microstructure, and mechanical properties are investigated with respect to wear performance.

1.4. PROJECT OUTLINE

Since previous studies had shown the potential of bainite in low carbon steels in terms of wear resistance, further investigations of this kind of steel were necessary to cover a wider spectrum of composition and mechanical properties. A project was proposed to study the properties of bainitic steels for the application in wheel/rail systems. The objective of the project was to develop high strength, wear resistant steels which are also tough, weldable and cost effective.

To accomplish the above objectives, six alloys were designed. The composition of the designed alloys is given in Table 1.2. Mo and B were used to ensure bainite transformations on continuous cooling. The variations of C, Mn, Cr and Ni are of most significance in the alloy design. Low carbon levels were used to achieve good toughness and weldability. A low carbon content was also beneficial in achieving granular bainite and improving wear resistance.[16] Ni is beneficial to toughness. 4% Mn was used to see if it can replace Ni and Cr to reach similar or better mechanical properties since Mn is much cheaper than Cr and Ni. Cr was expected to contribute to an improved wear resistance and fatigue resistance according to a previous investigation.[36]

Table 1.2 Composition of Designed Bainitic Steels (wt-%)

Steel	C	Mn	Ni	Cr	Si	Mo	B
1	0.2	2	0	2	1.0	0.5	0.003
2	0.12	4	0	0	0.25	0.5	0.003
3	0.12	2	2	2	0.25	0.5	0.003
4	0.04	4	0	0	0.25	0.5	0.003
5	0.04	2	2	2	0.25	0.5	0.003
6	0.25	2	0	2	2.0	0.5	0.003

In the current study, the following aspects were examined:

1) Microstructural changes with alloying elements and heat treatment;
2) Wear, deformation and mechanical properties of the bainitic steels;
3) Effect of carbon content at low levels ($<0.3\%$) on wear performance and mechanical properties;
4) Effect of alloying elements on microstructure and mechanical properties; and
5) Weldability of the low carbon bainitic steels.
6) Interaction of wear resistance between top and bottom rollers in Amsler wear tests.

The project was carried out in two phases. In the first phase, the first five steels were investigated. In the second phase, the sixth alloy was designed on the basis of results from the first five steels and the properties of this alloy were then investigated. For this reason, chapters two through four cover the first five steels and chapter six deals with the sixth alloy exclusively.

CHAPTER 2

EXPERIMENTAL PROCEDURES

2.1. MATERIALS

Three kinds of steels were investigated with respect to microstructure, mechanical properties, wear performance and weldability. These steels were:

- Five experimental low-carbon Mo-B steels,
- A pearlitic head-hardened rail steel, and
- An austenitic Mn steel.

In addition, as a counter part material for wear testing in an Amsler machine, a class C wheel steel was used for bottom rollers.

The low-carbon Mo-B steels, designated as J1, J2, J3, J4 and J5, were produced by Bethlehem Steel Corporation. All 500 lb heats were made in a vacuum induction furnace backfilled with argon. The ingots, approximately 9"×9"×24", were soaked at 2350 °F (1288 °C) for at least 2 hours and then rolled to 3"×3" bars in 23 passes. The finishing temperatures ranged between 1725 - 1750 °F (940 - 954 °C).

The chemical compositions of the liquid steels, provided by the manufacturer, are listed in Table 2.1(a), while the chemistry of the solid steels (products), analyzed by Oregon Steel Mills using a spark spectrum technique is listed in Table 2.1(b). The alloying contents obtained from both analyses were quite similar but the carbon contents of the solid steels were generally lower than those of the liquid steels.

X136 is a pearlitic head-hardened rail steel investigated for wear performance. The composition of this steel is given in Table 2.2(a) and the mechanical properties in Table 2.2(b). Table 2.3 gives the composition of a class C wheel steel that is a pearlitic steel designated as W5. The hardness of W5 was 31 HRC.

The chemistry of an austenitic Mn steel, provided by the Association of American Railroads, has not been provided. However, the typical composition of Hadfield's steel is 1.2% carbon and 12% manganese.[206] This kind of steel is generally used for a frog steel. In this investigation, the steel was in the as-wrought condition.

2.2. HEAT TREATMENT OF THE Mo-B STEELS

In order to investigate the effect of cooling rate on materials properties, some of the steels were re-austenitized and then cooled in air or quenched in water. Eventually, the experimental specimens were divided into three categories on the basis of thermal history: *as-received*, *air-cooled* and *water-quenched*. The heat treatment parameters are given in Table 2.4.

2.3. MICROSTRUCTURAL CHARACTERIZATION

The microstructural characterization was carried out using optical metallography and transmission electron microscopy (TEM). For the optical metallography, the specimens were polished and etched with Vilella's reagent and 5% Nital. The observations were carried out on a Nikon Epiphot microscope.

The TEM specimens were prepared by mechanically thinning the 3 mm diameter disks to approximately 100 μm on abrasive papers. Then the disks were electro-polished and perforated in a solution of 5% perchloric acid in methanol at a temperature below -40°C. The TEM observations were carried out in a Hitachi H800 with an accelerating voltage of 200 kV and a Jeol 100CX with 100 kV.

2.4. GRAIN SIZE MEASUREMENT

The prior austenite grain sizes of some samples were measured using a circular intercept procedure defined in ASTM standard No. E112-88.[207] However, the number of fields used was less than required since the grain boundaries were not well revealed in all specimens. Therefore, the results represent a rough estimation rather than an accurate determination.

In a grain size measurement, for each field at a given magnification, the number of intersections (N) of grain boundaries and a three-ring pattern was counted while scoring intersections at the junction of three grains as 2 counts rather than the theoretical 1 1/2. An average number of intersections ($\bar{N}$) was derived by

$$\overline{N} = \frac{\sum_{i=1}^{n} N_i}{n}$$

where N_i is the number of intersection in the *i*th field, and n the number of fields measured. Using the equation

$$G = ASTM\ No. = 10.00 + 2\log_2(\overline{N}/L)$$

where L is the total length of circumference in the three-ring pattern, a nominal ASTM number G at that magnification was obtained. The real ASTM number defined at 100× was then obtained by subtracting Q from G, where Q is a correction factor calculated with the equation

$$Q = 2\log_2(M/M_b)$$

where M is the magnification used and M_b the basic magnification, i.e., 100×. The final grain size was reported by converting the real ASTM No. to the nominal diameter of average grain section according to Table 2 in ASTM standard E112-88.[207]

2.5. HARDNESS MEASUREMENT

The hardness of the steels was measured on the Rockwell C scale for the Mo-B steels, X136 and W5. Brinell hardness of the Mo-B steels was also measured. For these steels, the measurements were performed on a lateral side of Amsler rollers, indicated by the dark area in Figure 2.1.

2.6. DETERMINATION OF PHASE TRANSFORMATION TEMPERATURES

The phase transformation temperatures of the Mo-B steels were determined using a Gleeble 1500 thermal simulator. During thermal cycle running, the dimensional changes of the specimen with temperature was recorded by means of dilatometry and therefore a curve of dilation versus temperature was obtained. The transformation temperature was determined at the point where the curve began to deviate from a linear relationship between dilation and temperature of the specimen. Figure 2.2 shows a dilation curve, illustrating how the transformation temperatures are determined.

The setup of a Gleeble experiment is schematically illustrated in Figure 2.3. In the vacuum specimen chamber, a sample was held at the two ends by copper fixtures and heated in the center through electrical resistance. A thermocouple, welded in the center of the specimen working area, was connected to a control panel to monitor the specimen temperature and provide information for temperature control. An L-shaped dilatometer was attached to the center of the specimen, measuring the dimensional change of the specimen in the y direction with temperature change. The specimen geometry is shown in Figure 2.4 and the configuration of specimen setup shown in Figure 2.5.

A computer was used to define controlling parameters for Gleeble thermal cycle runs, acquire data during the thermal cycle runs, and process the data after testing. A plotter is used to represent results graphically.

The Ac_1 and Ac_3 temperatures of the Mo-B steels were determined by dilatometry with a heating rate of 0.2778 °C/s (1000 °C/hr).

To investigate phase transformations during continuous cooling, a sample was heated at 2 °C/s to 970 °C, held for 15 minutes and then cooled at 0.4, 2, 10 or 25 °C/s controlled by computer programs. The transformation temperatures were determined from the dilation curves as described above.

2.7. ROLLING/SLIDING WEAR TESTS

2.7.1. Amsler Machine

The wear performance of the materials was investigated under rolling/sliding conditions. An Amsler machine was used to generate rolling/sliding interaction with two cylindrical specimens as a pair for each test.

Figure 2.6(a) shows a photograph of the machine. This machine has two shafts with the lower shaft rotating 1.104 times faster than the upper one. Cylindrical specimens or rollers, are fixed at the end of each shaft. The two rollers contact each other with a contact pressure applied through a spring loading mechanism. The contact configuration is shown in Figure 2.6(b).

Due to the difference in tangential speed between top and bottom roller surfaces, sliding occurs at the contact surface. With the rolling/sliding movement, a slide/roll ratio or creepage (γ) is defined as

$$\gamma = \frac{l_s}{l_r}$$

where l_s is the sliding distance relative to contact surfaces and l_r the average rolling distance of the top and bottom rollers. Since the bottom shaft rotates 1.104 times faster than the top, the creepage is given by

$$\gamma = \frac{2(1.104d_2 - d_1)}{d_1 + 1.104d_2}$$

where d_1 and d_2 are the diameters of top and bottom rollers, respectively. The creepage can be adjusted by changing the roller diameter.

A maximum Hertzian contact pressure was obtained through a load applied to the rollers using Hertzian theory.[208] The maximum Hertzian contact pressure P_0 is calculated using the equation

$$P_0 = 0.418\left(\frac{LE}{WR}\right)^{1/2}$$

where L is the normal load applied to the rollers, W contact width of the rollers, E Young's modulus, and R given by

$$\frac{1}{R} = \frac{1}{R_1} + \frac{1}{R_2}$$

where R_1 and R_2 are the roller's radii. In this investigation, a Young's modulus of 2.1×10^5 MPa was used for all Amsler rollers.

2.7.2. Wear Tests

The geometry of the rollers are shown in Figure 2.7. For the Mo-B steels, the rollers were taken from the rolled bars with the roller's axis parallel to the longitudinal direction of the bars. For X136, the rollers were taken from a rail with the axis parallel to the longitudinal direction of the rail. The rollers of the austenitic Mn steel were taken from a plate with the roller axis parallel to the height direction. The orientations of rollers to the bulk materials are shown in Figures 2.8(a)–(c). The bottom rollers were taken from a class C wheel with the orientation shown in Figure 2.8(d).

Prior to running a test, the rollers were cleaned with soap and the contact surfaces were degreased with ethanol and acetone. During a test, both top and bottom rollers were removed periodically to measure the weight on an electronic balance with a precision of 0.1 milligram. The weight loss due to wear was then calculated and a curve of weight loss against revolutions was plotted. The wear rate was obtained using linear regression from the steady wear stage indicated by the plot. During the test, a compressed air blast was used to minimize an increase in temperature by removing heat generated by friction on specimen surfaces of and thereby minimized oxidation of the worn surfaces.

The initial wear rate obtained from the test was expressed in the unit of grams/revolution. This was then converted and normalized to μg/m/mm, the wear rate being expressed by the weight loss after unit sliding distance in unit contact width.

In each weight measurement interval, diameter and width measurements were also taken. An average diameter was obtained from two diameter measurements perpendicular to each other. An average width was obtained from four points which were used for diameter measurements. The procedure is illustrated in Figure 2.9.

In each test, the top roller is the material to be investigated and the bottom roller a counterpart, always being W5. The maximum contact pressures used in the tests were

500, 900, 1220, 1450 and 1700 MPa and the slide/roll ratio was set at 35%. The materials of top rollers, heat treatments and the contact pressures are summarized in Table 2.5.

2.8. ROLLING/SLIDING DEFORMATION TESTS

The deformation tests under rolling/sliding conditions were also conducted in the Amsler machine. The tests were carried out with a slide/roll ratio of 10% and at the maximum Hertzian contact pressures of 1295 and 1600 MPa. The test configuration is similar to that of the wear test, but the gear system of the machine was adjusted to allow the upper shaft to oscillate in its axial direction. The top roller, when fixed on the upper shaft, moved approximately 3 mm on either side of the centerline of the bottom roller every 3 seconds. Both top and bottom rollers were of the same materials. The geometry profile of the specimens was the same as that used in wear testing except that only 35 mm diameter rollers were used to get a 10% longitudinal slide/roll ratio. To achieve deformation without wear, drops of lubricant were applied uniformly on the surface of the rollers before starting the test and before resuming the test after taking measurements.

During a test, both top and bottom specimens were removed from the machine periodically to measure the variations in diameter and width. The measurement procedures for diameter and width of rollers were the same as that for wear testing rollers. Curves of variations in width and diameter of the rollers against revolutions were obtained to represent the deformation behavior of the materials under rolling/sliding conditions.

2.9. TESTING OF MECHANICAL PROPERTIES

The tensile tests and Charpy V-notch impact tests were carried out on the Mo-B steels under as-received and water-quenched conditions. The geometry of a tensile specimen is shown in Figure 2.10, complying with ASTM standard E8-91.[209] The dimension of a Charpy V-notch sample is shown in Figure 2.11, in accordance with ASTM standard E23-92.[210] The impact toughness tests were carried out at room temperature in a drop pendulum tester with a capacity of 264 ft-lb.

2.10. WELDABILITY TESTING

The weldability of steels was evaluated by conducting Tekken tests. The testing method, officially named the *Method of Y-groove Cracking Test*, was initiated and developed by the Japanese and is defined in the Japanese Industrial Standard JIS Z 3158. The Tekken test is used to evaluate the susceptibility of a material to cold cracking induced by hydrogen in the heat affected zone (HAZ) as well as in the weld metal. Since the welding groove is in the "y" shape, it provides very severe constraint for cracking.

The configuration of a Tekken sample is shown in Figure 2.12. An entire test piece was composed of two parts that were welded together before testing. After the test piece had been pre-heated to 200 °C using the flame of a torch, the test weldment was made in the center portion of the groove. To avoid toe and crater cracking in the testing section, the welding was run in the path shown in Figure 2.13. After welding, the specimens were stored for more than 72 hours to allow time for cracks to develop. The sample was then sliced into six pieces in the transverse section relative to the welds with a uniform spacing along the weld, Figure 2.13. Metallographic specimens were prepared on the transversely sectioned surfaces and the surfaces etched with 5% Nital were observed for cracking occurrence in the HAZ and the weld metal.

The welding method used was gas metal arc welding (GMAW). Solid wire 120S-1 of 1/16 inch in diameter was used as filler material. The specifications of this material are listed in Table 2.6 according to the L-Tec Catalog. The shielding gas used in the tests consisted of 95% argon, 2% oxygen and 3% carbon dioxide. For the as-received steels J1 and air-cooled J2, the heat input was 100 kJ/in and for the water-quenched J1, the heat input was 71 kJ/in. It was estimated that the cooling rate between 800 and 500 °C would be slower than 10 °C/s. A summary of the welding test data is given in Table 2.7.

2.11. ANALYSIS OF AMSLER WEAR ROLLERS

The features of worn surfaces of the Amsler rollers were observed in a Zeiss SEM with an accelerating voltage of 20 kV. Subsurface characteristics were observed by means of optical metallography in the section cut perpendicularly to the roller axis (Figure 2.14). To protect worn surface from being distorted by cutting and grinding, the sample was plated with nickel beforehand.

The microhardness of the section from the worn surface towards the center was measured using a microhardness tester on the Knoop scale with a load of 1000 grams. The path of measurement is also illustrated in Figure 2.14.

2.12. FRACTOGRAPHIC ANALYSIS

The fracture surface of Charpy impact specimens was examined macroscopically in a stereo-microscope and microscopically in a scanning electron microscope.

Table 2.1 Composition of the Experimental Mo-B Steels (wt-%)

(a) Analysis of Liquid Steels

Steel No.	C	Mn	P	S	Si	Ni	Cr	Mo	Al	Ti	B
J1	0.21	2	0.013	0.01	0.97	0	2.01	0.51	0.025	0.038	0.003
J2	0.13	4.04	0.013	0.008	0.28	0	0	0.51	0.023	0.035	0.003
J3	0.09	2.04	0.013	0.011	0.28	2.03	1.98	0.5	0.02	0.039	0.003
J4	0.034	2.1	0.014	0.009	0.29	2.1	2.1	0.53	0.019	0.035	0.003
J5	0.039	4.1	0.012	0.009	0.29	0	0	0.51	0.019	0.037	0.003

Table 2.1 Composition of the Experimental Mo-B Steels (cont.)

(b) Analysis of Solid Steels

Steel No.	C	Mn	P	S	Si	Cu	Ni	V	Nb	Al	Cr	Mo
J1	.181	2.01	.010	.0131	1.13	<.001	.008	<.005	<.005	.029	1.94	.482
J2	.115	3.97	.009	.0133	.270	<.001	.015	<.005	<.005	.028	.017	.474
J3	.077	2.03	.009	.0082	.270	<.001	1.93	<.005	.006	.028	1.97	.475
J4	.023	2.02	.009	.0071	.268	<.001	1.93	<.005	.006	.026	1.96	.475
J5	.026	4.04	.009	.0137	.272	<.001	.019	<.005	<.005	.025	.018	.469

Steel No.	Ti	Sn	B	Zr	Ca	As	Pb	Sb	Bi	N*	O*	
J1	.025	.001	.0027	<.0040	.0042	<.0004	.0061	<.0020	.0022	.00074	.0013	
J2	.038	<.001	.0027	<.0040	.0017	.0010	.0100	<.0020	.0023	.001	.0027	
J3	.026	<.001	.0031	.0046	.0016	<.0004	.0073	<.0020	.0024	.00092	.0033	
J4	.023	<.001	.0030	.0047	.0016	<.0004	.0075	<.0020	.0025	.001	.0038	
J5	.037	<.001	.0030	<.0040	.0016	.0016	.0110	<.0020	.0024	.00095	.0028	

* *Oxygen and nitrogen were analyzed by Esco corporation using Leco approach.*

Table 2.2(a) Composition of the Pearlitic Rail Steel X136 (wt-%)

C	Mn	P	S	Si	Cr
0.794	0.913	0.018	0.010	0.663	0.473

Table 2.2(b) Mechanical Properties of the Pearlitic Rail Steel X136

Steel	Y.S. (ksi)	UTS (ksi)	RA (%)	El (%)	Hardness* (HRC)
X136	126	191	40	13.3	36

* *The hardness was determined on a lateral side of an Amsler roller by measuring 12 points along periphery of the roller. Hardness readings varied from 33.9 to 38.1 HRC with an average of 36.3 HRC. The population standard deviation was 1.631 and sample standard deviation was 1.711.*

Table 2.3 Composition of the Class C Wheel Steel W5*

C	Cr	Mo	Mn	Si	S	P	Cu	Ni	V
0.66	.036	.014	.684	.528	.022	.002	.089	.029	.009

* *The hardness of W5 was determined in a similar manner for X136 by measuring 8 points along the periphery of an Amsler roller. The average hardness was 30.8 with the lowest hardness reading of 28.3 HRC and the highest 33.5 HRC. The population and sample standard deviations were 1.589 and 1.699, respectively.*

Table 2.4 Heat Treatment of the Mo-B Steels

Steel	Austenitizing Temperature (°C)	Holding Time (min)[*]	Air Cooling	Water Quenching
J1	910	15	✓	✓
J2	900	15	✓	✓
J3	900	15	✓	✓
J4	900	10	✓	✓
J5	930	15	✓	✓

[*] *After the sample was put into the furnace, the holding time commenced when the furnace temperature came back to the austenitizing temperature.*

Table 2.5 Contact Pressures Used in the Amsler Wear Tests with a Slide/Roll Ratio of 35%

Steel	Contact Pressure (MPa)				
	500	900	1220	1450	1700
J1-as	✓	✓	✓	✓	✓
J2-as	✓	✓	✓	✓	✓
J3-as	✓		✓		✓
J4-as	✓	✓	✓	✓	✓
J5-as	✓		✓		✓
J1-ac			✓		
J2-ac			✓		
J3-ac			✓		
J4-ac			✓		
J5-ac			✓		
J1-wq	✓		✓		✓
J2-wq	✓		✓		✓
J3-wq			✓		
J4-wq	✓		✓		✓
J5-wq			✓		
X136	✓		✓		✓
Mn steel			✓		✓

Key:
as — as received
ac — air cooled
wq — water quenched

Table 2.6 Chemistry and Properties of 120S-1

(a) Chemical Composition of 120S-1 (wt-%)

C	0.06-0.08
Mn	1.20-1.35
Si	0.30-0.40
Ni	2.40-2.70
Cr	0.30-0.50
Mo	0.40-0.50

(b) Mechanical Properties of 120S-1

Tensile Strength (ksi)	120-125
Yield Strength (ksi)	110-115
Elongation (%)	15-18
Reduction of Area(%)	50-65
Charpy V-Notch	
@ 0°F (ft-lbs)	95-110
@ -60°F (ft-lbs)	70-80

Table 2.7 Weldability Test Conditions

Materials	As-received J1
	Air-cooled J2
	Water-quenched J1
Type of Test	Tekken test
Welding Method	Gas Metal Arc Welding
Filler Material	120S-1
Shielding Gas	95%Ar + 2%O_2 + 3%CO_2
Heat Input (kJ/in)	100 (for J1-as and J2-ac)
	71 (for J1-wq)
Preheat Temperature (°C)	200

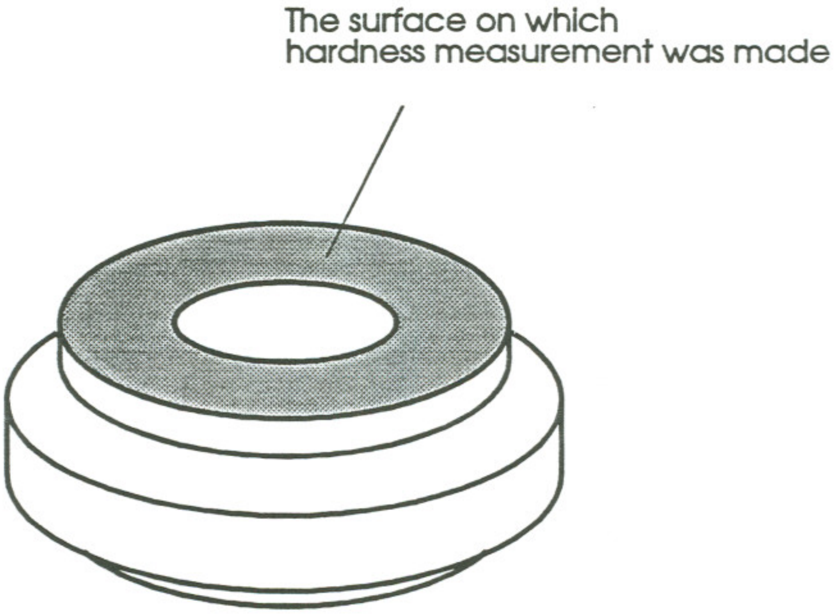

Figure 2.1 Hardness measurement on an Amsler roller

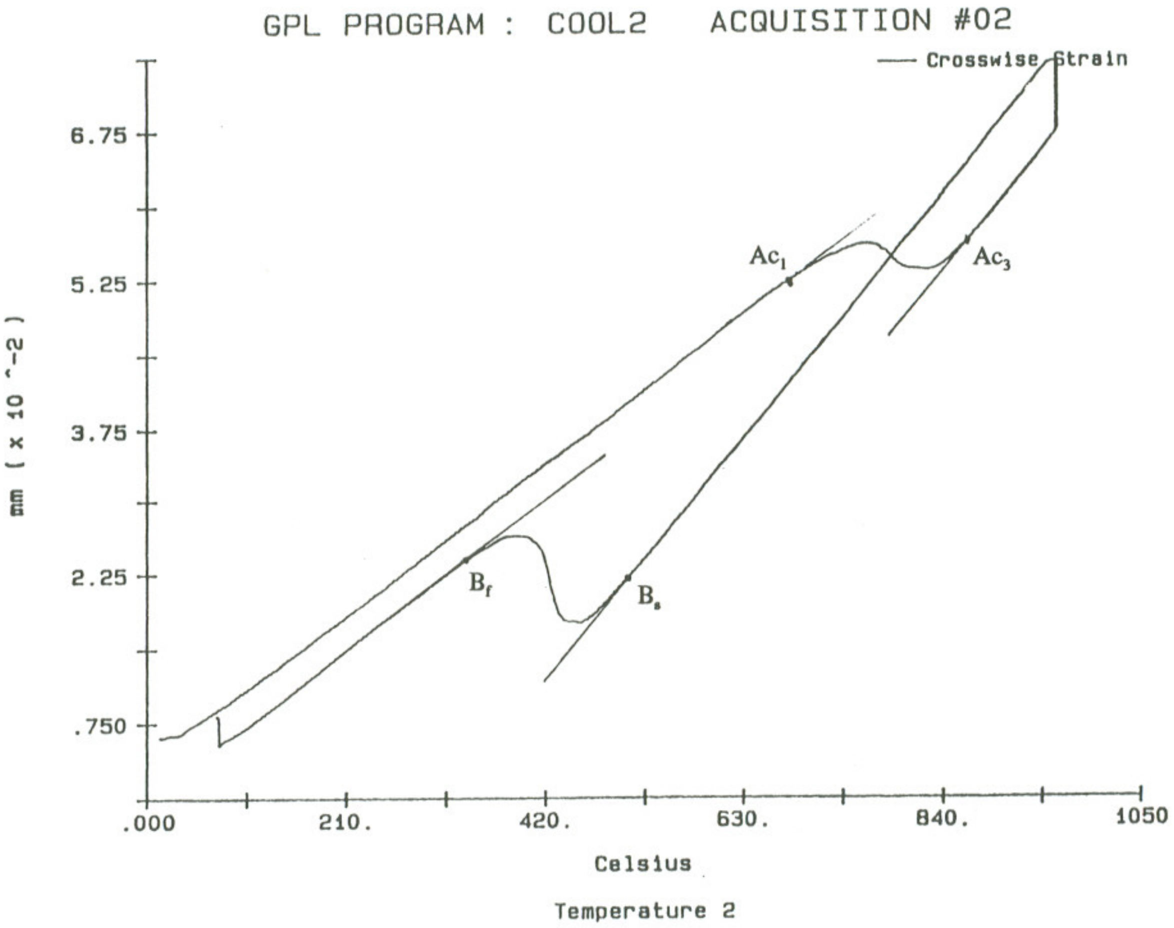

Figure 2.2 Determination of transformation temperatures from a dilation curve

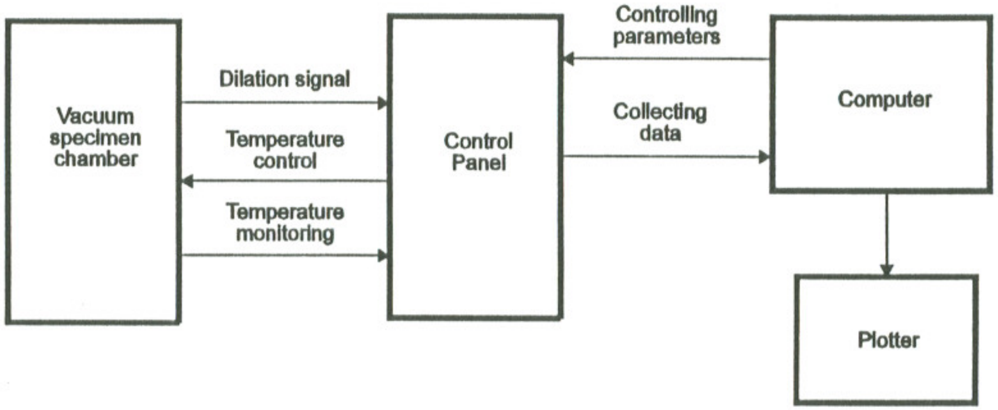

Figure 2.3 Set-up of a Gleeble experiment

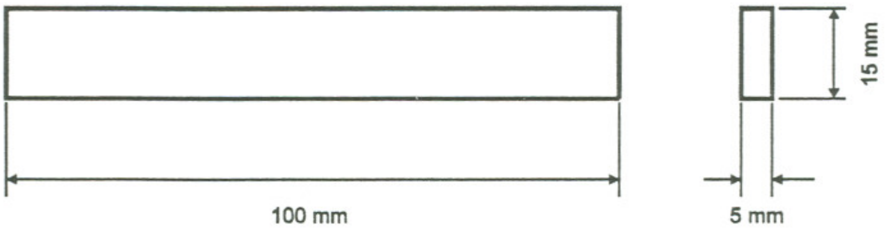

Figure 2.4 Geometry of a Gleeble specimen

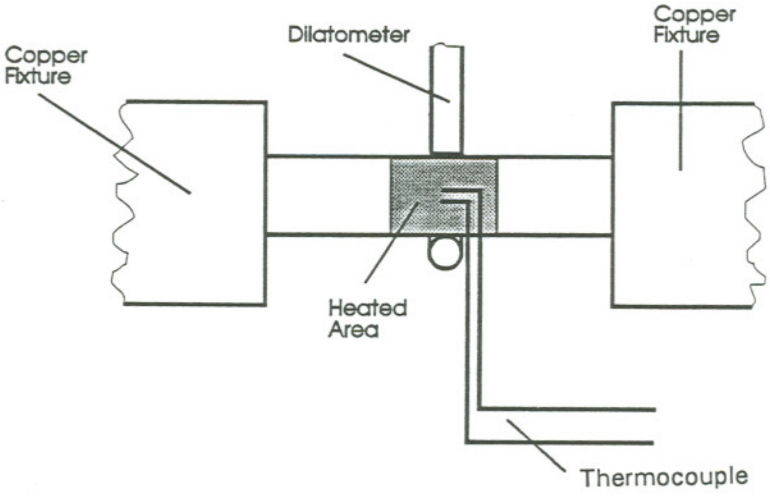

Figure 2.5 Specimen set-up for a Gleeble thermal run with a dilatometer

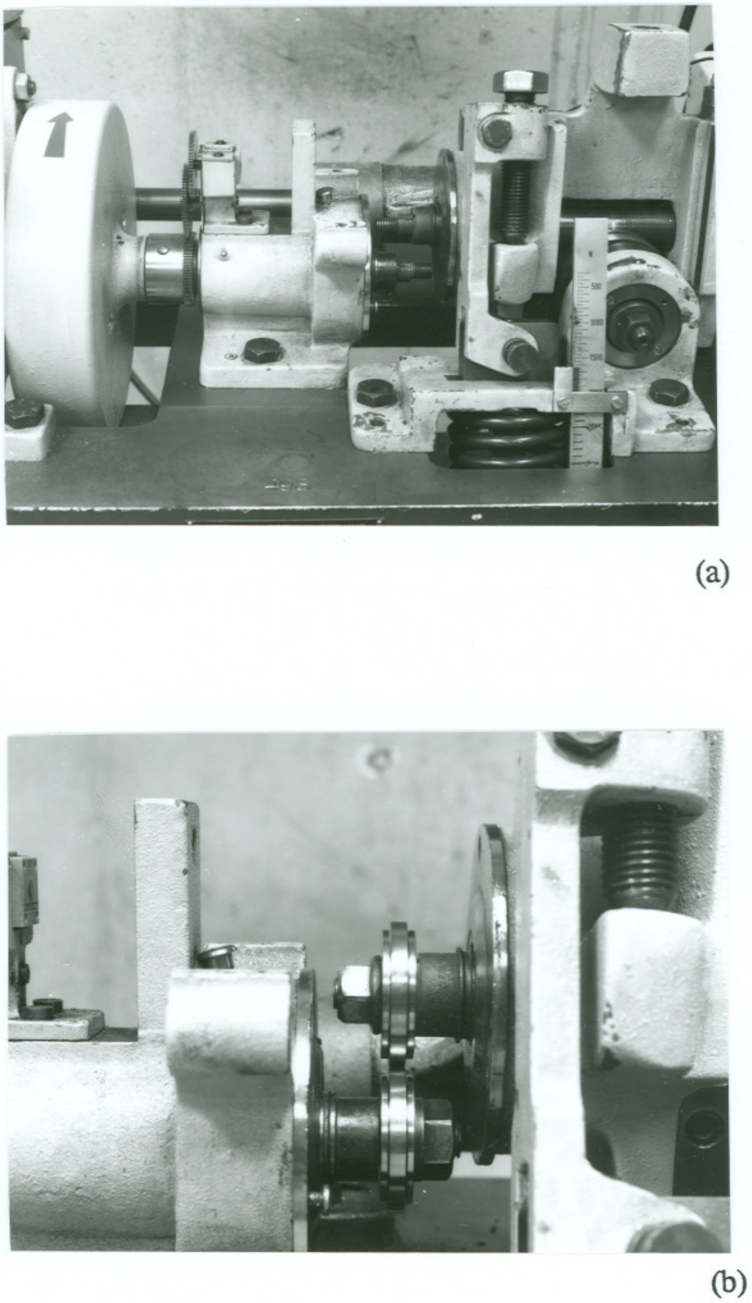

(a)

(b)

Figure 2.6 Amsler machine for wear and deformation testing
(a) Overview of the machine (b) Roller set-up for a wear test

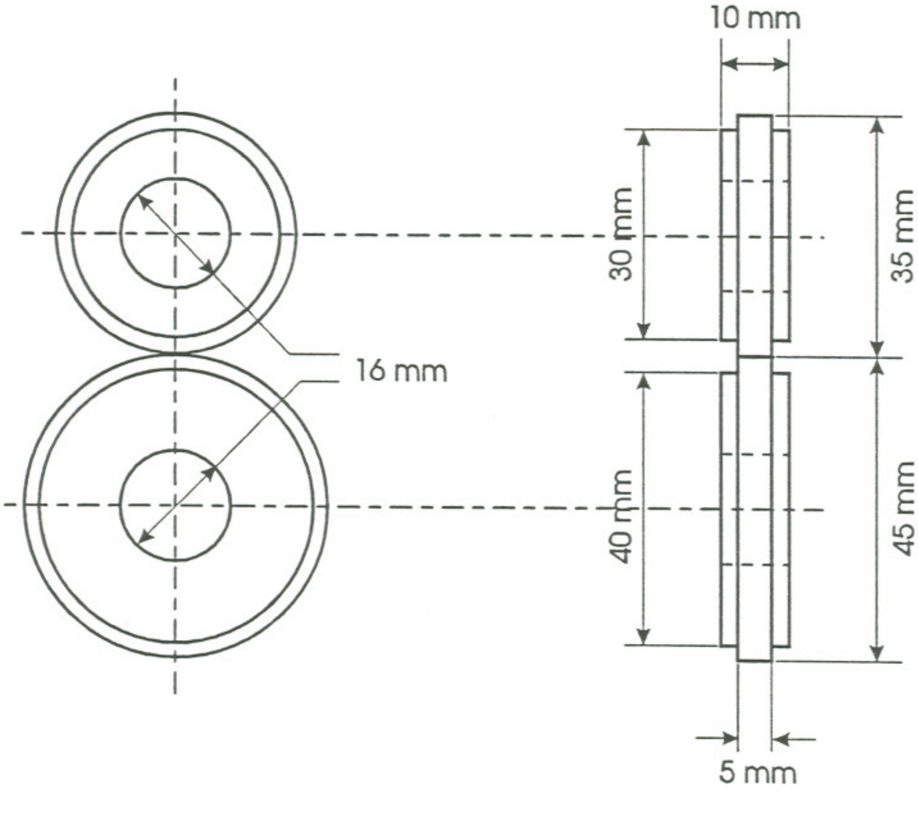

Figure 2.7 Geometry of Amsler rollers for wear testing

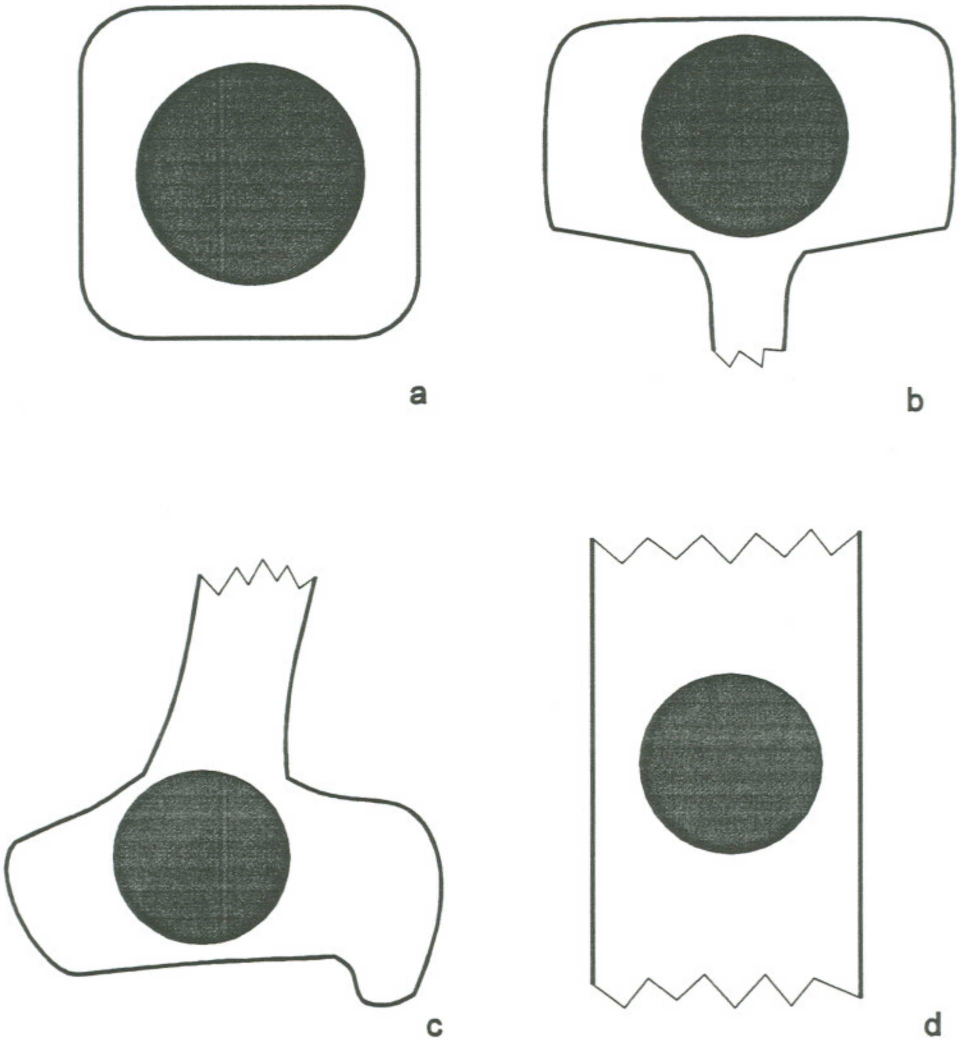

Figure 2.8 Orientation of Amsler rollers taken from bulk materials
(a) Rollers from Mo-B bainitic steel bars
(b) Rollers from a X136 rail steel
(c) Rollers from an austenitic Mn steel
(d) Bottom rollers from a wheel of class C wheel steel

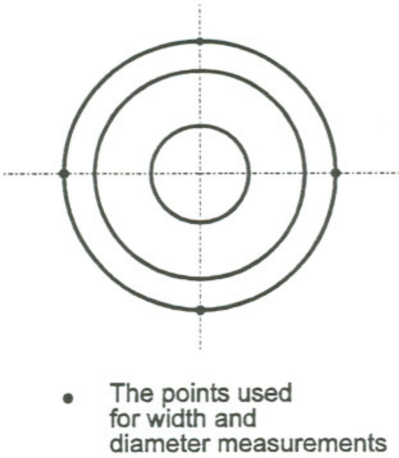

Figure 2.9 Dimensional measurements on an Amsler roller

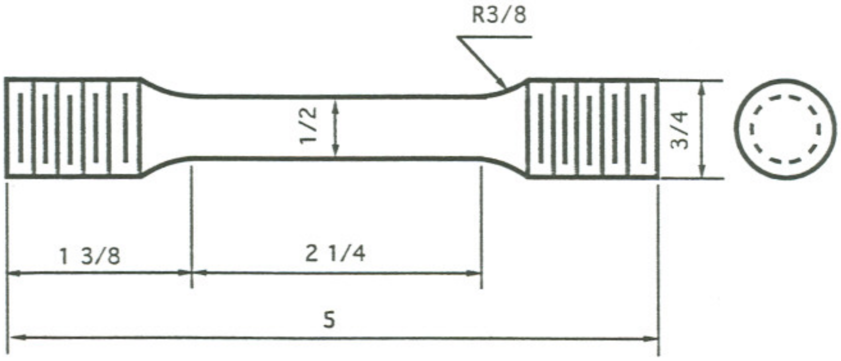

Dimensions in inches

Figure 2.10 Geometry of a tensile specimen

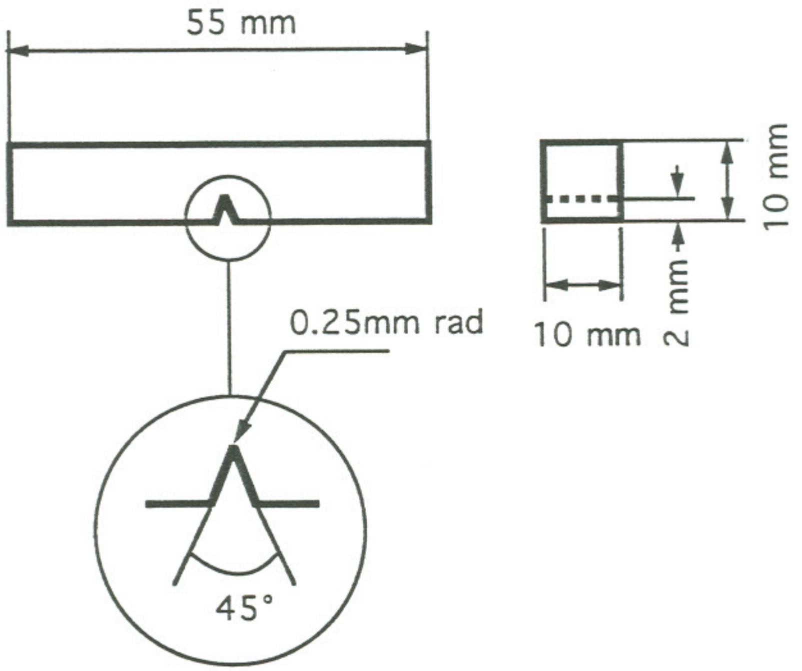

Figure 2.11 Geometry of a Charpy V-notch impact specimen

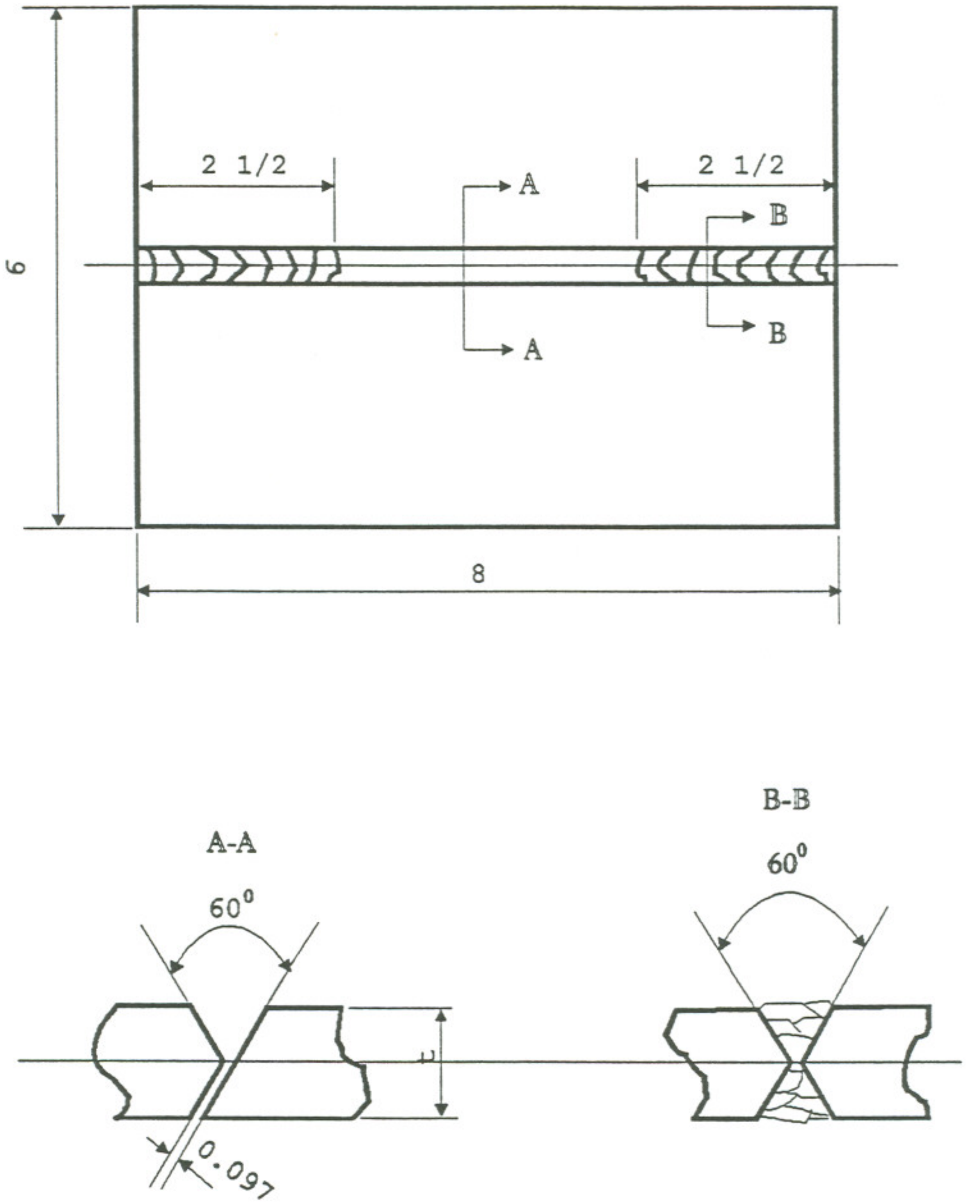

Dimension in inches

t = 1 inch

Figure 2.12 Configuration of a Tekken specimen

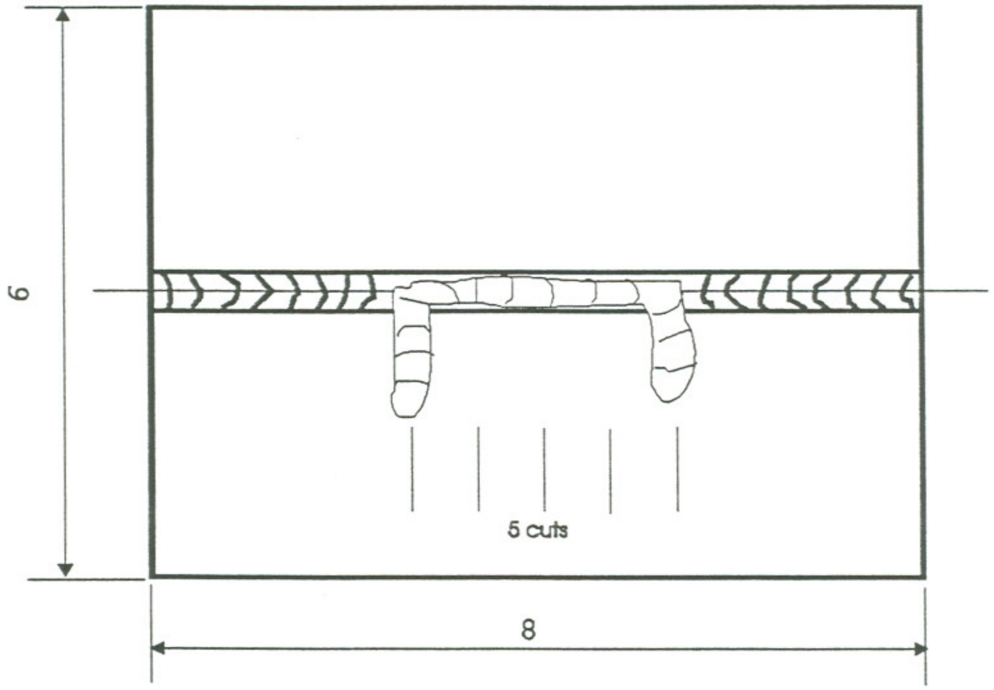

Dimension in inches

Figure 2.13 Welding path and sectioning of a Tekken specimen

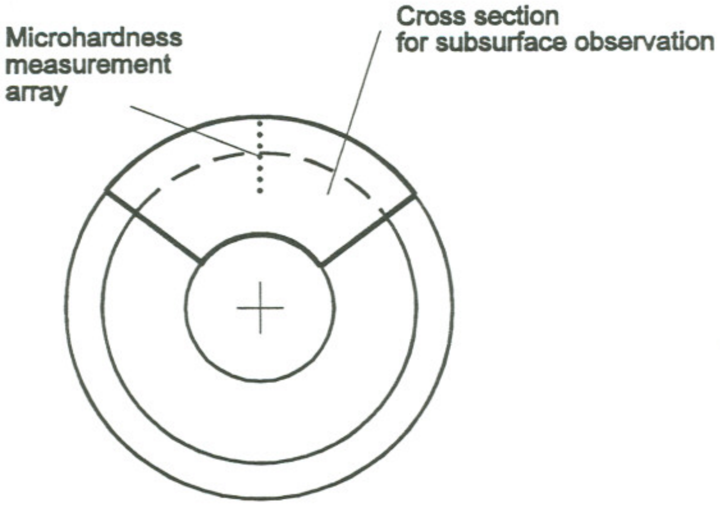

Figure 2.14 Cross section of an Amsler roller for subsurface analysis

CHAPTER 3

EXPERIMENTAL RESULTS

3.1. MICROSTRUCTURE OF THE Mo-B STEELS

3.1.1. Metallography of the As-Received Steels

The microstructure of the as-received steels was examined in an optical microscope. As shown in Figure 3.1, packets characterized by features with different contrast and orientations were found in prior austenite grains. Due to the limited resolution of the optical microscope and the complexity of microstructure on continuous cooling, no further details of phases were identified with these micrographs. Therefore, the microstructure of these steels was characterized by means of transmission electron microscopy.

3.1.2. Transmission Electron Microscopy of the Mo-B Steels

3.1.2.1. The as-received steels

The TEM observations revealed that in the as-received J1, a lath structure was predominant although there is some massive ferrite. The lath ferrite was heavily dislocated as shown in Figure 3.2(a). Retained austenite was found in elongated and blocky forms as shown in Figures 3.2(b) and 3.2(c). The retained austenite was clearly revealed by a dark field image in Figure 3.2(c) with a reflection of $(020)_\gamma$ (Figure 3.2(d)). The elongated retained austenite was located in the lath ferrite boundaries and the blocky retained austenite could cross the ferritic lath. A twinned structure shown in Figure 3.2(e) was found in the steel, but only occasionally and at generally high magnifications (>50,000×). Although its crystallography was not identified due to its small size, this feature is presumably a twinned martensite-retained austenite island (M-A island) since its morphology resembles the M-A islands reported in the literature. The structure of this steel is therefore predominantly carbide-free bainite with some blocky retained austenite, M-A islands and non lath ferrite, i.e., a mixture of carbide-free bainite and granular bainite.

The microstructure of the as-received J2 was more complex. In most areas, carbides precipitated in ferrite laths at an angle to the long axis of the laths, showing a morphology of lower bainite. Such a structure was predominant and is shown in Figure 3.3(a). It was found, however, that in some ferrite laths there were no carbide precipitates (Figure 3.3(b)). In addition, in some areas, carbides formed in the massive ferrite. In these areas, as shown in Figure 3.3(c), carbides precipitated in a single direction. M-A islands (Figure 3.3(d)) were found occasionally. This steel has a microstructure of predominantly lower bainite with some massive ferrite with and without carbides.

A microstructure of massive ferrite with high density dislocations was found to be predominant in the as-received J3. M-A islands were produced in this steel. Figure 3.4(a) presents a highly dislocated massive ferrite and Figure 3.4(b) shows a M-A island. This steel consists of granular bainite.

The microstructure of J4 is quite similar to J3, but with a greater number of M-A islands. This structure is shown in Figure 3.5.

Lath ferrite is well developed in J5. At the lath boundaries retained austenite was found. No carbides or M-A islands were revealed. The microstructure of this steel is basically carbide-free bainite, consisting of lath ferrite and retained austenite (Figure 3.6).

3.1.2.2. The air-cooled steels

The microstructure of the air-cooled steel J1 is shown in Figure 3.7. Figure 3.7(a) shows that ferrite laths were well developed and the retained austenite thin films were located in the lath boundaries. In this steel, a needle-shaped structure was very distinct (Figure 3.7(b)), but the morphology was different from a M-A island. This structure is presumably martensite like that reported by Narasimha Rao *et al.*[211] The microstructure of this steel is carbide-free bainite with needle-shaped martensite.

Figure 3.8 shows the microstructure of the air-cooled J4. A heavily dislocated lath ferrite was revealed but no M-A islands were found (Figure 3.8(a)). The cell structures formed by tangled dislocations were found in some areas and are shown in Figure 3.8(b).

3.1.2.3. The water-quenched steels

In the water-quenched J1, heavily dislocated lath ferrite was predominant (Figure 3.9(a)). The thin films of retained austenite were entrapped in the lath boundaries, as shown in Figure 3.9(b). Figure 3.9(c) shows the corresponding dark field image of Figure 3.9(b) using the $02\bar{2}$ diffraction spot of austenite (Figure 3.9(d)). In this steel, more needle-shaped martensite was found than in the air-cooled J1. Usually the needles are agglomerated and juxtaposed in groups, as shown in Figure 3.9(e). The microstructure of this steel was similar to that of the air-cooled J1, but the features of the ferrite laths and martensite were much enhanced. This steel consists of carbide-free bainite with martensite.

The microstructure of the water-quenched J2 was composed of lath ferrite (Figure 3.10(a)) and massive ferrite, Figure 3.10(b). Needle-shaped martensite was found in some areas (Figure 3.10(c)) and no carbides were detected.

The microstructure of the water-quenched J3 consisted of lath and massive ferrite, but the former was greater than the latter. Figure 3.11 shows the microstructure of this steel.

The water-quenched J4 achieved a microstructure consisting of predominant ferrite laths (Figure 3.12(a)) and some massive ferrite (Figure 3.12(b)). The diffraction pattern (Figure 3.12(c)) shows that only ferrite existed in this structure.

The microstructure of the water-quenched J5 was also composed of lath and massive ferrite (Figures 3.13(a) and (b)). No thin films of retained austenite were discerned in the lath boundaries.

The water-quenched J3, J4 and J5 are basically bainitic ferrite in both lath and massive forms. Such a microstructure was also found in the ultra-low carbon weld metals in a study of Singh.[212]

The microstructures of the Mo-B steels are summarized below.

	As-received	Air-cooled	Water-quenched
J1	lath ferrite retained austenite massive ferrite few M-A islands	lath ferrite thin films of retained austenite in lath boundaries needle-shaped martensite	lath ferrite thin films of retained austenite in lath boundaries needle-shaped martensite
J2	lower bainite lath ferrite w/o carbides massive ferrite w/ carbides few M-A islands		lath ferrite massive ferrite needle-shaped martensite
J3	massive ferrite M-A islands		lath ferrite massive ferrite
J4	similar to J3-as but more M-A islands	lath ferrite	lath ferrite massive ferrite
J5	lath ferrite thin films of retained austenite in lath boundaries		lath ferrite massive ferrite

3.2. CCT DIAGRAMS OF THE Mo-B STEELS

The phase transformations of high carbon J1 and low carbon J4 were investigated using a Gleeble thermal simulator over a wide range of cooling rates between 0.4 and 25 °C/s. Each temperature-dilation curve indicates that only one transformation happened since the geometric expansion of a specimen caused by phase transformation appeared only once. It was found that for each steel, the transformation temperature generally remained constant, regardless of cooling rate. The transformation start temperature of J1 was measured to be about 435 °C and that of J4 about 550 °C. Since the transformation was able to occur at 0.4 °C/s at such a low temperature, the transformation was believed to be a bainite transformation. Therefore, the transformation start temperatures were designated as B_s. The measurement results are listed in Table 3.1. It is seen that the B_s was significantly depressed in the high carbon steel J1.

Figures 3.14 and 3.15 show the CCT curves for J1 and J4, respectively. The curves indicate that only bainitic structures were obtained over a wide range of cooling rate since no martensite transformation was detected.

3.3. GRAIN SIZE OF THE STEELS

The prior austenite grain size measurements were taken only on some steels because not all steels would etch well enough to show grain boundaries. Table 3.2 lists the grain size of J2, J4 and J5 in the as-received state. The as-received steels have almost the same grain size, leading to an assumption that the grain size of all the as-received steels was about 55 μm. The grain size of the air-cooled J4 was found to be greater than 90 μm, suggesting that the grains grew significantly by furnace heat treatment.

3.4. Ac_1 AND Ac_3 OF THE BAINITIC STEELS

Since the grain size of the air-cooled J4 exhibited a large grain size of greater than 90 μm, it was felt necessary to reduce the grain size by lowering the austenitizing temperatures. Hence, the Ac_1 and Ac_3 were measured so that an austenitizing temperature just above the Ac_3 could be used in subsequent heat treatments. Unfortunately, the results shown in Table 3.3. indicate that the measured Ac_3 was very close to the austenitizing temperatures used in the previous heat treatment. Therefore, no further action was taken to adjust austenitizing temperatures.

Table 3.3 also contains the calculated Ac_3 temperatures for comparison. The calculated temperatures were obtained using the equation developed by Andrews,[213] shown below:

$$Ac_3\ (^\circ C) = 910-203\sqrt{C}-15.2Ni+44.7Si+104V+31.5Mo+13.1W$$
$$-(30Mn+11Cr+20Cu-700P-400Al-120As-400Ti)\quad (wt\text{-}\%)$$

It is seen that the calculated values are consistently lower than the measured ones. This suggests that the empirical equation is generally limited to the range in which the materials were tested.

3.5. MECHANICAL PROPERTIES OF THE BAINITIC STEELS

The mechanical properties of the bainitic steels were examined in terms of strength, ductility, impact toughness and hardness. The results are given in Tables 3.4 and 3.5.

3.5.1. Hardness of the Steels

The hardness of the bainitic steels is tabulated in Table 3.5. and shown in Figure 3.16. It is apparent that the hardness of the steels was increased by heat treatment, but the degree varied with steel. Water-quenching resulted in almost the same hardness as air-cooling did for J1, J2 and J4, but led to a substantially higher hardness for J5.

Figure 3.17 shows a linear relationship of hardness values between Rockwell and Brinell scales as measured for these steels. With linear regression, the relationship is given as

$$HRC = 2.75 + 0.10\ HB, \qquad (r = 0.97)$$
$$\text{or} \qquad HB = 10\ HRC - 27.5$$

where HRC is the hardness on the Rockwell scale, HB the Brinell scale and r is the correlation coefficient.

3.5.2. Strength and Ductility

The strengths of the steels are shown in Figure 3.18. It is seen that water quenching increased both ultimate tensile strength and 0.2% proof stress. The extent of improvement was evaluated using the equation

$$\Delta\sigma_{in}\ (\%) = \frac{\sigma_{wq} - \sigma_{as}}{\sigma_{as}} \times 100\%$$

where $\Delta\sigma_{in}$ is the strength increase by percentage, σ_{wq} is the strength of water-quenched steels and σ_{as} is the strength of as-received steels. Figure 3.19 shows that the improvement of yield strength was greater than that of ultimate tensile strength.

Figure 3.18 also demonstrates that the strength of higher carbon steels was greater than that of lower carbon steels for both as-received and water-quenched steels.

The ductility of the steels are shown in Figure 3.20. Both reduction of area and elongation were reduced by water quenching. The degree to which water quenching decreased ductility is illustrated in Figure 3.21. For both elongation and reduction of area, the high carbon steel J1 exhibited the greatest change by water quenching. There was no significant change in reduction of area for J3.

It seems that ductility was decreased by an increase in carbon content since higher carbon steels showed lower elongation and reduction of area than lower carbon steels.

3.5.3. Impact Toughness

The results of Charpy impact toughness at room temperature are shown in Figure 3.22. For the as-received steels, J1 showed the lowest toughness. The toughness of J2, J3 and J4 were quite similar and at a higher level.

Water quenching did not exhibit a consistent influence on toughness. The toughnesses of J1 and J5 were increased by water quenching, but those of the rest were decreased. After quenching in water, J1 through J4 exhibited similar toughnesses and J5 showed the highest toughness.

Brittle features were revealed on all fracture surfaces at low magnification (only a few times of magnification)and no ductile areas were found on the these surfaces. SEM observations revealed that the fracture belonged to a quasi-cleavage mode. Figure 3.23 shows the fractography of some steels. In some areas, ductile dimples were found, as shown in Figure 3.24. In the SEM, the packet size on the fracture surface was not generally revealed, but could, in some instances, be measured and found to be about 20 μm.

3.6. WEAR PERFORMANCE OF STEELS — BAINITE, PEARLITE AND AUSTENITE

The wear resistance of the steels was evaluated at various contact pressures with a slide/roll ratio of 35%. The wear rates of all the steels tested are given in Table 3.6.

3.6.1. Re-evaluation of the Reproducibility of the Amsler Machine

Although no systematic tests were performed to investigate the reproducibility of the Amsler machine in the present study, the data of wear rates for reproducibility[214] were re-processed. The evaluation of the reproducibility with 95% confidence was then achieved in terms of relative error.

Assuming that the data follow a normal distribution, the original data[214] and the re-evaluation results are tabulated in Table 3.7. The maximum relative error obtained was 10%. In the current study, some tests were performed twice using the as-received

J1 and J4 at a contact pressure of 1220 MPa, the relative error for these tests was calculated using the equation

$$\epsilon = \frac{\dot{W}_{max} - \dot{W}_{min}}{\dot{W}_{min}}$$

where ε is the relative error, $\dot{w}_{max}$ and $\dot{w}_{min}$ are the maximum and minimum wear rates, respectively. The maximum relative error was found to be 6.7%, falling within the presumed 10%. Therefore, ±10% was considered to be the scatter band for a wear rate for each test.

3.6.2. Rolling/Sliding Wear of the Bainitic Steels

Wear rates were obtained based on weight loss measurements. Figure 3.25 shows the wear rates of the bainitic steels tested at 1220 MPa. Heat treatment exhibited a great influence on the wear rate of the steels. For each steel of a given composition, the as-received steel showed the highest wear rate and the water quenched steel the lowest wear rate. However, the degree to which the wear rate was decreased by heat treatment varied with the steel. J1 experienced the greatest change while J4 the slightest. Consequently, the relative wear resistance also varied with heat treatment. Herein the relative wear resistance refers to the ranking of wear resistance of the steels in each heat treatment group (or at each contact pressure level as will be mentioned later on) and wear resistance is reciprocal to wear rate. J1, for example, did not show an outstanding wear resistance in the as-received steel group, but it exhibited the highest wear resistance in the water-quenched group.

The variation in wear rate with contact pressure for the as-received steels is presented in Figure 3.26. The wear rate of J1 increased with an increase in contact pressure in a linear manner. For J2 and J3, however, the wear rate did not increase at high contact pressures as fast as at low contact pressures. For J4 and J5, the wear rate increased with contact pressure increasing at lower pressures, but at high contact pressures over approximately 1220 MPa, the wear rate tended to be decreased by increasing contact pressure.

The relative wear resistance also varied with contact pressure level. At 500 MPa, the as-received J1 exhibited the best wear resistance, but at 1700 MPa its wear resistance was much lower than that of J4.

As at 1220 MPa, water quenching increased the wear resistance of J1 and J4 at 500 MPa and 1700 MPa. It is apparent in Figure 3.27 that this effect was much stronger for J1 than for J4. For J1, water quenching reduced the wear rate about 80%, while for J4, its wear rate was reduced about 28%. Because of the significant reduction in wear rate, the water-quenched J1 excelled over all other steels at each contact pressure in terms of wear resistance.

3.6.3. Wear Resistance of X136 and Mn Steels

It is well known that for pearlitic rail steels, high hardness indicates high wear resistance. For this reason, a high hardness pearlitic steel X136 was chosen to be investigated with respect to wear resistance and a comparison was made with the bainitic steels. Further, the wear performance of an austenitic manganese steel, which is often used to make frog steels, was also investigated. The wear rates of X136 and the Mn steel are shown in Figure 3.28. Compared with the as-received bainitic steels, X136 exhibited the lowest wear rates at each contact pressure. However, its wear rate was higher than that of the water-quenched J1. It was noted that there was a variation of 4 – 5 HRC in hardness in the periphery of the X136 rollers, but no abnormal wear behavior was observed with reference to the other steels. The austenitic Mn steel exhibited superior wear resistance to all the other steels and the wear rates were almost zero even at 1700 MPa.

3.6.4. Wear Behavior of the Pearlitic Wheel Steel W5

The pearlitic wheel steel W5 was used to make bottom rollers as a counterpart material in the Amsler wear testing. Although the weight loss of the top rollers increased linearly with revolutions after a break-in period in most tests, the weight loss vs. revolutions curves for the bottom rollers did not always exhibit a linear relationship. Figure 3.29(a) shows examples of a linear curve for a top roller and a non-linear curve for a bottom roller. For a bottom roller, if the curve is not linear, the wear rate was derived through the data points which correspond to their counterpart points for the top roller, as shown in Figure 3.29(b). The wear rates of the bottom rollers are also listed in Table 3.6.

Figures 3.30 and 3.31 show the wear rates of both top and bottom rollers for a wide range of contact pressure 500 – 1700 MPa. Coupled with top rollers of the bainitic steels, the wear rates of bottom rollers were generally far lower than those of their top counterparts. It was noted that for the water-quenched J1/W5 pair, i.e., the top roller is the water-quenched J1 and the bottom roller W5, the differences in wear rate between the rollers were not significant and that the bottom roller W5 even exhibited a higher wear rate than the top roller (water-quenched J1) at 1700 MPa. For the X136/W5 pairs, the difference in wear rate between the rollers decreased as contact pressure increased. Wear rates of both rollers were very close for the Mn steel/W5 pairs.

3.7. ROLLING/SLIDING DEFORMATION BEHAVIOR

The resistance to deformation under rolling/sliding conditions was tested in the Amsler machine. With oil on the surface of the rollers, wear was effectively prevented. During a test, the rollers were deformed by stretching the surface to both sides of the rollers and the diameter of the specimens was reduced accordingly. The deformation in terms of roller width increase or diameter decrease of both top and bottom rollers at 1295 MPa is plotted in Figures 3.32 and 3.33 as a function of revolutions. The results indicate that the as-received J4 experienced a significant deformation, but the other steels exhibited quite good deformation resistance. The top roller of J4 suffered slightly more deformation than the bottom one.

The effect of contact pressure on deformation was investigated for the as-received J1. Figure 3.34 indicates that deformation was increased by increasing the contact pressure. It was found that at 1295 MPa, the deformation accumulation became very small after an initial period of time. At 1700 MPa, however, deformation continued substantially with revolutions. By defining the deformation rate as width increase divided by revolutions, the deformation rate was derived using a linear regression. The deformation rate was 1.5×10^{-6} mm/rev at 1295 MPa, and 1.8×10^{-5} mm/rev at 1600 MPa. With the contact pressure increased from 1295 MPa to 1600 MPa, the deformation rate was increased by an order of magnitude.

The subsurface of wear test rollers was investigated. The microstructures in Figure 3.35 indicate that a deformation layer was generated below the worn surfaces. The microstructure of the subsurface was distorted towards an orientation parallel to the surface in the rolling direction. Although the depth of deformation layer was not uniform, especially at high contact pressure, the measurements taken under an optical microscope indicate that the deformation depth of the as-received J1 at 1220 MPa was about 30 μm and 40 — 60 μm at 1700 MPa. It is not surprising that higher contact pressure produced greater deformation. In rolling/sliding wear, the deformed layers were work hardened. Figure 3.36 shows the variation in hardness from the surface towards the center of the specimen. The maximum hardness produced near the surface was about 480 HK and that of bulk material about 420 HK.

3.8. WORN SURFACE OF THE AMSLER WEAR ROLLERS

The worn surface of the Amsler wear rollers were observed in a SEM. In the bainitic steel category, J1 and J4 were investigated. J1, a high carbon steel (0.18%C), demonstrated good wear performance in the water-quenched condition. J4, chosen as a representative of low carbon steel (0.023%C), showed better wear resistance at higher contact pressures than J1 in the as-received conditions.

The worn surface morphologies of the rollers with different heat treatments and contact pressures are shown in Figures 3.37(a) — (g) for the bainitic steels. Generally speaking, the wear mode of these rollers was Type III wear, as first characterized by Bolton and Clayton[18] in pearlitic steels and later applied to bainitic steels.[37] In these steels, large flakes were produced. The deformation on the surface was discerned through the gouging grooves in the rolling direction. The photographs indicate that the degree of deformation varied with heat treatment and contact pressure. Since there is no way to measure the surface deformation (semi-)quantitatively in the wear situation, the observation was only qualitative.

Compared with the as-received J1 at 1700 MPa, the worn surface of the water-quenched J1 was much smoother (Figures 3.37(c) and (g)). The as-received steel J1 showed large thin flakes attached to the surface and evidence of the accumulative deformation was indicated by the gouging traces and ridges on the surface. The water-quenched J1 surface was smooth, Figure 3.37(g), with far fewer deformed ridges and large flakes. This suggests that less deformation was experienced and much less material was removed during wear. Concurrently, the wear rate of the water-quenched J1 was much lower than that of the as-received J1.

In the water-quenched J1, small pits and cracks perpendicular to the rolling direction were observed (Figures 3.37(g) and 3.38). Since the deformation occurred in the rolling/sliding direction, it is likely that the pits were produced by stretching the microcrack in this direction. Figure 3.39 shows the close up of a pit and the illustration of a possible formation mechanism.

The worn surfaces of the pearlitic steel X136 are shown in Figure 3.40. Typical Type III wear was produced at 1700 MPa as demonstrated in Figure 3.40(a). Figure 3.40(b) reveals the worn surface generated at 1220 MPa after 450 revolutions, for which wear rate continuously decreased as the wear process continued. The weight loss curve for this test is shown in Figure 3.41. It was noted that the wear rate reported in this investigation came from the linear portion of the curve during the early period of the test.

The worn surfaces of the Mn austenitic steel were very smooth, corresponding to its low wear rates. At the beginning of the wear test, small dents were uniformly produced on the surface. For a short period of time, the number of dents continued to increase and the surface became rougher. After this period, however, the worn surface was rolled smoother and the dents gradually disappeared as the test continued. As a result, the final worn surface was quite smooth and the wear rate was very low. Figure 3.42 shows the morphology of the worn surfaces of the Mn steel rollers. No Type III wear was produced on this steel.

The observations revealed that the worn surface of the bottom rollers always presented the same features as the top rollers although the wear rate of the bottom rollers was generally lower than that of the top rollers.

3.9. WELDABILITY OF THE BAINITIC STEELS

The weldability of steels is often indicated by carbon equivalent (CE). Yurioka[215] reported that there are at least eight formulae for CE currently being used. These formulae are divided into three groups (A, B and C) according to their applicability to various types of steels.[215] In group A, the CEs are characterized by 1/6 as the coefficient of Mn. This group includes CE(IIW), CE(WES) and CE(Stout II), which are applicable to plain carbon and carbon-manganese steels.[216] Pcm, CE(Graville) and CE(Duren) are classified in Group B. These CEs are believed to have better assessment for low-carbon low-alloy steels. The CEs in Group C, including CE(Stout I) and CEN, have taken into account the interactions between carbon and other elements and therefore have a wider applicability.

Of these formulae, three CEs that are most important and frequently use are given below:

$$A \quad CE\ (IIW) = C + \frac{Mn}{6} + \frac{Cu+Ni}{15} + \frac{Cr+Mo+V}{5};$$

$$B \quad Pcm = C + \frac{Si}{30} + \frac{Mn+Cu+Cr}{20} + \frac{Ni}{60} + \frac{Mo}{15} + \frac{V}{10} + 5B; \quad and$$

$$C \quad CEN = C + A(C)\cdot\left[\frac{Si}{24} + \frac{Mn}{6} + \frac{Cu}{15} + \frac{Ni}{20} + \frac{Cr+Mo+Nb+V}{5} + 5B\right]$$

$$where \quad A(C) = 0.75 + 0.25\tanh[20(C-0.12)].$$

In the above equations, the alloying contents are expressed in weight percentage. In the current study, the CEs of the bainitic steels, given in Table 3.8, were calculated using these equations. It is evident that for a given steel, the CEs could be quite different depending on which equation was used. CE(IIW) values seem to be always the highest and Pcm the lowest.

To prevent cold cracking, preheating is sometimes necessary. Using the methodology developed by Yurioka *et al.*,[217] the preheat temperatures for the bainitic steels was estimated for Tekken testing using the program developed by Dighde.[218] Based on the assumptions that the hydrogen content is 5 ml/100gm and that heat input is 1.7 kJ/mm, the lowest preheat temperature was predicted to be 144 °C for J5. No preheat temperature was obtained for J1 because the program was terminated during execution due to overflow of some intermittent values in calculation. The results obtained with this program are given in Table 3.8 using CEN.

As far as experiments are concerned, Ashton and Johnson[219] reported that for a fully bainitic structure with a hardness level about 420 HV10 (~42 HRC), an excellent weldability was achieved with a minimum of 100 °C preheat temperature. With the composition provided by Ashton and Johnson,[219] the CEN of the steel was calculated to be 0.63.

Based on the above analysis, the susceptibilities of J1 and J2 to cold cracking induced by hydrogen were evaluated using Tekken testing with a preheat temperature of 200°C. After welding, the examination of weldments in cross sections was carried out. No evidence of cold cracking was found in either heat affected zone or in the weld metal for all specimens. The result indicates that even under a water-quenching condition, the high carbon steel J1 still has a good weldability. However, lack of fusion was found at the beginning of the weld and then disappeared in all test specimens. Figure 3.43(a) shows the weldment of the as-received J1 without cracking. Figure 3.43(b) reveals the lack of fusion found in the same steel.

Table 3.1 B_s of the Mo-B Bainitic Steels (°C)

	0.4 °C/s	2 °C/s	10 °C/s	25 °C/s
J1	441	434	436	440
J4	560	551	554	545

Table 3.2 Grain Size of the Mo-B Steels

Steel No.	ASTM No.	Grain Dia. (μm)	Heat Treatment
J2-as	5.2	60	as-received
J4-as	5.3	59	as-received
J5-as	5.5	54	as-received
J4		>90	furnace, 870°C, air cooled
J4		>90	furnace, 900°C, air cooled

Table 3.3 Ac_1 and Ac_3 with Austenitizing Temperatures (°C)

	Ac_1	Ac_3	Austenitizing Temperature
J1	758	896 (823)*	910
J2	677	865 (777)	900
J4	722	865 (816)	900

* *The data in parentheses are calculated values using Andrews' equation.*[213]

Table 3.4 Mechanical Properties of the Bainitic Steels

STEEL No.	UTS		0.2% YS		ELN.	RED. OF AREA	IMPACT TOUGHNESS
	(ksi)	(MPa)	(ksi)	(MPa)	(%)	(%)	(ft-lb)
J1-as	197.2	1359	122.8	847	14.5	39.3	6.5
J2-as	167.0	1151	120.4	830	16.0	55.0	13.0
J3-as	167.5	1155	114.8	792	16.3	58.8	12.3
J4-as	137.0	945	104.6	721	18.0	69.5	12.8
J5-as	130.4	899	93.5	645	18.0	70.3	10.3
J1-wq	237.3	1636	168.1	1159	10.3	33.5	9.3
J2-wq	204.8	1412	155.6	1073	13.3	50.0	8.5
J3-wq	182.4	1258	138.5	955	14.3	59.0	9.5
J4-wq	150.2	1036	122.0	841	14.8	67.3	8.5
J5-wq	150.5	1038	124.5	858	15.3	65.8	12.0

Key:
as – as received
wq – water quenched

Table 3.5 Hardness of the Mo-B Steels

Steel	Heat Treatment	HRC	HB
J1-as	as-received	40	363
J2-as		35	319
J3-as		35	302
J4-as		27	242
J5-as		26	237
J1-ac	air-cooled	44	401
J2-ac		41	363
J3-ac		37	321
J4-ac		28	243
J5-ac		27	241
J1-wq	water-quenched	43	415
J2-wq		40	375
J3-wq		40	363
J4-wq		29	271
J5-wq		34	288

Table 3.6 Wear Rates of Steels at Various Contact Pressures with a Slide/Roll Ratio of 35% (μg/m/mm)

Steel	Contact Pressure (MPa)									
	500		900		1220		1450		1700	
	Top	Bottom	Top	Bottom	Top	Bottom	Top	Bottom	Top	Bottom
J1-as	1555	337	6735	1271	13489	2857	18173	4344	20313	6091
J2-as	2794	309	10943	1034	17807	2445	20641	3056	21018	4341
J3-as	4691	420			15790	2037			16843	3827
J4-as	3254	205	8593	452	11608	1133	10140	1033	9786	1818
J5-as	3858	118			17449	828			12614	591
J1-ac					8172	2348				
J2-ac					11925	2680				
J3-ac					13611	2156				
J4-ac					10759	1161				
J5-ac					13816	750				
J1-wq	346	167			2374	1697			4429	5227
J2-wq					6454	2167				
J3-wq					9418	2159				
J4-wq	2274	257			8334	894			7112	257
J5-wq					9524	894				
X136	928	27			6439	2940			8149	7545
Mn steel					126	82			156	247

as — as received
ac — air cooled
wq — water quenched

Table 3.7 Wear Rates (μg/m) and Statistical Analysis for Reproducibility Evaluation of the Amsler Machine under Rolling/Sliding Conditions

Test	1220 MPa		900 MPa	
	Rail (top)	Wheel (bottom)	Rail (top)	Wheel (bottom)
1	116100	12200	69600	7100
2	162200	13300	63600	6900
3	140700	13800	61700	6100
4	153900	13100	66000	7100
5	137600	12400	65600	7100
6	141000	12600	66000	6900
7	136400	14000		
α	0.05	0.05	0.05	0.05
n	7	7	6	6
$\bar{x}$	141128.57	13057.14	65416.67	6866.67
s	14540.48	692.48	2658.13	388.16
$t_{\alpha/2,n-1}$	2.4469	2.4469	2.5706	2.5706
$t_{\alpha/2,n-1}(s/\sqrt{n})$	13447.64	640.43	3055.81	446.23
RE	9.5%	4.9%	4.7%	6.5%

$100(1-\alpha)\%$: confidence
n: number of tests
s: sample standard deviation
$\bar{x}$: average value
$t_{\alpha/2,n-1}$: upper $100(\alpha/2)$ percentile point of the *t* distribution
RE: relative error

$$RE = \frac{t_{\alpha/2,n-1}\frac{s}{\sqrt{n}}}{\bar{x}}$$

Table 3.8 Carbon Equivalents and Preheat Temperatures (T_{ph}) Prediction of the Bainitic Steels

	J1	J2	J3	J4	J5
CE(IIW)	1.001	0.876	1.033	0.975	0.798
Pcm	0.462	0.369	0.365	0.310	0.285
CEN	1.026	0.684	0.625	0.506	0.434
T_{ph}, °C	-	275	247	212	144

(a) J1

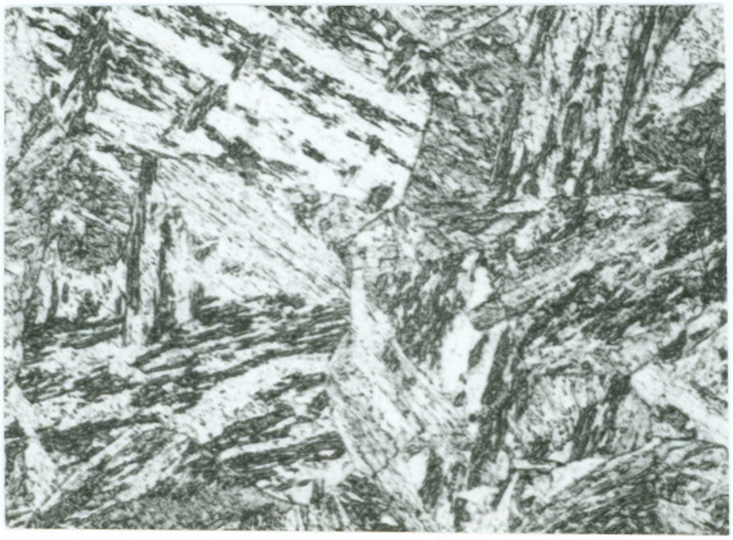

(b) J2

Figure 3.1 Optical micrographs of the as-received Mo-B steels

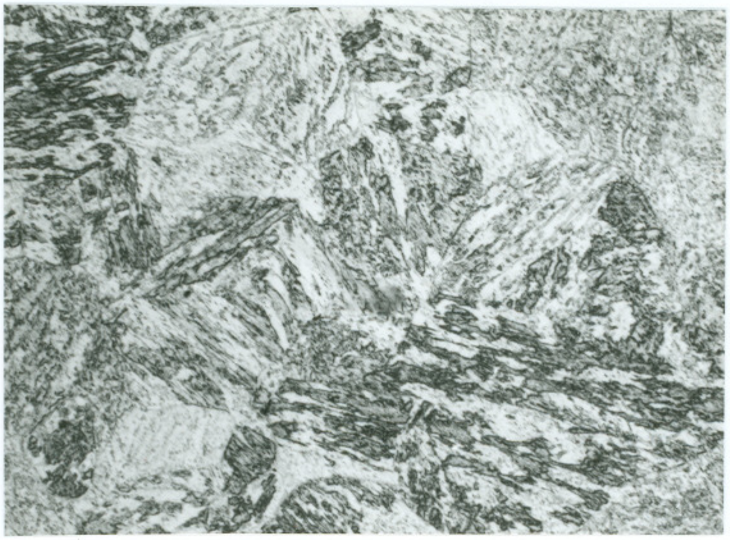

(c) J3 25 μm

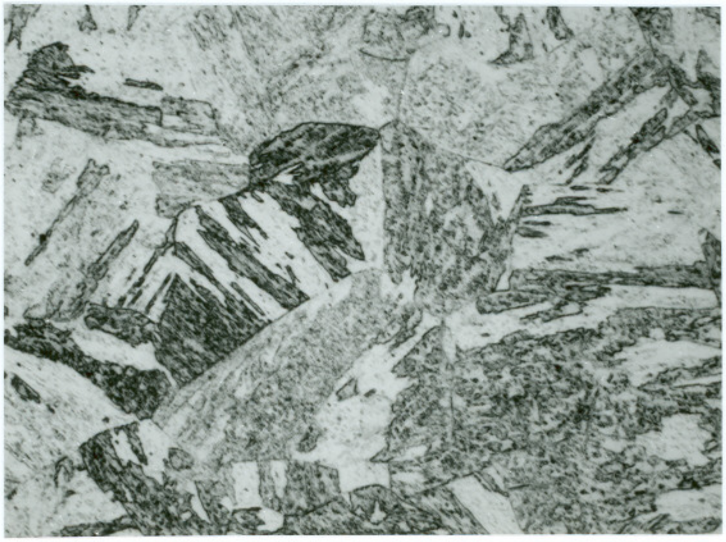

(d) J4 25 μm

Figure 3.1 Optical micrographs of the as-received Mo-B steels (continued)

(e) J5

Figure 3.1 Optical micrographs of the as-received Mo-B steels (continued)

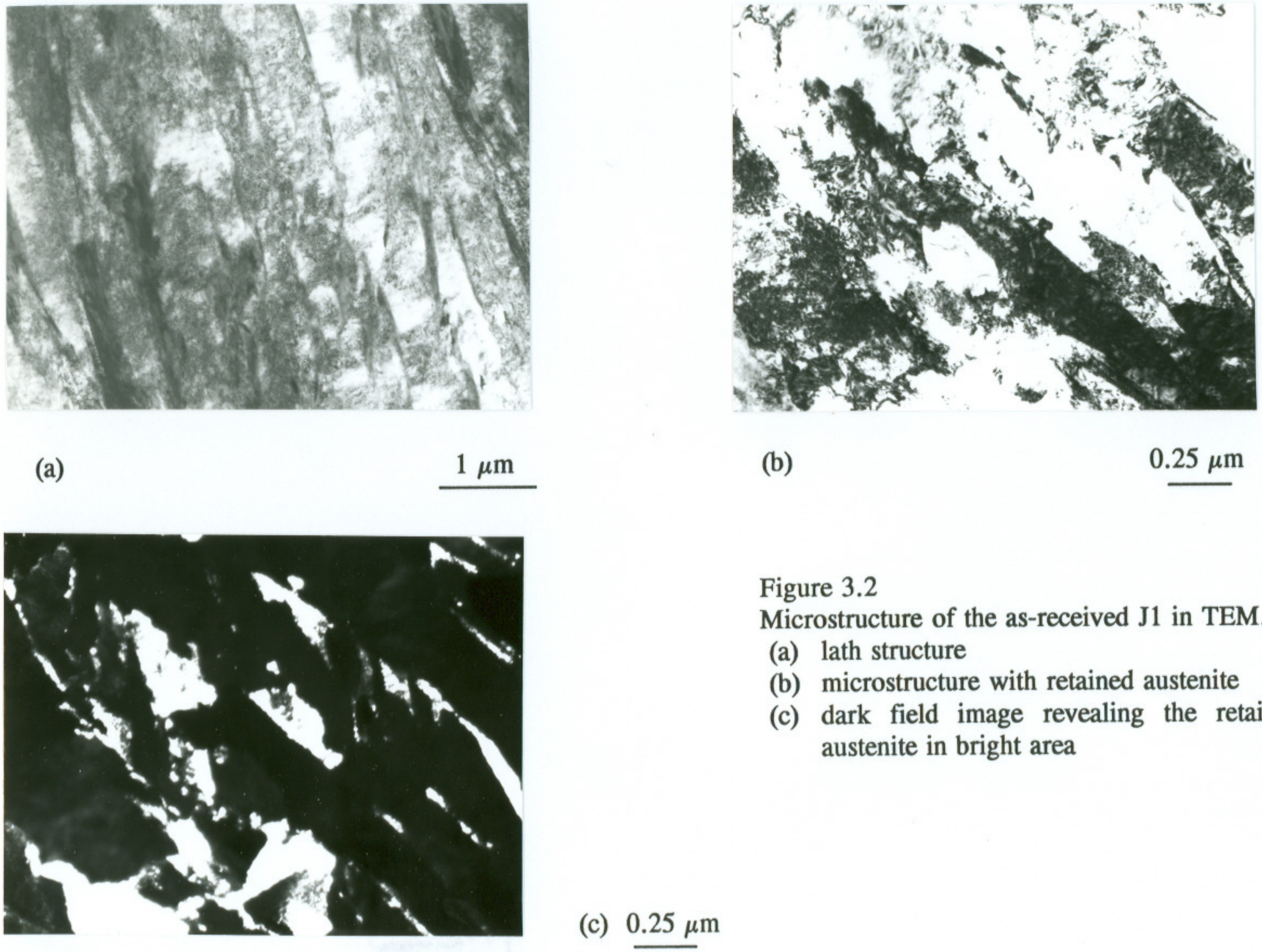

Figure 3.2
Microstructure of the as-received J1 in TEM.
(a) lath structure
(b) microstructure with retained austenite
(c) dark field image revealing the retained austenite in bright area

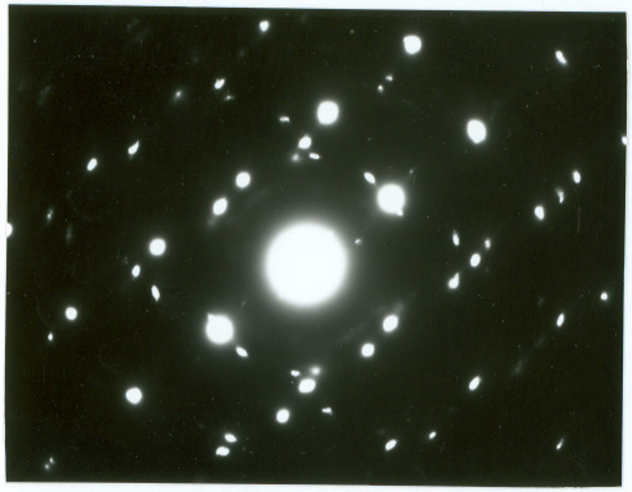

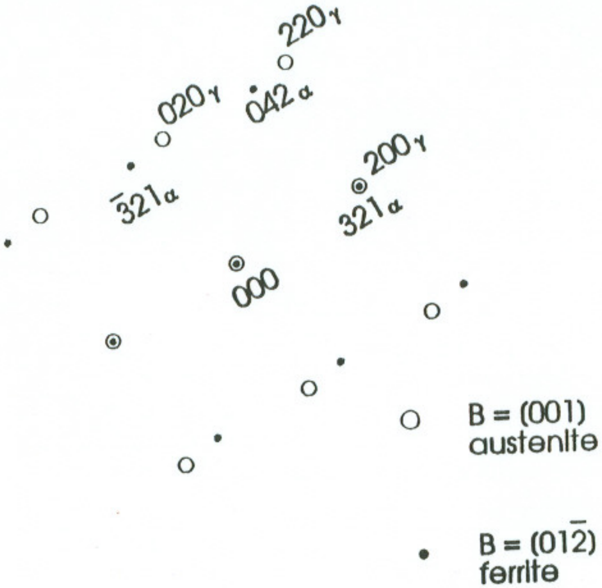

(d)

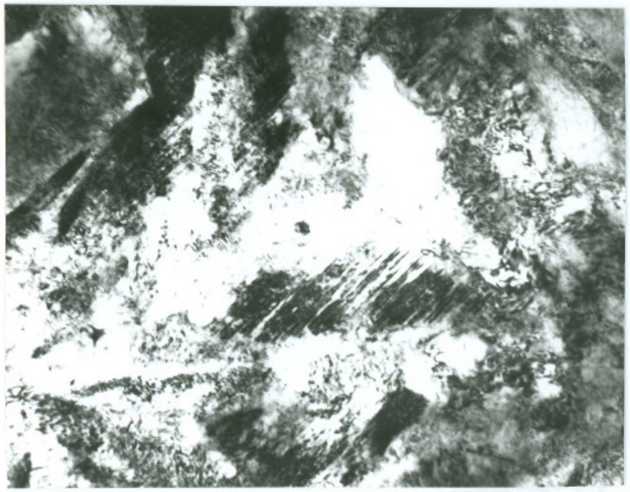

(e) 0.20 μm

Figure 3.2
Microstructure of the as-received J1 in TEM.
(d) diffraction pattern
(e) M-A island

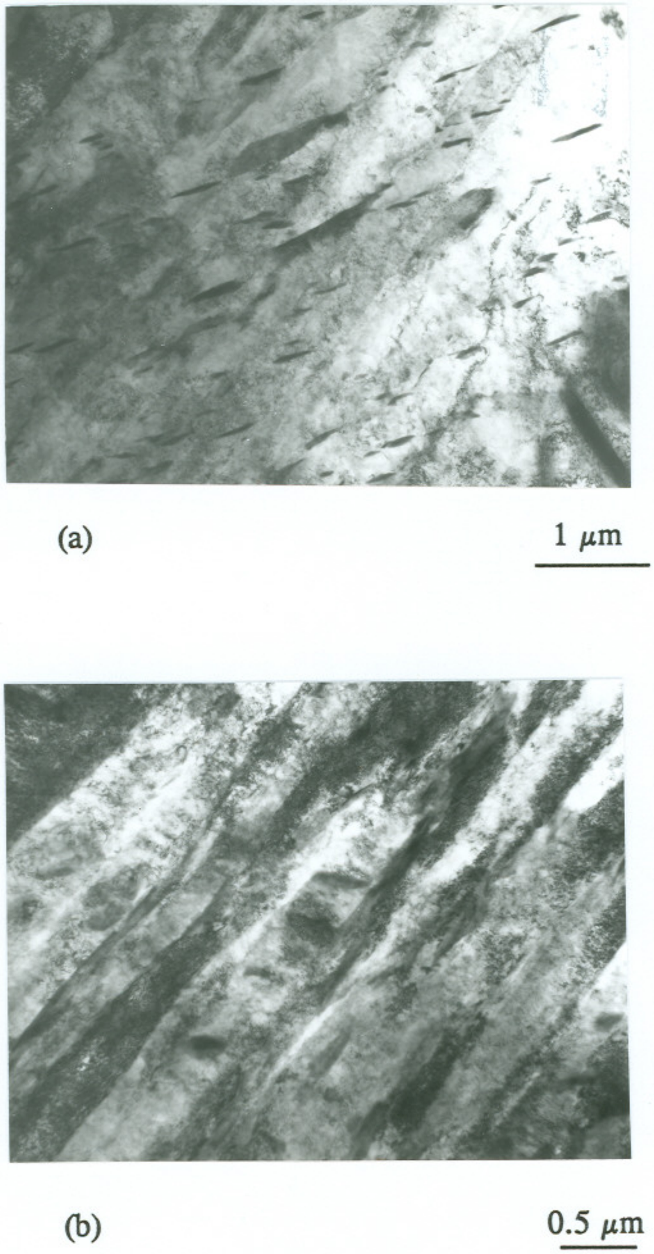

Figure 3.3 Microstructure of the as-received J2 in TEM
(a) microstructure of carbide precipitates lying at an angle to laths, exhibiting a morphology of lower bainite
(b) lath structures without carbides

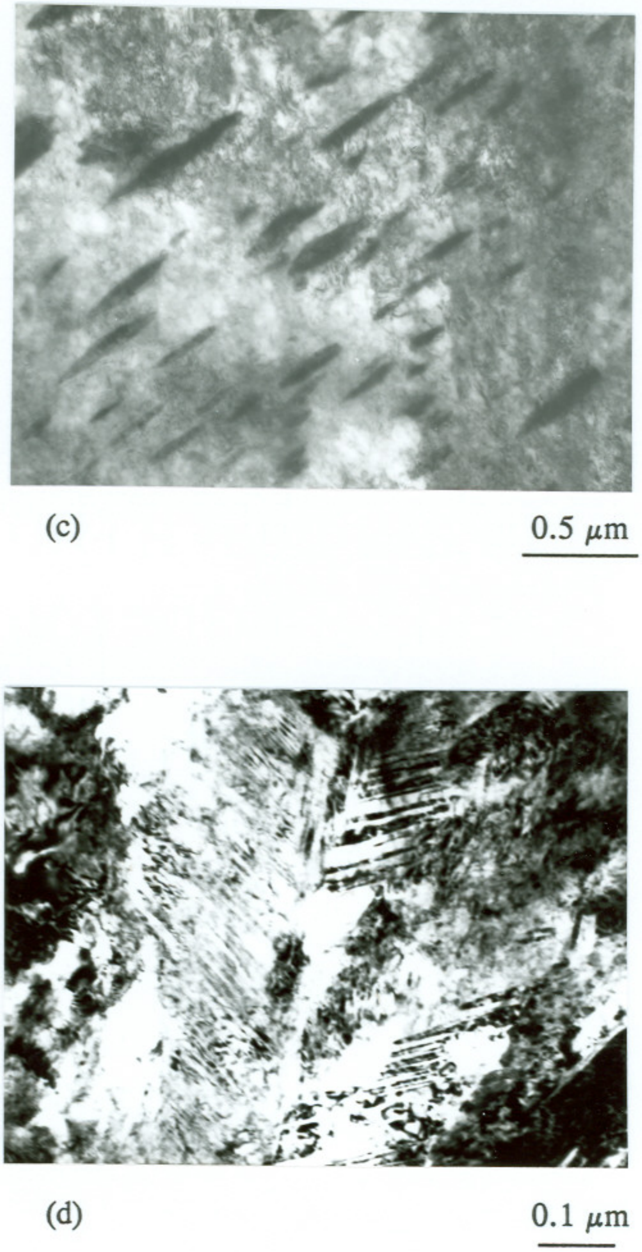

Figure 3.3 Microstructure of the as-received J2 in TEM
(c) carbide precipitates in massive ferrite
(d) twinned structure in the steel

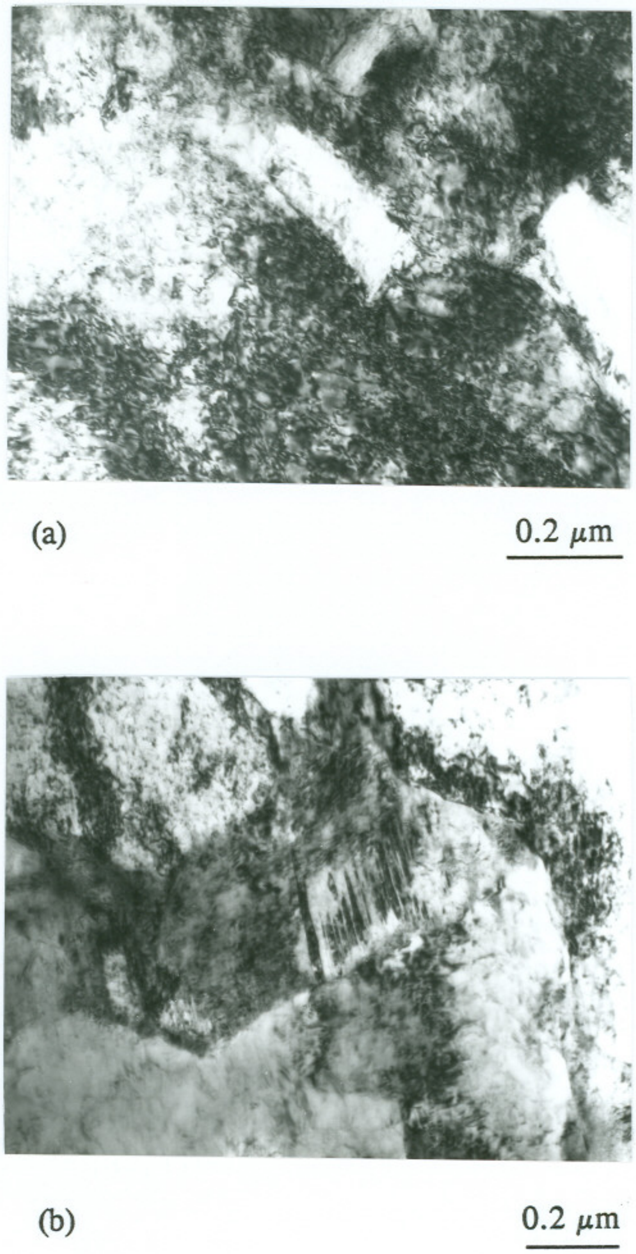

Figure 3.4 Microstructure of the as-received J3 in TEM
(a) massive ferrite
(b) a M-A constituent

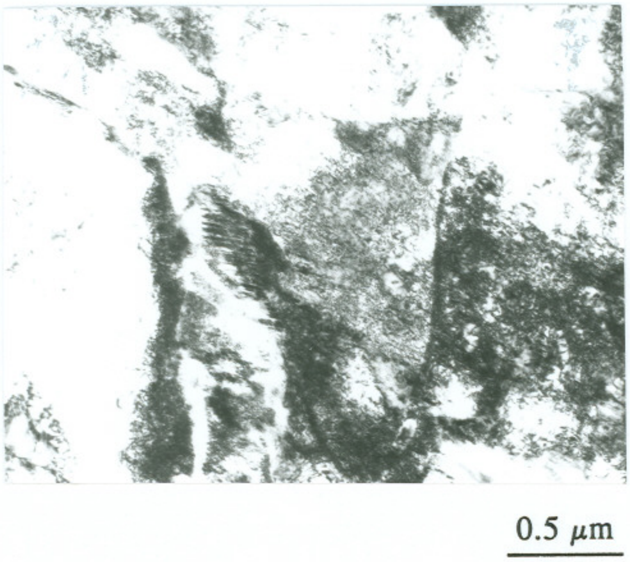

Figure 3.5 Microstructure of the as-received J4 in TEM massive ferrite with twinned martensite

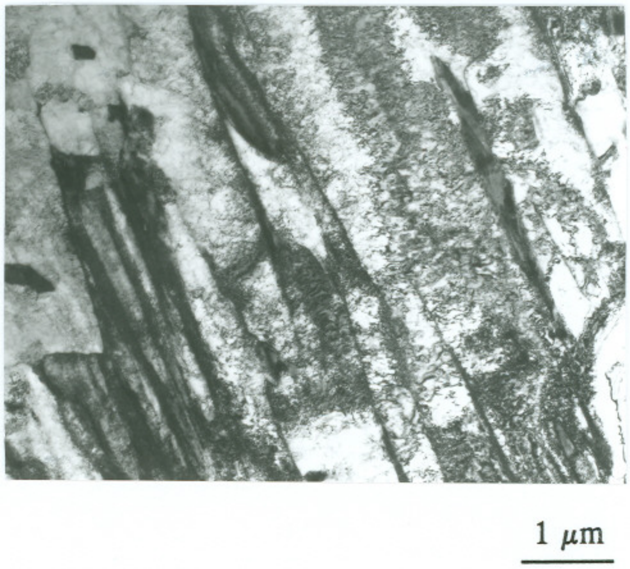

Figure 3.6 Microstructure of the as-received J5 in TEM

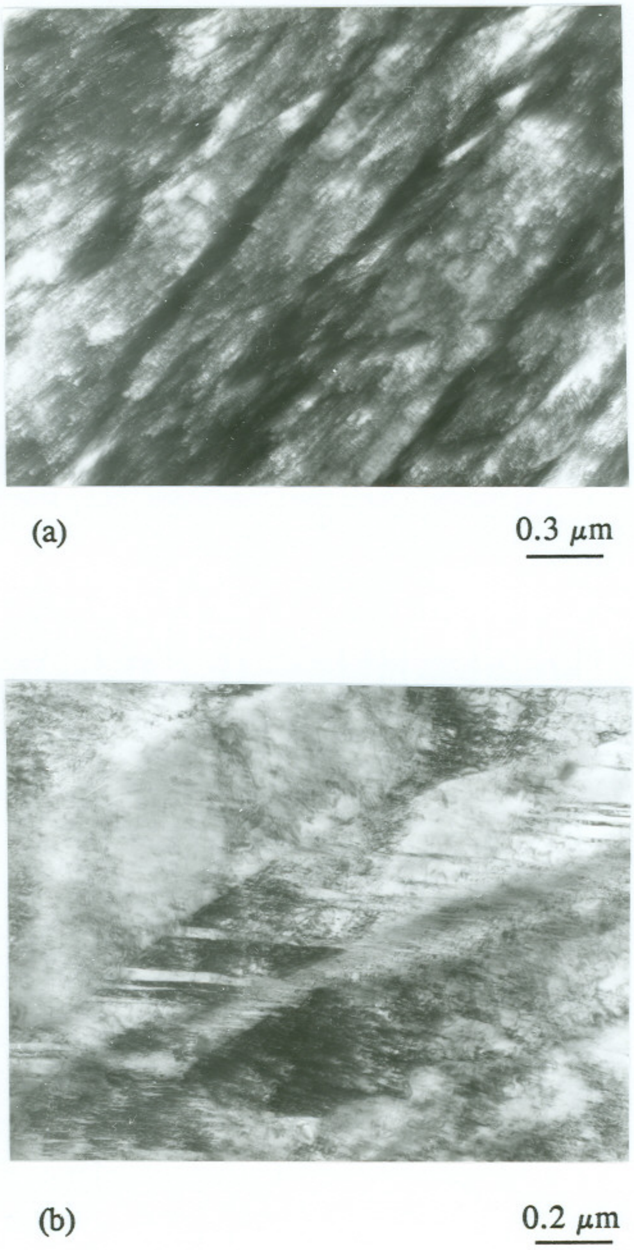

Figure 3.7 Microstructure of the air-cooled J1 in TEM
(a) lath ferrite and retained austenite
(b) needle shaped martensite

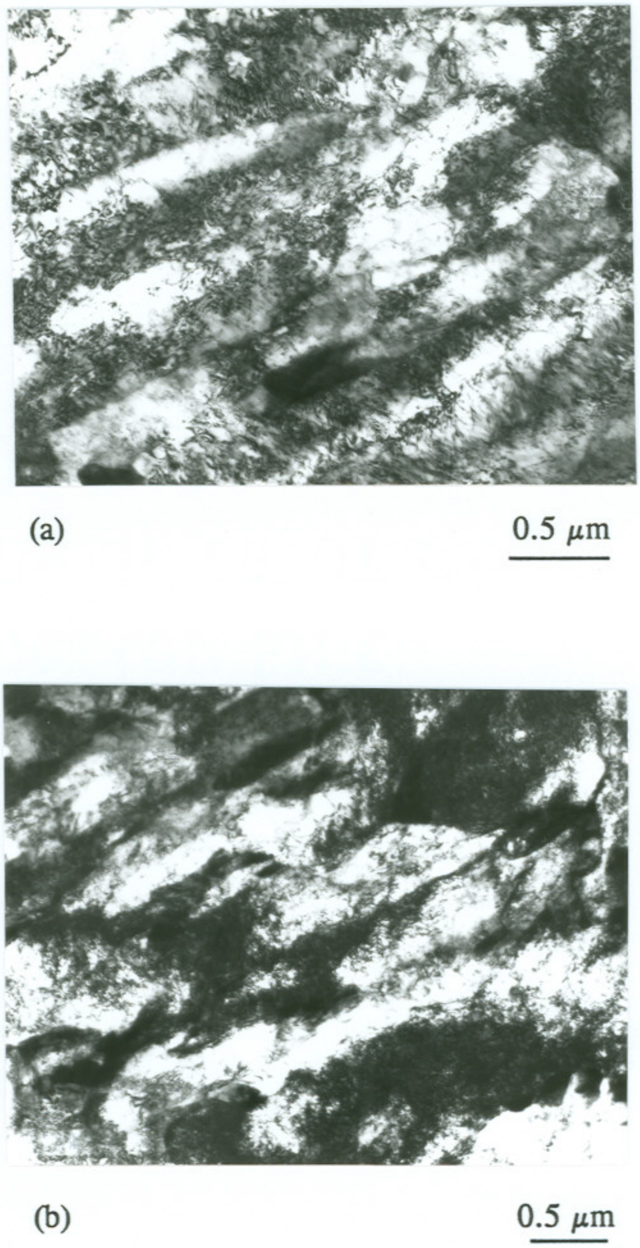

Figure 3.8 Microstructure of the air-cooled J4 in TEM
(a) lath structure (b) cell structure

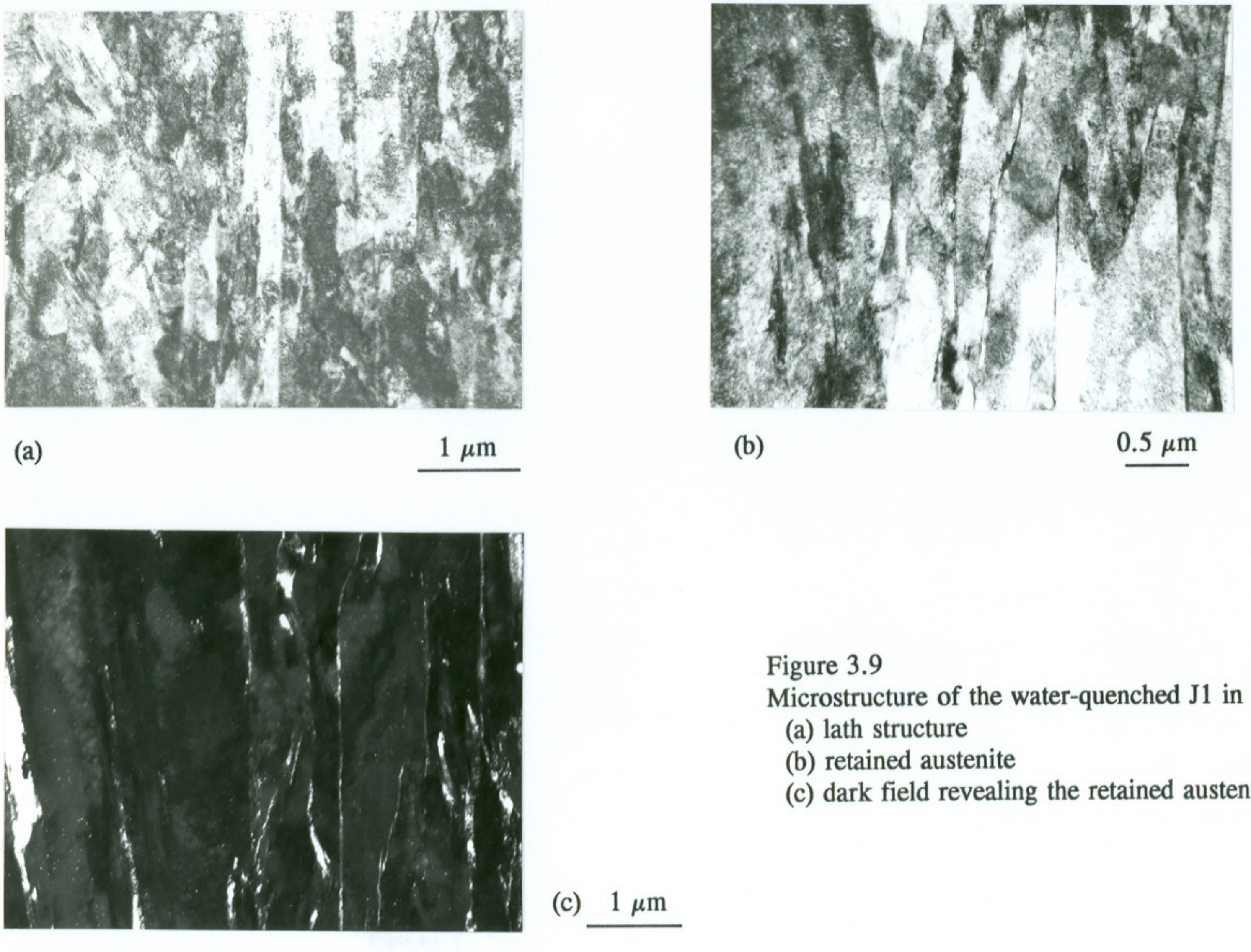

Figure 3.9
Microstructure of the water-quenched J1 in TEM
(a) lath structure
(b) retained austenite
(c) dark field revealing the retained austenite

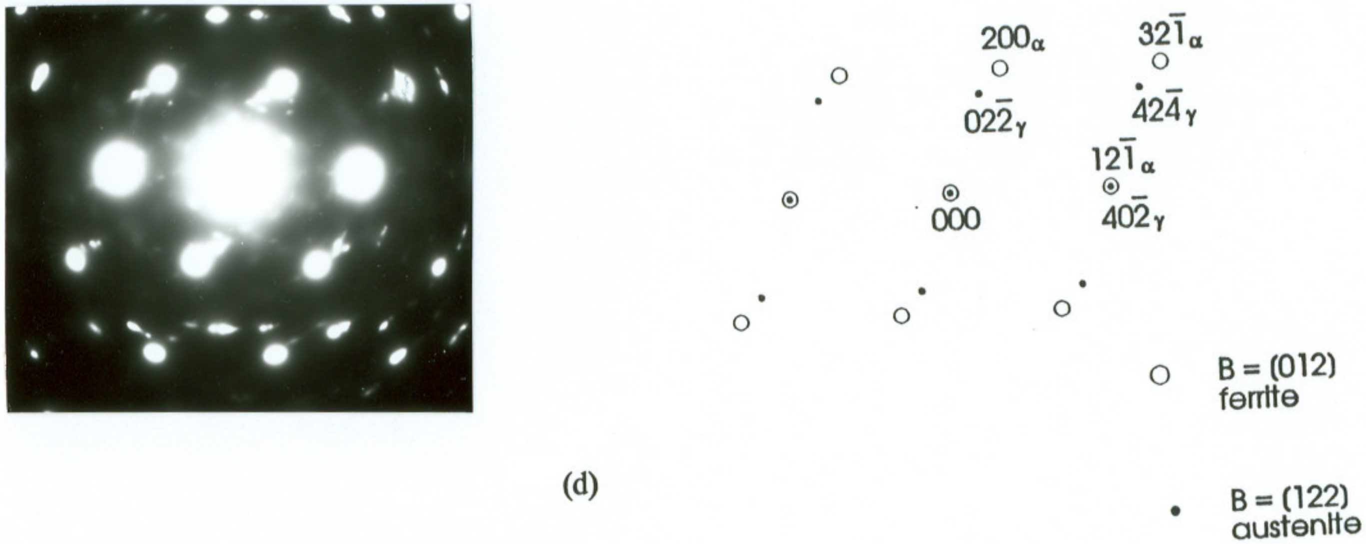

(d)

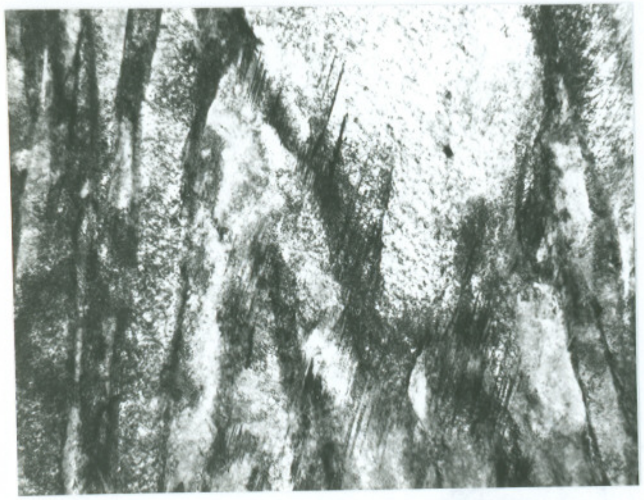

(e) 0.5 μm

Figure 3.9
Microstructure of the water-quenched J1 in TEM
(d) diffraction pattern corresponding to (c)
(e) needle shaped martensite

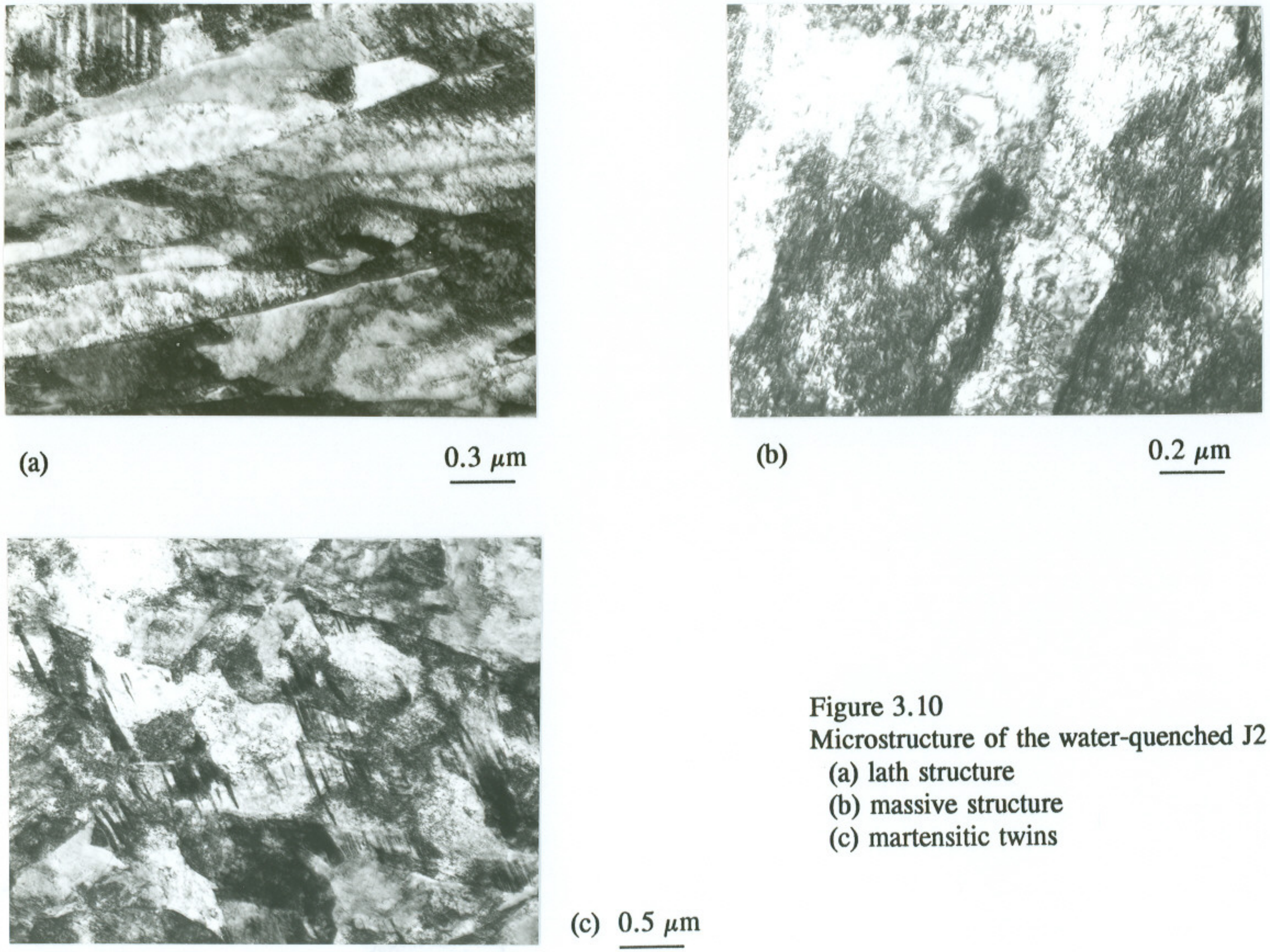

Figure 3.10
Microstructure of the water-quenched J2 in TEM
(a) lath structure
(b) massive structure
(c) martensitic twins

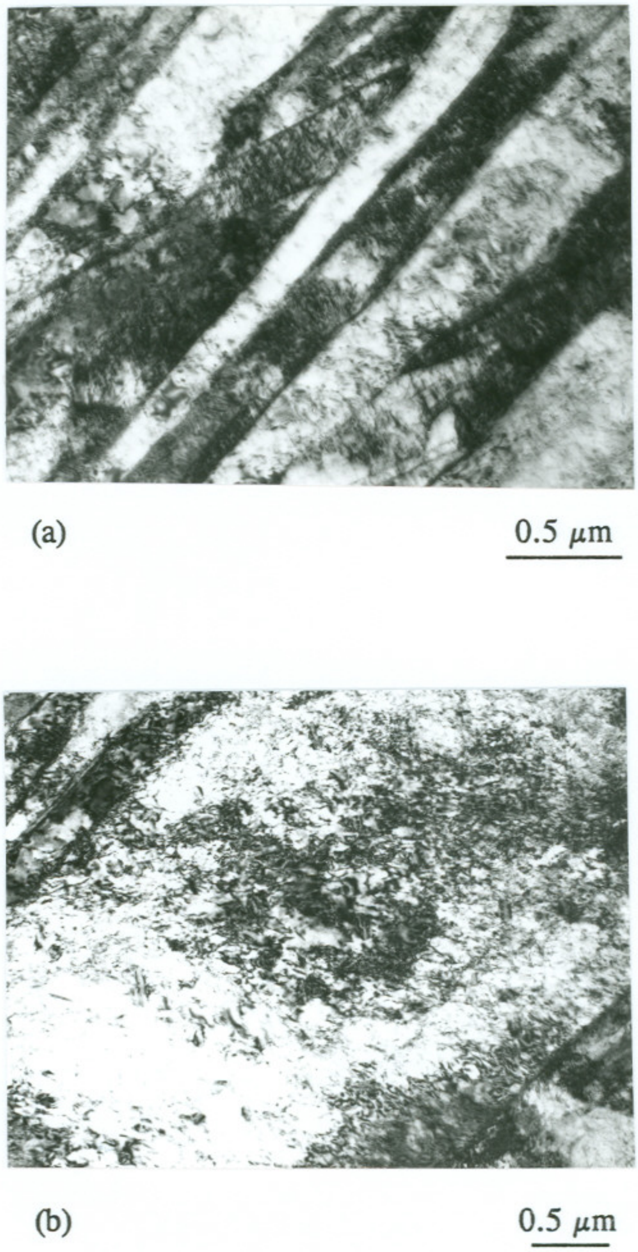

Figure 3.11 Microstructure of the water-quenched J3 in TEM
(a) lath structure (b) massive structure

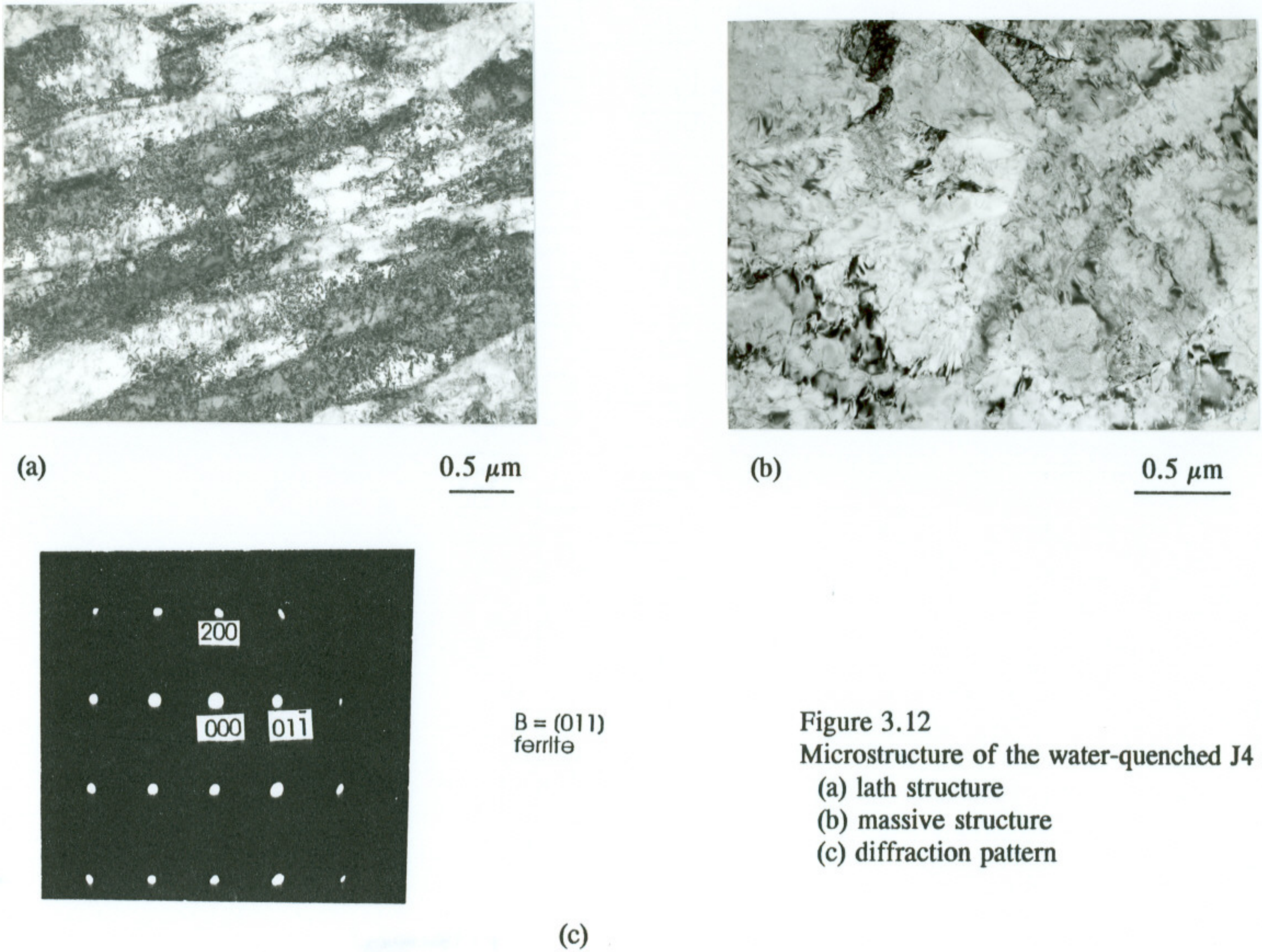

Figure 3.12
Microstructure of the water-quenched J4 in TEM
(a) lath structure
(b) massive structure
(c) diffraction pattern

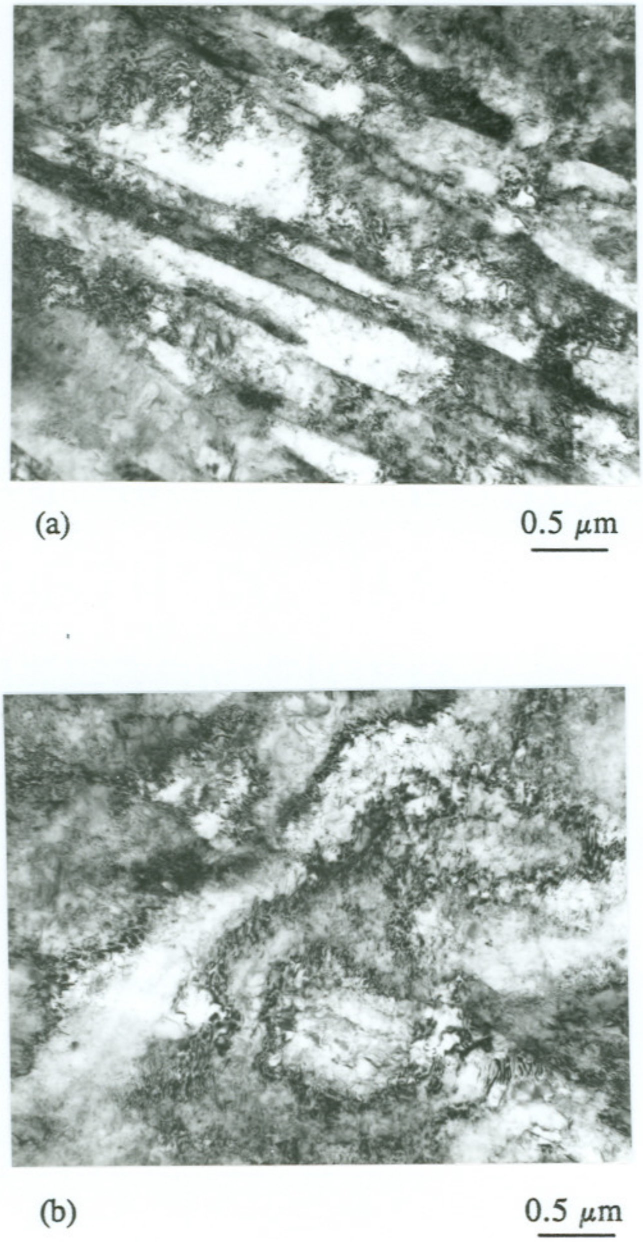

Figure 3.13 Microstructure of the water-quenched J5 in TEM
(a) lath structure (b) massive structure

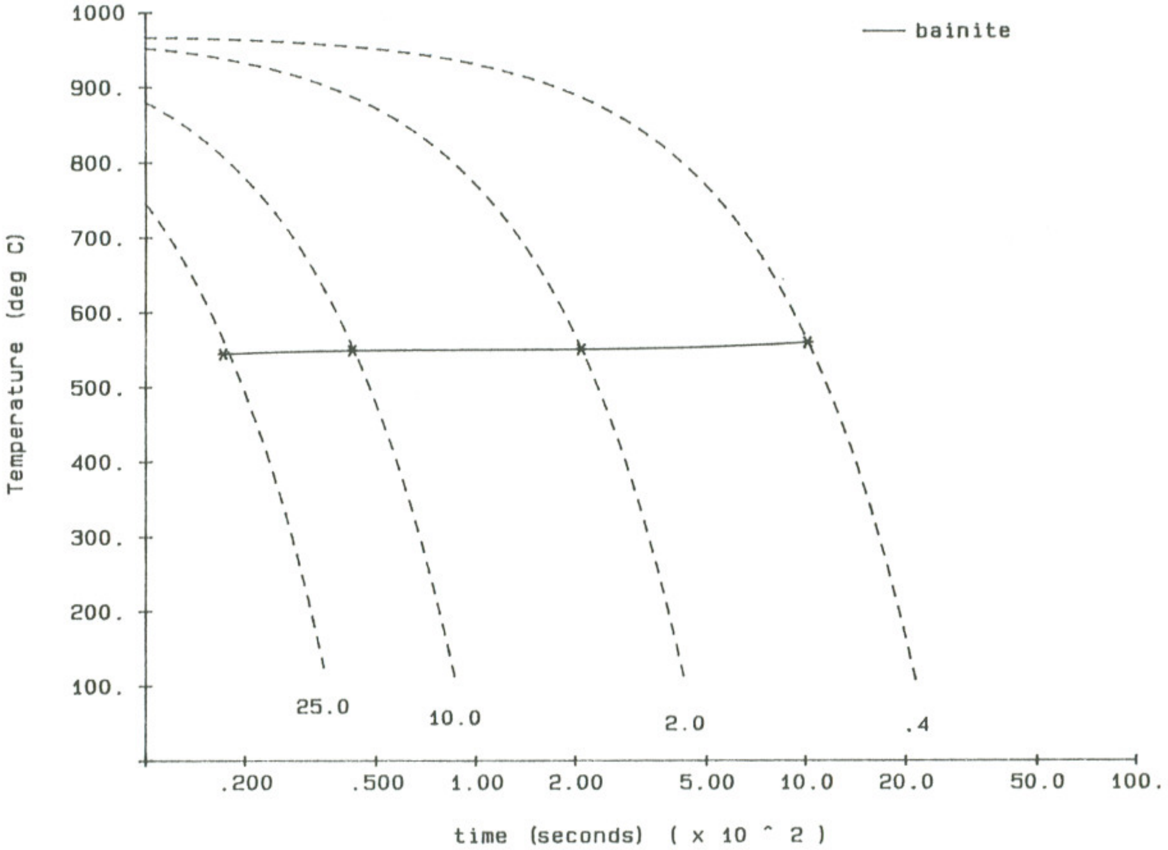

Figure 3.14 CCT curve for J1

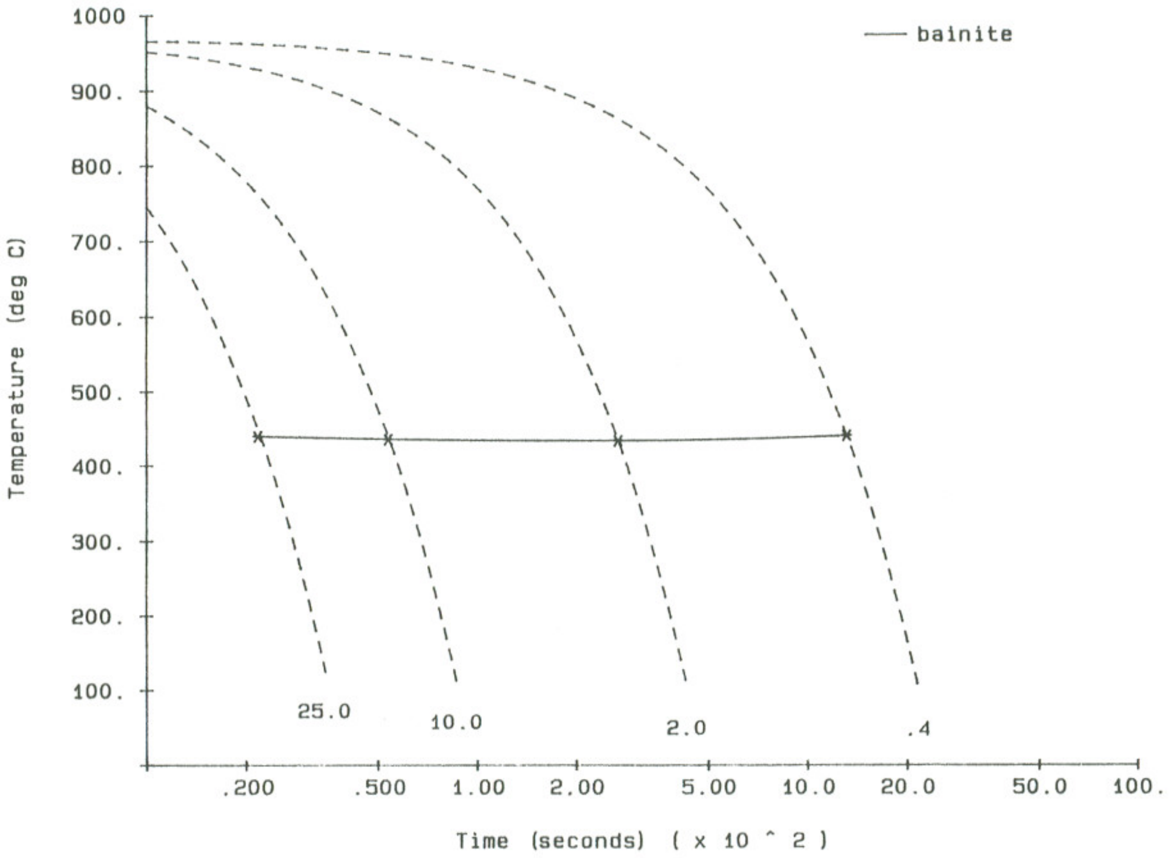

Figure 3.15 CCT curve for J4

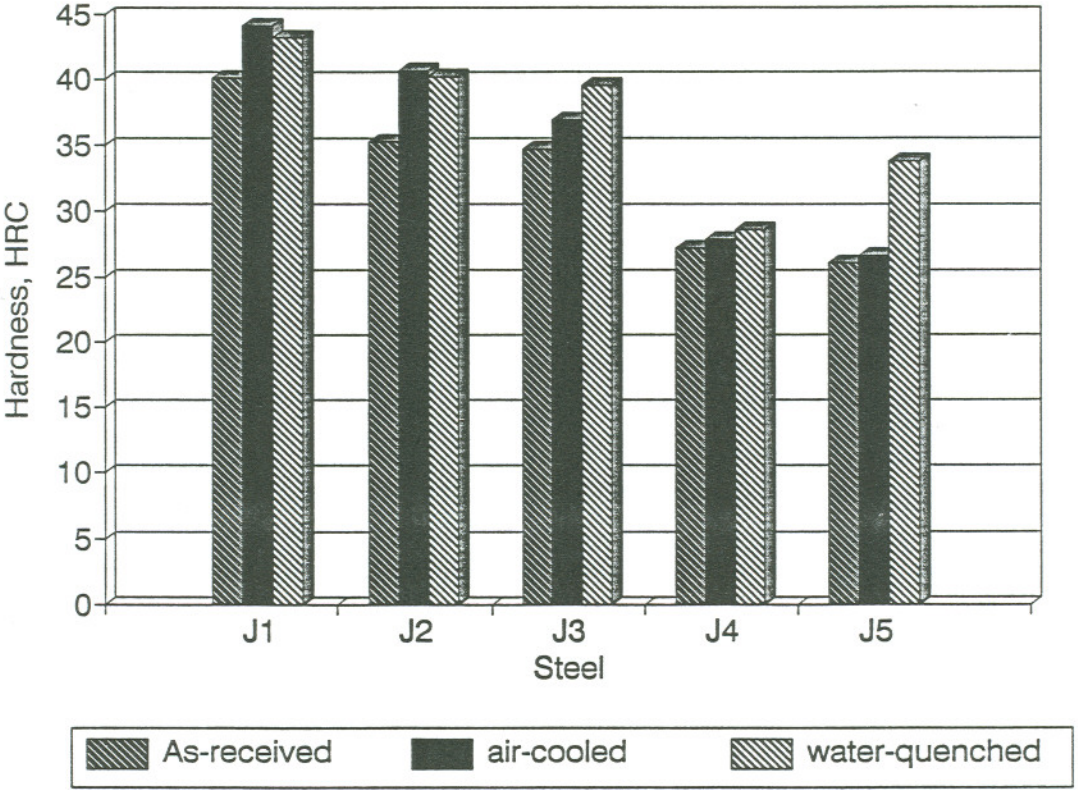

Figure 3.16 Hardness of the Mo-B bainitic steels

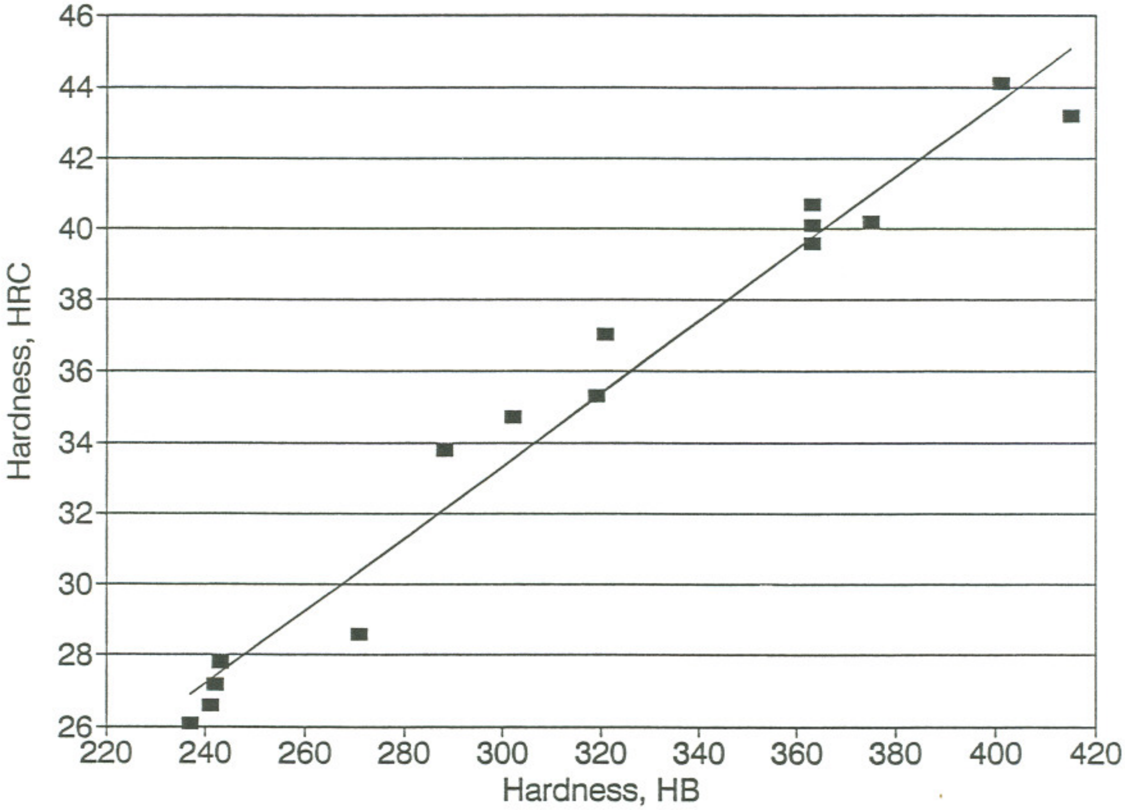

Figure 3.17 Relationship of hardness between the Rockwell C and the Brinell scales

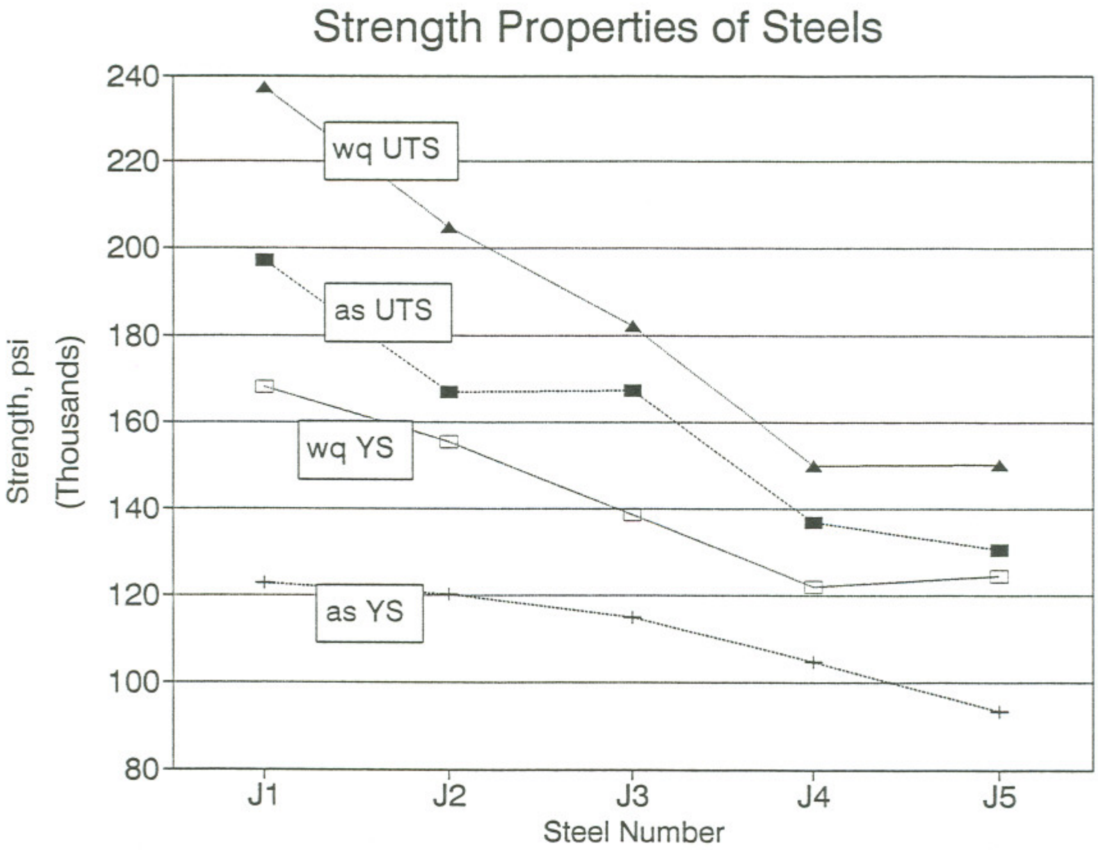

Figure 3.18 Strength of the bainitic steels

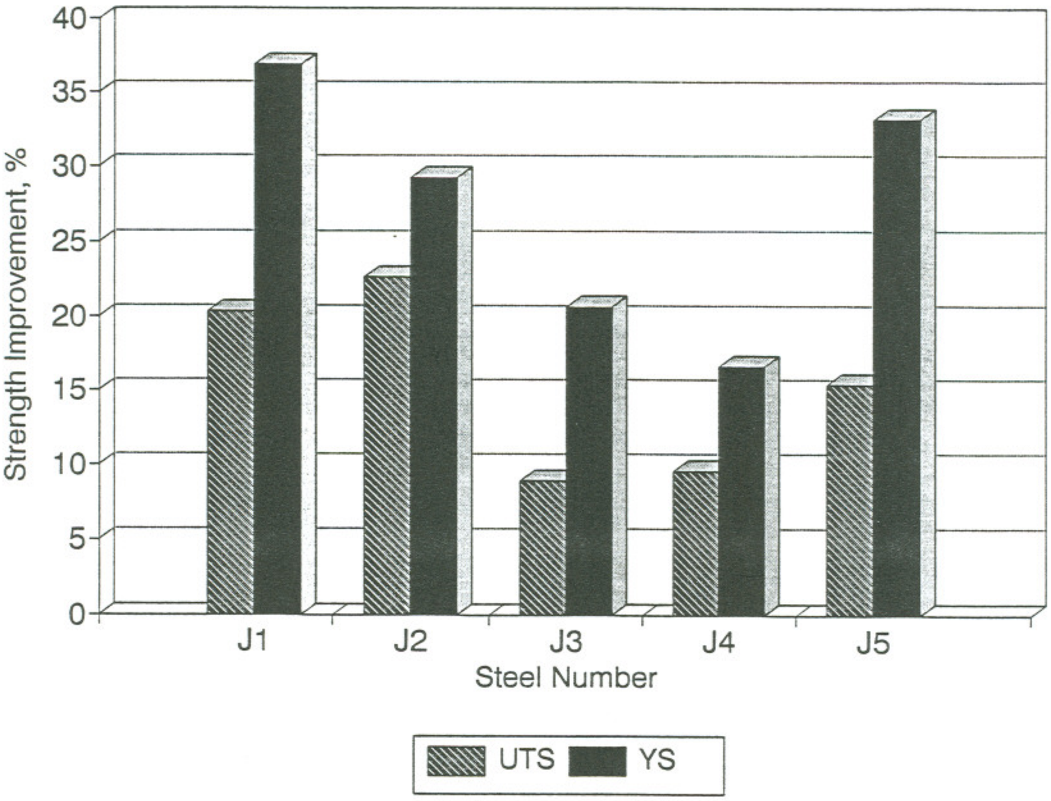

Figure 3.19 The improvement of strength by water quenching

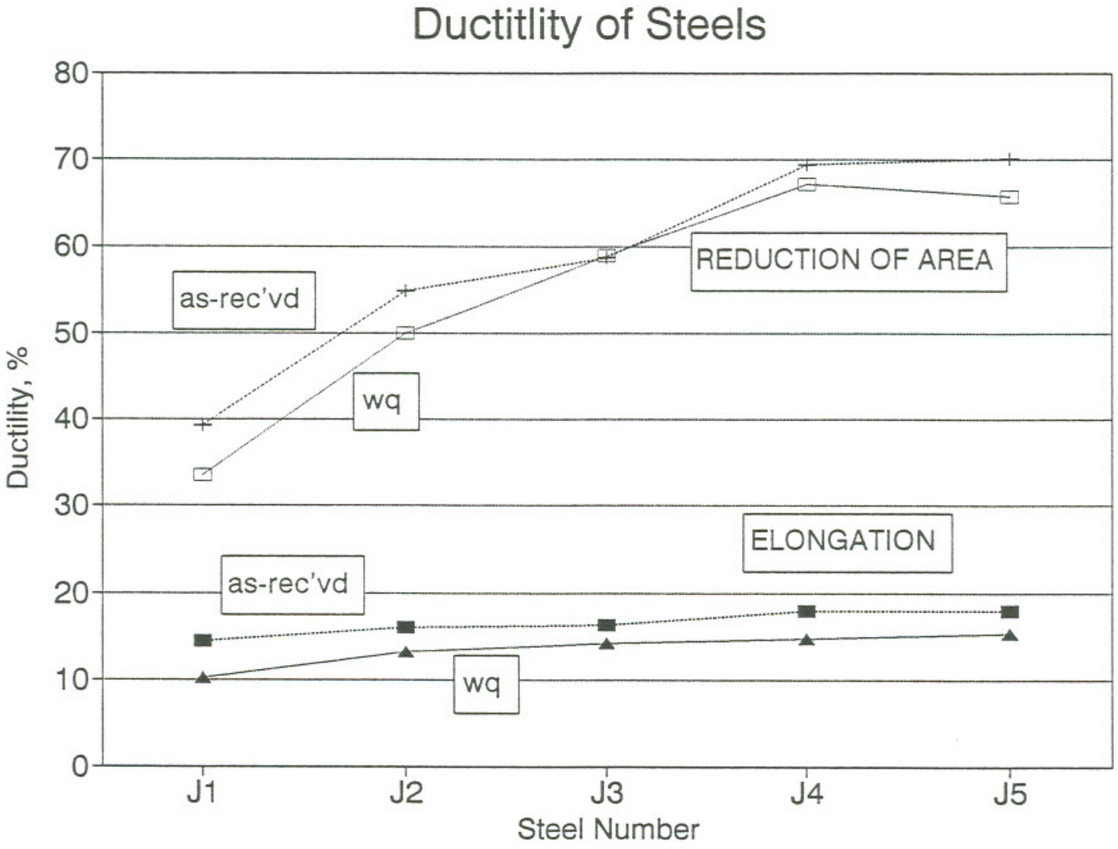

Figure 3.20 Ductility of the bainitic steels

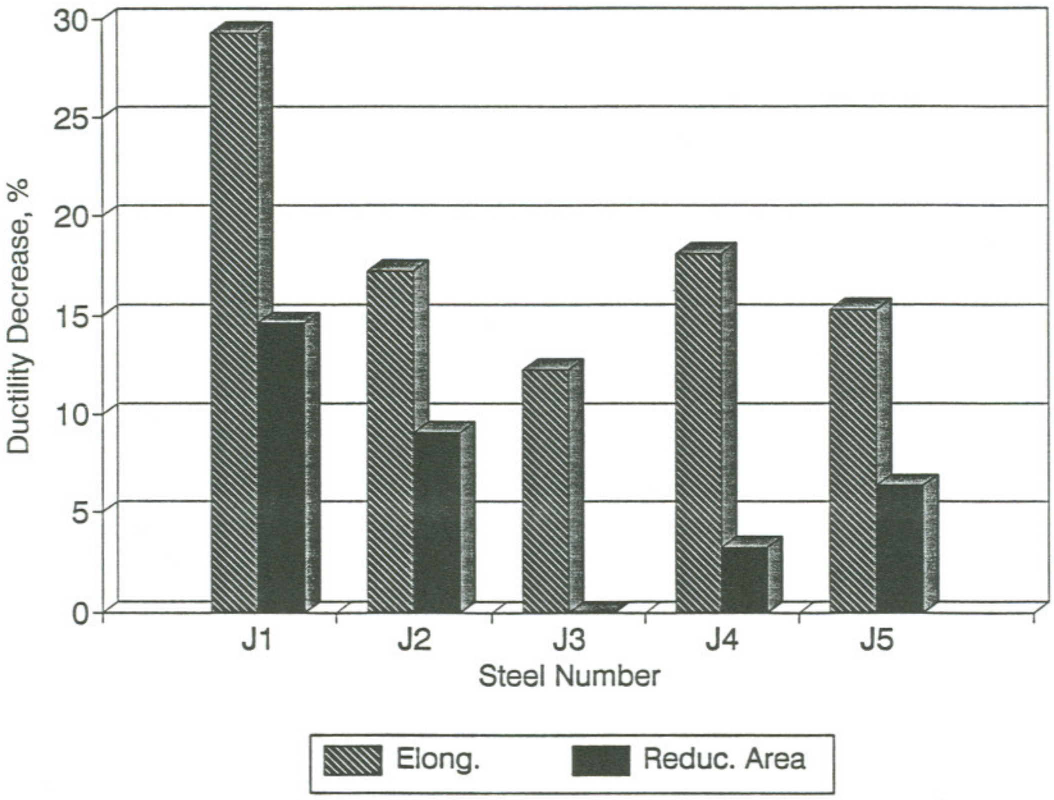

Figure 3.21 The deterioration of ductility by water quenching

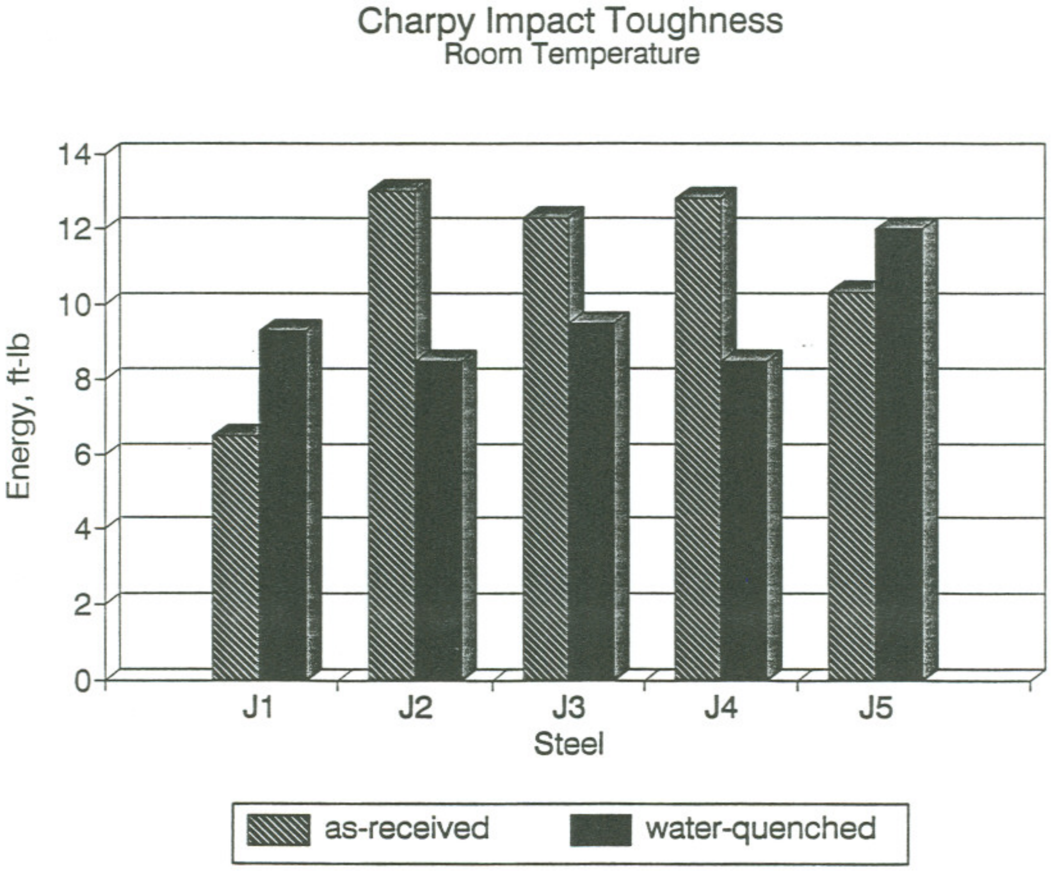

Figure 3.22 Charpy impact toughness of the bainitic steels

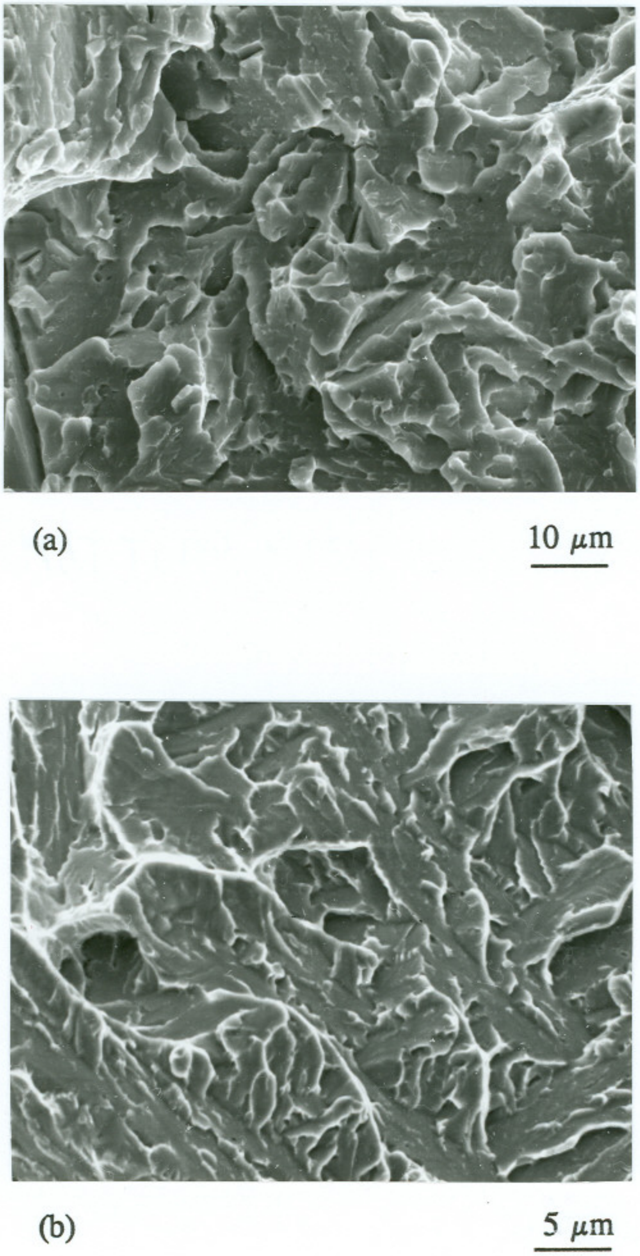

Figure 3.23 Fracture surfaces of the impact specimens
(a) J1-as (b) J2-as

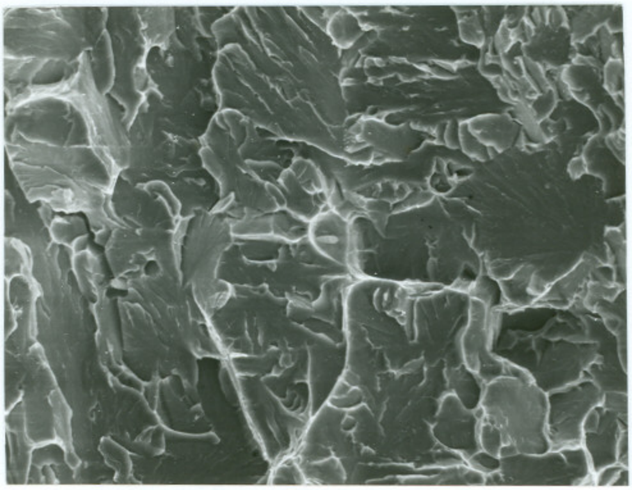

(c) 20 μm

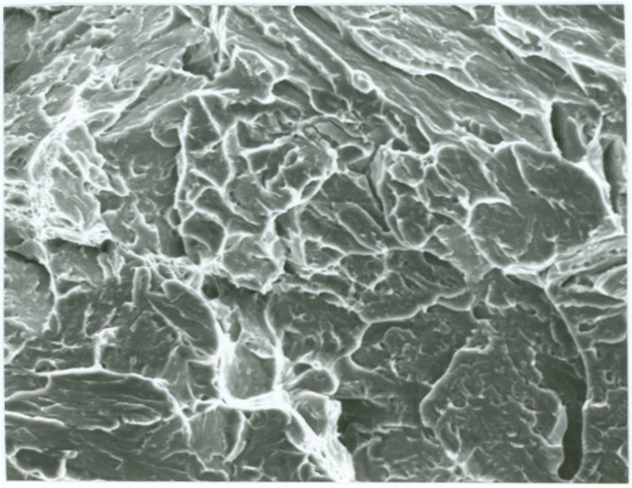

(b) 10 μm

Figure 3.23 Fracture surfaces of the impact specimens
(c) J4-as (d) J1-wq

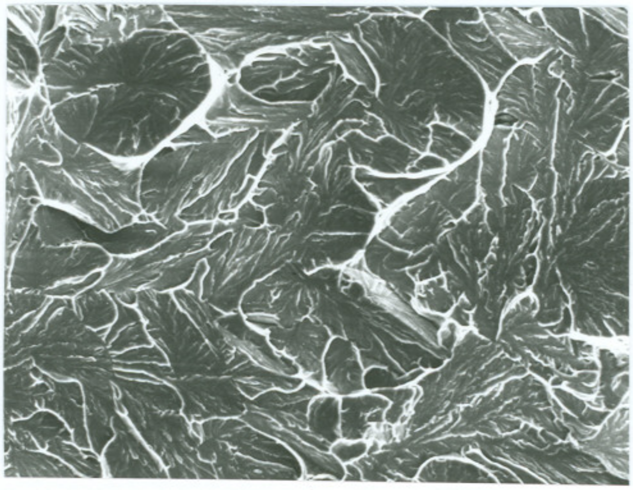

(c) 20 μm

Figure 3.23 Fracture surfaces of the impact specimens
(e) J4-wq

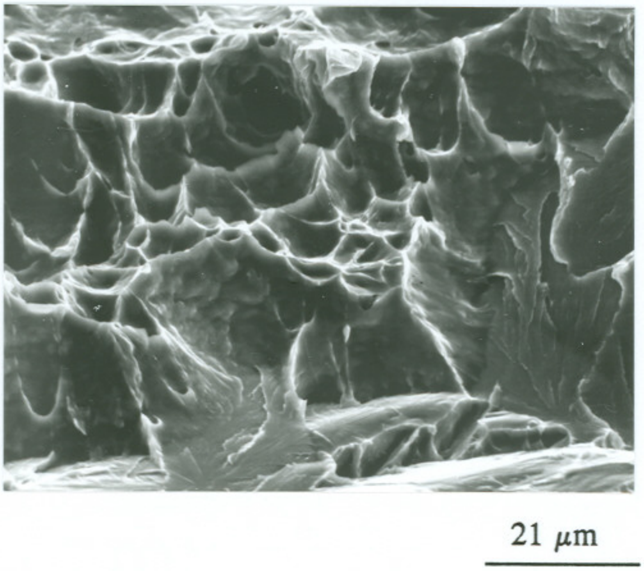

Figure 3.24 Dimples on the fracture surface

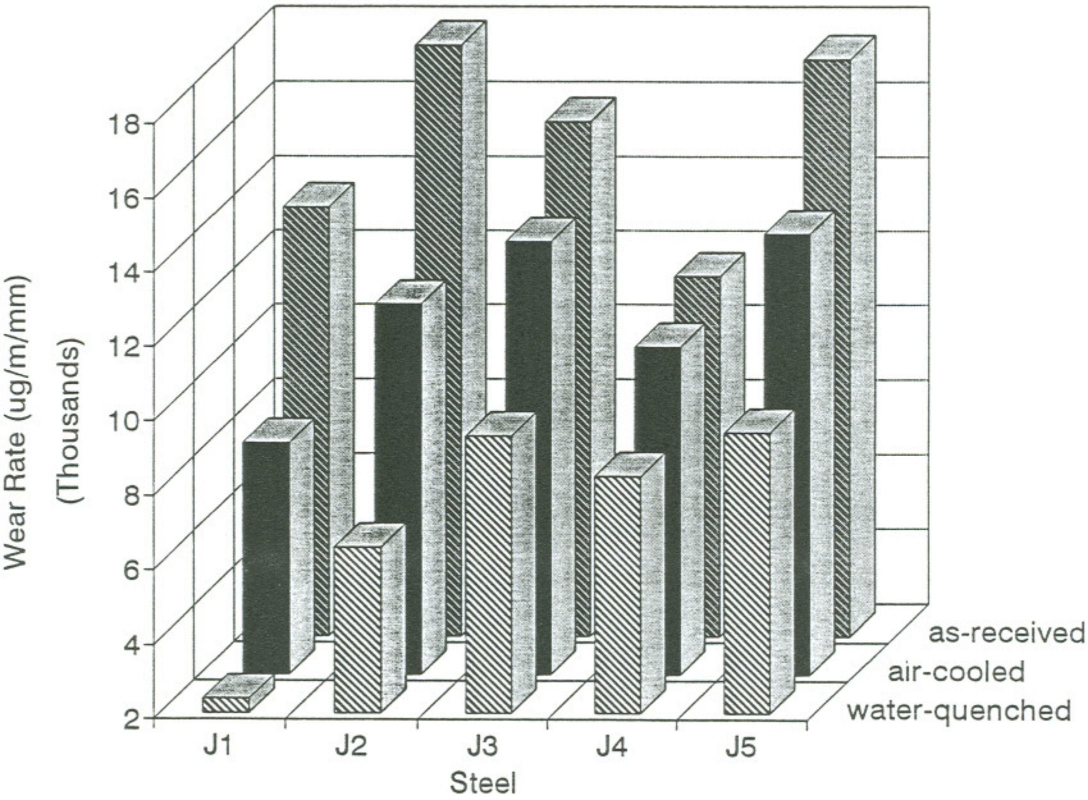

Figure 3.25 Wear rate of the as-received bainitic steels at 1220 MPa

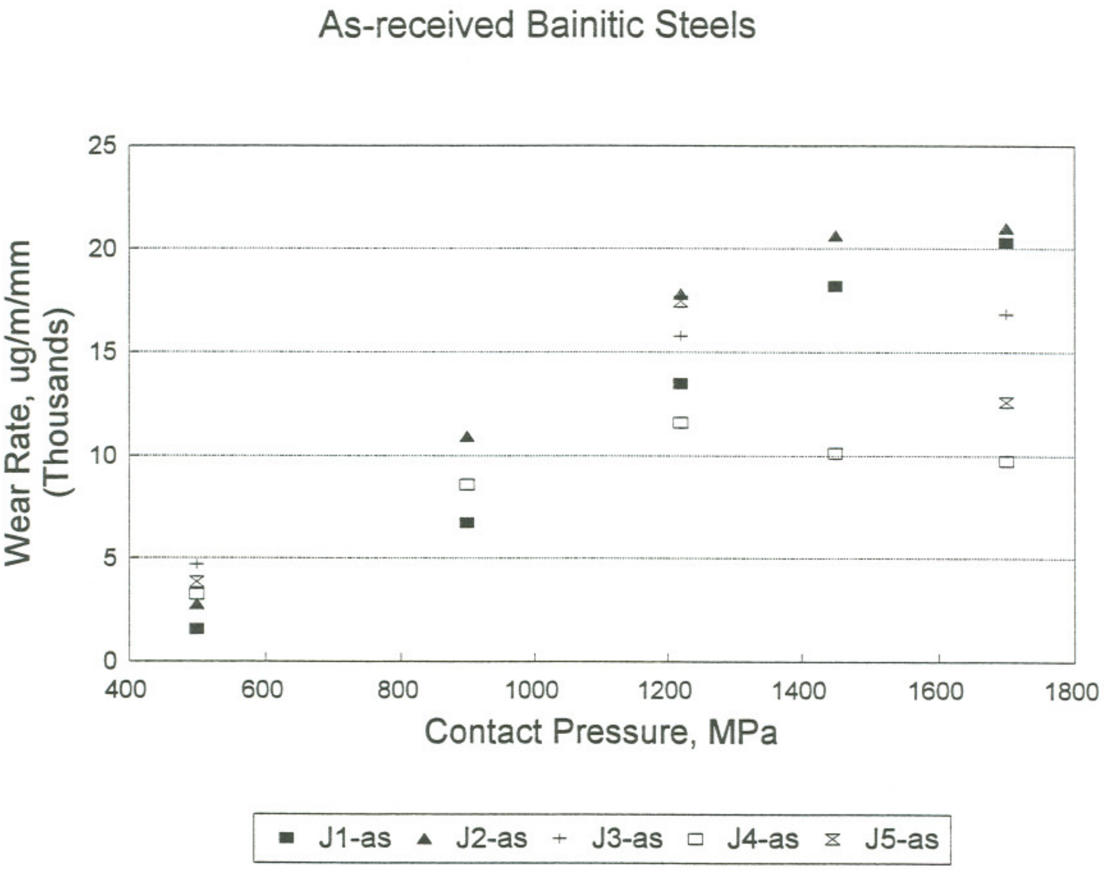

Figure 3.26 Variation of wear rate with contact pressure

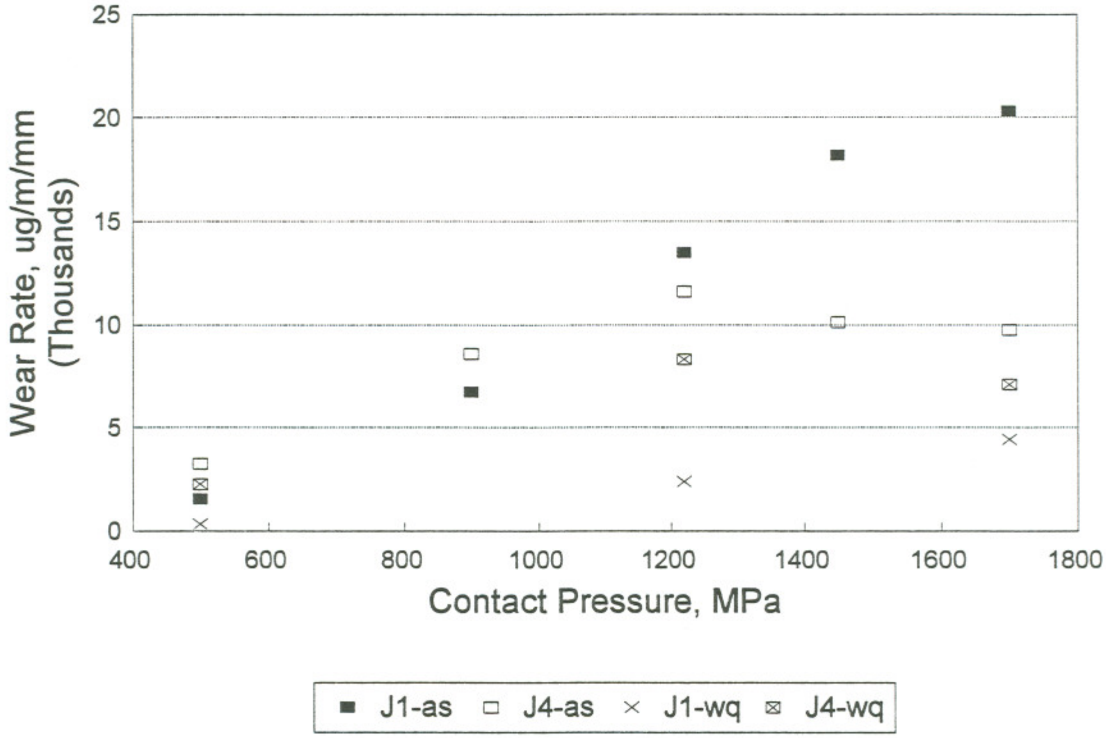

Figure 3.27 Effect of water-quenching on wear rate

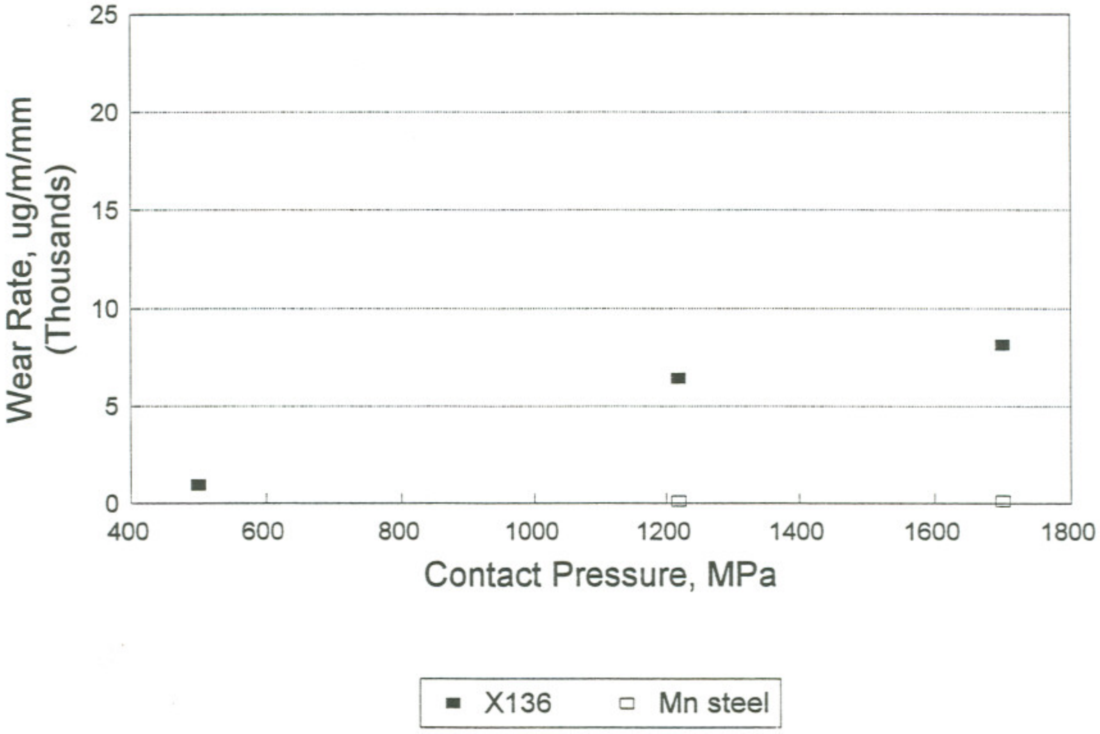

Figure 3.28 Wear behavior of X136 and austenitic Mn steels

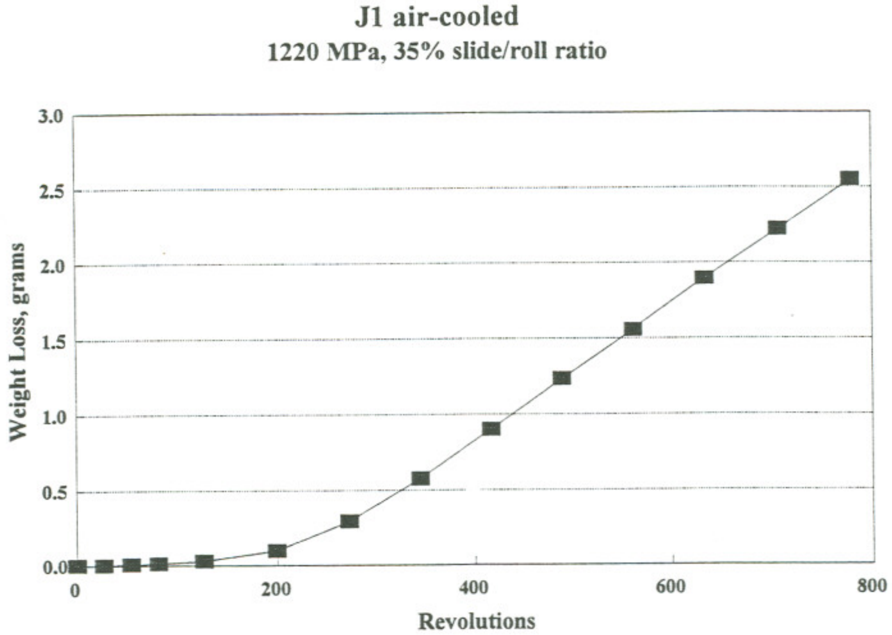
J1 air-cooled
1220 MPa, 35% slide/roll ratio

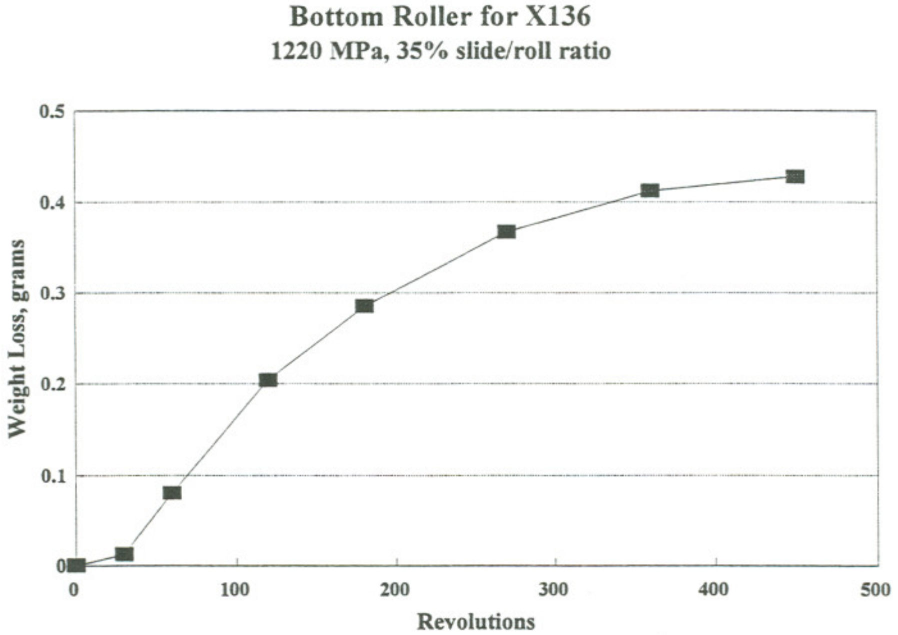
Bottom Roller for X136
1220 MPa, 35% slide/roll ratio

Figure 3.29 Weight loss vs. revolutions during wear test
(a) a linear relationship for a top roller
and non-linear relationship for a bottom roller

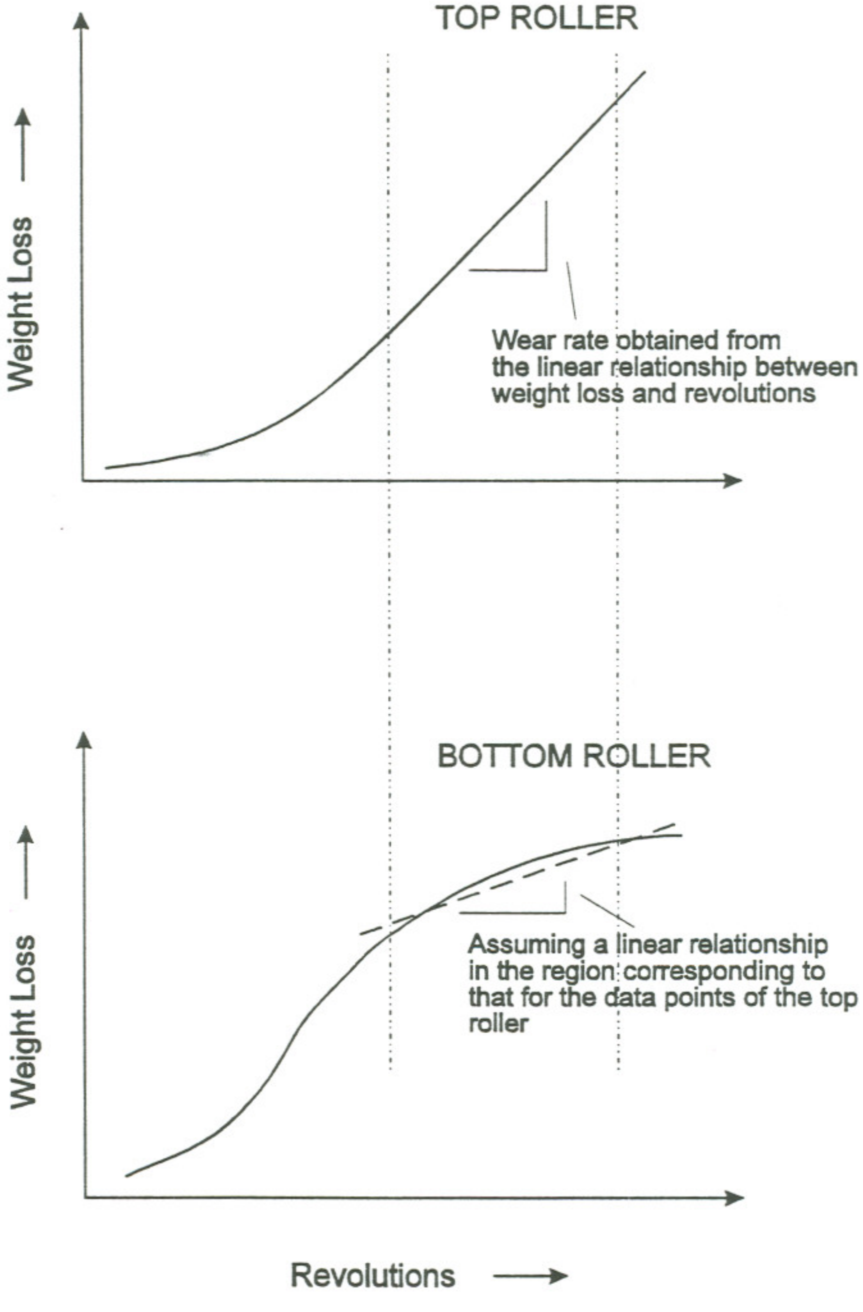

Figure 3.29 Weight loss vs. revolutions during wear test (b) an illustration as to how a wear rate is obtained from a non-linear wear curve for a bottom roller

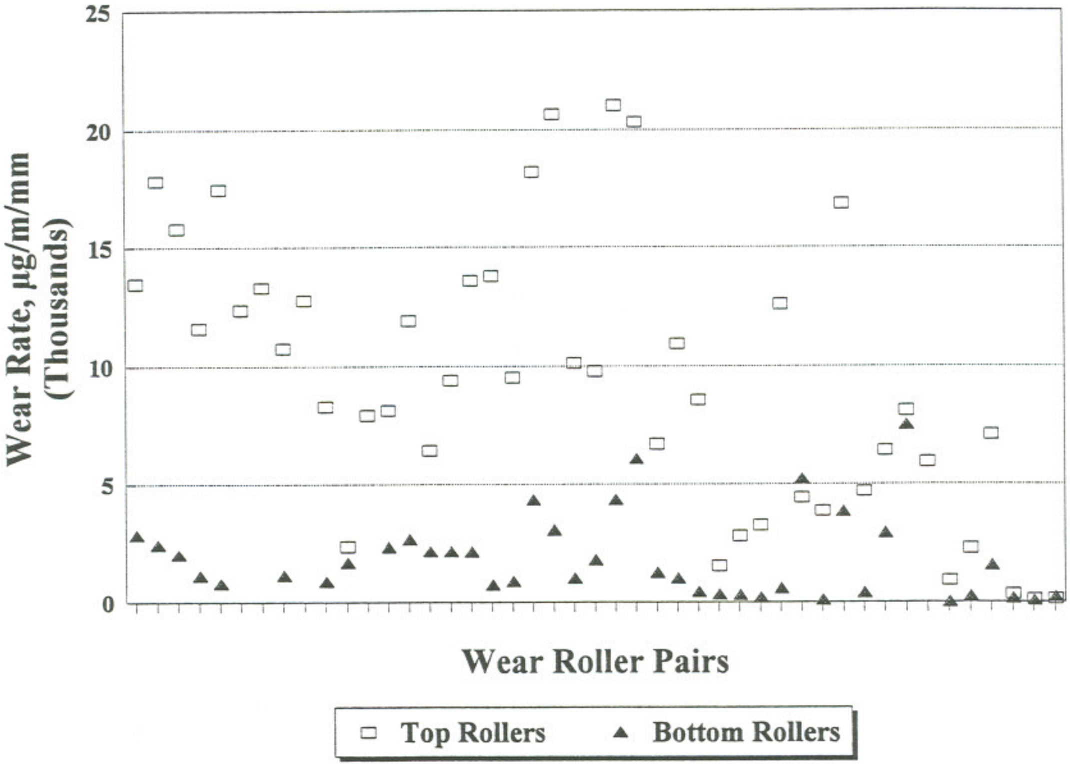

Figure 3.30 Wear behavior of both top and bottom rollers

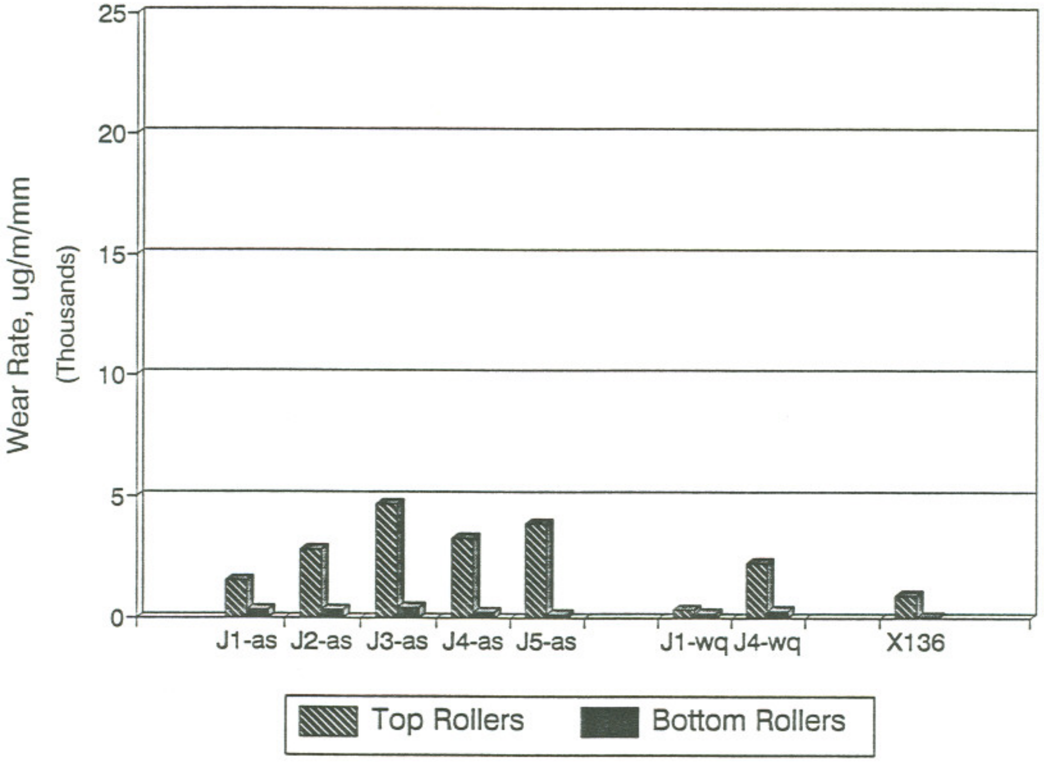

Figure 3.31 Comparison of wear rates between the top and bottom rollers at various pressures
(a) 500 MPa

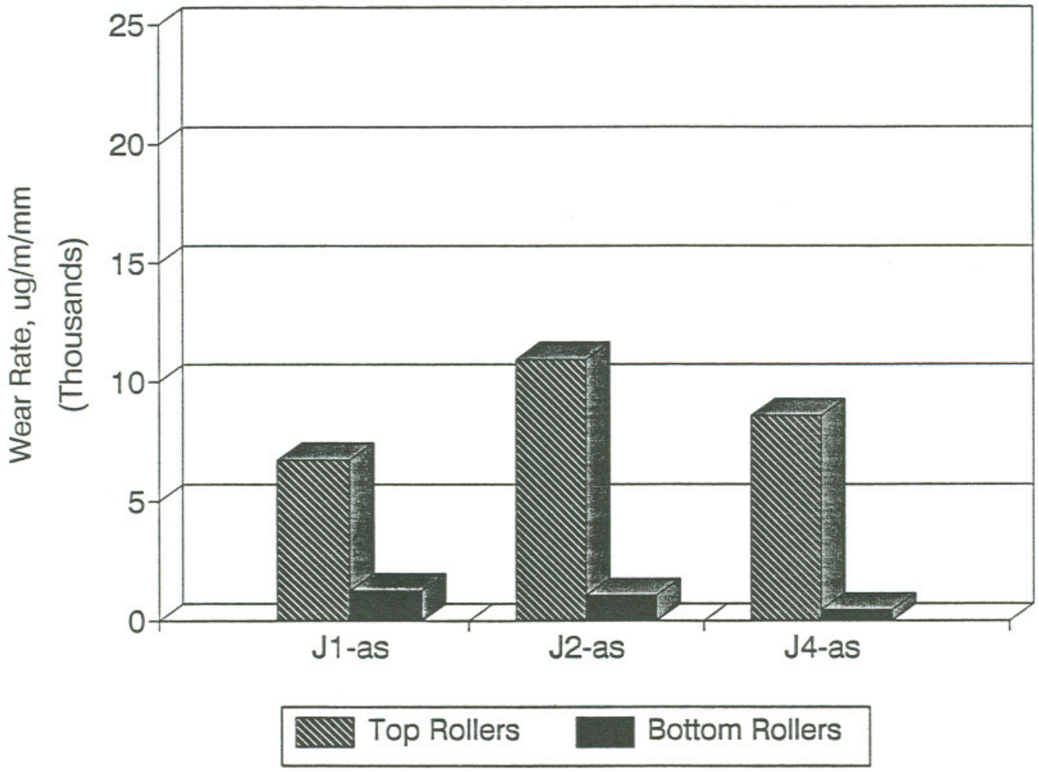

Figure 3.31 Comparison of wear rates between the top and bottom rollers at various pressures
(b) 900 MPa

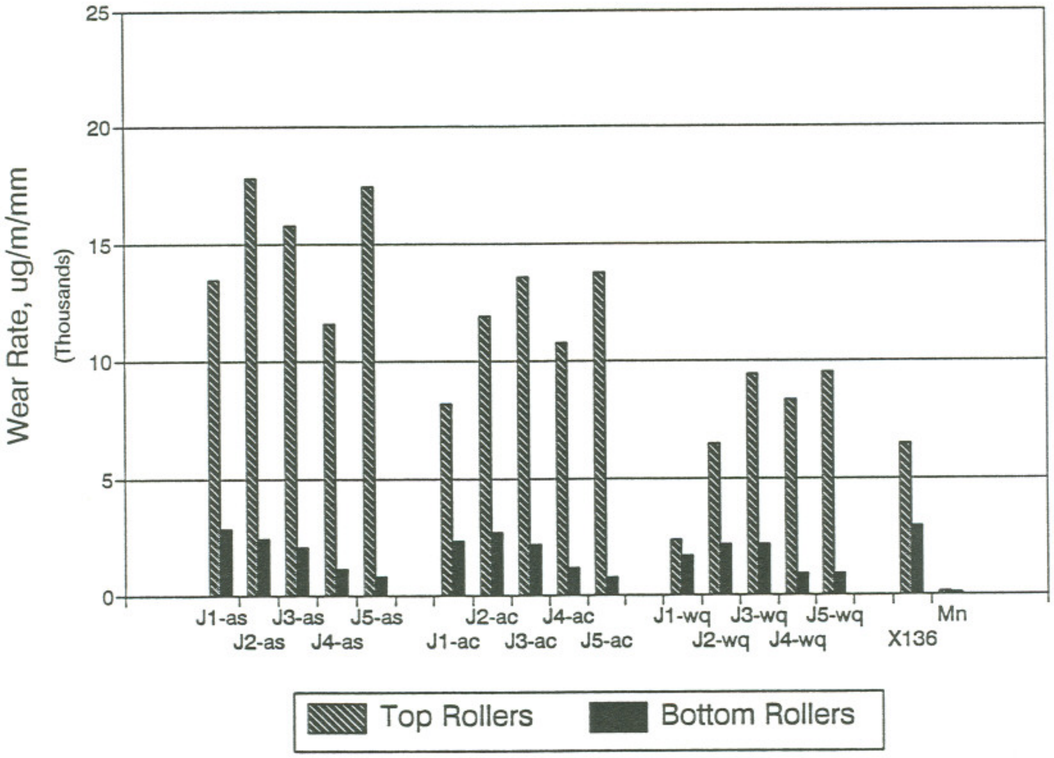

Figure 3.31 Comparison of wear rates between the top and bottom rollers at various pressures
(c) 1200 MPa

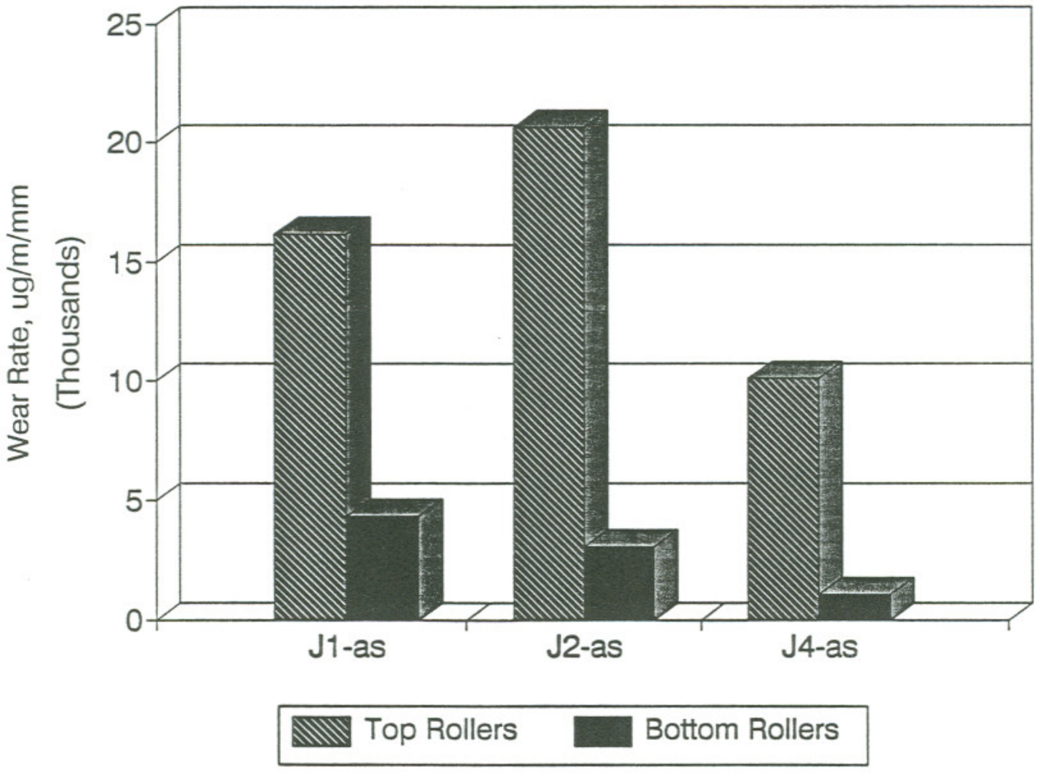

Figure 3.31 Comparison of wear rates between the top and bottom rollers at various pressures
(d) 1450 MPa

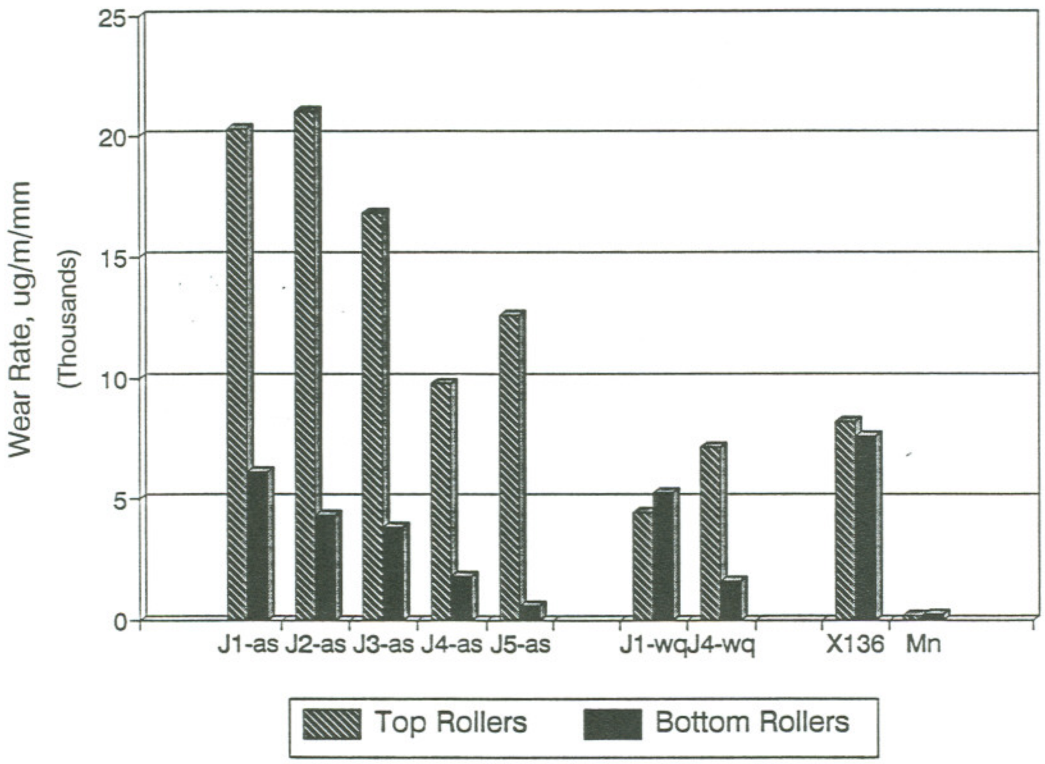

Figure 3.31 Comparison of wear rates between the top and bottom rollers at various pressures
(e) 1700 MPa

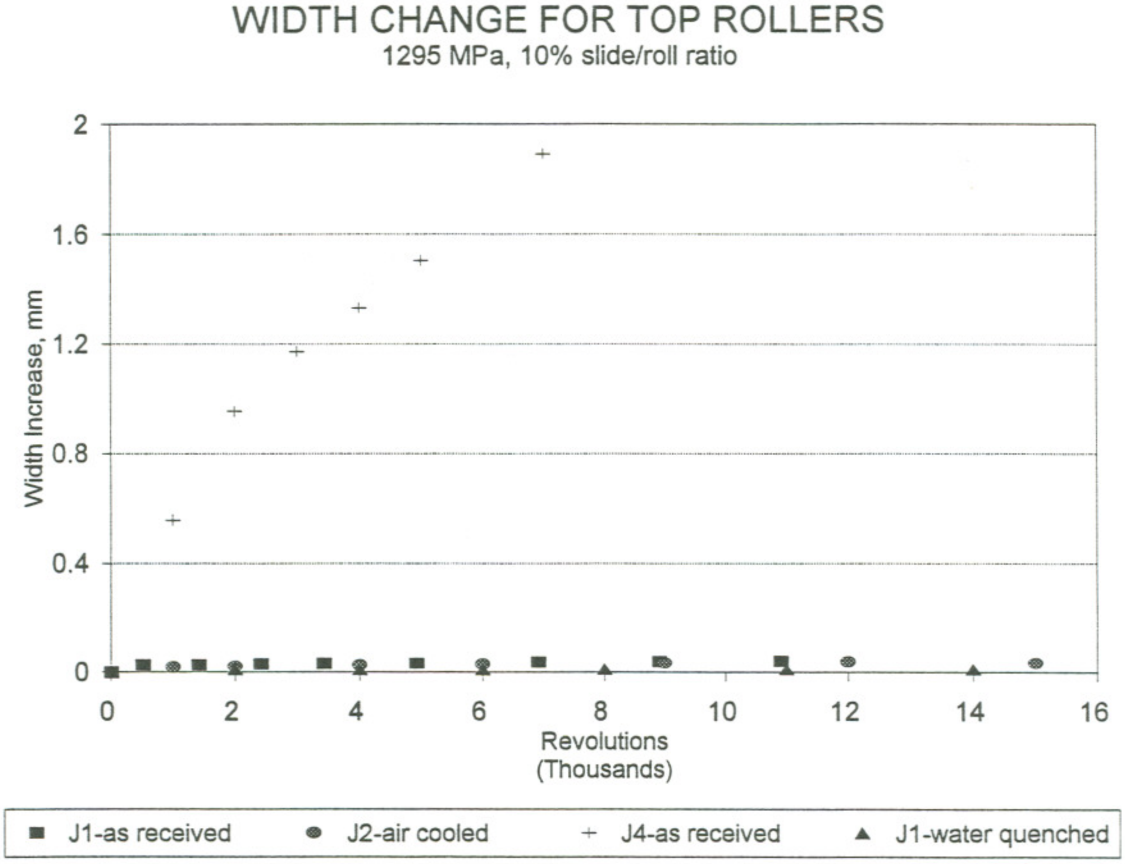

Figure 3.32 Width change of rollers during deformation test
(a) top rollers

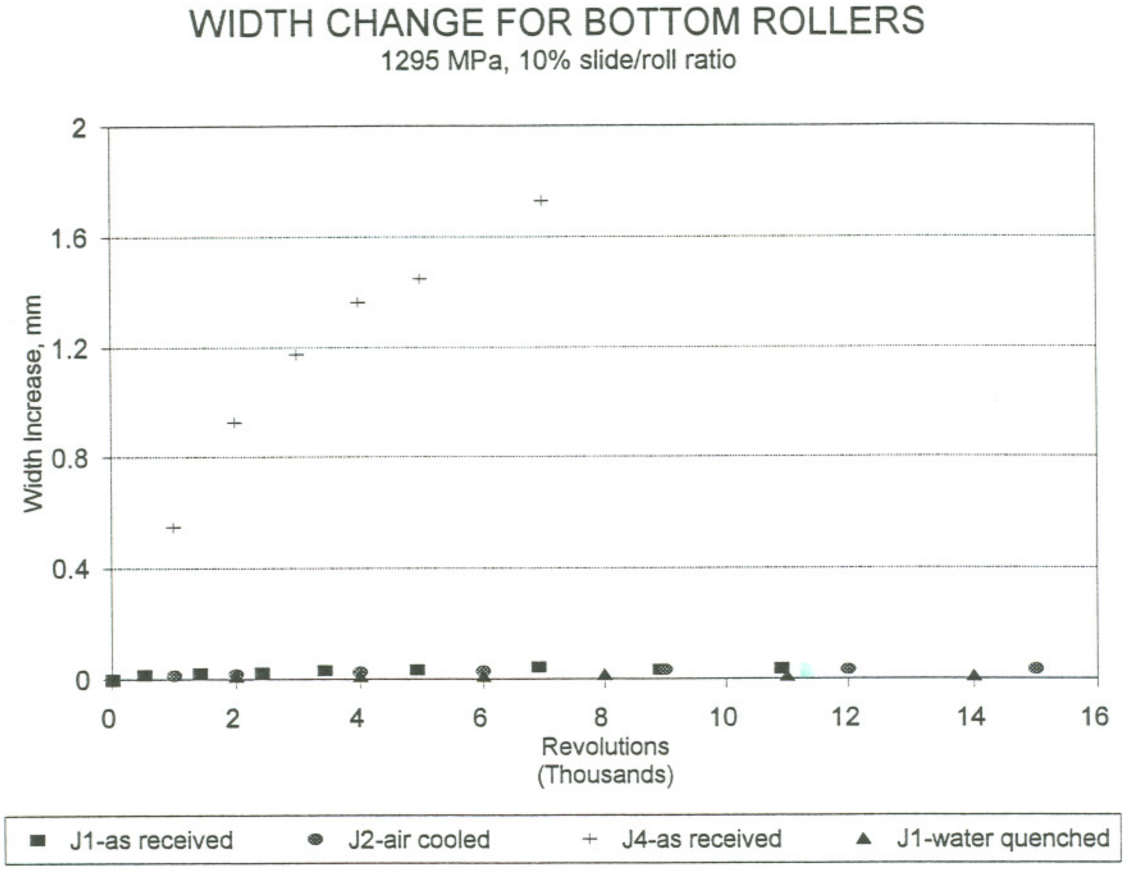

Figure 3.32 Width change of rollers during deformation test
(b) bottom rollers

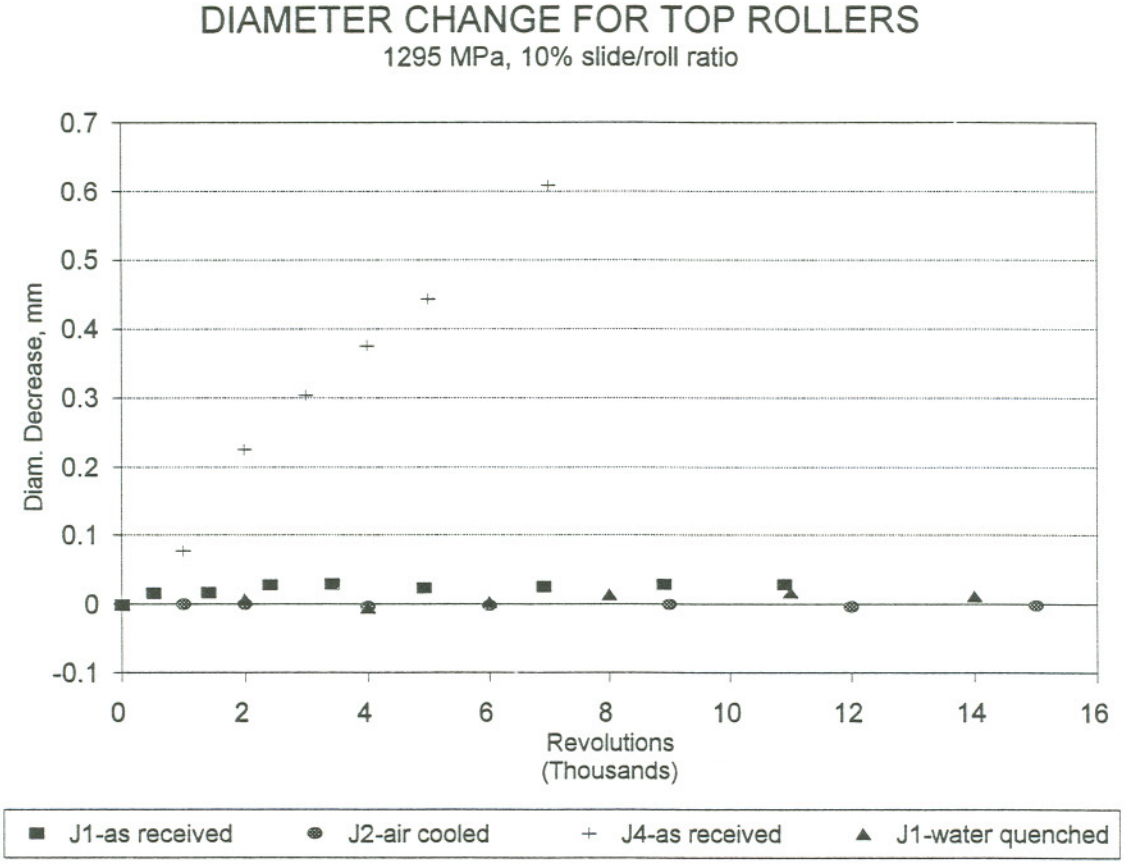

Figure 3.33 Diameter change of rollers during deformation test
(a) top rollers

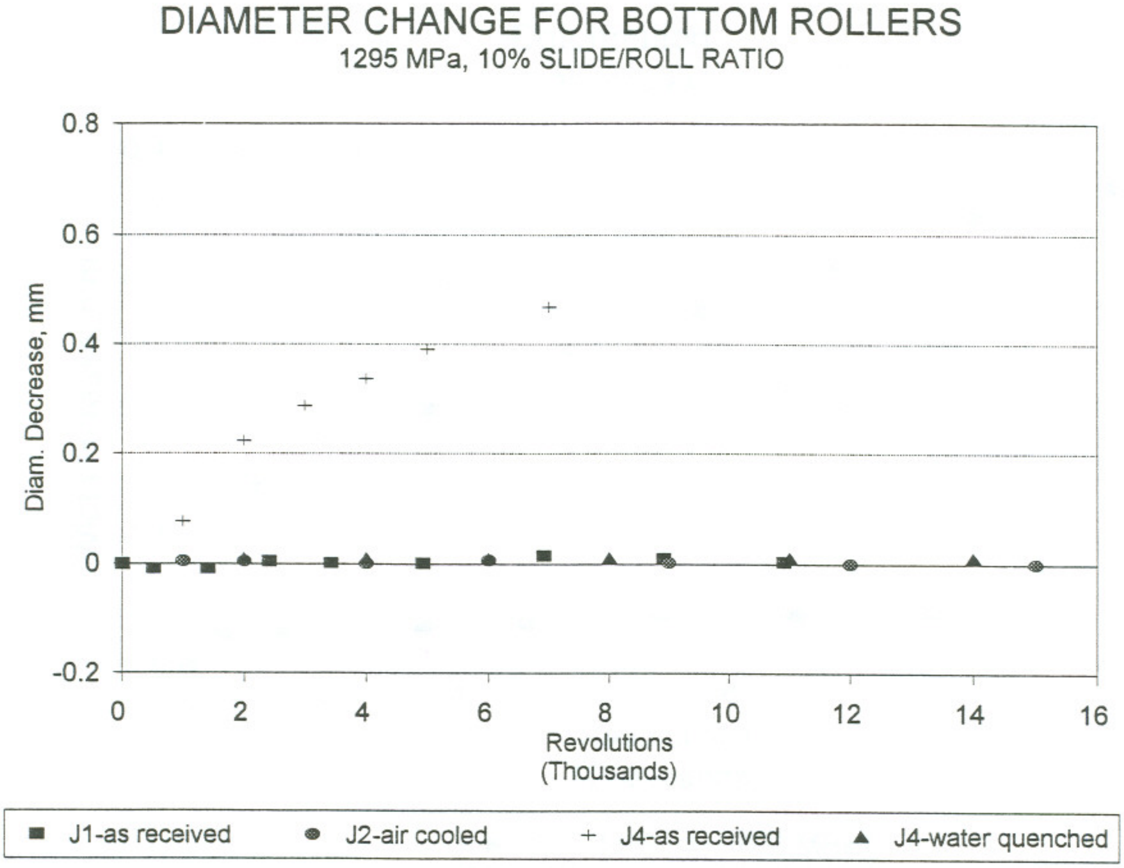

Figure 3.33 Diameter change of rollers during deformation test
(b) bottom rollers

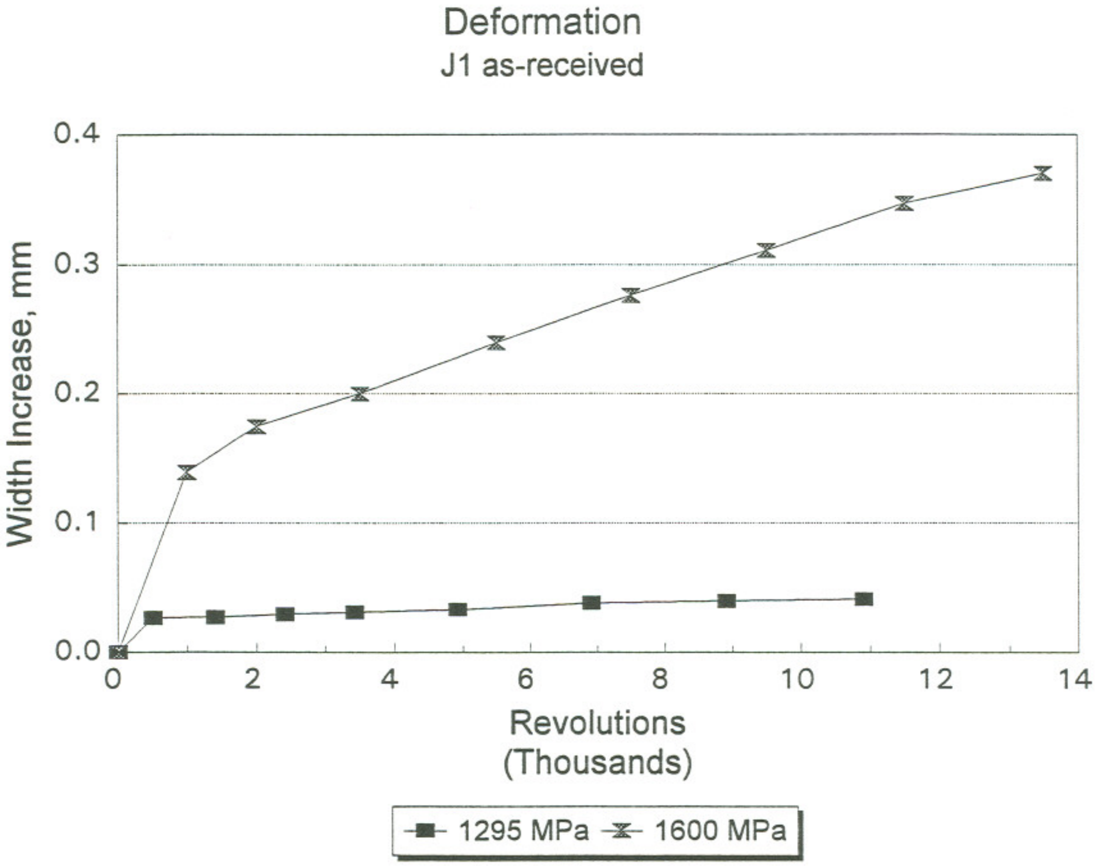

Figure 3.34 Effect of contact pressure on deformation

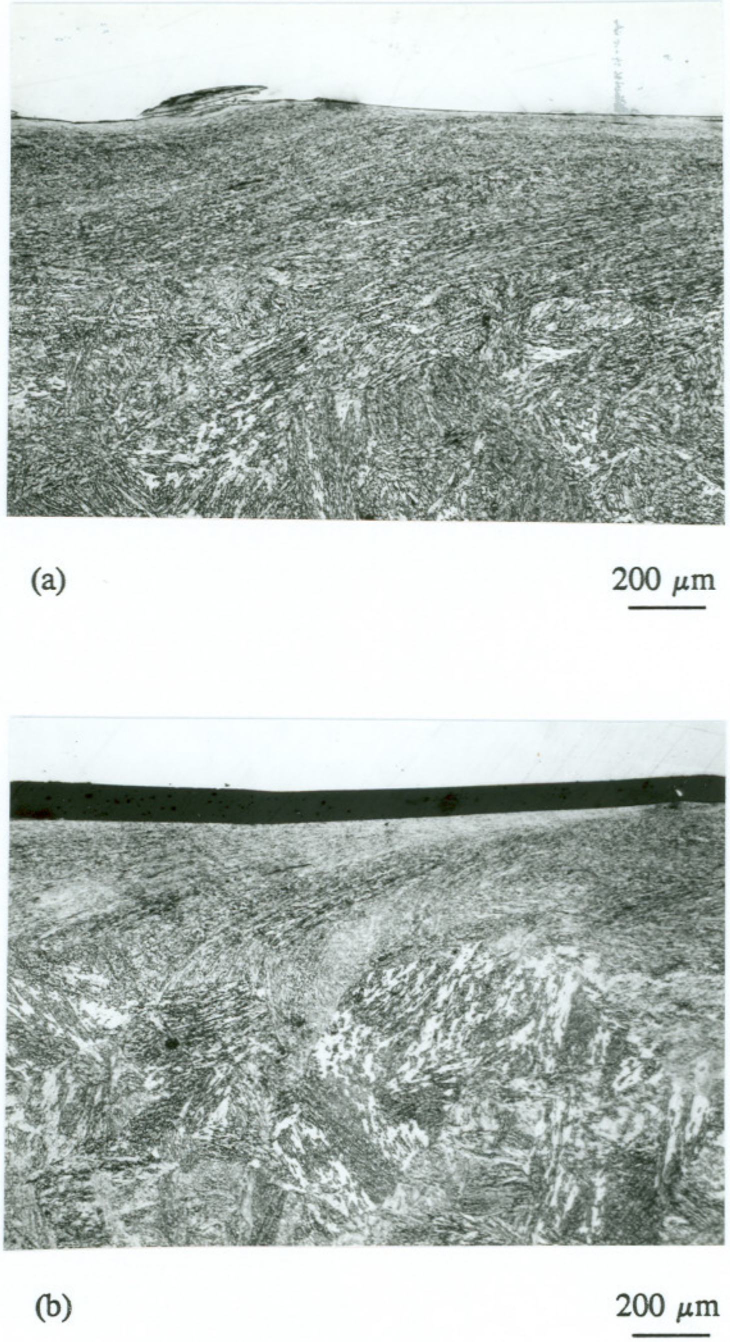

Figure 3.35 Subsurface of worn rollers
(a) 1700 MPa (b) 1220 MPa

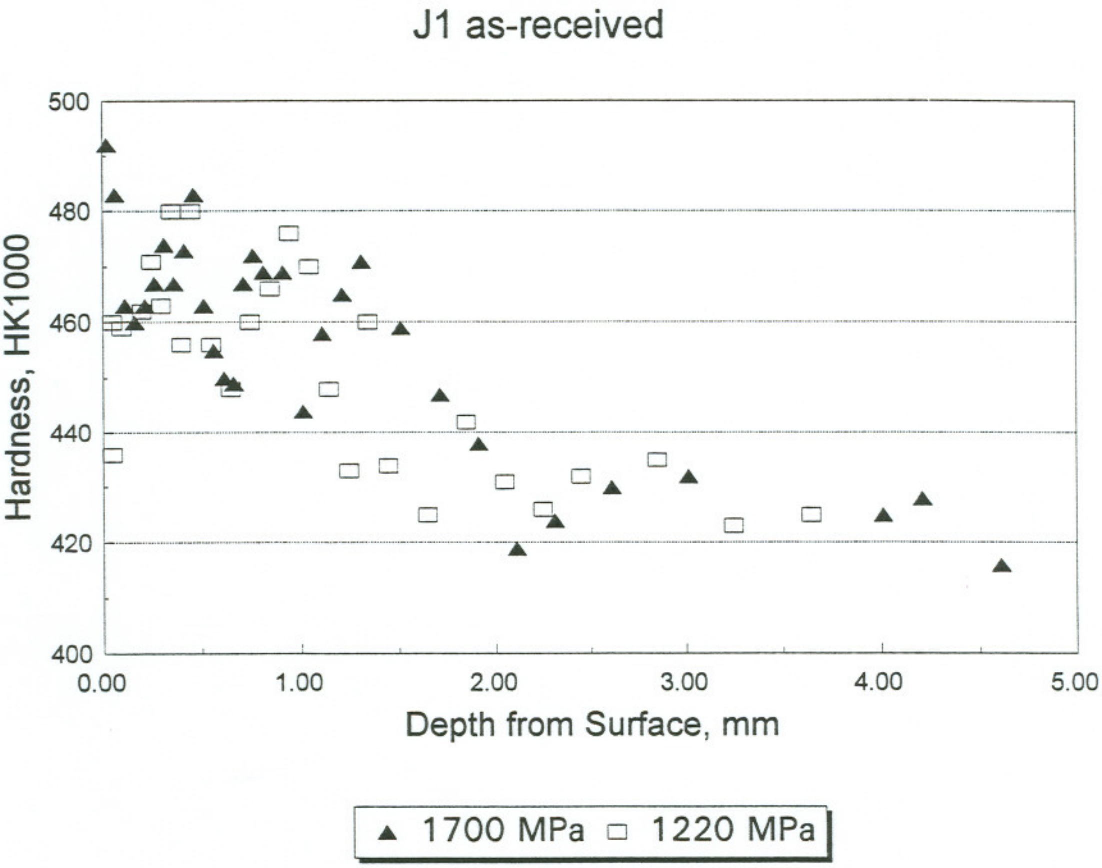

Figure 3.36 Hardness profile of deformed layers

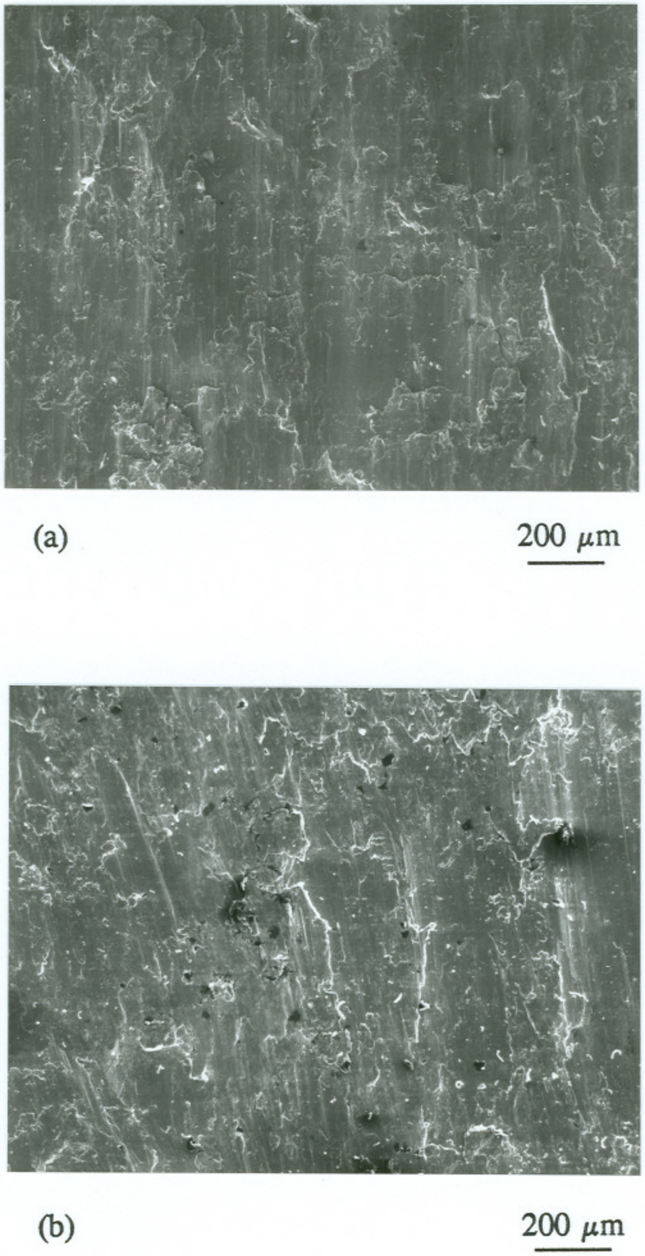

Figure 3.37 Worn surfaces of the bainitic steels
(a) J1-as 500 MPa (b) J1-as 1220 MPa

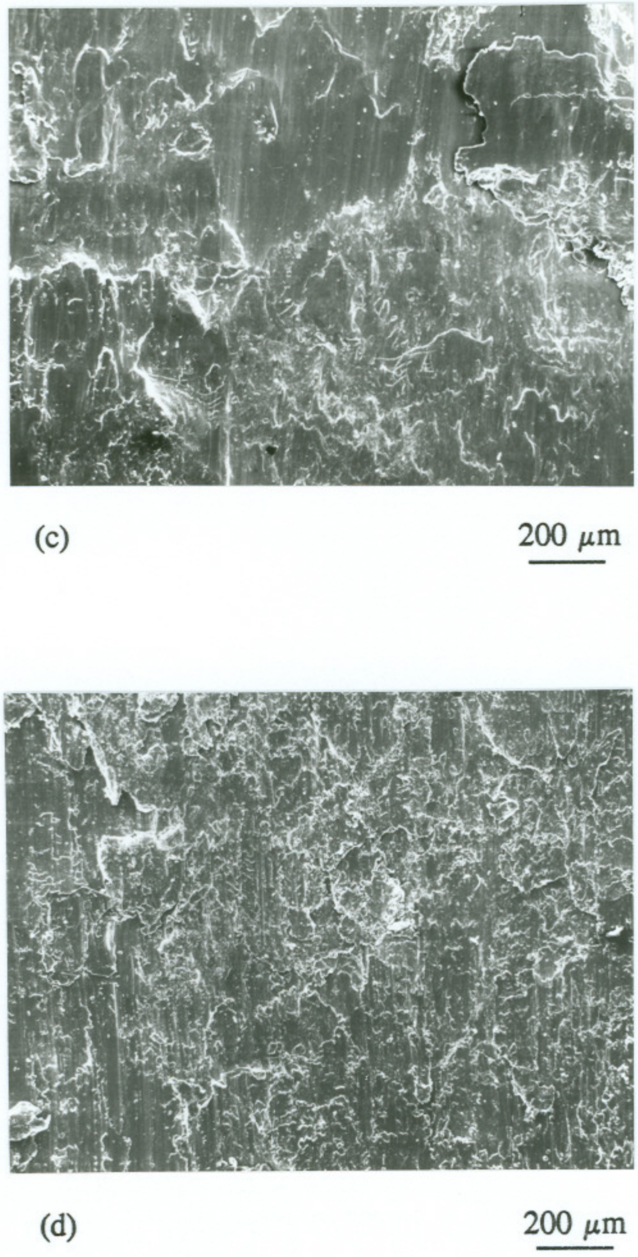

Figure 3.37 Worn surfaces of the bainitic steels
(c) J1-as 1700 MPa (d) J4-as 500 MPa

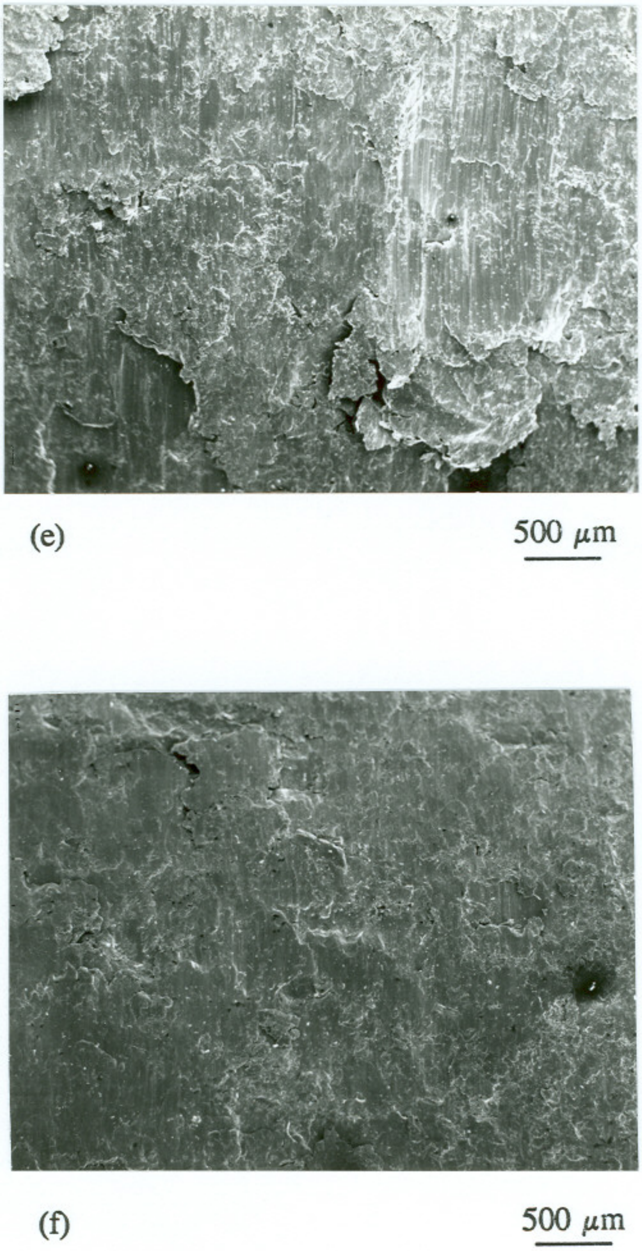

Figure 3.37 Worn surfaces of the bainitic steels
(e) J4-as 1220 MPa (f) J4-as 1700 MPa

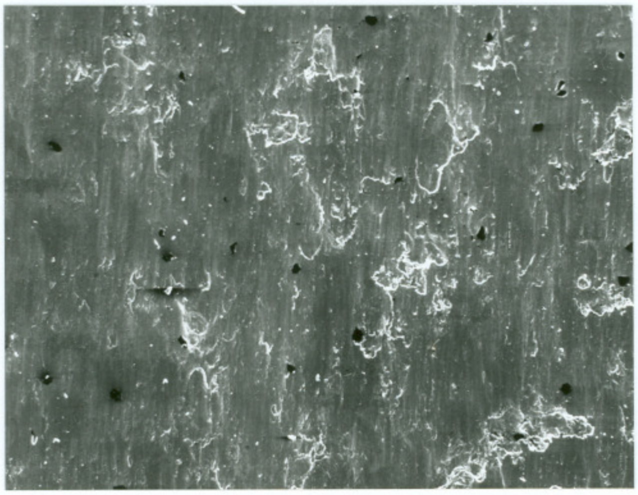

(g) 200 μm

Figure 3.37 Worn surfaces of the bainitic steels
(g) J1-wq 1700 MPa

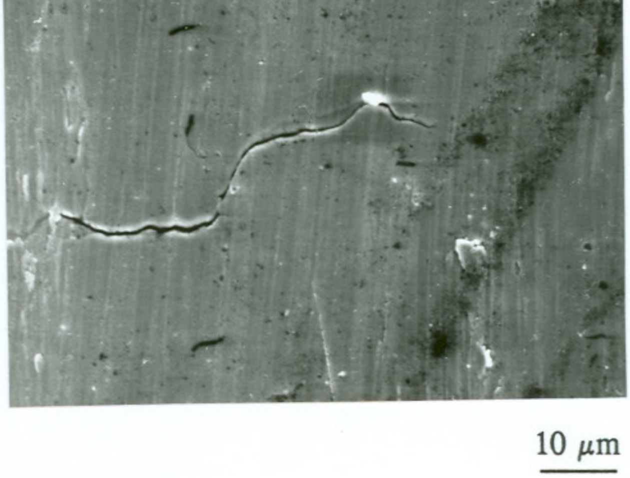

Figure 3.38 Microcracks on a worn surface

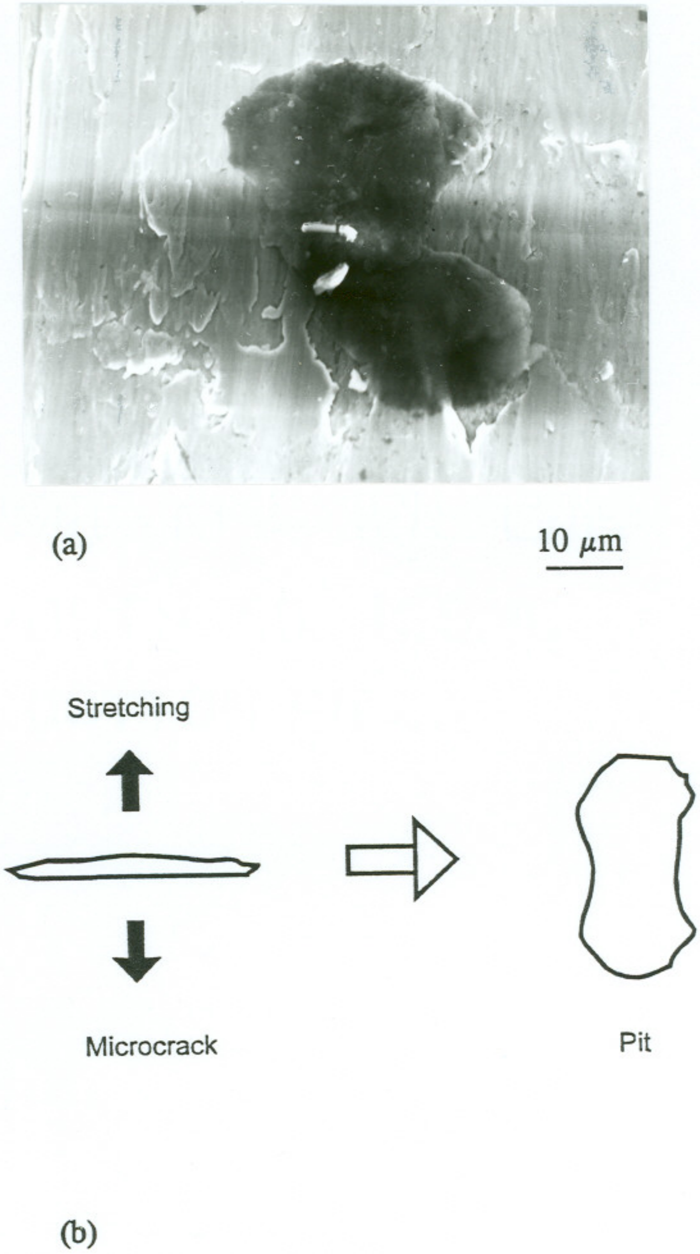

Figure 3.39 Pit formation during wear
(a) close-up of a pit
(b) schematic presentation of the formation of a pit

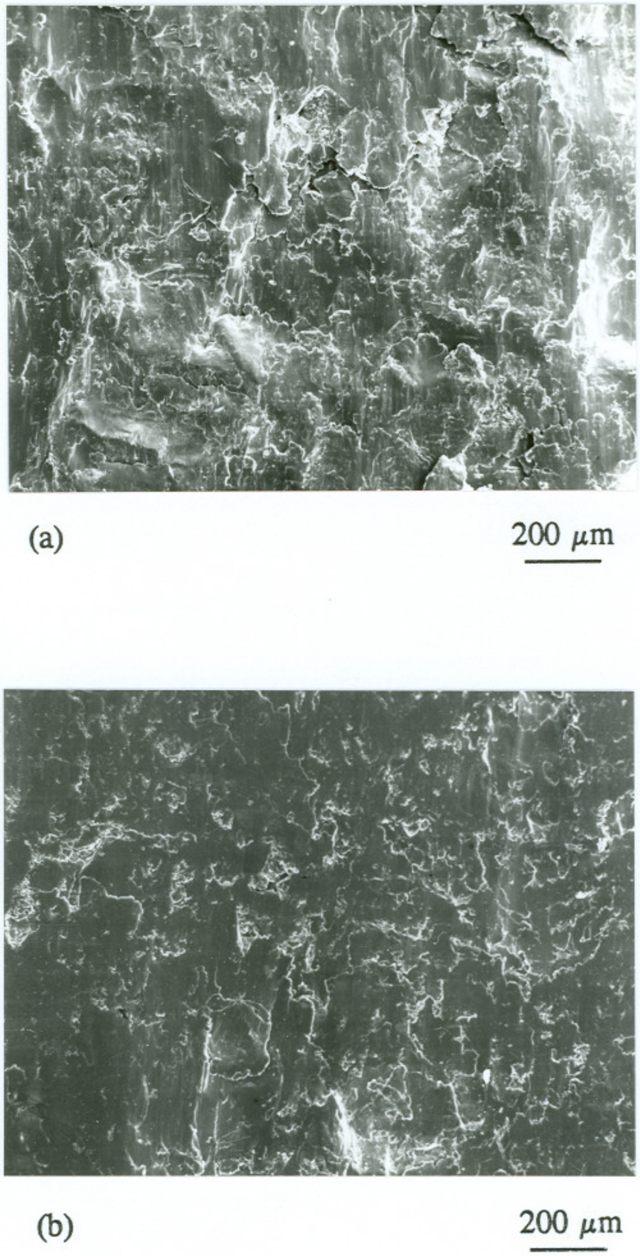

Figure 3.40 Worn surfaces of X136
(a) 1700 MPa (b) 1220 MPa

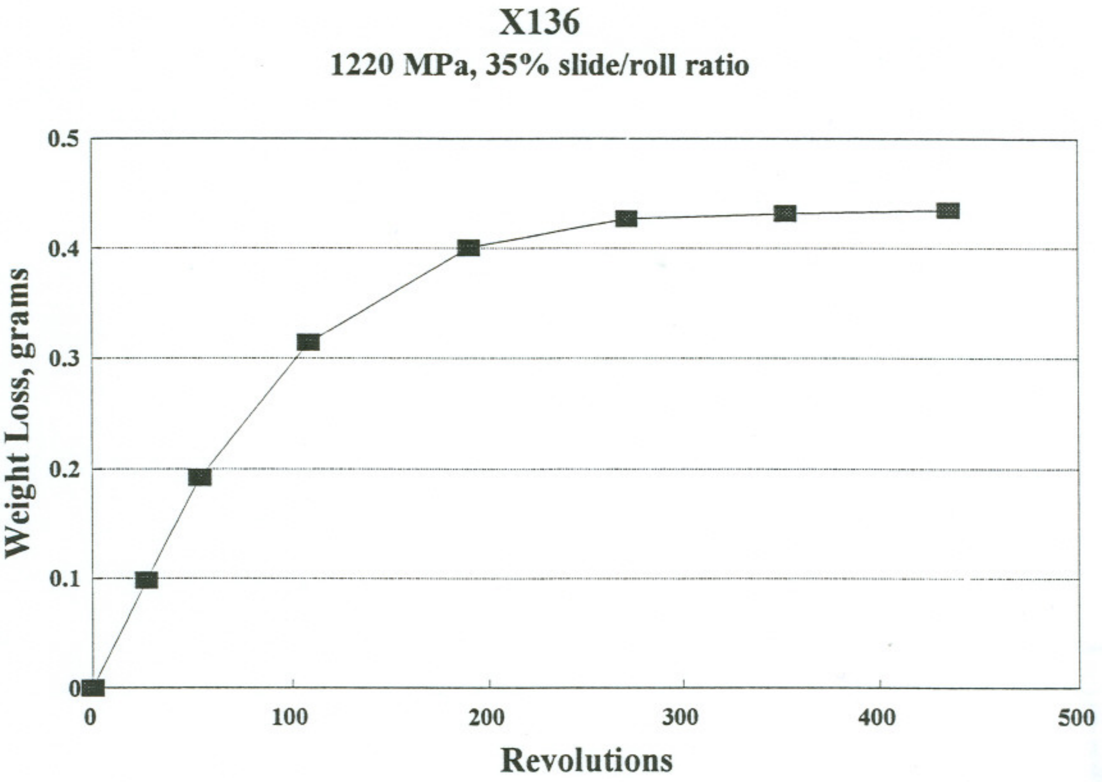

Figure 3.41 A level-off curve for X136

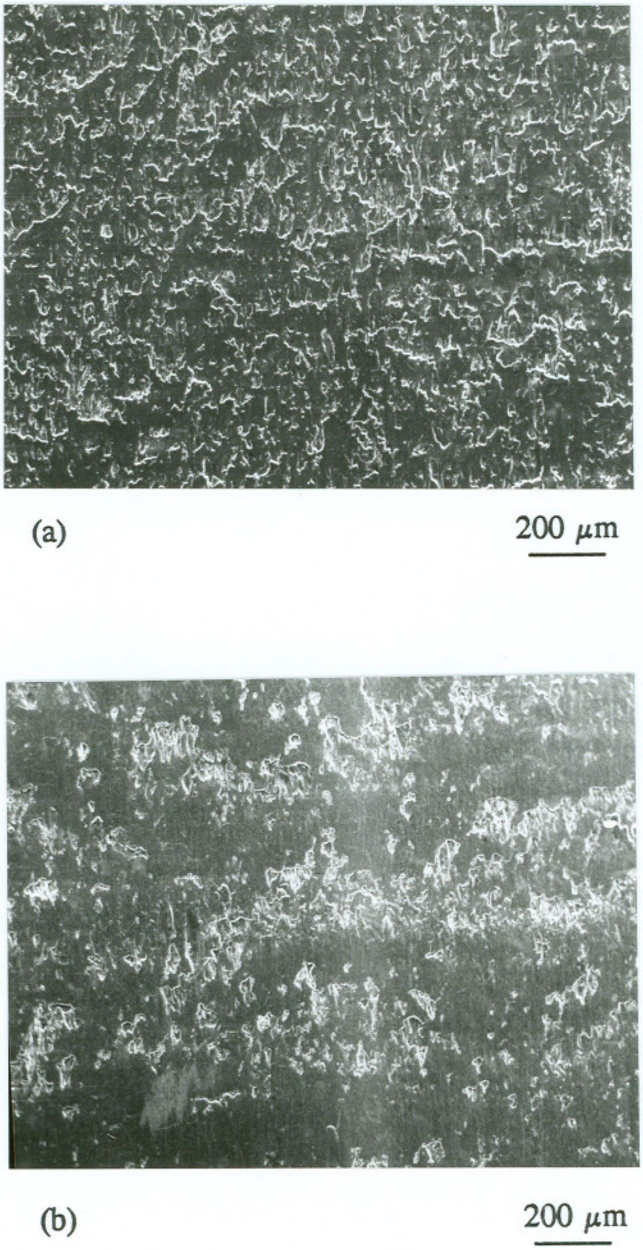

Figure 3.42 Worn surfaces of the austenitic manganese steel
(a) 1220 MPa (b) 1700 MPa

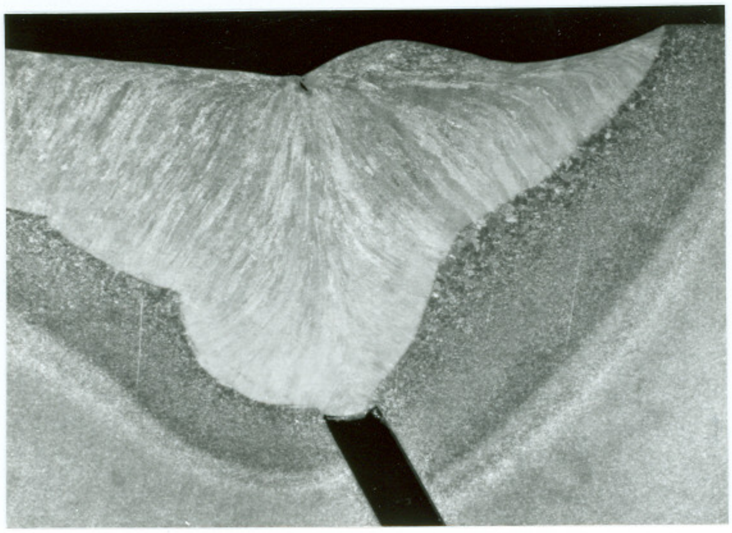

(a)

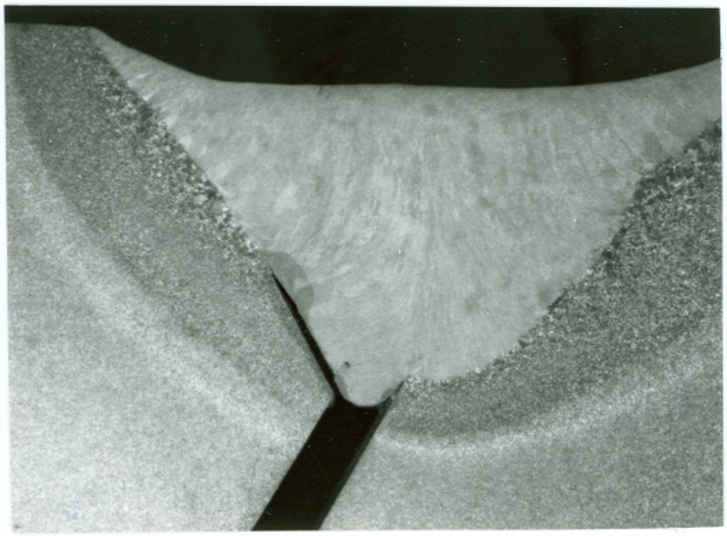

(b)

Figure 3.43 Weldment of J1
(a) no cracking (b) lack of fusion

CHAPTER 4

DISCUSSION

4.1. MICROSTRUCTURE OF THE Mo-B STEELS

The optical micrographs in Figure 3.1 show the very different microstructural morphologies of the as-received steels. However, it is difficult to use them to characterize or identify the microstructure. Therefore, an electron microscope was used to reveal finer structures. The TEM work has demonstrated that the matrix of the microstructure is bainitic ferrite in two morphologies: lath-like and massive. Other constituents found in the steels include M-A islands, retained austenite, carbides and needle-shaped martensite. The presence and distribution of these constituents vary with the composition and heat treatment of the steels.

Figures 3.15 and 3.16 suggest that for J1 and J4, the transformation product is bainite over a wide range of cooling rate. Furthermore, the bainite start transformation temperature does not change much with cooling rate. This is consistent with what Ohmori *et al*. reported.[39] They found that for Cu-Ni-Cr-Mo-V alloy steels with carbon contents between 0.12% and 0.22%, the B_s did not change with cooling rate. Bramfitt and Speer[41] also stated that bainite with an almost constant transformation start temperature can be produced over a wide range of cooling rates.

The relationship between B_s and the composition of steels was not determined experimentally in the present study since there had not been enough number of steels with various alloying element levels for statistical analysis. However, it was still an interesting topic and the relationship between B$_s$ and composition was evaluated using empirical equations developed by other workers.[37,220-222] Steven and Haynes[220] developed an equation for isothermal transformations in the form

$$B_s\ (^\circ C) = 830-270C-90Mn-37Ni-70Cr-83Cr \quad (wt\text{-}\%) \qquad (1)$$

For continuous cooling transformations, Bodnar and Taylor[221] obtained an equation in the form

$$B_s\ (^\circ C) = 719 - 127C - 50Mn - 31Ni - 27Cr - 61Mo \quad (wt\text{-}\%) \qquad (2)$$

Another equation Bodnar *et al.*[222] proposed is

$$B_s\ (^\circ C) = 844 - 597C - 63Mn - 16Ni - 78Cr \quad (wt\text{-}\%) \qquad (3)$$

In a recent investigation, Devanathan[37] found under continuous cooling the bainite transformation follows the relationship

$$B_s\ (^\circ C) = 721 - 598C - 85Mn - 43Cr \quad (wt\text{-}\%) \qquad (4)$$

The B$_s$'s of the steels J1 through J5 calculated using these equations are given in Table 4.1 and illustrated in Figure 4.1 along with the experimental data for J1 and J4. It is shown that great differences were produced in calculating the B$_s$ with these equations. The discrepancy in B$_s$ for a given steel could be as great as 210°C. In addition, the relative values of B$_s$ for these steels varied with the equation used. Table 4.1 and Figure 4.1 reveal that these equations generally are not able to predict the B$_s$'s of the steels in the current study although equation (3) gave the closest results to the measured ones. These variations and disagreements suggest that the empirical equations are not universally applicable to all steels while each one may fit well for the steels used to derive it. Generally speaking, the derivation of an empirical equation is strongly dependent upon the composition, metallurgical conditions and processing procedures of steels.

It has been found that microstructure varies with cooling rate for steels within the bainite transformation region in a CCT diagram.[39-41,223,224] Some observations have been well documented by Bramfitt and Speer.[41] The variation in morphology of continuously cooled bainite could be considerable, depending on the composition of the steel. It was reported that the microstructure changes from auto-tempered martensite to lower bainite to upper bainite and finally to granular bainite as the cooling rate decreases.[39,41,223] Ohmori *et al.*[39] found that type BI, BII or BIII bainite could be produced by changing the cooling rate. It should be mentioned, however, that the terminology for depicting bainite produced under continuous cooling conditions has never been consistent and led to some confusion.

The microstructural variations with cooling rate was also found in the current study. For the bainitic ferrite, more lath ferrite is produced and the amount of massive ferrite decreased as the cooling rate increases. Also, the lath boundaries are better defined by faster cooling. In the present study, *massive* refers to the structure where no boundaries can be defined on a comparable scale with respect to a *lath* structure. Although the term *massive* has been frequently used in the literature, confusion still exists. In the early investigations, a microstructure without acicular features was termed *massive* with the limited resolution of optical metallography and early electron microscopy, and a "granular bainite" was described as consisting of massive ferrite with M-A islands[40]. As TEM techniques were improved, this massive structure was later found to be composed of laths on a much finer scale.[45,225-229] However, non-lath matrices have also been found on such fine scales in the TEM and the term *massive* is still used in the literature.[38,46,49,230,231]

The morphology of retained austenite also changes with cooling rate. In the as-received J1, the retained austenite exists in either blocky or elongated forms. In the water-quenched J1, only thin films of retained austenite were found between ferrite laths. This kind of structure was reportedly obtained by quenching medium carbon steels[129,232] or by isothermal treatment in Si steels.[131,150,169] It is believed that the thin films of retained austenite, which are thermal and mechanical stable, lead to a good combination of strength and toughness. From the viewpoint of transformation thermodynamics, Bhadeshia and Edmonds[150] suggest that this kind of microstructure can be optimized by (1) reducing the overall carbon content of the alloy so that a critical concentration in the austenite, at which displacive transformation becomes impossible, is reached at a later stage in the transformation; and (2) modifying substitutional alloying additions such that the T_0 curve, which is the locus of points where the austenite and ferrite free energy curves intersect,[131] is shifted to higher austenite carbon contents. With the above theory, they obtained a steel that exhibited a better combination of strength and toughness by reducing carbon content and replacing Mn by Ni.[131,150]

No carbides were found in the as-received J1 although the carbon content was 0.18%. This is attributed to the addition of 1.13%Si. Due to the relative insolubility of Si in cementite, Si is rejected by a diffusion control mechanism at the transformation front. A subsequent silicon concentration built-up during the early stage of growth increases the activity of carbon locally, which reduces the carbon flux and finally inhibits the further development of the cementite embryo.[233]

In the as-received J2, the presence of a large number of carbides is attributed to 0.12%C and a low silicon content. In this steel, 0.27% Si was not able to inhibit the precipitation of carbides. The absence of carbides in the water-quenched specimens suggests that fast cooling can suppress the formation of carbides.

The martensite-retained austenite islands (M-A islands) were found in the as-received J1 through J4. But only in J3 and J4, were these islands frequently observed.

Increasing the cooling rate reduced the number of islands. In the water-quenched steels, the M-A islands were completely suppressed by the fast cooling rate.

The M-A islands were found by Habraken and Economopoulos[40] in association with granular bainite. They proposed that the formation of M-A islands was associated with a dehomogenization of the parent austenite. When the cooling rate is low, large carbon-enriched clusters would be formed and subsequently transformed to martensite-retained austenite islands. Buchi *et al.*[223] found that the islands of retained austenite in a matrix of acicular ferrite look like the granular bainite mentioned by Habraken and suggested that this structure forms because carbon quickly diffuses away from the ferrite/austenite interface at slow cooling rates, preventing the formation of interlath cementite. The increased carbon concentration in the remaining austenite stabilizes the austenite from further transformation, leading to the formation of granular bainite.

Biss and Cryderman[45] proposed a similar model, suggesting that at faster cooling rates within the bainite transformation region, a steep carbon concentration gradient is developed on the austenite side with a high carbon supersaturation at the ferrite/austenite interface. This supersaturation leads to the precipitation of cementite at the interface as the transformation proceeds. At slower cooling rates, the carbon concentration gradient is lower and carbon supersaturation at the interface is also lower. This low supersaturation makes it more difficult, or even unlikely, for carbides to precipitate and thereby leads to the formation of M-A islands. A schematic representation of the carbon concentration at the ferrite/austenite interface is shown in Figure 4.2. In the present study, the M-A islands were found in the as-received steels which experienced relatively slow cooling rates in comparison with the air-cooled and water-quenched steels. This is consistent with the general result that granular bainite forms at slow cooling rates within the bainite transformation region.

Katsumata *et al.*[234] investigated the formation of a granular structure in a 0.06%C-1.5%Mn-0.5%Cr-0.022%Ti-0.0022%B steel at a cooling rate of 1.7°C/s. They found that at the early stage of the transformation, lath-like bainitic ferrite formed. As the transformation continued, parts of neighboring laths of bainitic ferrite coalesced and then the length of untransformed austenite shortened during slow cooling. Finally, the island-shaped retained austenite formed when the transformation finished. They estimated that 60% of the untransformed austenite transformed to martensite and 40% was retained as austenite at temperatures below the transformation finish temperature of 460°C.

It is known that carbides form at high cooling rates and M-A islands form at slow cooling rates. However, no systematic study has been reported on the critical cooling rate, that is, the lowest cooling rate to inhibit the formation of M-A islands. It seems that the critical cooling rate is a function of the composition of the material. In the present study, carbides precipitated only in the as-received J2, where a mixed structure with predominantly lower bainite was produced. This suggests that the alloying contents, especially carbon content, influence the transformation characteristics of steels. With the composition of J2, lower bainite can be produced at the cooling rate produced by air cooling. Furthermore, the mixed microstructure of J2 also suggests that various transformations can occur at the same cooling rate. The transformations may take place in different temperature ranges and/or even in the same temperature range during cooling. Since the current study did not concentrate on transformation mechanisms, no further investigation has been carried out on this aspect. The microstructure of the as-received J2 indicates that the air cooling rate was much faster than that required for the formation of granular bainite. It is inferred that martensite is likely to form if cooling rate is further increased. This idea is supported by the needle-shaped martensite was observed in the water-quenched J2 and J1, Figures 3.9(e) and 3.10(c).

The presence of retained austenite and the formation of needle-shaped martensite is associated with the carbon enrichment in austenite. When a steel is cooled down from the austenitic region, the partition of carbon results in the supersaturation in the remaining austenite during transformation. However, the degree of supersaturation varies. If the supersaturation is high enough to suppress the M_s below room temperature, the remaining austenite is retained and observed at room temperature. When the carbon content is not high enough to suppress M_s to lower than room temperature but is high enough to activate the martensite transformation above room temperature, martensite is produced at fast cooling rates. A carbon content in the retained austenite, which was reported to be about 3 at-%[232] or 1.55 wt-%,[235] is high enough to produce twinned martensite.

4.2. MECHANICAL PROPERTIES OF THE BAINITIC STEELS

The strengths of the bainitic steels in the as-received condition are fairly high with respect to conventional HSLA steels. The yield strengths are in the range 93.5 — 127 ksi (644 — 846 MPa) and the ultimate tensile strengths 130 — 197 ksi (899 — 1360 MPa). Water-quenching further increases the strengths of these steels to 124.5 — 168 ksi (858 — 1159 MPa) yield strength and 140.5 — 237 ksi (1037 — 1636 MPa) ultimate strength. These strengths are much higher than conventional HSLA steels which have yield strengths in the range 290 — 550 MPa and ultimate tensile strengths in the range 415 — 700 MPa.[236] Hot rolled 0.15%C steels with a bainitic structure was reported to possess yield strengths in the range 450 — 900 MPa,[237] which are comparable to the as-received bainitic steels in the current study.

Of bainitic steels, a high dislocation density makes a significant contribution to strength. In the present study, high density dislocations were detected in the bainitic ferrite matrix although no quantitative analysis was made. It was reported that the dislocation density in upper bainite are in the range 10^9 — 10^{10} cm^{-2} [105] and that a dislocation density of the order of 10^4 m^{-2} may contribute to an increase in strength of 145 MPa.[104] Garcia *et al.*[238] point out that in the ultra-low carbon bainitic (ULCB) steels, whose microstructure is generally lath ferrite with a network of high density dislocations, high strengths mainly arise from solid solution and dislocation strengthening.[238] The heavily dislocated structure in bainite may be partly inherited from the prior austenite.[106,107]

For bainitic steels, strength is also associated with the change in the bainite transformation temperature. It has been well documented that strength increases as B_{50} decreases.[92] B_{50} is the temperature at which 50% bainite transformation is accomplished. Steven and Haynes[220] empirically established the relationships between B_{50} and B_s by

$$B_{50}\ (°C) = B_s\ (°C) - 60,$$

where B_s was correlated to the alloying elements using eqn. (1) mentioned earlier in this chapter.

As far as the alloying elements are concerned, carbon content was found to play a significant part in determining the strength for the bainitic steels J1 through J5. As carbon content increases, strength increases. The interaction between interstitial elements (C, N) and dislocations makes a great contribution to strength.[98] Substitutional elements also influence the strength of bainite. Mn, Cr, Mo, Ni, Ti, V, and W were found to increase strengths, but their effects are far less than carbon.[91] Using the linear relationship between strength and transformation temperature and between B_s (or B_{50}) and composition, Pickering[91] related tensile strength to composition in the following formula:

$$\sigma\ (MPa) = 15.4[16+125C+15(Mn+Cr)+12Mo+6W+8Ni+4Cu+25(V+Ti)]$$

where σ is the tensile strength in MPa and all the element concentrations are in weight percent. It should be noted that the equation was derived by combining the relationship between the strength and the 50% bainite transformation temperature and that between the 50% bainite transformation temperature and the composition of bainitic steels, not an empirical equation obtained by direct correlation between the strength and composition. The range of carbon content for the equation is 0.05 – 0.20%.

In the present study, the effects of alloying elements of C, Cr, Ni, and Mn on the 0.2% yield strength and ultimate tensile strength were quantitatively analyzed using multiple element linear regression. In regression, the estimated strength $\hat{\sigma}$ could be expressed in the form

$$\hat{\sigma} = b_0 + b_1C + b_2Cr + b_3Ni + b_4Mn$$

where C, Cr, Ni and Mn are element concentrations in weight percent and their values are known variables. Table 4.2 gives the results for the coefficients b_0 through b_4. Retaining one decimal point for the coefficients, the empirical equations are given below:

For the as-received steels,

$$\sigma_y\ (ksi) = 479.7 + 226.3C - 105.1Cr + 10.7Ni - 96.6Mn \quad (wt\text{-}\%)$$

$$\sigma_u\ (ksi) = -421.4 + 515.5C + 133.4Cr + 9.0Ni + 132.6Mn \quad (wt\text{-}\%)$$

For the water-quenched bainitic steels,

$$\sigma_y\ (ksi) = 266.7 + 320.3C - 42.3Cr + 3.0Ni - 37.1Mn \quad (wt\text{-}\%)$$

$$\sigma_u\ (ksi) = 180.8 + 601.2C - 15.3Cr + 4.3Ni - 11.3Mn \quad (wt\text{-}\%)$$

where σ_y and σ_u are yield and ultimate tensile strengths, respectively. The strengths estimated using the above empirical equations are given in Table 4.3, along with the measured values. The estimated values exactly match the measured values, indicating that the linear relationship is very good.

The equations indicate that carbon is the dominant element in controlling strength. Ni does not make a great contribution to strength. It is noted that a negative effect of Cr and Mn on strength has been found in three equations. This effect is stronger on the yield strength of the as-received steels than the water-quenched steels because of greater absolute values of the coefficients. No reports of the negative effect of Cr and Mn have been found in the literature for bainite structures. For polygonal ferrite structures, however, a negative effect of chromium was reported by Pickering in a study on the solid solution hardening effects of alloying elements.[239] In an earlier study, Irvine and Pickering[240] found that 1%Cr could reduce yield strength by 4.5 ksi in ferrite. In a solid solution, manganese addition generally increases strength by a solid solution strengthening mechanism. In the current study, solid solution strengthening is believed an important mechanism since there are no carbides in most steels. However, manganese bears a negative coefficient in the above strength equations. One possible reason for the negative coefficients in the present study is that there were not enough variations in Cr and Mn contents in these steels. Consequently, the statistical approach might not be able to produce a result that represents the general trend of alloying element effects on strength in a wider compositional range.

It is worthwhile noting that water quenching exerts more impact on increasing yield strength than increasing tensile strength, with the former a critical consideration of material selection in most mechanical designing. Faster cooling yields a significant increase in yield strength, as indicated in Figure 3.19.

The variation in ductility is associated with the change in strength. Ductilities are decreased while strengths are increased by water quenching. Figure 3.21 shows that cooling rate has greater influence on elongation than on reduction of area. Carbon content also seems to have a great influence on ductility. A linear relationship between carbon content and ductility is presented in Figure 4.3. For the as-received steels, we have

$$\delta\ (\%) = 18.4 - 22.1(\%C)$$

$$\psi\ (\%) = 74.6 - 190.3(\%C)$$

For the water-quenched steels, we have

$$\delta\ (\%) = 16.0 - 28.9(\%C)$$

$$\psi\ (\%) = 72.6 - 207.9(\%C)$$

where δ is elongation and ψ reduction of area. These equations clearly indicate that carbon content exerts a much stronger effect on reduction of area than on elongation.

Table 3.4 shows that J4 and J5 have similar strengths and ductilities in both the as-received and water-quenched conditions. These mechanical testing results indicate that 4%Mn yields similar mechanical properties to 2%Mn, 2%Cr and 2%Ni at an ultra low carbon level (~ 0.025%). At a higher carbon level (~ 0.1%), 4%Mn in J2 achieved similar mechanical properties compared to 2%Mn, 2%Cr and 2%Ni in J3 in the as-received conditions. By water quenching, J2 yielded a slightly higher strength than J3. This may be attributed to the higher carbon content in J2. The carbon content exhibited a stronger effect on strength in the water-quenched condition as shown in the strength equations derived above. These results appear to suggest that at the same carbon level, 4%Mn may have a similar effect to 2%Mn, 2%Cr and 2%Ni on mechanical properties.

From the strength equations at a given carbon content, the contributions of Mn, Cr and Ni to the yield and ultimate tensile strengths are given below:

Strength (ksi)	4%Mn	2%Mn-2%Cr-2%Ni	Difference
σ_y^{as}	-386.4	-382	4.4
σ_u^{as}	530.4	550	-19.6
σ_y^{wq}	-148.4	-152.8	-4.4
σ_u^{wq}	-45.2	-44.6	0.6

where σ_y and σ_u are yield and ultimate strengths, respectively and the superscripts *as* and *wq* refer to as-received and water-quenched conditions, respectively. 4%Mn produces similar strengths to what 2%Mn-2%Cr-2%Ni do.

Fractographic analysis has shown that the Charpy impact specimens experienced brittle fracture at room temperature. Water-quenching can either increase or decrease impact toughness, depending upon the composition of the steel (Figure 3.22). The fractographs (Figures 3.23(a) and (b)) show that the water-quenched J1 exhibits more ductile features than the as-received J1, in agreement with the measured toughness. The increase in toughness of the water-quenched J1 could be attributed to the thin films of retained austenite. The retained austenite in the lath boundaries absorbs energy and retards the propagation of cracks from one lath to another. Quasi-cleavage fracture revealed by means of SEM causes the low toughness of these steels.

The ductile-brittle transition temperature of the bainitic steels has been estimated. Using Figure 4.4(a)[50] and assuming a prior austenite grain size of 60 μm (close to the actual grain size of the steels), the transition temperature was calculated to be 60°C. Assume the facet size is 20 μm (based on the fractographic observation), using Figure 4.4(b) for the bainitic structures,[120] the transition temperature was estimated to be 75°C, close to the former estimation of 60°C. This analysis suggests that the fracture at room temperature should be brittle, which is consistent with the experimental results. According to the equations used, reducing grain size or facet size could effectively reduce the transition temperature, thereby leading to ductile fracture and higher toughness. Therefore, the large grain size is probably one reason for the low toughness of the steels.

Another possible reason for the low toughness is the presence of B and Ti in the steels. Boron (coupled with Mo) is often used to produce bainitic structures on continuous cooling since it retards the formation of proeutectoid ferrite and the pearlite transformation. Maitrepierre *et al.*[161] noted that both B and Ti are detrimental to toughness. Thomas and Chen also found that boron-treated (0.0016%B) steels exhibited inferior impact toughness to boron-free steels.[166] For low carbon steels (< 0.2%C) with 0.5%Mo, 0.003%B might be excessive for ensuring a bainitic structure. Titanium is generally used to protect boron from being combined with nitrogen to form boronitrides. Thelning[241] proposed that the amount of titanium needed to combine with nitrogen can be estimated using the equation

$$Ti = 5(N - 0.002) \qquad (wt\text{-}\%)$$

In steels J1 through J5, the nitrogen contents are in the range 0.00074% to 0.001%. Therefore, no titanium is needed according to this equation. However, the actual content of titanium is 0.023% or more in these steels. The excess titanium might lead to low toughness.

The mechanism by which B or Ti deteriorates toughness is not fully understood. Maitrepierre *et al.*[161] cited that boron has an intrinsic adverse effect on toughness. The detrimental effect on toughness in weld metals was reported to be attributed to the presence of finely dispersed TiN in ferrite.[242,243] A deteriorating impact toughness is often associated with the presence of boronitride or titanium nitride particles. However, in the present study, such particles were not found.

Compared with the bainitic steels reported in the literature, the toughness of the steels in the present study is comparable to that of some steels,[23,144,244] but lower than that of others.[115,245,246] Although they are not as high as expected, the toughnesses of these bainitic steels are significantly higher than those of conventional pearlitic rail steels. The toughness of pearlitic steel is generally in the range 2 to 4 ft·lb at room temperature.[247]

4.3. ROLLING/SLIDING WEAR BEHAVIOR OF BAINITIC, PEARLITIC AND AUSTENITIC STEELS

In the current study, wear resistance is evaluated on the basis of weight loss. when The relative wear resistance (wear resistance of one steel compared with the other steels) of the as-received steels varies with contact pressure (Figure 3.26). This indicates that the relative wear resistance can be influenced by operating conditions. To evaluate the wear performance of a material, operating conditions must be considered in addition to the properties of the material.

It has been noted that the wear behavior of the as-received bainitic steels is differentiated by carbon content. For high carbon steels (J1 and J2), the wear rate increases with an increase in contact pressure. For low carbon steels (J4 and J5), a fall in wear rate occurred at high contact pressures. This fall leads to a superior wear resistance of low carbon steels at high contact pressures. J3, which has a carbon content at a medium level, exhibit an intermediate wear rate at high contact pressure. Such behavior with respect to carbon content is associated with mechanical properties and deformation resistance of the steels. It was found that the low wear rate of the low carbon steels at high contact pressures was achieved at the expense of great deformation.

To understand the wear performance of the steels, deformation behavior must be investigated. Under rolling/sliding conditions, deformation can be depicted in two aspects: macro and micro. The macro deformation refers to the geometric changes of Amsler rollers that can be measured with respect to dimensional changes of the specimens. The micro deformation refers to the deformation of surface and subsurface of the rollers on much smaller scales, and generally observed in optical and scanning electron microscopes. The deformation behavior in the current study was investigated in both wear tests and deformation tests. Unfortunately, the macro deformation behavior in the current study were not well defined for the specimens in the wear tests because the measurements of dimensional changes could not always reflect the geometric changes of the specimens accurately or comprehensively. In contrast, the deformation behavior of the steels was well defined in the deformation tests. To isolate deformation from wear, specifically designed deformation tests were conducted in the Amsler rig. In these tests, wear was eliminated by lubricating the contact surfaces of the Amsler rollers. The results indicate that lower carbon steels experience larger deformation than higher carbon steels (Figures 3.32 and 3.33) at the same contact pressure. This is consistent with ductility results obtained in tensile tests. A higher ductility for low carbon steels than high carbon steels indicates that low carbon steels experienced larger deformation before rupture. These results suggest that lower carbon steels would experience greater deformation than high carbon steels in rolling/sliding wear at a given contact pressure.

The difference of steels in enduring deformation before fracture may explain the variation in the relative wear resistance with contact pressure. It is known that material loss comes from the fracture of surface material. The more fracture that occurs, the more material loss, and the higher the wear rate could be. At a low contact pressure, the deformation of both high carbon and low carbon steels is low. In this case, the fracture of the surface material is determined by the strength of the material. High strength results in less fracture, thereby leading to a low wear rate. At a high contact pressure, a low carbon steel experiences much higher deformation than a high carbon steel before fracture occurs. The large deformation retards the detachment of fractured flakes from the bulk material and thereby reduced the wear rate of the material. The observation of the worn surface revealed that the a fractured flake could experienced further deformation in the subsequent wear process by rolling/sliding and overlapped by other fracture debris.

The relationship between bulk hardness and wear rate is shown in Figure 4.5 for the bainitic steels. The data presented in this figure come from all bainitic steels used in the present study, regardless of heat treatment. At each contact pressure, there is a rough trend that wear rate decreases with an increase in hardness. However, since scatter bands are very large, especially at 1220 MPa, such a trend is very weak. Generally, bulk hardness is not a strong indicator of wear resistance for these steels.

It was reported that wear resistance could be improved with an increase in impact toughness under a dry sliding condition.[248] In the current study, the wear resistance of the steels was also correlated to the impact toughness as shown in Figure 4.6. Figure 4.6 shows that no simple relationship between wear rate and toughness could be established. As the range of toughness variations is very narrow and all impact fracture happens only in a brittle mode, it would be very difficult to establish a clear relationship in this situation.

It has been seen that cooling rate has a great influence on wear resistance; faster cooling rate consistently decreases wear rate at all contact pressures investigated. This is associated with the microstructural changes caused by various cooling rates. For the high carbon steel J1, water-quenching increased the wear resistance dramatically. This effect is conspicuously demonstrated at 1700 MPa. The significant change in microstructure by fast cooling in J1 is that thin films of retained austenite have been developed at the ferrite lath boundaries, suppressing the formation of blocky retained austenite within bainite laths. In addition, needle-shaped martensite (rather than M-A islands) was produced by fast cooling. It is hypothesized that these factors contributed to an improvement in wear resistance. For J2, faster cooling changed the microstructure from lower bainite to lath ferrite plus needle-shaped martensite. Such a structure also increases wear resistance significantly (Figure 3.25). It seems that the needle-shaped martensite plays a role in improving wear resistance to some extent.

In J3 and J4, the formation of M-A islands was suppressed by fast cooling and more lath ferrite was produced at the expense of massive ferrite. These changes resulted in a decrease in wear rate of the steels. For low carbon bainitic steels, Devanathan[37] found that a 0.04%C steel with fewer M-A islands exhibited a lower wear rate than a 0.1%C steel that had more M-A islands. He proposed that the hardness difference between matrix and M-A islands possibly leads to cracking at their interface, thereby leading to higher wear rates. However, there has been no report providing direct evidence of interfacial cracking during a wear process. Under tension conditions, Xu *et* *al.*[231] found that microcracks nucleated at the M-A island/ferrite interface. In contrast, Zhang *et al.*[230] found that M-A islands deformed and failed in a ductile manner in room temperature straining.

Although both needle-shaped martensite and M-A islands contain martensite, they seem to exert opposite influences on wear resistance. The reason for that is unclear because there is no direct evidence to indicate how they act during a wear process. However, it is noted that the morphology of the needle-shaped martensite is different from that of a M-A island. The separate needles in the former may reduce local stress concentration under the wear surface and thereby improve wear resistance. Also, this structure improves the overall strength of the material, which in turn enhances wear resistance.

Despite the fact that no substantial change in microstructure for J5 has been found, the wear rate was still decreased by fast cooling. The increase in wear resistance may be associated with the increase in strength. A higher dislocation density produced by a faster cooling rate could contribute to decreasing the wear rate. No reports about the effect of dislocation density on wear resistance have been found in the literature, but there are studies regarding dislocation cell structures.[249-253] In lubricated wear, the cell walls were believed weak and could generate cracks resulting in wear particles.[253]

In summary, the following tendencies of microstructural changes have been observed with an increase in cooling rate in the current study:

1) more lath ferrite is produced with reduced massive ferrite;
2) thin films of retained austenite are developed while blocky retained austenite is suppressed;
3) carbides are suppressed; and
4) needle-shaped martensite forms.

If one associates the wear rates with these microstructural changes in the bainitic steels, it seems that lath ferrite, thin films of retained austenite and needle-shaped martensite are potentially beneficial to wear resistance whereas carbides and M-A islands may deteriorate wear resistance.

It is very significant that the water-quenched J1 demonstrates the best wear resistance of all the bainitic and pearlitic steels tested. This outstanding performance is attributed to the relatively high carbon content and the corresponding microstructure consisting of carbide-free bainite plus needle-shaped martensite. It is possible that better wear resistance could be achieved by adding more carbon to the steel if this kind of microstructure is retained.

The wear resistance of a pearlitic rail steel X136 was found to be better than all the as-received bainitic steels at each contact pressure in the investigation although the mechanical properties of X136 are quite similar to those of the as-received J1 (see Tables 2.2(b), 3.5 and 3.4). This result agrees with the finding in some studies[11,21,25,34] that with similar hardness (or mechanical properties), the wear resistance of pearlitic steel is better than bainitic steel. Garnham and Beynon[23] attributed the better wear resistance of pearlitic steels to a structural alignment. They found that in pearlitic steels, a large fraction of carbide plates were aligned in the rolling direction and exposed to the surface due to deformation. The exposed carbide plates improve wear resistance. Once the alignment breaks down, the wear resistance of pearlitic steels with respect to bainitic steels is more likely to depend on the bulk hardness. Ichinose, *et al.*[35] also attributed the better wear resistance than bainite to the carbide distribution at the surface.

Devanathan and Clayton[254] investigated the relationship between wear rate and contact pressure for pearlitic and bainitic steels. They found that at contact pressures in the range 500 — 1220 MPa at a slide/roll ratio of 35%, the wear rate of bainitic steels increases linearly with an increase in contact pressure while a parabolic trend is shown for the pearlitic steel, Figure 4.7. In an earlier study, the parabolic relationship for pearlitic rail steels was also reported by Danks.[214] With this trend, Devanathan and Clayton[254] inferred that at higher contact pressure than 1220 MPa, the wear resistance of bainitic steels could be better than that of pearlitic steels. To gain some insight of this issue, the wear tests were carried out at 1450 MPa and 1700 MPa for bainitic steels and 1700 MPa for a pearlitic steel in the present study. The results have shown that even at 1700 MPa, the as-received bainitic steels wore faster than the pearlitic steel, especially for high carbon steels. However, the water-quenched J1 showed a better wear resistance than the pearlitic steel. In the investigation by Devanathan and Clayton,[254] the bainitic steels shows a structure of granular bainite or carbide-free bainite. The difference in the water-quenched J1 is that needle-shaped martensite was produced. Furthermore, for the pearlitic steel in the current study, a linear relationship is established between wear rate and contact pressure (Figure 3.28), inconsistent with the parabolic relationship reported by Devanathan and Clayton[254] or Danks.[214] For the bainitic steels, although a linear relationship is established at contact pressures between 500 and 1220 MPa, it cannot be extended to higher contact pressures (Figure 3.26).

A strong effect of carbon content in bainitic steels was shown in the study by Devanathan and Clayton,[254] where wear rate increased with an increase in carbon content. In the current study, however, no consistent effect of carbon content on wear rate was found as the relative wear resistance varied with contact pressure. As far as the microstructure is concerned, a general trend found in the current study is that the wear resistance is improved by more lath ferrite and fewer M-A islands, suggesting that the more carbide-free bainite that is produced, the better the wear resistance. This is also in disagreement with the observation that granular bainite produced in the low carbon steel possesses better wear resistance than carbide-free bainite.[37] Since more steels and a wider range of microstructural changes and contact pressures have been involved in the current study, the previous results can now be viewed in a broader context.

The wear rates of the bainitic steels are compared with those of pearlitic steels in Figure 4.8. The steels presented in this figure were tested at 1220 MPa with a slide/roll ratio of 35%. The X136 is one of the highest wear resistant steels in the pearlitic steel group. Generally speaking, the J-series bainitic steels investigated in the present study are comparable to the high hardness pearlitic steels. The wear rates of bainitic steels investigated by Devanathan[37] (designated as D-bainite) fall within the overall bainitic steel scatter band. The wear rate of pearlitic steels is sensitive to hardness, whereas the link between wear rate of bainitic steels and hardness is tenuous. A similar pattern was reported by Clayton *et al.*[36] under pure sliding conditions, but in their study the scatter bands were much narrower for both bainitic and pearlitic steels.

The austenitic manganese steel has shown superior wear resistance to all the other steels tested. This can be attributed to its tremendous work hardening capability under heavy loading conditions. Such work hardening produces a high strength layer near the working surface, which in turn protects the surface from further deterioration, whether from wear or deformation. The analysis of worn surfaces indicates that no Type III wear occurred. During wear testing, it was found that small pits were produced on the surface at the beginning of the test. The number of pits increased as the test proceeded, but eventually saturated. Continuing the test, the debris produced early on were removed subsequently and no more pits produced. Meanwhile, the rough worn surface arising from previously formed pits was rolled repeatedly and the surface became smoother and smoother. This process is obviously different from the Type III wear mode.

The deformation behavior under rolling/sliding conditions was investigated in the current study. High carbon steels (J1 and J2) demonstrated much better resistance to deformation than did low carbon steel (J4). This is consistent with the strength and ductility of materials under tension conditions. Tensile tests revealed that the high carbon bainitic steels are able to withstand high stress and experience small deformation before fracture. It is inferred that under rolling/sliding conditions, the steels behave the same way. High strength and low ductility suggests high deformation resistance.

The Amsler deformation behavior of the bainitic steels in the current study is compared with that of the bainitic steels investigated in a previous study.[37] Figure 4.9. shows that J1 and J2 exhibit a similar deformation resistance to the D0.52%C steel and is much better than the D0.1%C steel. Although the carbon contents of J1 and J2 are quite different from that of D0.52%C steel, their hardnesses are almost the same. The hardnesses of the as-received J1, air-cooled J2 and D0.52%C steel are 40, 41 and 40 HRC, respectively. The deformation resistance of the as-received J4 is lower than the D0.04%C steel although they have granular bainite. There is a slight difference in hardness between the as-received J4 (27 HRC) and the D0.04%C steel (29 HRC).

The deformation of the bainitic steels was also compared with that of the CrMo pearlitic steels, Figure 4.10. In this figure, the deformation is expressed in terms of diameter change of the rollers with a formula $(D_0 - D)/D_0$, where D_0 and D are the initial diameter and the diameter during test, respectively. J1 and J2 demonstrate the best deformation resistance and the as-received J4 shows the most severe deformation. This figure also shows that the deformation resistance increases with an increase in hardness.

The above comparison suggests that the Amsler deformation behavior is associated with tensile properties. High deformation resistance could be achieved with high strength and low ductility. Hardness could be an indicator for judging deformation resistance, irrespective of microstructure.

4.4. INTERACTION BETWEEN TOP AND BOTTOM ROLLERS

Although all bottom rollers were made from the same material, i.e. W5, their wear rates varied with the change in material of the top rollers (Figure 3.30). This suggests that the wear performance of a material is not only determined by its own properties, it is also a function of its mating material. *Wear ratio* is used to indicate the relationship of wear between the top and bottom rollers. Here, the *wear ratio* is defined as the wear rate of the top roller divided by that of the bottom roller. The greater the ratio (if it is greater than 1), the faster the top roller wears than the bottom roller. If the wear ratio is less than 1, the top roller wears slower than the bottom roller.

Figure 4.11, showing the wear ratios for the bainitic steel/W5 pairs at 1220 MPa, indicates that the bainitic steels always wore faster than the pearlitic steel W5 since the wear ratios are greater than 1 in all cases. This figure seems to suggest that a faster cooling rate of the top roller would reduce the wear ratio or the difference in wear rate between the top and bottom rollers. A similar effect of water quenching of the top rollers was found at the other contact pressures, as shown in Figure 4.12. At 1220 MPa, the wear ratio appears a function of carbon content in each heat treatment category of the top rollers. Lowering carbon content could increase the difference in wear rate between the two rollers. The lower the carbon content of the top rollers, the faster it wears with respect to the bottom roller. At the other contact pressures as shown in Figure 4.12, the lower carbon steel J4/W5 pair showed higher wear ratios than the higher carbon steel J1/W5 pair, similar to that at 1220 MPa. It seems that there might be some relationship between wear ratio and heat treatment and carbon content of the top rollers. However, a big difference in wear ratio was revealed in Figure 4.11 and Figure 4.13 between J4 and J5 although their carbon contents are quite similar. Furthermore, the strengths and ductility of J4 and J5 are also very close. It suggests that the variation in wear ratio cannot simply be interpreted in terms of carbon content or mechanical properties. Microstructure could be another factor considered to influence the wear interaction between the top and bottom rollers. It is noted that the microstructure of the as-received J4 is granular bainite and that the as-received J5 exhibits a microstructure of carbide-free bainite. Probably, various microstructures respond differently to wear under a given condition. However, no conclusions can be drawn in this study since only two steels were compared. Further investigations are needed to get more insight into this issue.

The wear ratios of all the materials at the contact pressures tested are illustrated in Figure 4.13. Figure 4.14 highlights the wear ratios of the as-received bainitic steels at various contact pressures. Figures 4.12 and 4.14 indicate that for the bainitic steel/W5 pairs, the wear ratio decreases as the contact pressure increases. X136/W5 and Mn/W5 pairs exhibited fairly low wear ratios in comparison with the bainitic steel/W5 pairs (Figures 4.13(c) and (e)).

Figures 3.30 and 3.31 demonstrate that a high wear rate of the top roller does not always result in a high wear rate of the bottom roller. For the as-received J5/W5 pair, for instance, the wear rates of the bottom roller were lower than that for the as-received J4/W5 pair although the wear rates of J5 were higher than that of J4 at the contact pressures investigated (Figures 3.31 (a), (c) and (e)). This gave rise to a higher wear ratio for the J5/W5 pairs than that for the J4/W5 pairs. Although the wear rate of the bottom rollers varied inconsistently with that of the top rollers, Figure 3.31(c) appears to show that heat treatment of the top rollers did not change the wear rate of the bottom rollers much at 1220 MPa.

Generally speaking, the wear rate of the bottom rollers is far less than the top rollers for the bainitic steel/W5 pairs. Only for the water-quenched J1/W5 pair, was the wear rate of the top roller close to that of the bottom roller and at 1700 MPa the wear rate of the top roller was slightly lower than that of the bottom roller (Figures 3.31(a), (c) and (e)). For the Mn steel/W5 pair, the difference in wear rate between both rollers was very small (Figures 3.31(c) and (e)). The wear ratio was 1.5 at 1220 MPa and 0.6 at 1700 MPa (Figures 4.13(c) and (e)). For these pairs, the wear rates were also very low, no severe wear or Type III wear was generated. In the current study, there was not the situation where the wear rate of the bottom roller was much higher than that of the top roller. This suggests that the total wear rate of a pair would be controlled by the wear of the top roller and that the wear rate of the bottom roller was constrained by the top roller.

The above analysis indicates that under rolling/sliding wear conditions, the wear rate of an individual specimen is dependent on both its own properties and the properties of the counterpart roller. Even though the bottom rollers are always from the same material, their wear rate varies with the change in material of the top rollers. In the current study, on one hand, no consistent pattern has been found as to how the top roller material influences the wear rate of the bottom roller. On the other hand, the wear resistance of top rollers is obviously influenced by heat treatment, microstructure and mechanical properties. The wear rate of a material is also closely associated with operating conditions. At various contact pressures, the relative wear resistance could be changed. Wear ratio is an indicator of relative wear performance of the materials in a wear pair. When a wear system comprises two materials, the wear ratio will tell which material wears faster than the other.

4.5. WEAR MECHANISM

For the bainitic steels, Type III wear was generated on all wear specimens under the conditions used in this investigation. The analysis of worn surfaces has shown that the wear features on the pearlitic bottom rollers were always the same as that on the top rollers. The observation of worn surfaces during wear tests reveals that wear begins on both top and bottom roller surfaces simultaneously and at the same contact areas. This result is consistent with what was observed by Devanathan.[37] It was also found that if the steels for the top rollers had the same composition, the initiation period was increased by a faster cooled top roller. Hereafter, the initiation period refers to the period from the beginning of test to the point when surface break-down just begins. It appears that the initiation period is influenced by the properties of the top roller. Since the material strength is increased with an increase in cooling rate, it is suggested that raising strength can improve the resistance to surface break-down. However, the simultaneous break-down of both top and bottom roller surface obscure the effect of strength because the strengths of the bottom rollers are different from those of top rollers. If strength were the factor that determines the break-down of surface, only one surface, for which the material strength is lower, should be broken down first. However, this is not observed. The simultaneous break-down of both surfaces would probably be attributed to three body abrasive wear. In the current study, the abrasive debris found on the worn surface

(Figure 4.15) indicate that abrasive wear is involved in the rolling/sliding process. It is possible that once one surface is broken down, the resultant debris could immediately penetrate the other surface with very high localized pressure. As a result, the surface of the other rollers begins to break down in a very short time. The three-body wear was also addressed by Devanathan[37] for the rolling/sliding wear where the debris produced by wear act as foreign particles.

Rolling/sliding wear is also associated with the deformation of materials. High capability of deformation would defer the fracture of material and thereby reduce the rate of weight loss. In Type III wear, significant deformation occurs on the worn surface. An example of the surface deformation is shown in Figure 4.16 by grooving traces in the rolling direction. The overlap of debris seen in the figure is a result of deformation. Once debris is formed, it may not be detached from the bulk material immediately. Rather, it could be rolled several times before detaching. During this time, new debris will be formed and deformed in the same process. As a result, an overlap of deformed debris is produced. Large debris could further be broken down to smaller pieces during rolling/sliding process as shown in Figure 4.17. A severe overlap suggests a slow rate of material detachment and a resultant low wear rate.

The phenomenon that wear rates of top rollers are far higher than their paired bottom rollers was also reported by other investigators.[15,23,37] However, the reason for such behavior was not clear. As far as the mutual influence of both rollers in an Amsler wear test was concerned, Clayton and Danks[255] conducted a series of experiments to determine the effect of the hardness differential of mating rollers on wear behavior. In that investigation, a CrMo rail steel was heat treated to provide a wide range of hardnesses 10 — 45 HRC. Then the steel was used to make both top and bottom rollers and the tests were conducted at a contact pressure of 1220 MPa with a slide/roll ratio of 35%. The results, given in Table 4.4, indicate that in most cases, the top roller wore faster than the bottom roller. The only tests where the top roller wore slower than the bottom roller were REW numbers 6 and 13. In addition, in REW 9, the wear rates of the both rollers were very close. From these results, no consistent effect of hardness on wear rates of both top and bottom rollers were observed. Clayton and Danks concluded that the overall picture is not obviously self consistent as to how hardness difference between mating rollers affects the wear behavior of any individual steel.

In the current study, the hardness of the bottom rollers was 32 HRC and that of the bainitic steels was in a range 26 — 44 HRC. Whether the hardness of the top roller is greater or less than that of the bottom roller, the bottom roller always wore slower than the top roller for the bainitic steel/W5 pairs. Therefore, no consistent effect of hardness on wear rate of the mating rollers was found, in agreement with that obtained by Clayton.[255] Alternatively, it was suspected that the different wear rate arises from the position of the rollers rather than material properties. To answer this question, Clayton[255] conducted another set of tests. In these tests, the same material was used for both top and bottom rollers, the only difference was the roller size. The results indicated that the smaller roller wore faster, whether it was on the top or the bottom position. This suggests that the size of roller does have an influence on wear behavior of the rollers. However, it was failed to use this to explain why in some cases the bigger bottom rollers wore faster than the smaller top rollers found both in the current study and that by Clayton and Danks.[255] The factors which would lead to a faster wear of the top roller seem to be far more complicated than expected.

It was found in some wear tests of the current study that at the beginning of the test, the weight of the bottom roller had increased while that of the top roller decreased. This suggests that material transfer may occur during the test. The debris detached from the top roller could be deposited on the bottom roller, reducing the weight loss of the bottom roller and consequently leading to a lower wear rate of the bottom roller. Therefore, material deposit might be a reason for lower wear rate of bottom rollers. This may partially explain why the wear ratio decreased as the wear rate of the top roller decreased. A decreased wear rate of the top roller indicates less deposition of wear debris of the top roller on the bottom roller and thereby reduces the possibility that the wear rate of the bottom roller would be reduced by the deposition of the debris from the top roller. In this situation, the difference in wear rate caused by the deposition between the rollers could be reduced. However, to fully understand this phenomenon, further study must be carried out.

Table 4.1 B_s (°C) of J1 through J5 Using Empirical Equations and Experimental Data

	Steven[220]	Bodnar[221]	Bodnar[222]	Devanathan[37]	Experimental
J1	424	513	457	358	438
J2	401	476	524	314	
J3	377	466	486	418	
J4	394	473	519	451	553
J5	418	484	572	361	

Table 4.2 Determination of b Values for the Bainitic Steels with Various Heat Treatments

	σ_y^{as}	σ_u^{as}	σ_y^{wq}	σ_u^{wq}
b_0	.4796935e+03	-.4214021e+03	.2667381e+03	.1807664e+03
b_1	.2262690e+03	.5155186e+03	.3202742e+03	.6012168e+03
b_2	-.1050664e+03	.1333770e+03	-.4232959+02	-.1525977e+01
b_3	.1073784e+02	.8989594e+01	.2979286e+01	.4328491e+01
b_4	-.9658105e+02	.1325625e+03	-.3707373e+02	-.1130664e+02

Key:

σ_y^{as} — yield strength of as-received steels
σ_u^{as} — ultimate tensile strength of as-received steels
σ_y^{wq} — yield strength of water-quenched steels
σ_u^{wq} — ultimate tensile strength of water-quenched steels

Table 4.3 Estimated Strengths in Comparison with Measured Strengths Using Empirical Equations

	σ_y		$\hat{\sigma}_y$		σ_u		$\hat{\sigma}_u$	
	ksi	MPa	ksi	MPa	ksi	MPa	ksi	MPa
J1-as	122.8	847	122.8	847	197.2	1,360	197.2	1,360
J2-as	120.4	830	120.4	830	167.0	1,151	167.0	1,151
J3-as	114.8	792	114.8	792	167.5	1,155	167.5	1,155
J4-as	104.6	721	104.6	721	137.0	945	137.0	945
J5-as	93.5	645	93.5	645	130.4	899	130.4	899
J1-wq	168.1	1,159	168.1	1,159	237.3	1,636	237.3	1,636
J2-wq	155.6	1,073	155.6	1,073	204.8	1,412	204.8	1,412
J3-wq	138.5	955	138.5	955	182.4	1,258	182.4	1,258
J4-wq	122.0	841	122.0	841	150.2	1,036	150.2	1,036
J5-wq	124.5	858	124.5	858	150.5	1,038	150.5	1,038

Key: as — as received
wq — water quenched
σ — measured values
$\hat{\sigma}$ — estimated values

Table 4.4 Wear Rate of the Amsler Rollers with Variations in Hardness for a CrMo Steel

		TOP ROLLER			
		A (45)	B (28)	C (16)	D (10)
BOTTOM	E (45)	*REW 1* 46/45 230/78 **I**	*REW 2* 27/42 60000/13000 **III**	*REW 3* 15/40 87000/6500 **III**	*REW 4* 9/41 45000/2900 **III**
	F (28)	*REW 5* 45/28 31000/19000 **III**	*REW 6* 28/29 16000/26000 **III**	*REW 7* 16/27 20000/12000 **III**	*REW 8* 10/26 129000/65000 **III**
	G (16)	*REW 9* 43/19 17000/16000 **III**	*REW 10* 26/15 119000/35000 **III**	*REW 11* 15/15 128000/25000 **III**	*REW 12* 10/16 91000/18000 **III**
	H (10)	*REW 13* 46/0 4300/11000 **III**	*REW 14* 28/7 44000/26000 **III**	*REW 15* 16/6 107000/23000 **III**	*REW 16* 10/0 124000/17000 **III**

Test Nomenclature

REW Test Number
Upper Roller Hardness/Lower Roller Hardness (Rc)
Upper Roller Wear Rate/Lower Roller Wear Rate (μg/m)
Wear Type

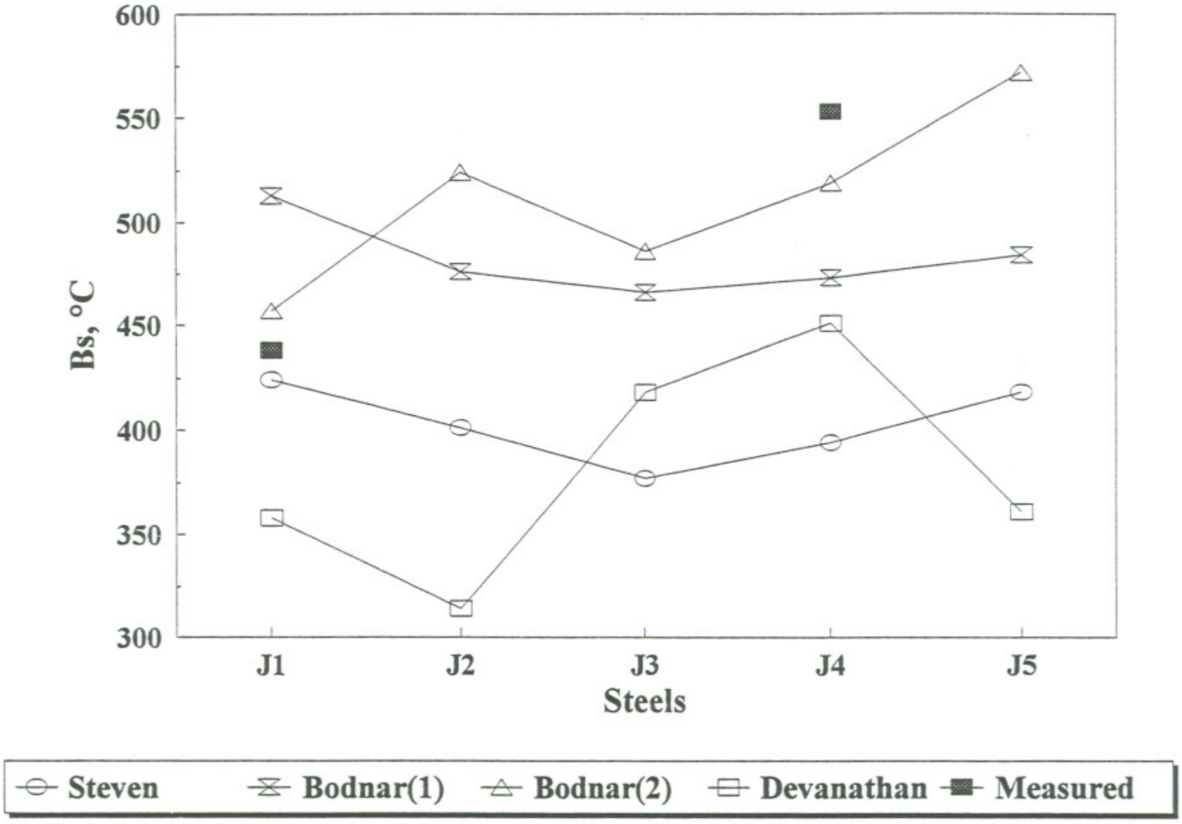

Figure 4.1 B_s of J1 through J5 from empirical equations and experiments

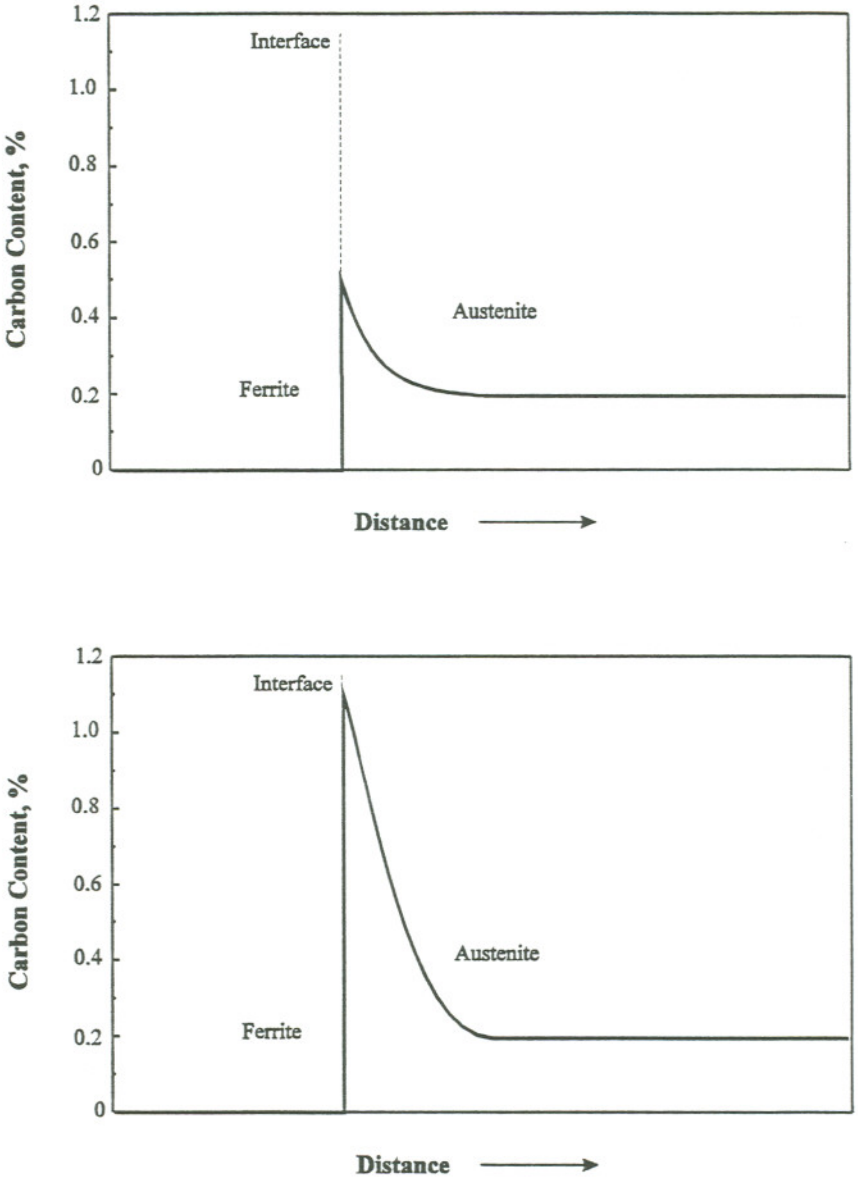

Figure 4.2 Carbon concentration at the austenite/ferrite interface

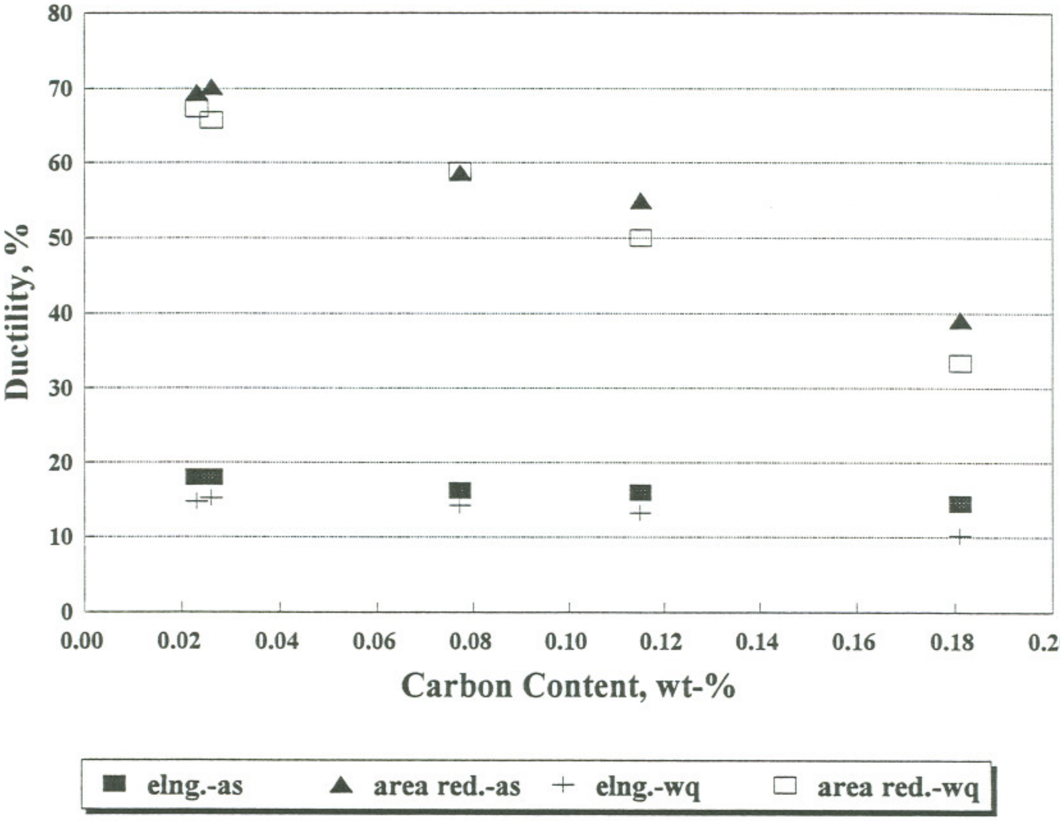

Figure 4.3 Effect of carbon content on ductility

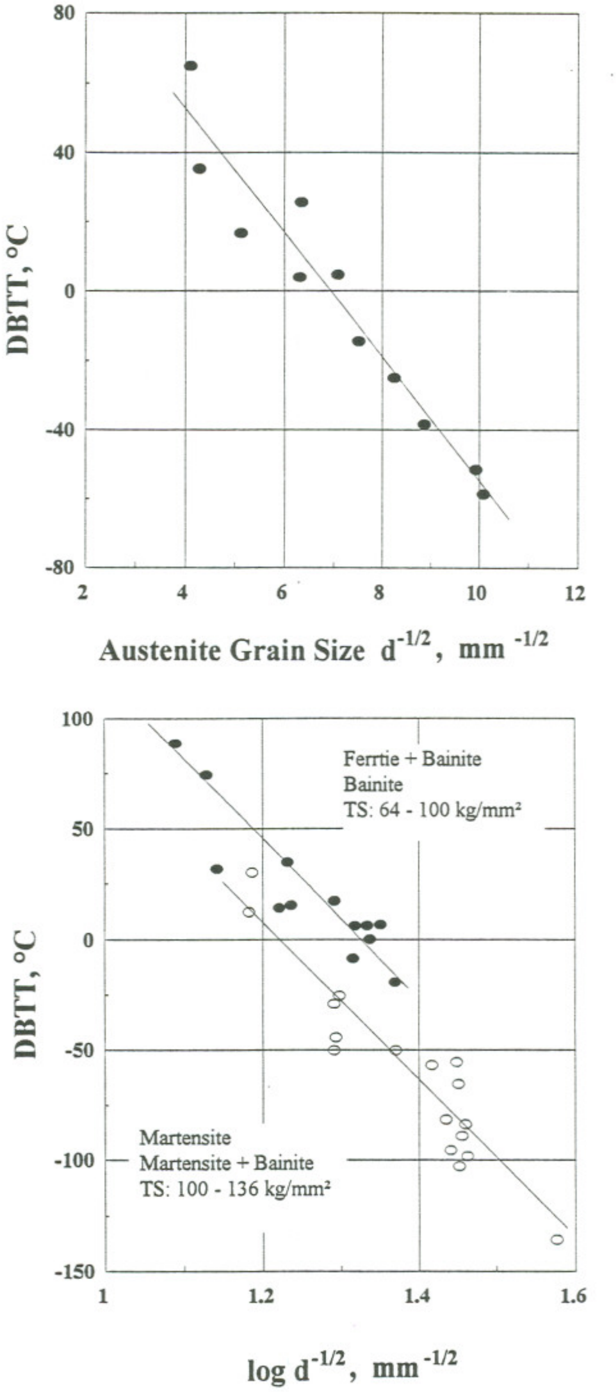

Figure 4.4 Effect of grain size on toughness
(a) DBTT vs austenite grain size[50]
(b) DBTT vs packet size[120]

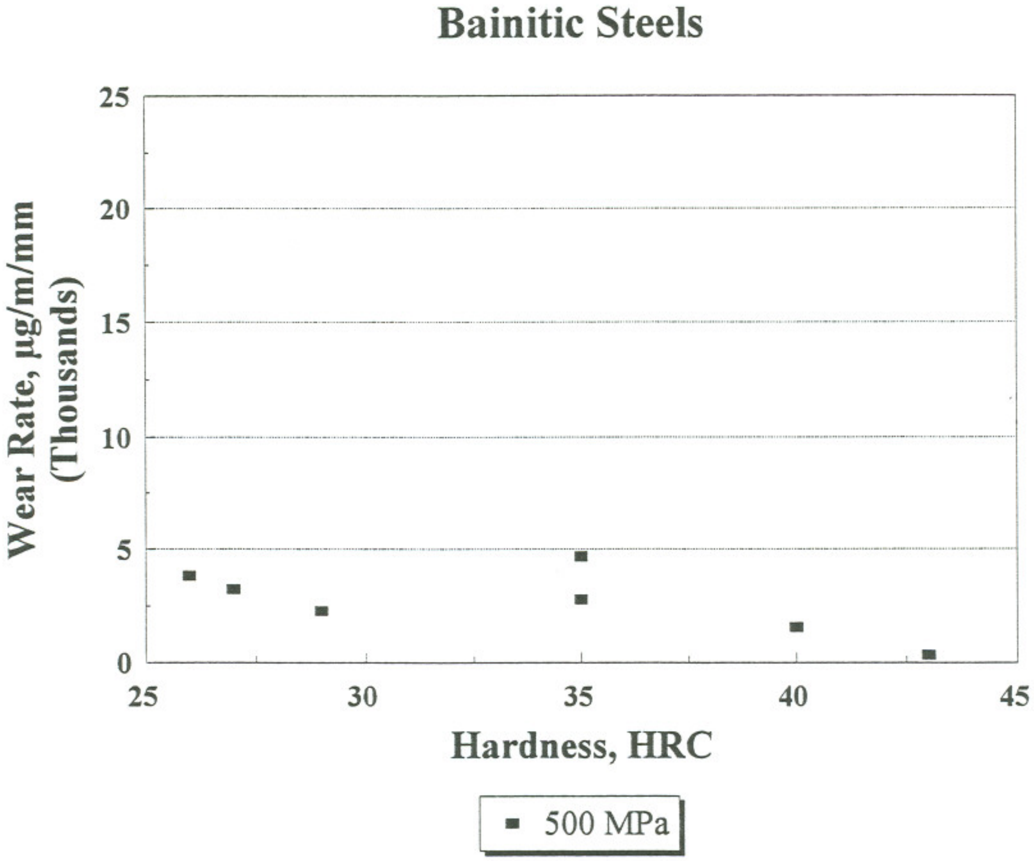

Figure 4.5 Relationship between hardness and wear rate
(a) 500 MPa

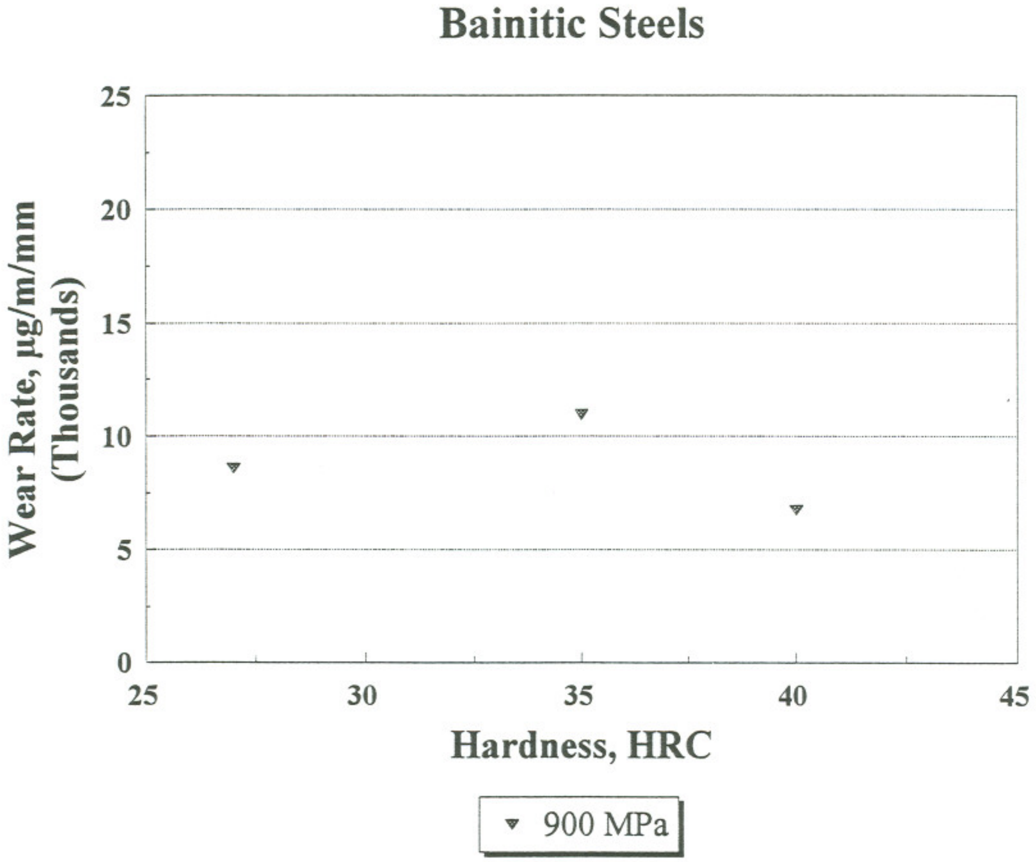

Figure 4.5 Relationship between hardness and wear rate
(b) 900 MPa

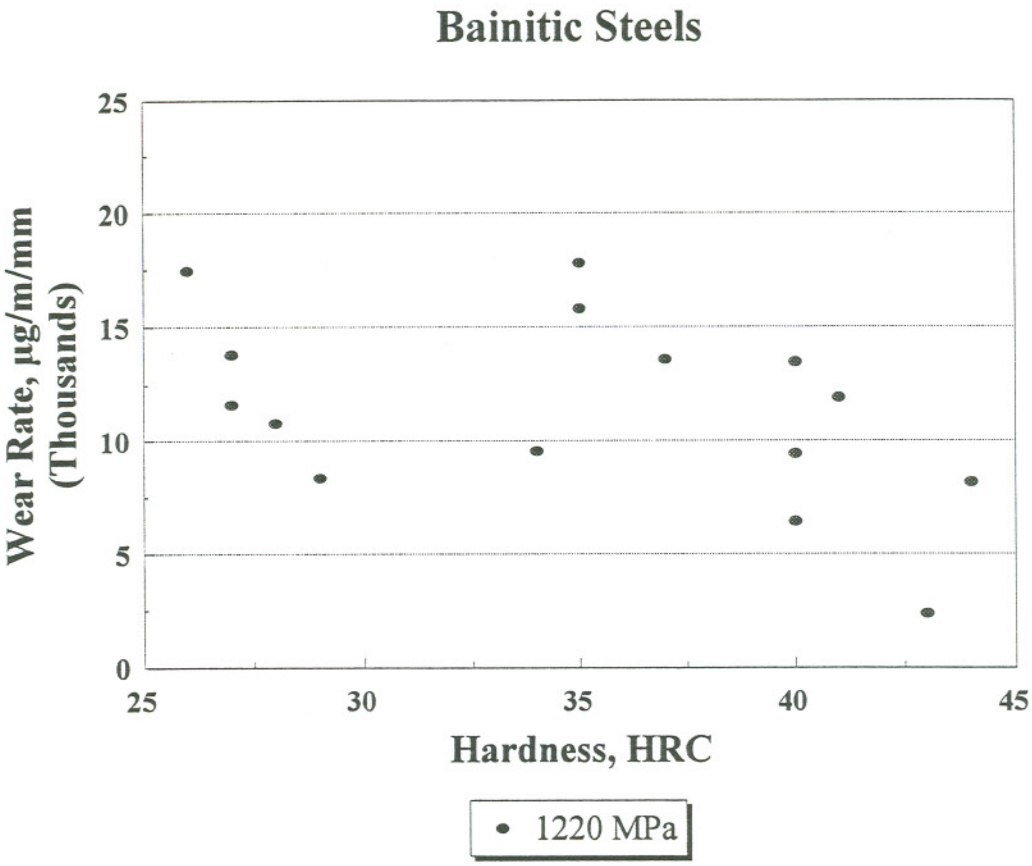

Figure 4.5 Relationship between hardness and wear rate
(c) 1220 MPa

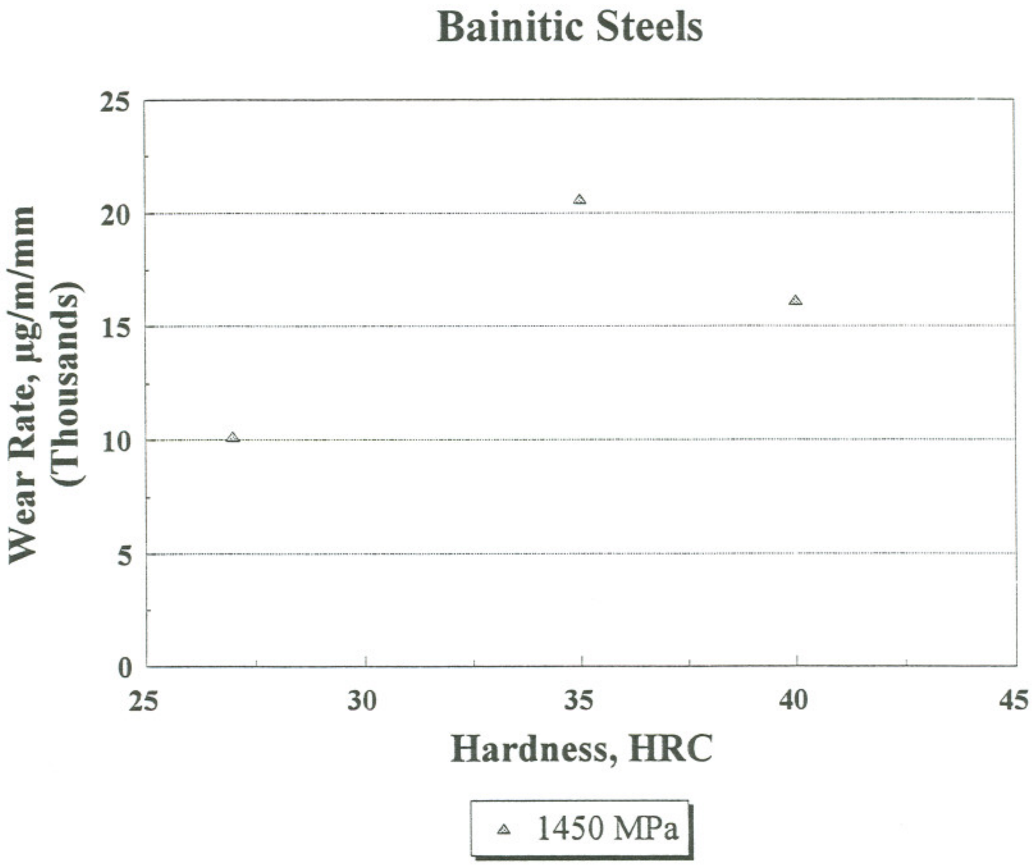

Figure 4.5 Relationship between hardness and wear rate
(d) 1450 MPa

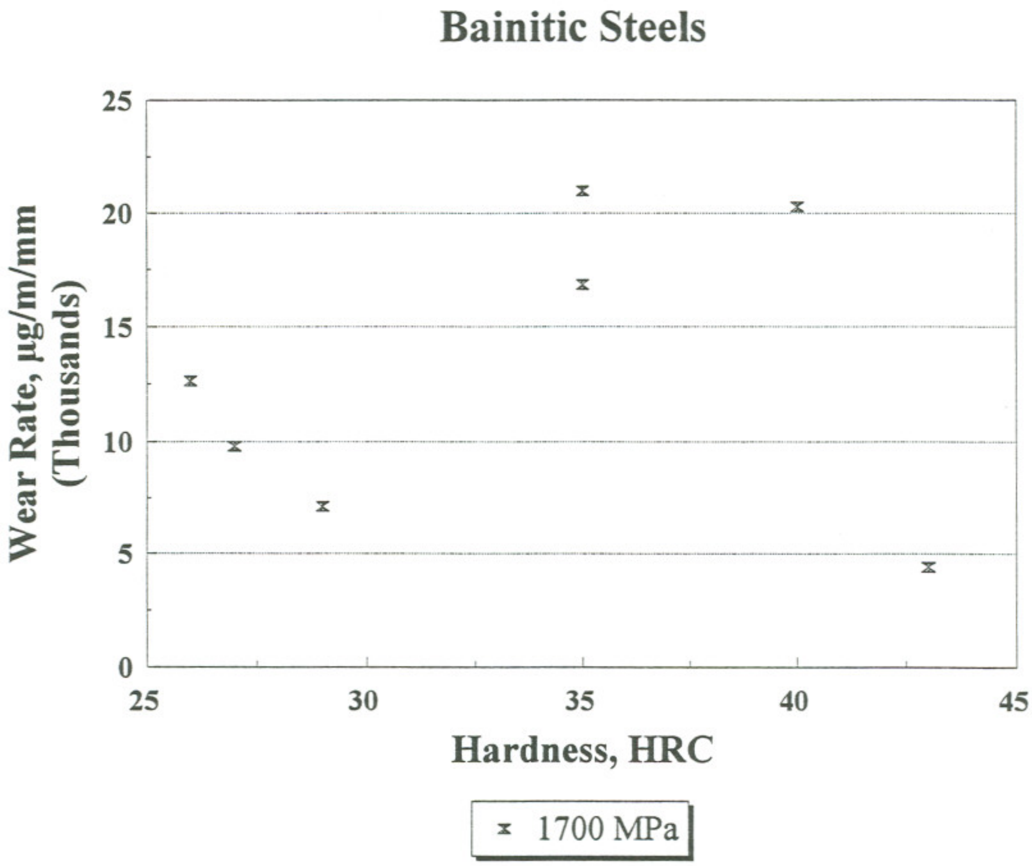

Figure 4.5 Relationship between hardness and wear rate
(e) 1700 MPa

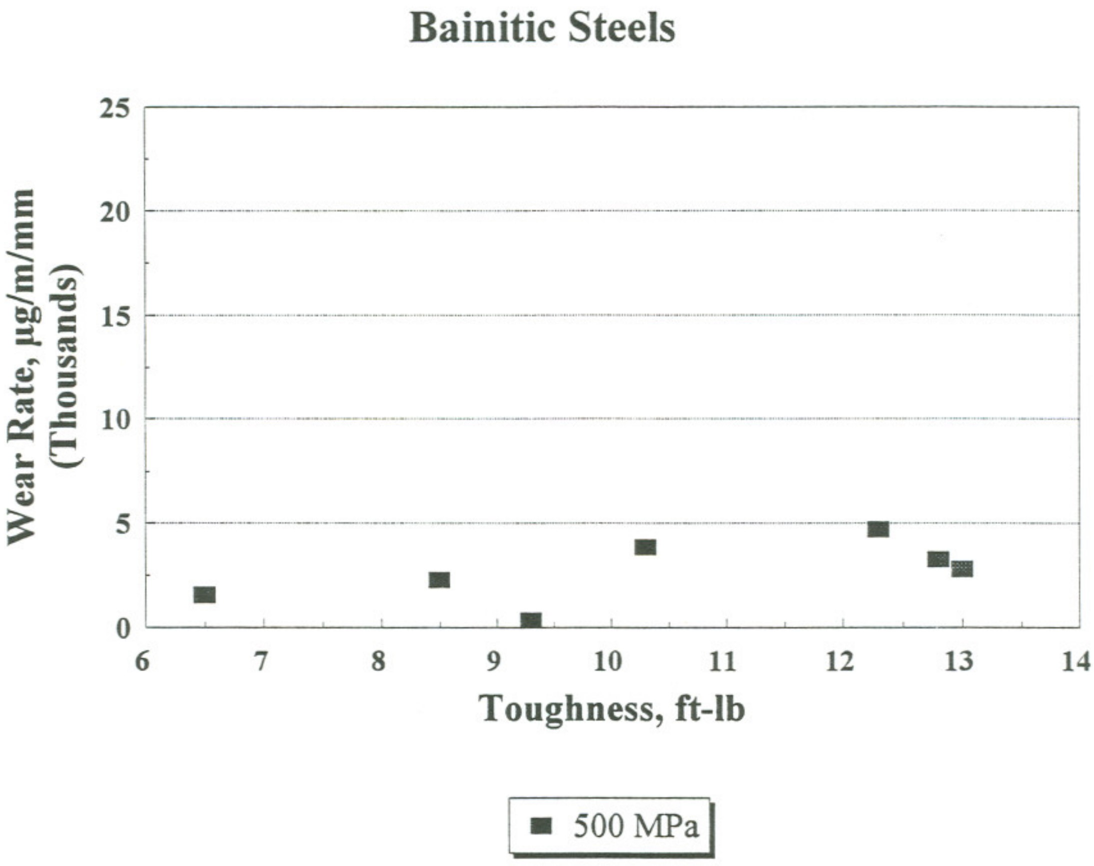

Figure 4.6 Wear rate against toughness for the bainitic steels
(a) 500 MPa

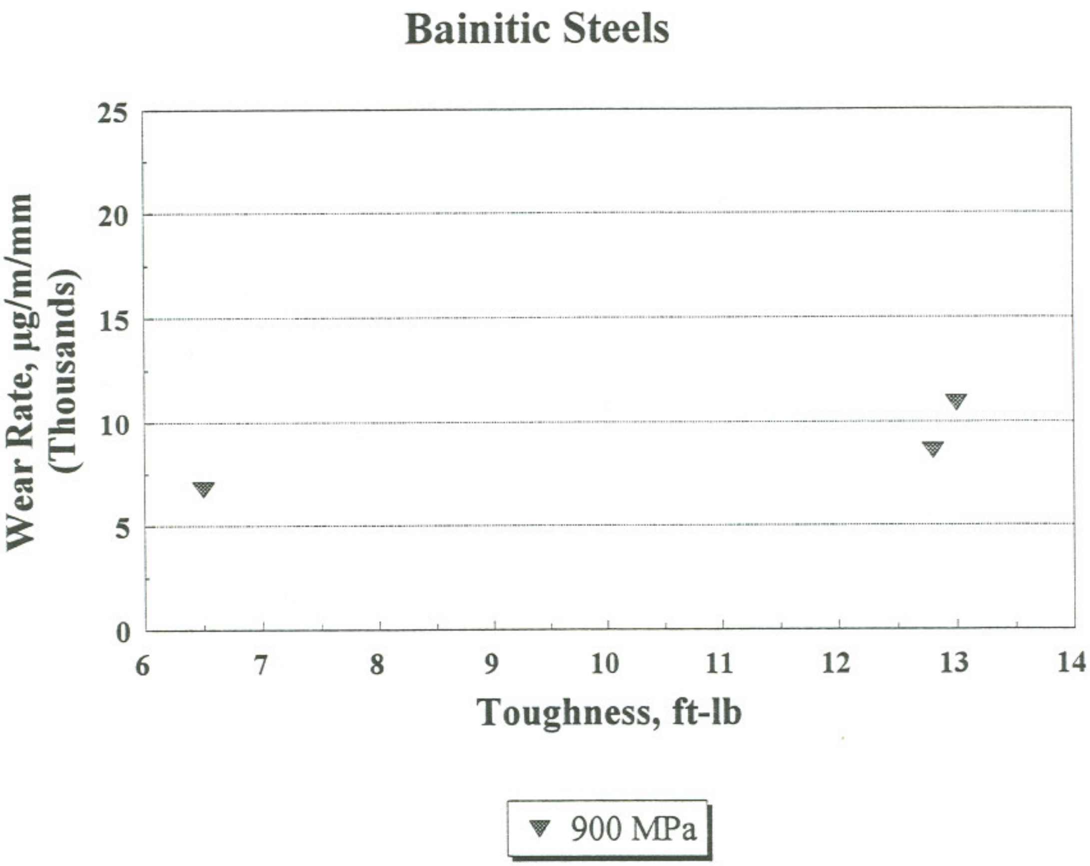

Figure 4.6 Wear rate against toughness for the bainitic steels
(b) 900 MPa

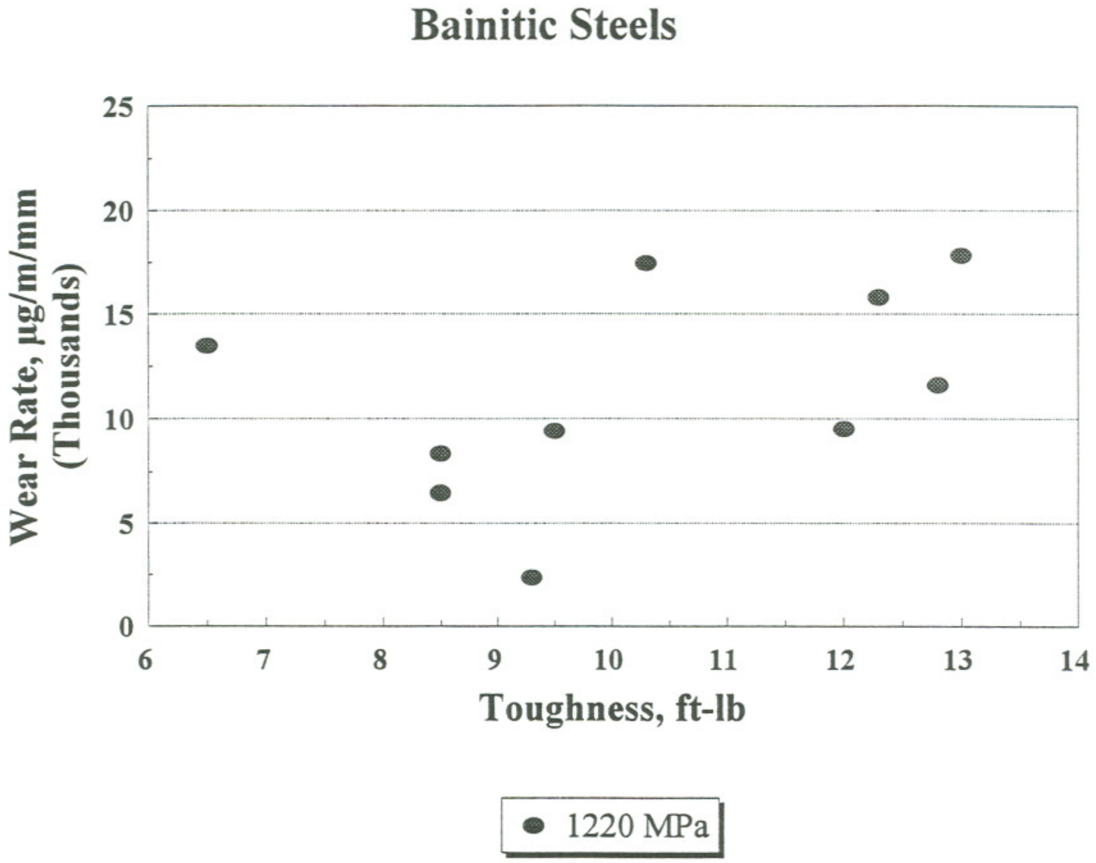

Figure 4.6 Wear rate against toughness for the bainitic steels (c) 1220 MPa

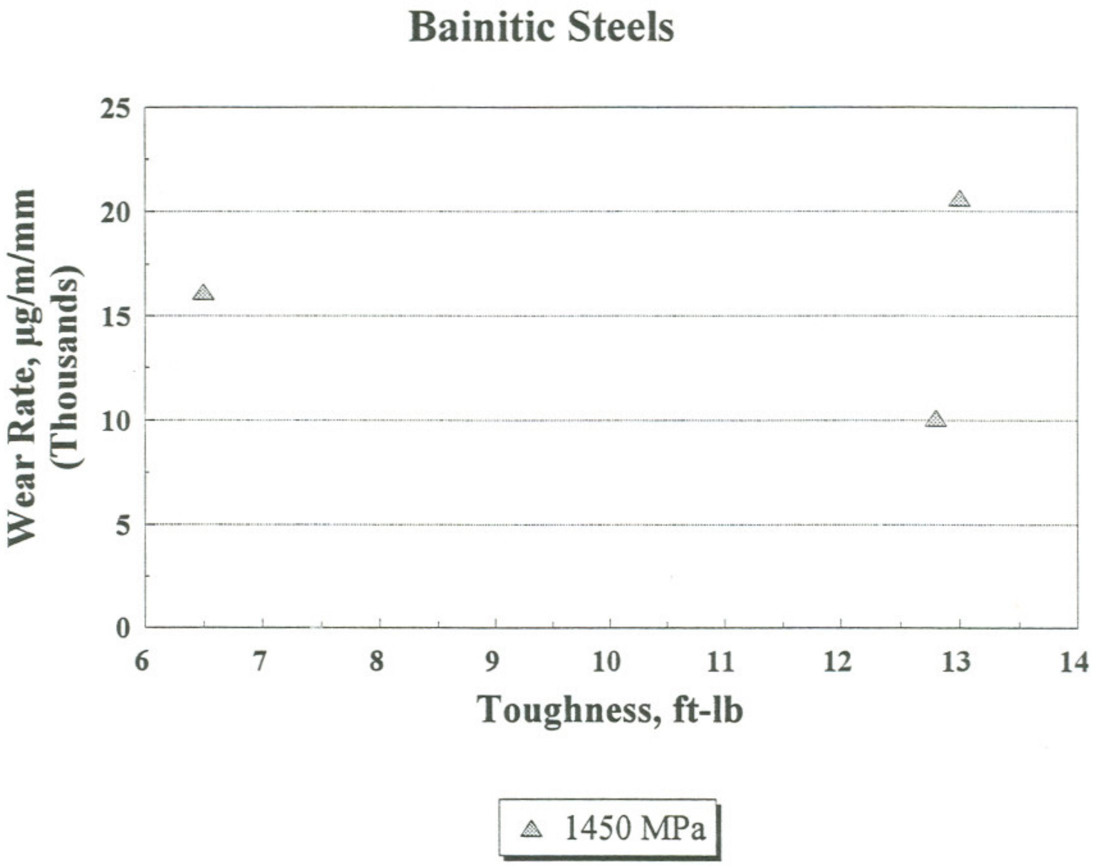

Figure 4.6 Wear rate against toughness for the bainitic steels
(d) 1450 MPa

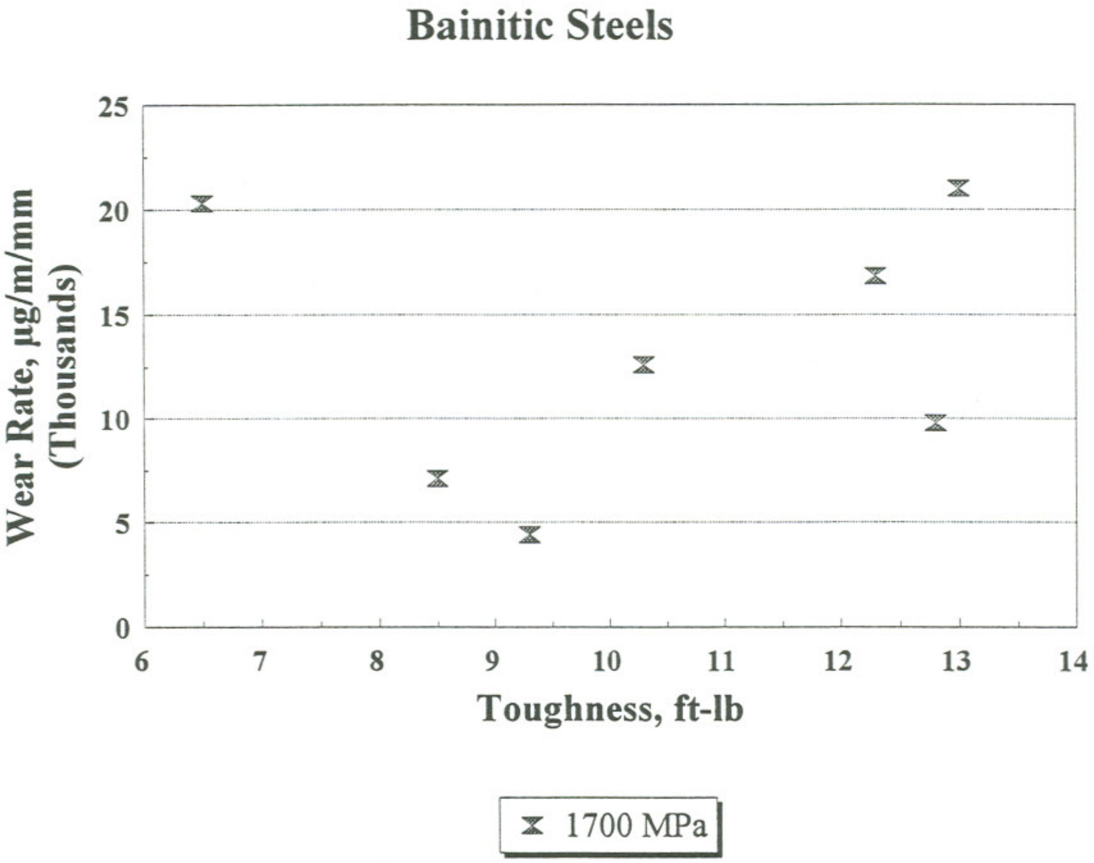

Figure 4.6 Wear rate against toughness for the bainitic steels
(e) 1700 MPa

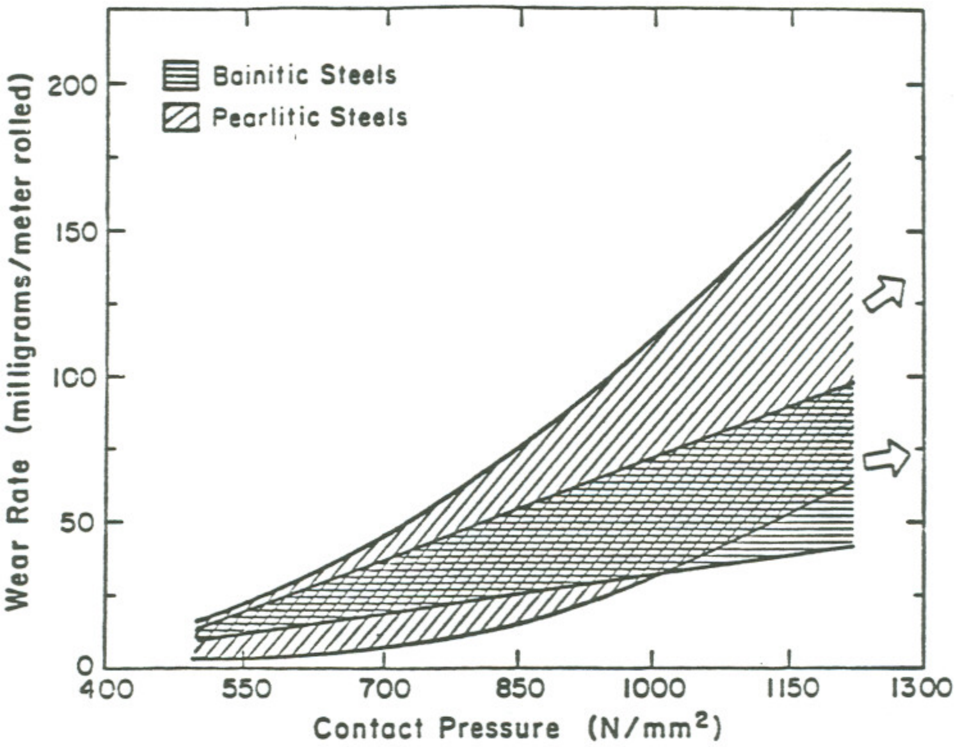

Figure 4.7 Wear rate vs contact pressure for bainitic and pearlitic steels

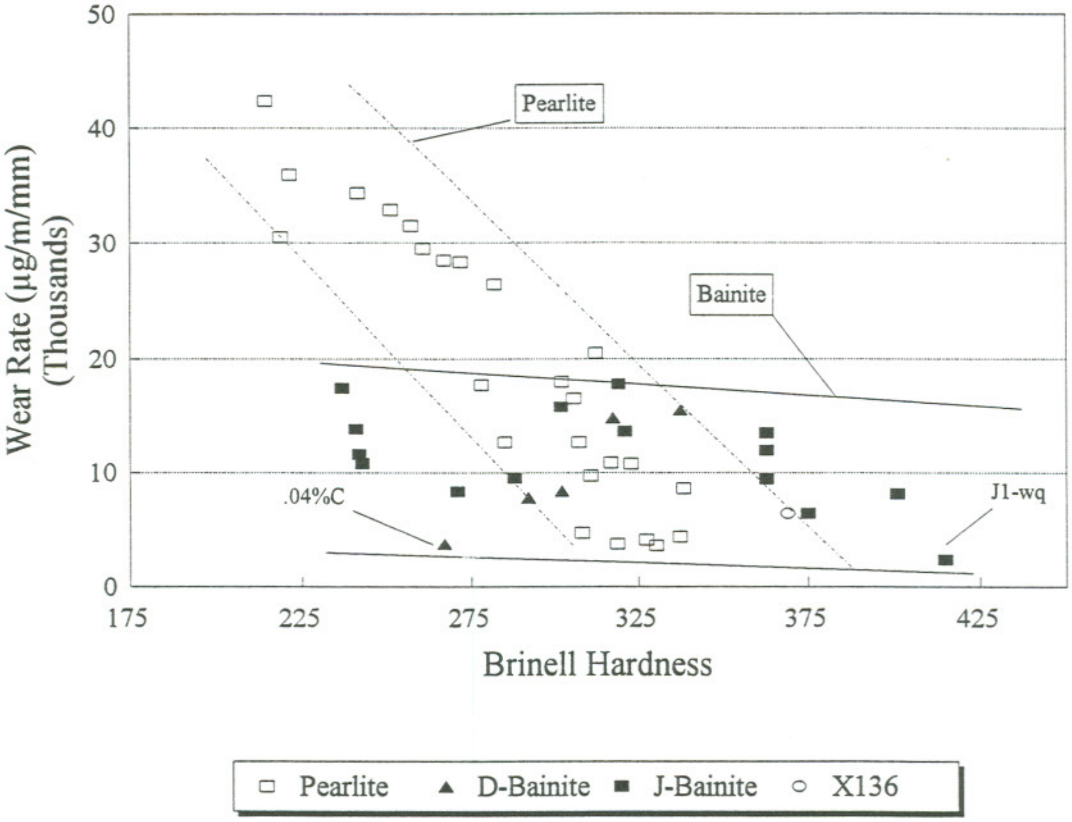

Figure 4.8 Effect of hardness on wear rate

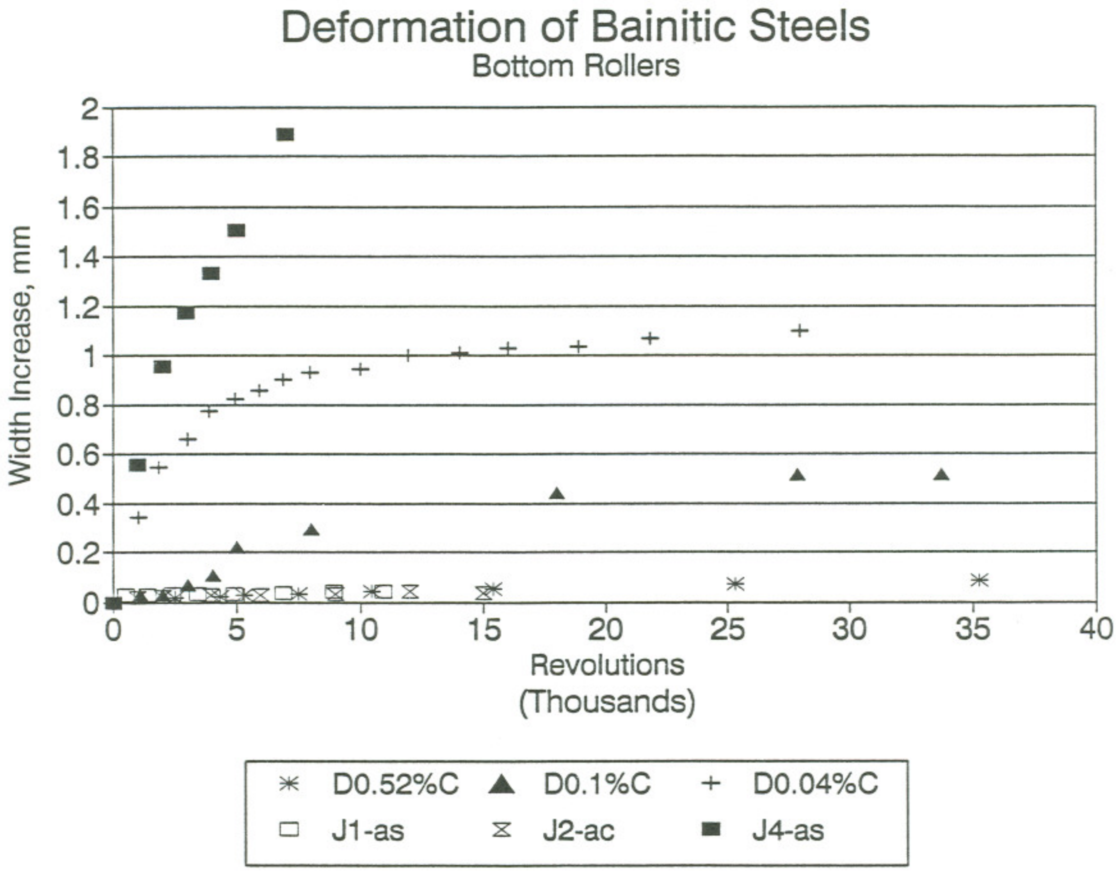

Figure 4.9 Deformation of bainitic steels

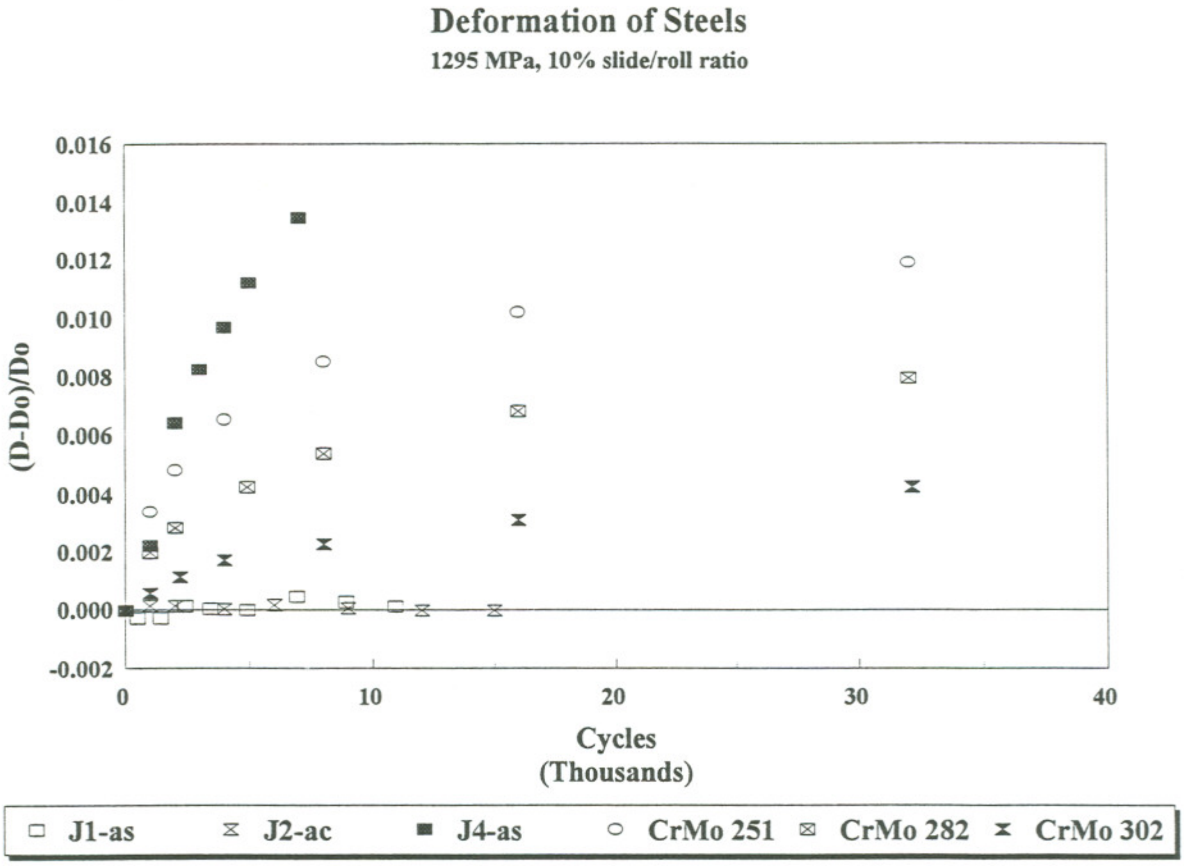

Figure 4.10 Comparison of deformation between bainitic and pearlitic steels

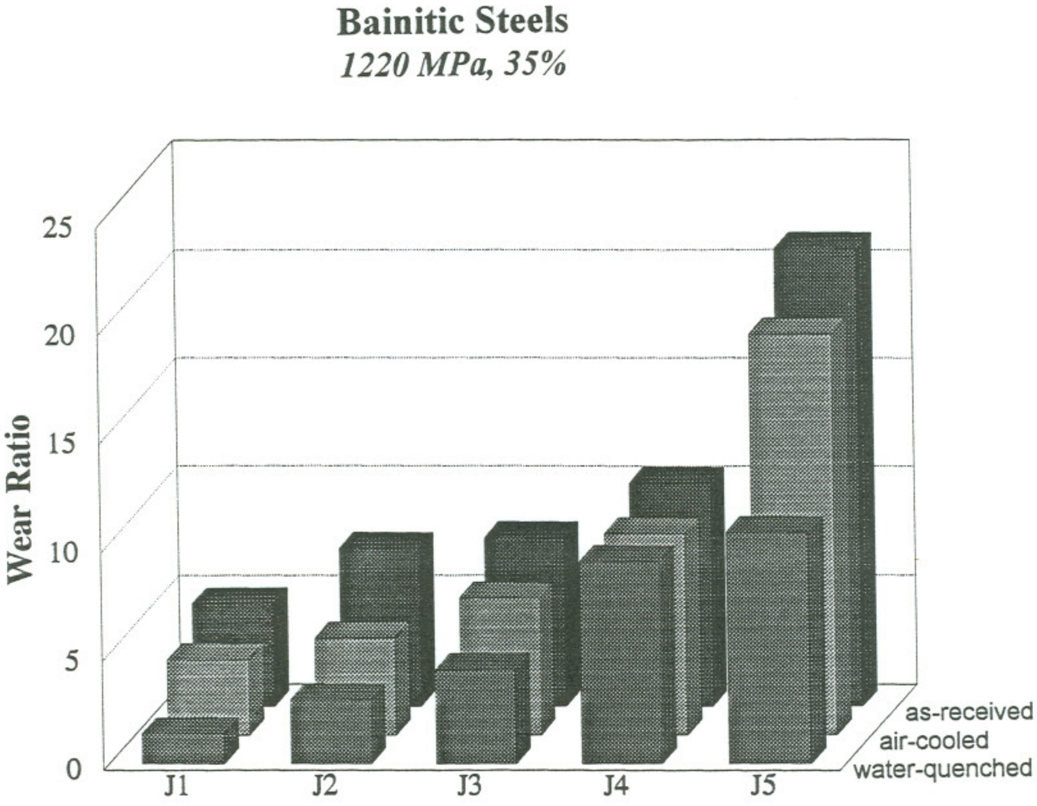

Figure 4.11 Wear ratio of the bainitic steels at 1220 MPa

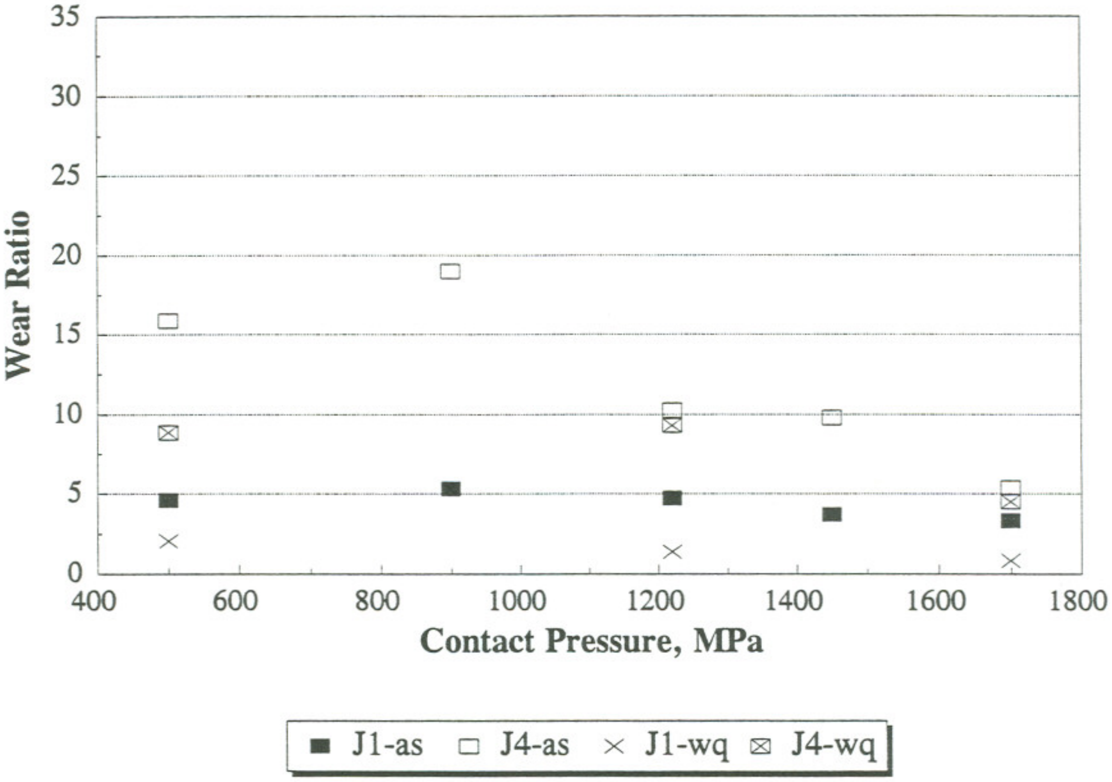

Figure 4.12 Effect of water-quenching on wear ratio

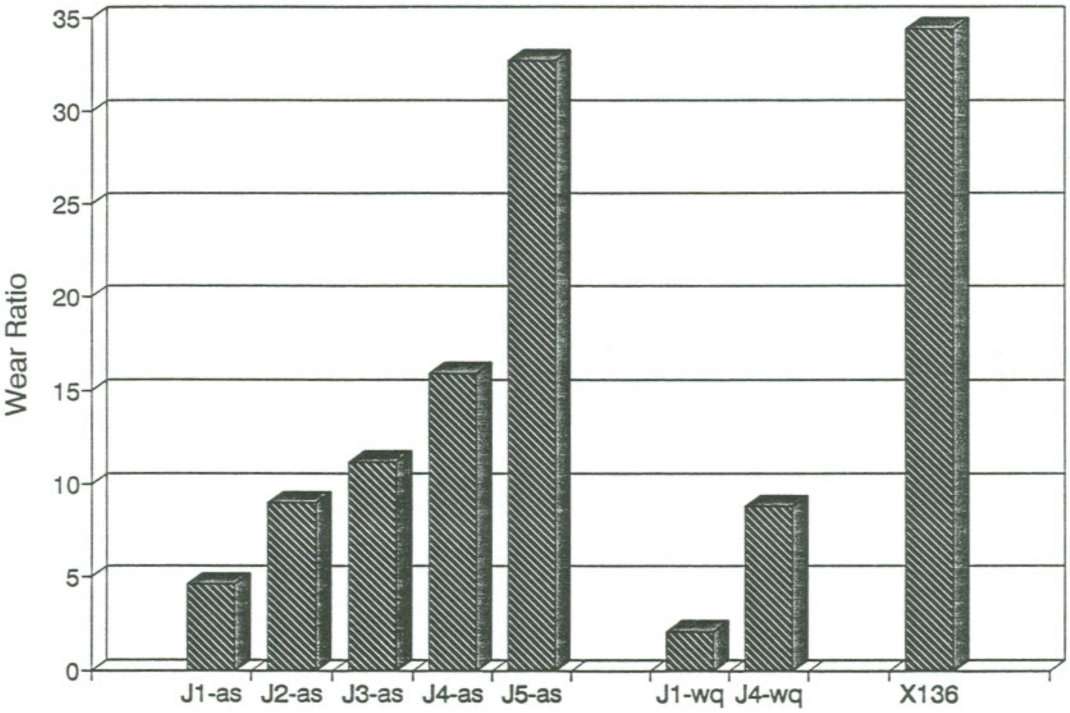

Figure 4.13 Wear ratio at various contact pressures
(a) 500 MPa

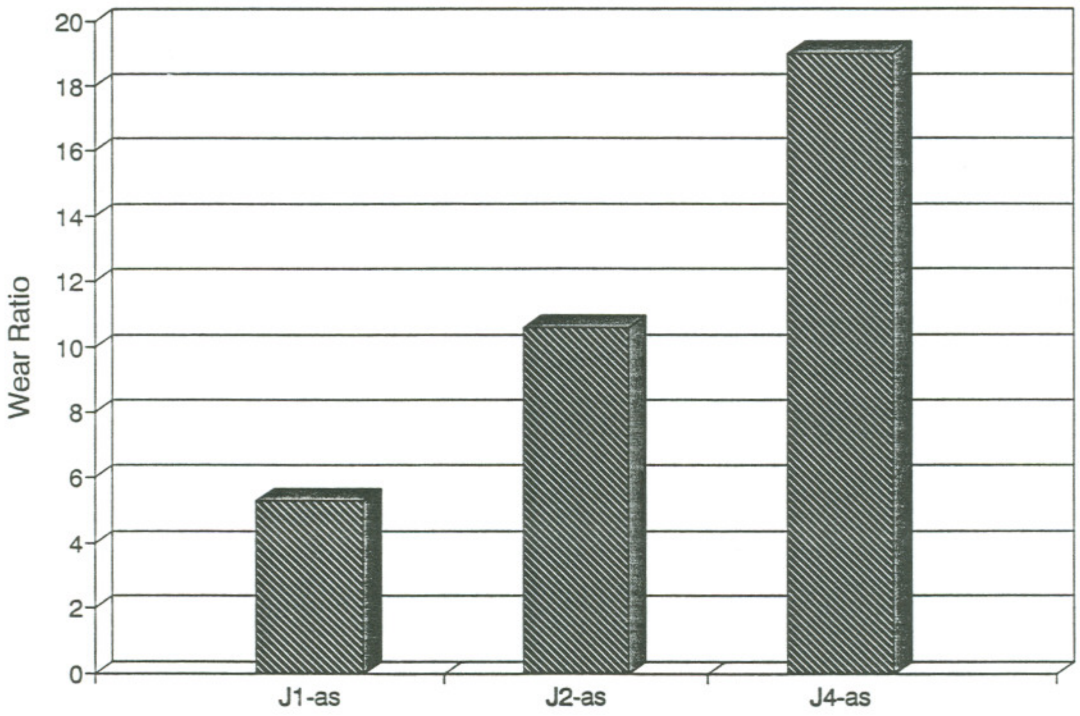

Figure 4.13 Wear ratio at various contact pressures
(b) 900 MPa

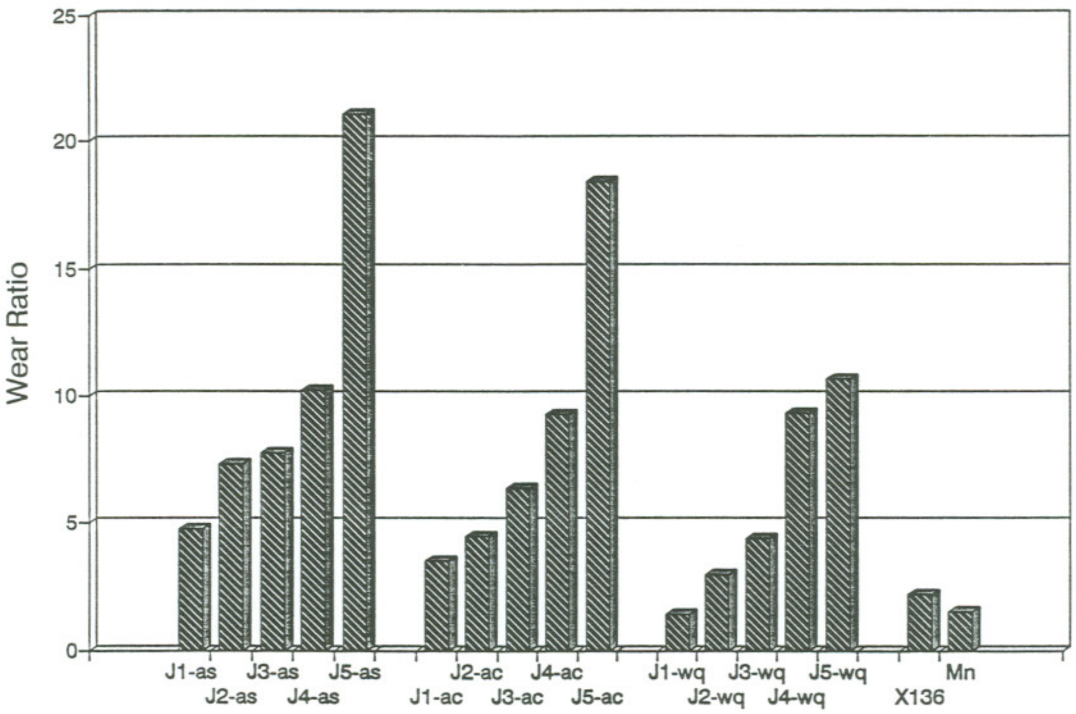

Figure 4.13 Wear ratio at various contact pressures
(c) 1220 MPa

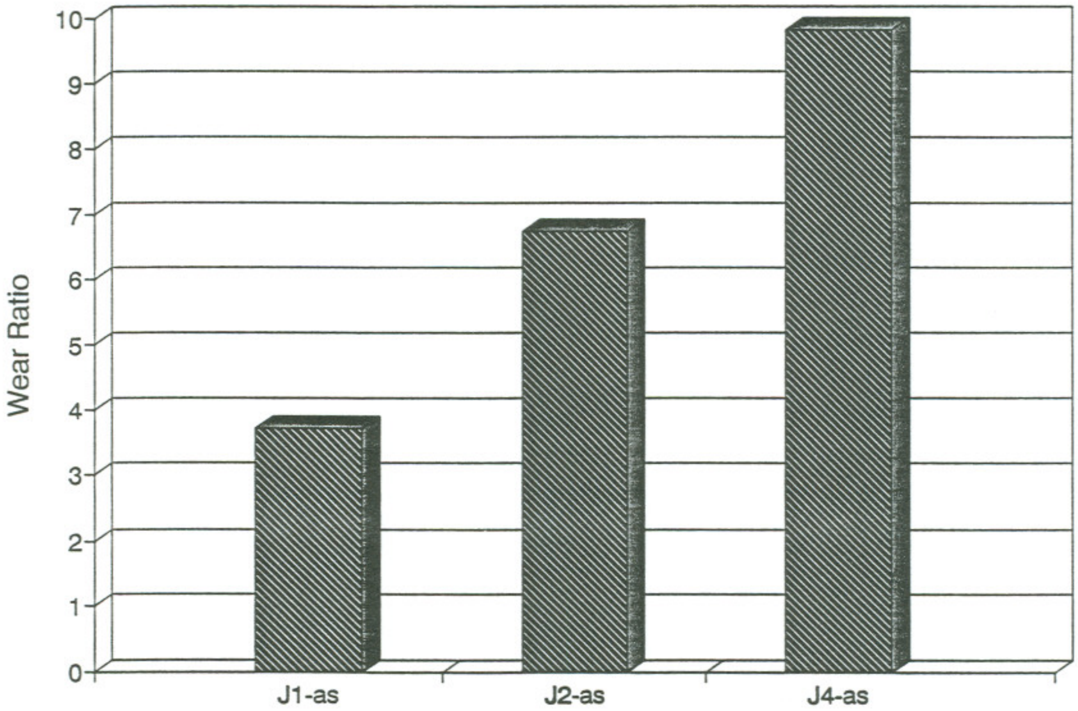

Figure 4.13 Wear ratio at various contact pressures
(d) 1450 MPa

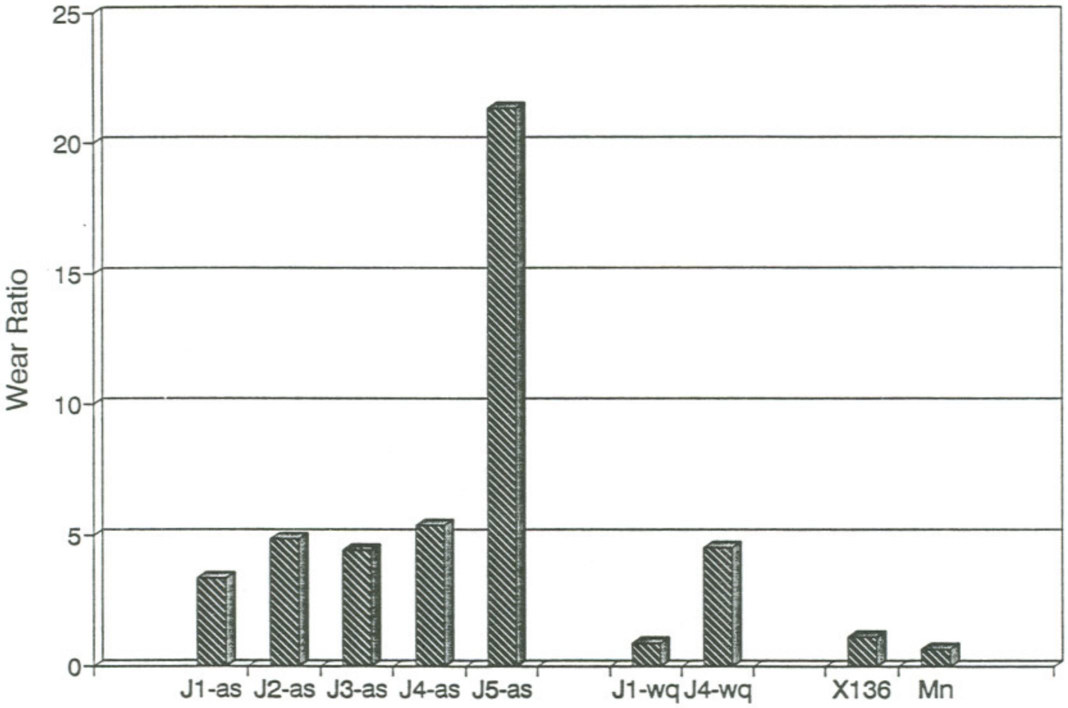

Figure 4.13 Wear ratio at various contact pressures
(e) 1700 MPa

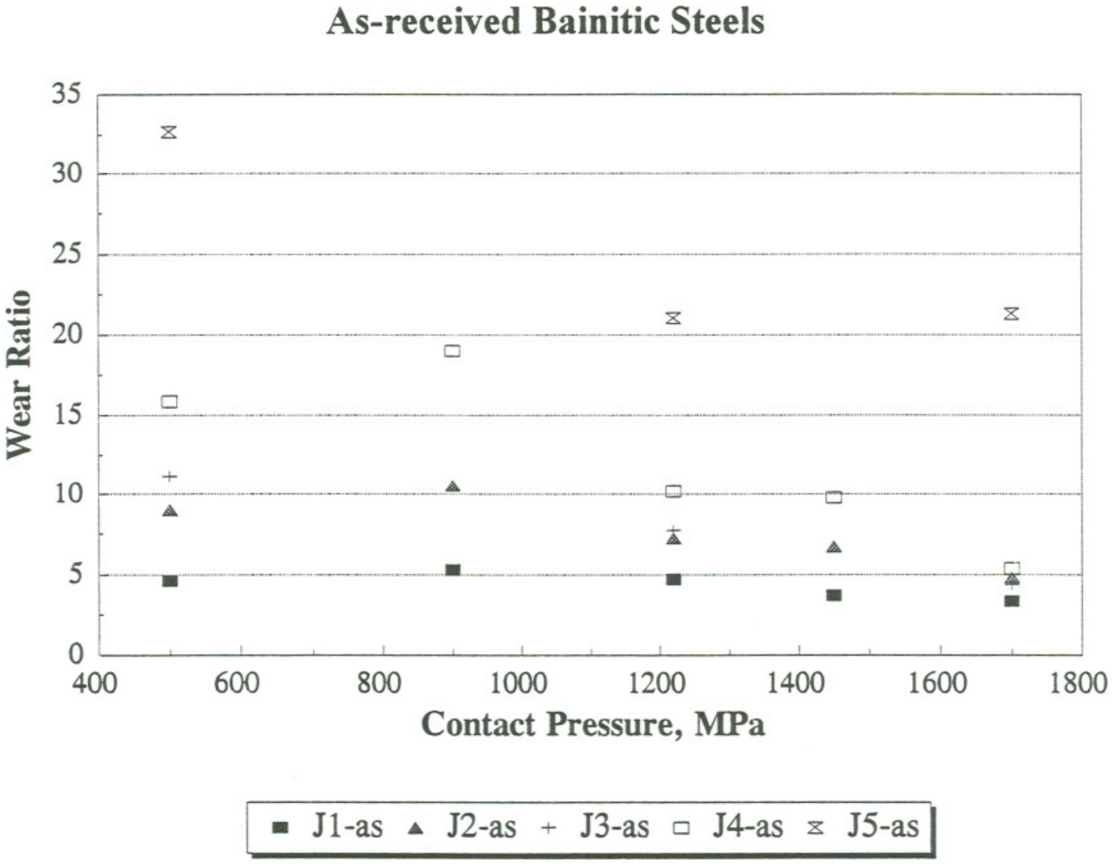

Figure 4.14 Effect of contact pressure on wear ratio of the as-received bainitic steels

Figure 4.15 Abrasive debris formed during rolling/sliding wear

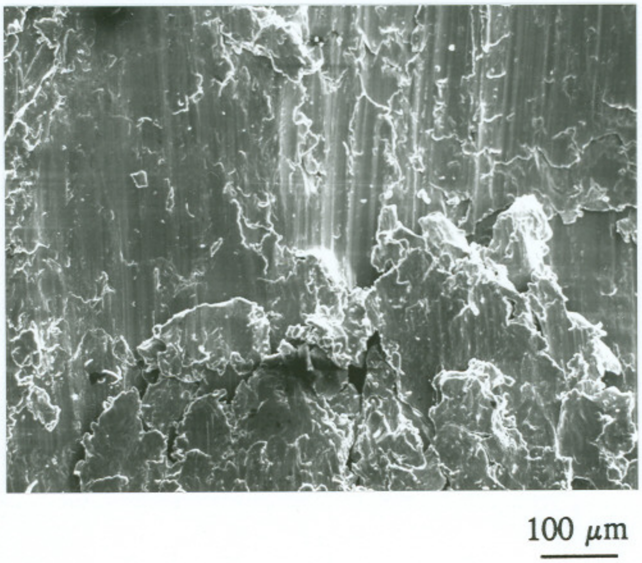

Figure 4.16 Deformed wear surface

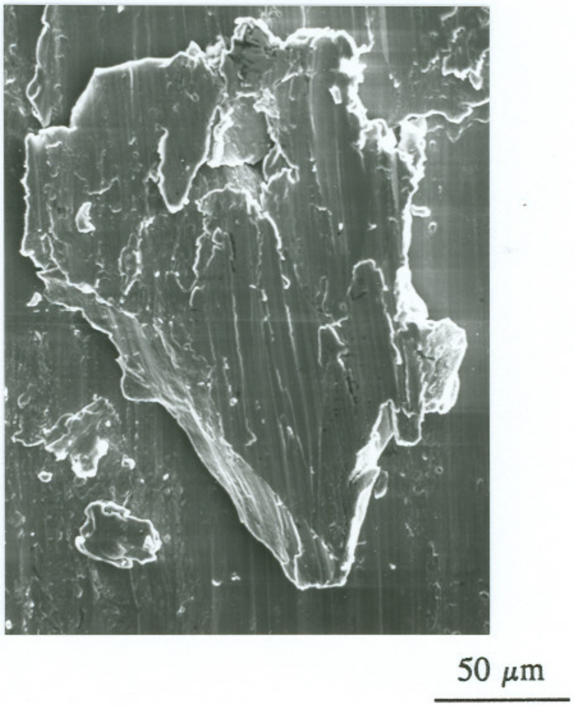

Figure 4.17 A fractured flake with severe deformation

CHAPTER 5

EXPERIMENTAL STEEL J6

5.1. ALLOY DESIGN

Steel J6 was developed on the basis of the investigations of the first five experimental bainitic steels J1 through J5. Of those steels, the water-quenched J1 exhibited the best overall properties in terms of mechanical properties and wear performance. Analysis has suggested that carbon is a predominant element in controlling the properties and that a microstructure consisting of carbide-free bainite and needle-shaped martensite is favorable.

Because of the superior performance of J1, its composition was modified to further improve the wear resistance. The carbon content was increased to 0.26%. To prevent the precipitation of carbides, Si was increased to 1.8%. The additions of Mn and Cr remained the same as in J1. A chemical analysis was carried out on both liquid and solid steel and the results are given in Table 5.1.

5.2. EXPERIMENTAL PROCEDURES

5.2.1. Manufacturing of Steel J6

Steel J6 was made in a vacuum induction furnace by Bethlehem Steel Corporation. An ingot, approximately 9"×9"×16" in dimension and about 500 lb in weight, was soaked at 2350 °F (1288 °C) for at least 2 hours and then rolled in 23 passes to a 3" × 3" square bar. The finishing rolling temperature was 1620 °F (882 °C).

5.2.2. Heat Treatment

The steel was investigated under two heat treatment conditions: as-received and water-quenched. The *as-received* condition refers to the hot-rolled condition referred to above. For the *water-quenched* condition, the steel was re-austenitized at 920 °C for 15 minutes and then quenched in water.

5.2.3. Microstructural Observations

The microstructural characterization was carried out using an optical microscopy, SEM and TEM. For the optical metallography, specimens were etched with 2% Nital and observed in a Nikon Epiphot microscope. The microstructure of the steel was also observed in a Zeiss scanning electron microscope using the metallographic specimens with an accelerating voltage of 20 kV. The TEM specimens were prepared as described in Section 2.3 and the microstructure investigated in a Hitachi H800.

5.2.4. Chemical Analysis with EDS

To investigate the element distribution in a banded structure found in the steel, the chemistry of the as-received J6 was analyzed using EDS in SEM with an accelerating voltage of 10 kV. A non-window mode was used in collecting specimen spectra and the ZAF correction employed in a semi-quantitative analysis of element concentrations.

5.2.5. Hardness Measurement

The hardness of the steel was measured on the Rockwell C scale on the bulk material or an Amsler roller as described in Chapter 2. The microhardness tests were carried out on the Knoop scale with loads of 100, 500 and 1000 grams, respectively, on the metallographic specimens.

5.2.6. Testing of Mechanical Properties

The tensile tests were conducted by Koon-Hall testing corporation, complying with ASTM standard E8-91.[209] The V-notch Charpy impact tests were conducted at room temperature on the as-received and water-quenched steels in accordance with ASTM standard E23-92.[210] The geometry of a tensile specimen is shown in Figure 2.10 and that of a Charpy V-notch sample in Figure 2.11.

5.2.7. Wear Testing

The wear tests of the as-received J6 were conducted using an Amsler machine under rolling/sliding conditions. The steel was tested at contact pressures of 1220 and 1700 MPa, respectively, with a slide/roll ratio of 35%. During a wear test, the width and diameter changes of both top and bottom rollers were measured while the measurement of weight loss of the rollers was taken. The details of the testing procedure are described in section 2.7.2.

5.3. RESULTS AND DISCUSSION

5.3.1. Microstructure of the Steel

The optical micrographs in Figure 5.1 show the microstructure of the as-received J6. A banded structure is clearly revealed in Figure 5.1(a) at a magnification of 50×. Bright narrow stripes run in the rolling direction. Figure 5.1(b) shows an evident lath-like feature at a magnification of 400× for the dark matrix. Figure 5.2 is a micrograph of the matrix obtained in the SEM at a magnification of 2000×. The orientation of lath-like ferrite is characterized by packets, in each of which the ferrite laths are parallel. A prior austenite grain boundary is also revealed in the micrograph. The microstructure of the white stripes observed in SEM looked similar to that of the matrix, but the contrast was much less.

In the TEM, carbide-free bainite was found in the as-received J6 as shown in Figure 5.3(a). Lath ferrite was heavily dislocated and thin films of retained austenite were located in the lath boundaries. In addition, very fine twinned martensite was found frequently at high magnifications above 100,000×. The twinned martensite, shown in Fig 5.3(b), usually has a shape resembling a M-A island in granular bainite. It was not known if the microstructure observed was in the matrix area or in a white stripe because the features of the area around the hole of a TEM specimen could not be determined during specimen preparation. The SEM observations seem to suggest that lath ferrite could also be predominant in the white stripes. However, it is worthwhile to investigate the difference between the matrix and white stripes because they have different microhardness and could affect the mechanical properties of the steel as will be discussed in the following sections.

Basically, the microstructure of the as-received J6 is composed of carbide-free bainite and fine twinned martensite islands.

The microstructure of the water-quenched J6 was observed in an optical microscope. Figure 5.4(a) shows that a banded structure was still present after water-quenching. The acicular feature of the matrix was not as evident in the water-quenched J6 as in the as-received J6 (Figure 5.4(b)). A micrograph of the white stripe in Figure 5.4(c) shows a more granular structure.

5.3.2. Wear Performance of the As-received J6

The wear rates of the as-received J6 are illustrated in Figure 5.5 accompanied by those of the water-quenched J1 and the wrought austenitic Mn steel. Table 5.2 gives the wear rates of both top and bottom rollers at contact pressures of 1220 and 1700 MPa. It is shown that the wear rate of the as-received J6 was much lower than that of the water-quenched J1 and comparable to that of the Mn austenitic steel.

Since the Mn steel exhibited the best wear resistance of the steels investigated before J6, a further comparison of J6 with the Mn steel is made. Figure 5.6 represents the overall wear performance of a wear system. In this figure, the "top" represents the top roller, i.e. J6 or Mn steel and the "bottom" refers to the bottom roller, which is a class C wheel steel W5. The "total" is the total wear rate of a wear pair, obtained by summing the wear rates of top and bottom rollers. At a contact pressure of 1220 MPa, the wear rate of the as-received J6 was lower than that of the Mn steel by about 40%. At 1700 MPa, the wear rate of the as-received J6 was slightly lower than that of the Mn steel. Figure 5.6 also shows that the bottom roller of the as-received J6/W5 pair wore faster than that of the Mn steel/W5 pair at both contact pressures although the top roller (the as-received J6) of the former wore slower than that (the Mn steel) of the latter. For the as-received J6/W5 pair, the top roller (the as-received J6) wore slower than the bottom roller (W5) at both 1220 and 1700 MPa. For the Mn steel/W5 pair, the top roller (the Mn steel) wore slower than the bottom roller (W5) at 1220 MPa, but faster at 1700 MPa.

The behavior that the top roller wore faster than the bottom roller for the as-received J6/W5 pairs is different from that of the first five bainitic steel/W5 pairs, for which the top roller wore much faster than the bottom roller (Figure 3.31), except for the water-quenched J1/W5 pair. It appears that the top roller could wear slower than the bottom roller when the wear rate of the top roller is low enough, as shown by the as-received J6 and the Mn steel. The transition of the relative wear between the top and bottom rollers is also influenced by the contact pressure as indicated by the Mn steel/W5 pairs (Figure 5.6). However, no conclusive statements should be reached without further study.

Figure 5.6 shows that the total wear rate of the as-received J6/W5 pair is lower than that of the Mn steel/W5 pair at 1220 MPa, but higher at 1700 MPa. For both steel/W5 pairs, higher contact pressure generated higher wear rate for both top and bottom rollers.

For the as-received J6, no Type III wear was generated on the worn surfaces of the rollers at both 1220 and 1700 MPa. During the early period of a test, wear debris were generated and removed, giving rise to an increased number of pits produced on the roller surface as the test proceeded. Meanwhile, the surfaces of the rollers were getting rougher. After this period, however, no large amount of debris was produced and the number of pits decreased as the test proceeded. The worn surfaces were rolled to become smoother and smoother. Figures 5.7 and 5.8 show the worn surfaces of the as-received J6 at 1220 and 1700 MPa, respectively. Fracture flakes produced on the surface were small and shallow. No large, overlapped and deformed fracture flakes were found. On the worn surfaces, there were no evident grooves, indicating little deformation during wear on a micro scale.

The dimensional changes of the as-received J6 rollers were investigated during the wear test. Unlike steels J1 through J5, the as-received J6 experienced a uniform spread of contact width and the edge of the spread surface was very smooth. Figure 5.9

shows the width increase of the as-received J6 rollers as well as the Mn austenitic steel rollers. At 1220 MPa, the width increase of the as-received J6 was nearly zero and at 1700 MPa, it was only about 0.1 mm. At a given contact pressure, the increase in width of the as-received J6 was much smaller than that of the Mn steel. The result indicates that the as-received J6 experienced very little deformation on a macro scale. Worn surface observations and width curves suggest that J6 is a deformation resistant material.

5.3.3. Mechanical Properties

Tensile tests and Charpy impact tests were conducted to evaluate the mechanical properties of the as-received J6 and water-quenched J6. Table 5.3 gives the hardness, strengths, ductility and toughness of J6 in both as-received and water-quenched conditions. With a carbon content of 0.25%, both yield and ultimate tensile strengths were increased with respect to J1. Water-quenching further increased the strengths of the steel. For J6, water-quenching also increased the ductility. J6 exhibited the highest strengths of the bainitic steels J1 through J6.

For the as-received J6, the hardness on the Rockwell C scale was not influenced by the banded structure in both longitudinal and cross sections of the steel bars with respect to the rolling direction. A constant hardness of 45 HRC was obtained in the longitudinal section and 46 HRC in the transverse section. However, microhardness varied significantly between the matrix and white stripes. In the longitudinal section, the hardness of the matrix was about 459 HK and that of the white stripes about 541 HK. In the cross section, the white stripes were in the form of discrete blocky islands or network to some degree and are referred to as white areas hereafter. In this section, in addition to the difference between the matrix and white area, the microhardness also varied in each area. The microhardness of the matrix was in a range of 438 – 501 HK and that of the white area in a range of 539 – 595 HK. The microhardness of the matrix was consistently lower than that of the white stripes.

By water quenching, the hardness of the steel was increased to 53 HRC. The microhardness was also increased, but the situation was more complicated than that of the as-received J6. Since a banded structure still existed, the microhardness measurement was carried out on both matrix and white stripes/areas. In a longitudinal section, the microhardness of the matrix and white stripes was 591 and 604, respectively; the difference was small. Moreover, the microhardness of the white stripes was not always higher than the matrix. In a cross section, the microhardness varied considerably in both the matrix and white area. The microhardness of the matrix varied in a range of 481 – 634 HK and that of the white area 518 – 687 HK. Statistically, the hardness of the white area was higher than that of the matrix. An average microhardness of the matrix was 552 HK and that of the white area 601 HK.

The microhardness difference between the matrix and white stripes is 82 HK in the longitudinal section for the as-received J6 and 13 HK for the water-quenched J6. Water quenching reduced the difference in microhardness between the matrix and white stripes although it did not eliminate or ever reduce the banded structure. It is believed that austenitizing at 920°C before water quenching reduced the inhomogeneity of the steel and imposed a favorable effect on mechanical properties.

The strengths of J6 in both heat treatment conditions were estimated using the strength equations developed on the basis of J1 through J5. In doing this estimation, the coefficient for each element was quoted from Table 4.2. The result given in Table 5.3 shows that the estimated values are very close to the tested ones. This suggests that the strength equations could be extrapolated to a higher carbon content and that they could provide estimations as a reference for further compositional modifications. However, it should be mentioned that compositional range and manufacturing procedures must be considered when the equations are applied to the steels in question. There is no universal equation that could fit all steels.

The estimation of the ductility of J6 is far away from the measured values. For the as-received J6, the estimated ductility is lower than the measured values and for the water-quenched J6, it is higher than the measured. It seems that the ductility cannot be determined only by the carbon content.

The V-notch impact toughness of J6 investigated at room temperature was 9.8 ft-lb for the as-received J6 and 6.5 ft-lb for the water-quenched J6. Water quenching decreased the toughness of the steel by 35% although it improved the toughness of J1. Interestingly, the toughness of the as-received J6 was close to that of the water-quenched J1 and the water-quenched J6 showed the same toughness as the as-received J1. The macro fracture surface observation showed that only brittle fracture occurred. The impact absorbed energy values were in the lower shelf of the impact curves for both the as-received and water-quenched specimens of J6.

5.3.4. Effect of Microstructure on Mechanical Properties

It has been shown that the strength of the as-received steel J6 is superior to that of the as-received J1. Increasing the carbon content as well as silicon content changes the microstructure of the steel. In the as-received J1, blocky retained austenite is present in the bainitic ferrite laths and elongated retained austenite is located along the ferrite lath boundaries. In addition, the ferrite laths are not as well developed as in the as-received J6. In the as-received J6, ferrite laths are well developed and thin films of retained austenite are well defined in the lath boundaries. This is a typical carbide-free bainitic structure. Moreover, there are very fine twinned martensite islands in the ferrite matrix. These islands could also contribute to enhancing the strength. It is postulated that the twinned martensite islands act as second-phase particles and increase the strength through a dispersion strengthening mechanism.

The effect of carbon is considered in two aspects. First, carbon is an element that increases the strength of a steel through solid solution strengthening. Second, carbon-enriched austenite transforms into fine twinned martensite islands as a strengthening constituent.

A banded structure caused an inhomogeneity in J6 and would inevitably influence the mechanical properties of the steel. An EDS analysis of the as-received J6 was carried out in a SEM and the result shown in Figure 5.10 indicates that manganese segregation might have occurred. Microhardness of the white stripes (541 HK) was much higher than that of the matrix (459 HK) in the as-received J6, but it is suspected that the manganese segregation alone cannot produce such a great difference in microhardness. Carbon enrichment is, therefore, considered another reason to cause such a high hardness. Unfortunately, no indication of carbon enrichment was found with the EDS analysis. This is probably due to the insensitivity and inaccuracy of EDS in quantitatively detecting light elements.

5.3.5. The Influences of Microstructure and Mechanical Properties on Wear Performance

It is undoubted that an increase in carbon content has resulted in a considerable improvement of the wear resistance of the as-received J6 with respect to J1. This improvement is associated with the microstructural changes and mechanical properties. As suggested for the first five bainitic steels, carbide-free bainitic structure would be beneficial to enhancing wear resistance. The microstructure of the as-received J6 turns out to be carbide-free bainite as expected and the wear resistance of this steel is improved in consistence with microstructural changes. High strength and low ductility suggest that J6 is highly resistant to deformation. This was confirmed by the small width changes of Amsler rollers experienced in the rolling/sliding wear tests and the smooth worn surfaces of the rollers. From the results of the first five bainitic steels, it was suggested that a high strength steel experiencing a small deformation under rolling/sliding conditions could lead to a low wear rate in terms of weight loss as for the water-quenched J1. The low wear rates of the as-received J6 are in agreement with this suggestion.

The effect of the banded structure on wear has not been investigated. It is assumed that the white stripes could act as a strengthening component and a deformation resistant element. In an Amsler roller, the white stripes were oriented in the roller axis direction and parallel to the roller surface. To understand the behavior of the banded structure under roller/sliding conditions, it is necessary to carry out a subsurface analysis of the worn roller in both longitudinal and transverse sections.

Although a banded structure was produced in J6, the strength, wear resistance and deformation resistance have been effectively improved by increasing the carbon content to 0.25%. The ductility of the as-received J6 was decreased dramatically compared with J1, but it was improved by water quenching. The toughness of J6 is comparable to that of J1. Carbide-free bainite is a favorable microstructure in terms of strength and wear performance. The effect of a banded structure on mechanical properties and wear performance is not clear and further study is needed.

Table 5.1 Composition of the Mo-B Steel J6 (wt-%)

(a) Analysis of liquid steel*

C	Mn	P	S	Si	Ni	Cr	Mo	Al	Ti	B
0.26	1.99	0.013	0.009	1.77	–	1.95	0.50	0.046	0.038	0.003

(b) Analysis of solid steel**

C	Mn	Si	Cr	Ni	Mo	Cu	S	O***
0.258	2.00	1.81	1.93	0.00	0.49	0.00	0.010	0.0022
P	Al	Ti	Zr	Co	Nb	V	W	N***
0.009	0.040	0.042	0.003	0.00	0.006	0.006	0.006	0.0013
B	Pb	Sn	As	Sb	Ca	Ce		
0.003	0.003	0.005	0.002	0.001	0.0016	0.004		

* *The composition was analyzed using spark spectrum and provided by Bhethlehem steel corporation.*

** *The composition was analyzed by Esco corporation using a spark spectrum technique.*

*** *The elements were analyzed by Esco corporation using Leco approach.*

Table 5.2 Wear Rates of the As-received J6/W5 Wear Test Pairs (μg/m/mm)

Contact Pressure (MPa)	J6-as (Top roller)	W5 (Bottom roller)
12208	78	106
1700	136	348

Table 5.3 Measured and Predicted Mechanical Properties of J6

	Hardness (HRC)	UTS		0.2% YS		ELN. (%)	RED. OF AREA (%)	IMPACT TOUGHNESS (ft-lb)
		ksi	MPa	ksi	MPa			
J6–as	45	222.1	1,531	145.4	1,003	4.2	6.7	9.8
J6–wq	53	284.9	1,964	199.2	1,373	10.2	30.2	6.5
J6–as*		236.5	1,631	141.5	976	12.9	27.0	
J6–wq*		284.8	1,964	193.7	1,336	8.8	20.7	

* *Predicted values using the strength and ductility equations presented in Chapter 4.*

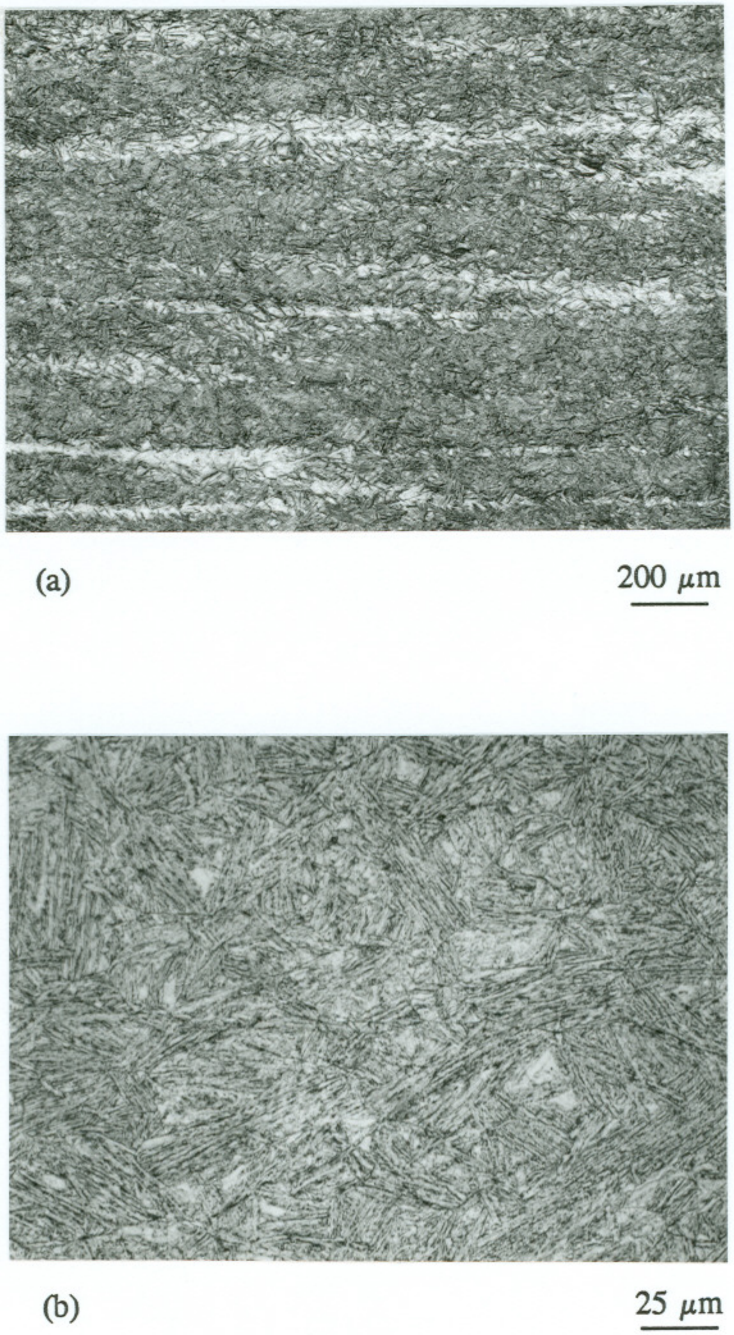

Figure 5.1 Optical micrographs showing the microstructure of the as-received J6

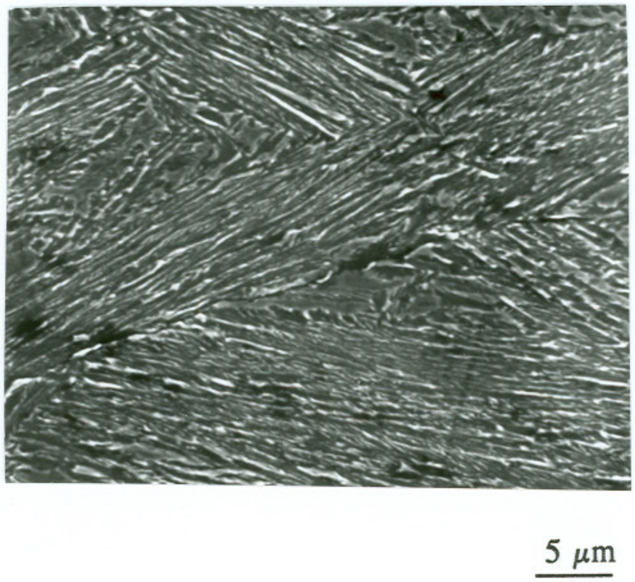

Figure 5.2 SEM micrograph of the as-received J6

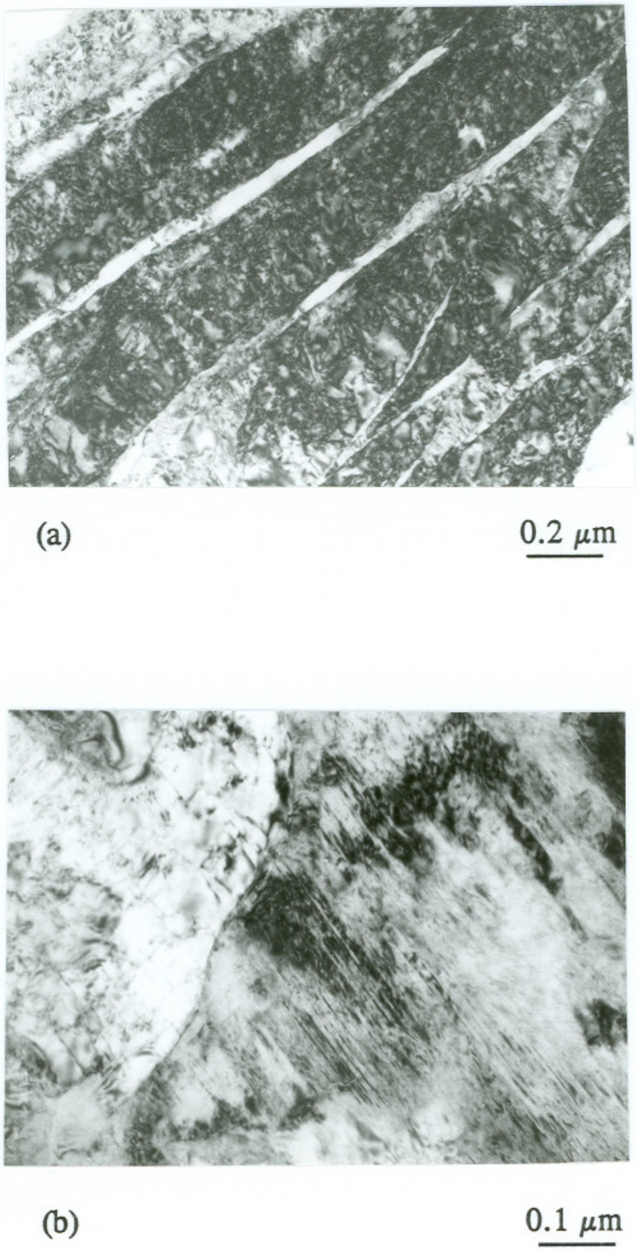

Figure 5.3 Microstructure of the as-received J6 in TEM
(a) carbide-free bainite
(b) twinned martensite

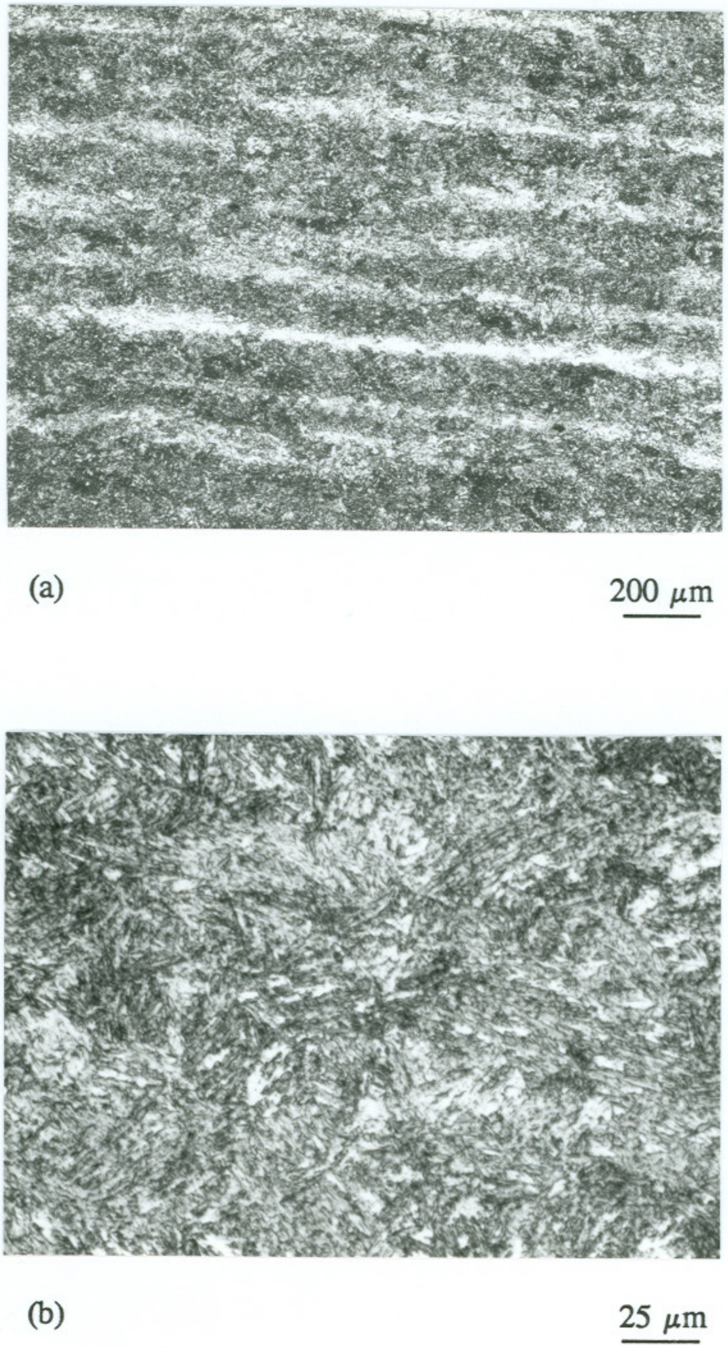

Figure 5.4 Microstructure of the water-quenched J6
(a) banded structure in the rolling direction
(b) matrix of the microstructure

(c)

Figure 5.4 Microstructure of the water-quenched J6
(c) a white band in the steel

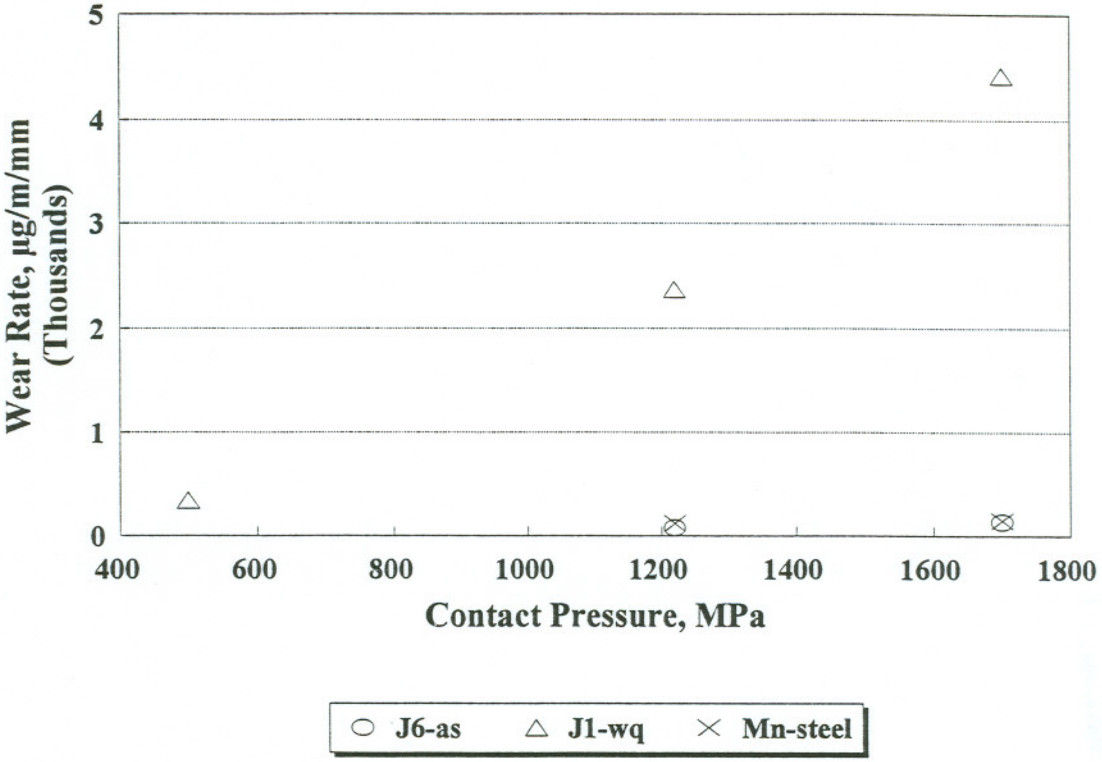

Figure 5.5 Wear rate of the as-received J6 in comparison with that of the water-quenched J1 and the austenite Mn steel

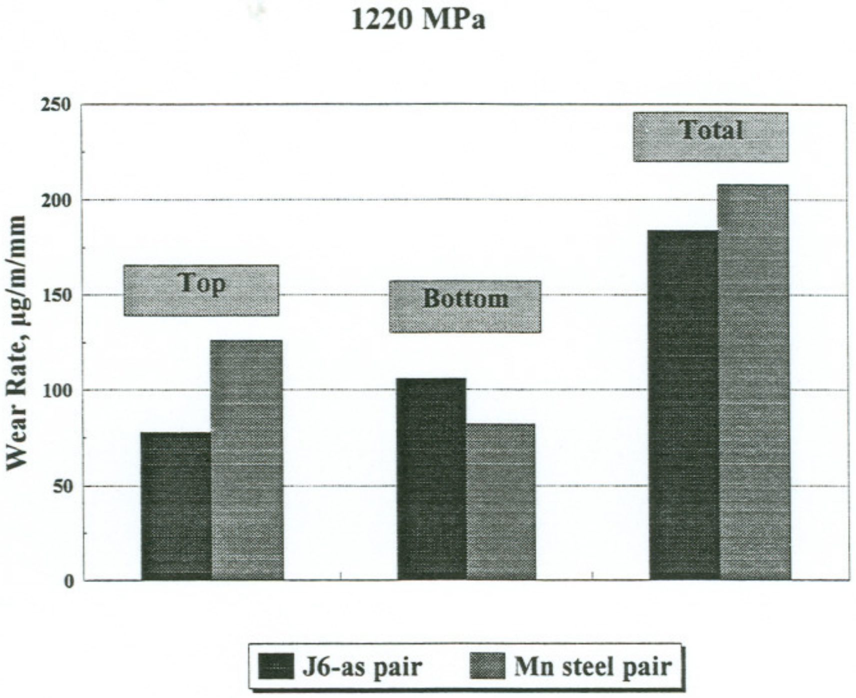

Figure 5.6 Wear of the as-received J6 and the Mn steel
(a) 1220 MPa

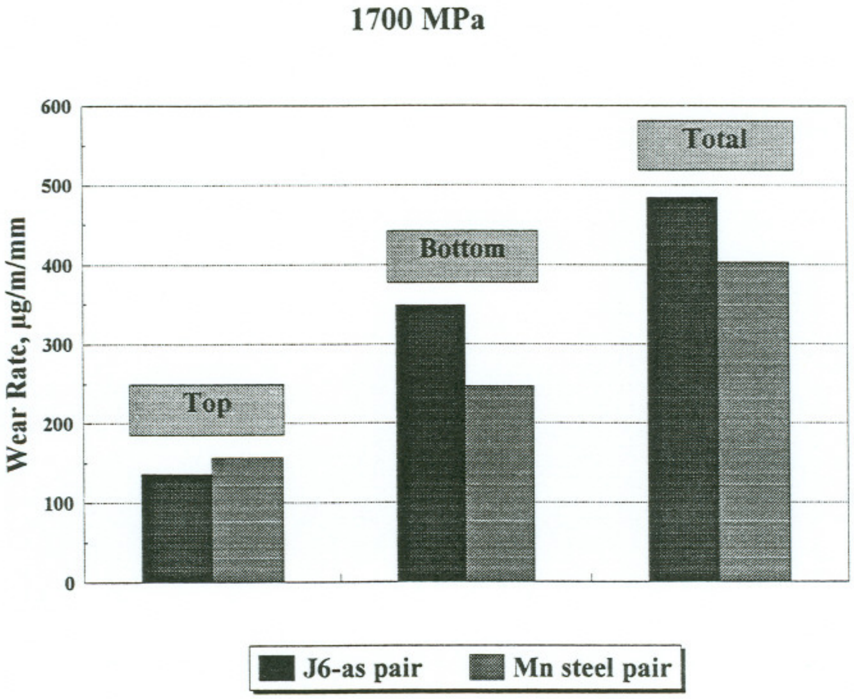

Figure 5.6 Wear of the as-received J6 and the Mn steel
(b) 1700 MPa

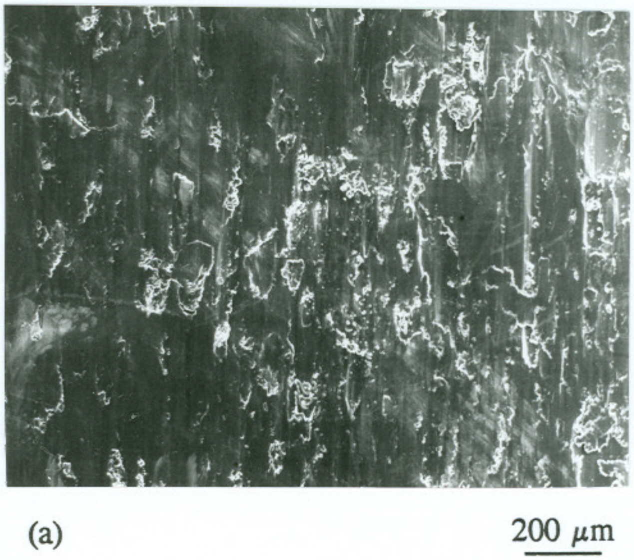

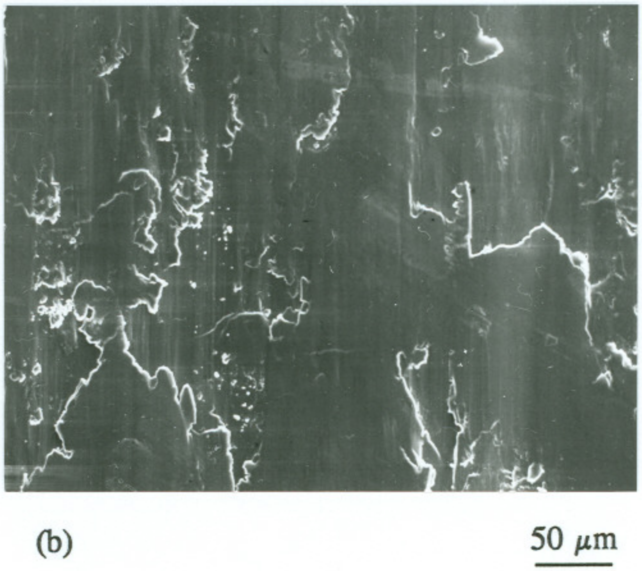

Figure 5.7 Worn surface of the as-received J6 at 1220 MPa
(a) general morphology (b) fracture lips

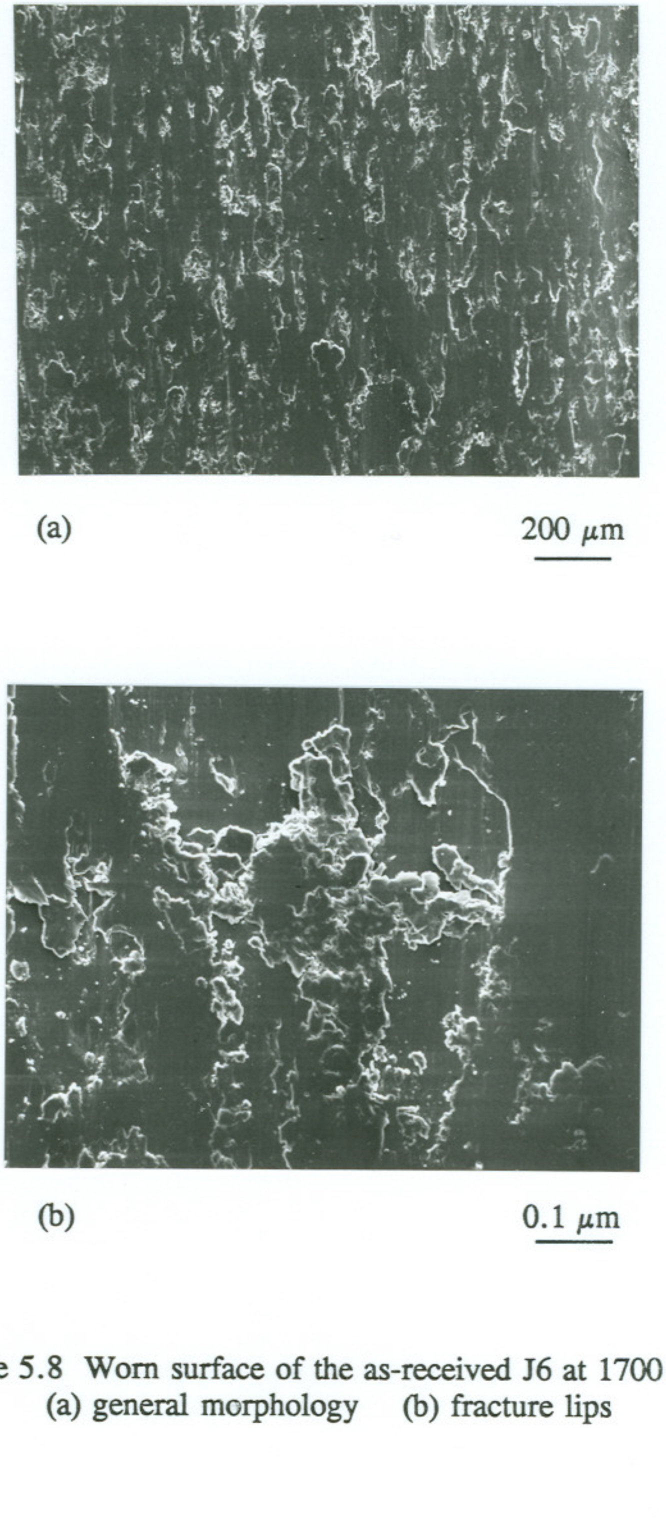

Figure 5.8 Worn surface of the as-received J6 at 1700 MPa
(a) general morphology (b) fracture lips

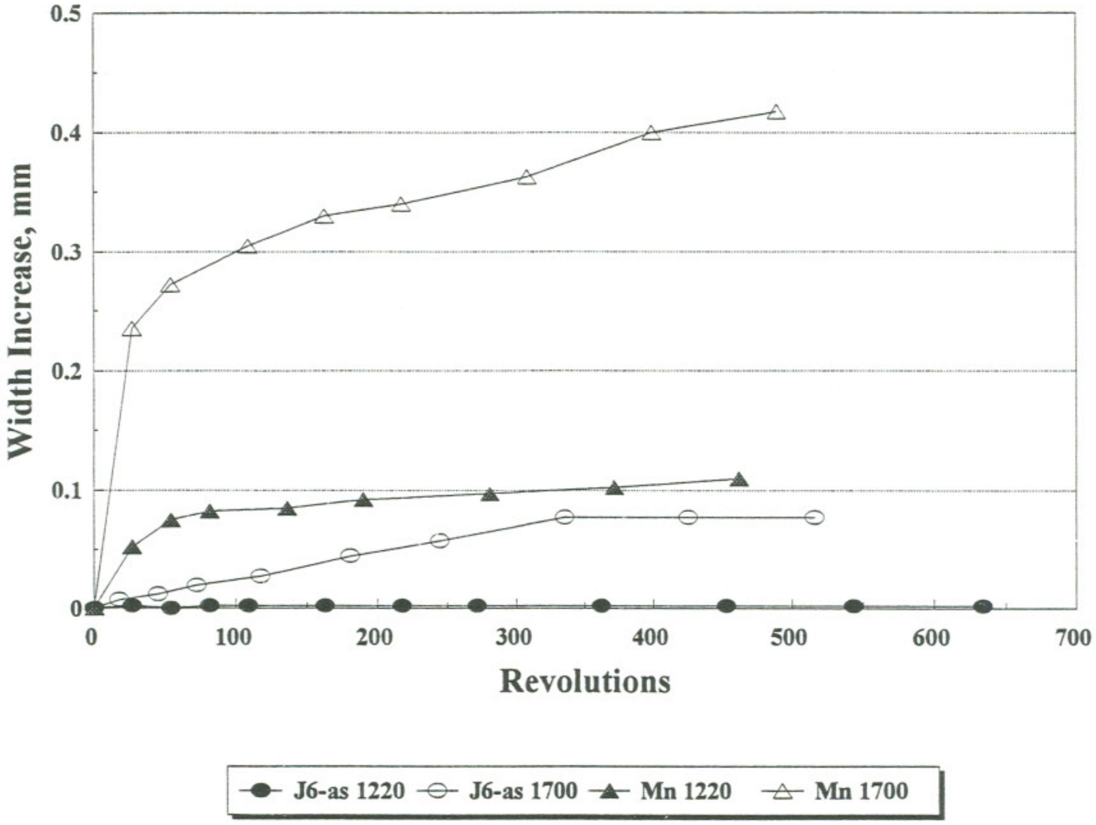

Figure 5.9 Width increase of the as-received J6 and the Mn steel at contact pressures of 1220 MPa and 1700 MPa

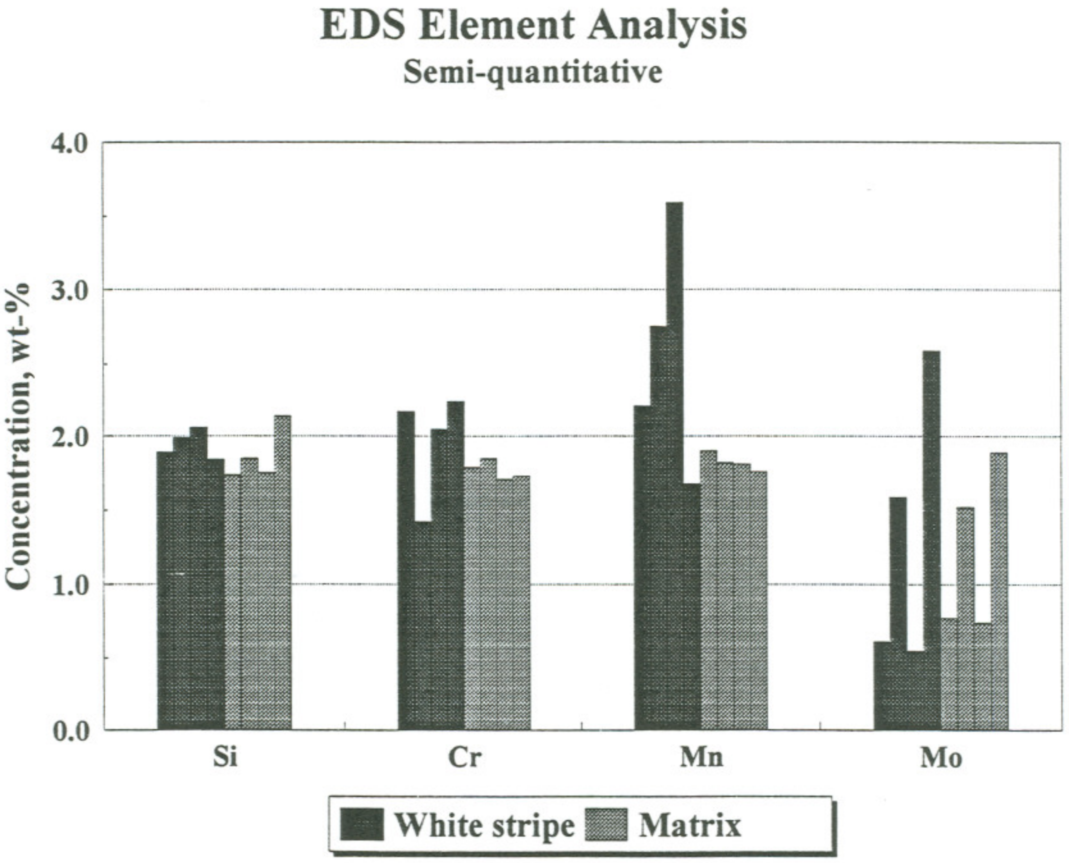

Figure 5.10 EDS analysis of the as-received J6

CONCLUSIONS

1. The microstructures of J1 through J6 were basically carbide-free bainite or granular bainite except for J2 that exhibited a predominant microstructure of lower bainite.

2. The bainitic ferrite in the steels were in two forms: massive and lath-like. Other constituents included M-A islands, retained austenite, twinned martensite (needle-shaped) and carbides. The amount and distribution of these constituents varied with the composition and heat treatment of the steels.

3. Cooling rate influenced the microstructure of the bainitic steels. A general tendency is that a faster cooling rate (1) produced more lath ferrite and less massive ferrite; (2) promoted the formation of thin films of retained austenite and reduced the blocky retained austenite; (3) hindered the formation of M-A islands and suppressed the precipitation of carbides; and (4) resulted in the needle-shaped martensite in the higher carbon steels.

4. Cooling rate also affects the mechanical properties of the bainitic steels. Water quenching generally increased both yield and ultimate tensile strengths of the steels, but decreased the ductility. For J6, however, the ductility was improved by water quenching. This is attributed to the austenitizing treatment that reduced the microstructural heterogeneity of the steel.

5. For a given carbon content, 4%Mn showed an equivalent effect on strength to a combination of 2%Mn, 2%Cr and 2%Ni.

6. At room temperature, water quenching could either increase or decrease the Charpy impact toughness of the bainitic steels, depending upon the composition of the steels. Brittle fracture occurred on all the specimens in both as-received and water-quenched conditions.

7. The impact toughness of the steels varied in the range 6 – 13 ft-lb at room temperature. This toughness is higher than that of conventional pearlitic rail steels.

8. For J1 through J5, the wear rate decreased as the cooling rate increased. For a given composition, water quenching produced the highest wear resistance.

9. A lath ferrite structure had a significant effect on improving wear resistance. Thin films of retained austenite and needle-shaped martensite might also contribute to the improved wear resistance. Carbides and M-A islands appeared to deteriorate the wear resistance of the bainitic steels.

10. Hardness and room temperature impact toughness did not show consistent effects on the wear resistance of the bainitic steels.

11. Of all the steels investigated, the as-received J6 showed the best wear resistance. The pearlitic rail steel X136 exhibited a better wear resistance than the as-received J1 through J5, but worse than the water-quenched J1. The wear rates of the austenitic Mn steel were much lower than those of the bainitic steels J1 – J5 and X136. However, the wear rates of the Mn steel were no lower than those of the as-received J6.

12. The deformation tests indicated that higher carbon steels J1 and J2 exhibited better deformation resistance than the bainitic and CrMo rail steels in previous investigations. The low carbon as-received J4 experienced great deformation. The as-received J6 appeared to be more deformation resistant than the Mn steel.

13. Carbon exhibited significant influences on microstructure, mechanical properties and wear performance of the bainitic steels. 0.25%C effectively increased the strength and wear resistance of J6 with a microstructure of carbide-free bainite.

14. The wear rate of the bottom roller varied with its counterpart top roller. A *wear ratio* was introduced to indicate the relative wear between the top and bottom rollers. For most tests in the current study, the top roller wore faster than the bottom roller. But in some cases, they are reversed. Further study is needed to clarify the factors that influence the interaction between the rollers.

15. 0.18%C J1 and 0.12%C J2 showed good weldability with a preheat temperature of 200 °C using Tekken test with the GMAW approach.

REFERENCES

1. D. Brooke, "The Advent of the Steel Rail, 1857-1914," *J. Transport History*, (1986) **vol.7, Part I**:18-31.

2. J. Dearden, "The Wear of Steel Rails: A Review of the Factors Involved," *Proc. of the Inst. Civil Engs, Part II*, London, UK, (1954) p.456.

3. J. Dearden, "The Wear of Steel Rails and Tyres In Service," *Wear*, (1960) **3**:43-59.

4. R.K. Steele and R.P. Reiff, "Rail: Its Behavior and Relationship to Total System Wear," *The 2nd International Heavy Haul Railway Conference, Pre-Conference Proceedings*, Colorado Springs, CO, USA, (1982) pp. 115-164(a).

5. J. Hannafious, "FAST/HAL Rail Performance," *Proc. Workshop on Heavy Axle Loads*, Pueblo, CO, USA, AAR, (1990) paper 10

6. M.B. Hargrove, F.S. Mitchell, R.K. Steele and R.E. Young, "The Wear Behavior of High Rails in the First Metallurgy Experiment, 0-135 MGT," *Report FRA/TTC-81/04*, US Dept. of Transportation, (1981)

7. R.K. Steele, "A Perspectival Review of Rail Behavior at FAST," *Report FRA/TTC-81/07*, US Dept. of Transportation, (1981)

8. R.K. Steele and T.J. Devine, "Wear of Rail/Wheel Systems," *Proc. Int. Sym. on Contact Mechanics and Wear of Rail/Wheel Systems*, Vancouver, Canada, (1982) pp. 293.

9. I. J. McEwen and R. F. Harvey, "Full Scale Wheel-on-Rail Wear Testing: Comparisons with Service Wear and a Developing Theoretical Predictive Method," *Lubrication Eng.*, (1985) **41(2)**:80-88.

10. J. Kalousek, G. Rosval and H. Ghonem, "Lateral Creepage and Its Effect on Wear in Rail Wheel Interface," *Contact Mechanics and Wear of Wheel Rail Systems*, J. Kalousek, R.V. Dukkipati and G.M.L. Gladwell eds. Univ. of Waterloo Press, (1983)

11. J. Kalousek, D. M. Fegredo and E. E. Laufer, "The Wear Resistance and Worn Metallography of Pearlite, Bainite and Tempered Martensite Rail Steel Microstructure of High Hardness," *Wear*, (1985) **105**:199-222.

12. P.J. Mutton, "The Influence of Microstructure on the Wear Behavior of Rail and Wheel Materials," *MAppS Thesis*, Univ. of Melbourne, (1985)

13. S. Kumar, J.S. Kim and B.R. Rajkumar, "A Laboratory Study of the Dynamic Nature of Wheel/Rail Contact," *Contact Mechanics and Wear of Wheel Rail Systems*, J. Kalousek, R.V. Dukkipati and G.M.L. Gladwell eds. Univ. of Waterloo Press, (1983)

14. K. Sugino, H. Kageyama and M. Sato, "Effect of Wheel Rail Profiles on Wear and Fatigue Behavior of Rail," *Contact Mechanics and Wear of Wheel Rail Systems II*, G.M. Gladwell, H. Ghonem and J. Kalousek eds. Univ. of Waterloo Press, (1987)

15. P. Clayton and D. Danks, "Effect of Interlamellar Spacing on the Wear Resistance of Eutectoid Steels under Rolling-Sliding Conditions," *Wear*, (1990) **135**:369-389.

16. R. Devanathan and P. Clayton, "Rolling/Sliding Wear Behavior of Three Bainitic Steels," *Wear of Behavior 1991, [Proc. Int. Conf.]*, ASME, (1991) pp. 91-100.

17. P. J. Bolton, P. Clayton and I. J. McEwan, "Wear of Rail and Tire Steels under Rolling Sliding Conditions," *ASLE Trans.*, (1982) **25**:17-24.

18. P. J. Bolton and P. Clayton, "Rolling-Sliding Wear Damage in Rail and Tyre Steels," *Wear*, (1984) **93**:145-165.

19. D. Danks and P. Clayton, "Comparison of the Wear Process for Eutectoid Rail Steels: Field and Laboratory Tests," *Wear*, (1987) **120**:233-250.

20. P. Clayton, D. Danks and R.K. Steele, "Assessment of Eutectoid Rail Steel Wear Performance Using Laboratory Tests," *Proc. Conf. Antiwear '88*, London, UK, The Royal Society, (1988)

21. P. Clayton and R. Devanathan, "Rolling/Sliding Wear Behavior of a Chromium-Molybdenum Rail Steel in Pearlitic and Bainitic Conditions," *Wear*, (1992) **156**:121-131.

22. W.H. Hodgson, J.K. Yates and R.R. Preston, "The Development of a Second Generation of Alloy Steel Rails for Heavy Haul Applications," *2nd Int. Heavy Haul Railway Conf*, Colorado Springs, CO, USA, (1982) pp. 207-215.

23. J. E. Garnham and J. H. Beynon, "Dry Rolling-Sliding Wear of Bainitic and Pearlitic Steels," *Wear*, (1992) **157**:81-109.

24. H. Ichinose, J. Takehara and M. Ueda, "High Strength Rails Produced by Two-Stage Flame Heating and Slack-Quenching," *2nd Int. Heavy Haul Railway Conf., Pre-Conf. Proc*, Colorado Springs, Colorado, USA, AAR et al., (1982) pp. 82-HH-19.

25. H. Masumoto, K. Sugino and H. Hayashida, "Development of Wear Resistant and Anti-Shelling High Strength Rails in Japan," *Heavy Haul Railways Conference [Proceedings]*, Perth, Western Australia, (1978) paper H1.

26. P. Clayton and M. B. P. Allery, "Metallurgical Aspects of Surface Damage Problems in Rails," *Can. Metall. Q.*, (1982) **21(1)**:31-46.

27. R. Nakumura, S. Owaku and N. Enomoto, "The Rail Shelly Crack in Japan," *Quarterly Report of the Railway Technical Research Institute of Japanese National Railways*, (1965) **6(3)**:34-44.

28. A. Ito and R. Kurihara, "Shelling of Rails Experienced in Japaneses Railways," *Bulletin of Permanent Way Soc. of Japan*, (1965) **13**:17-32.

29. H. Masumoto, K. Sugino, S. Nisida, R. Kurihara and S. Matsuyama, "Some Features and Metallurgical Considerations of Surface Defects in Rail due to Contact Fatigue," *Rail Steels -- Developments, Processing, and Use, [Symp.]*, Denver, Co, USA, ASTM STP 644, (1976) pp. 233-255.

30. S. Way, "Pitting due to Rolling Contact," *Trans. ASME, J. App. Mech*, (1935) **57**:A49-A58.

31. P. Clayton and D. N. Hill, "Rolling Contact Fatigue of a Rail Steel," *Wear*, (1987) **117**:319-334.

32. M. Sato, "Wear and Rolling Contact Fatigue of Rail Steels," *MS Thesis*, Ohio State Univ., (1991)

33. P. Clayton, R. Devanathan, N. Jin and R.K. Steele, "A Review of Bainitic Steels for Wheel/Rail Contact," *Rail Quality and Maintenance for Modern Railway Operation, [Int. Conf.]*, Delft, The Netherlands, Kluwer Academic Phblishers, (1992) pp. 41-51.

34. W. Heller and R. Schweitzer, "Hardness, Microstructure and Wear Behavior of Steel Rails," *2nd Int. Heavy Haul Railway Conf., Pre-Conf. Proc*, Colorado Springs, CO, USA, (1982) pp. 82-HH-26.

35. H. Ichinose, J. Takehara, N.Iwasaki and M. Ueda, "An Investigation on Contact Fatigue and Wear Resistance Behavior in Rail Steels," *Heavy Haul Railways Conference [Proceedings]*, Perth, Weatern Australia, (1978) paper I.3.

36. P. Clayton, K. J. Sawley, P. J. Bolton and G. M. Pell, "Wear Behavior of Bainitic Steels," *Wear*, (1987) **120**:199-220.

37. R. Devanathan, "Wear Behavior of Bainitic Steels," *Ph.D Thesis*, Beaverton, USA, Oregon Graduate Institute, (1991)

38. R. L. Klueh and A. M. Nasreldin, "Microstructure and Mechanical Properties of a 3Cr-1.5Mo Steel," *Metall. Trans. A*, (1987) **18A**:1279-1290.

39. Y. Ohmori, H. Ohtani and T. Kunitake, "The Bainite in Low Carbon Low Alloy High Strength Steels," *Trans. ISIJ*, (1971) **11**:250-259.

40. L.J. Habraken and M. Economopoulos, "Bainitic Microstructures in Low-Carbon Alloy Steels and Their Mechanical Properties," *Transformation and Hardenability in Steels*, Ann Arbor, MI, USA, Climax Molybdenum Co., (1967) pp. 69-107.

41. B. L. Bramfitt and J. G. Speer, "A Perspective on the Morphology of Bainite," *Metall. Trans. A*, (1990) **21A**:817-829.

42. T. Araki, K. Shibata and M. Enomoto, "Reviewed Concept on the Microstructural Identification and Terminology of Low Carbon Ferrous Bainites," *Martesitic Transformation, [Conf. Proc.]*, Sydney, Australia, Materials Science Forum Vols. 56-58, (1989) pp. 275-280.

43. D.V. Edmonds, "Bainitic Structures," *Metals Handbook*, 9th ed., vol.9, (1993) pp. 662-667.

44. D. N. Shackleton and P. M. Kelly, "The Crystallography of Cementite Precipitation in the Bainite Transformation," *Acta Metall.*, (1967) **15**:979-992.

45. V. Biss and R. L. Cryderman, "Martensite and Retained Austenite in Hot-Rolled, Low-Carbon Bainitic Steels," *Metall. Trans.*, (1971) **2**:2267-2276.

46. P. L. Mangonon, "Effect of Alloying Elements on the Microstructure and Properties of a Hot-Rolled Low-Carbon Low-Alloy Bainitic Steel," *Metall. Trans. A*, (1976) **7A**:1389-1400.

47. Z. Bojarski and T. Bold, "Structure and Properties of Carbide-Free Bainite," *Acta Metall.*, (1974) **22**:1223-1234.

48. H.K.D.H. Bhadeshia, *Bainite in Steels*, Inst. of Metals, (1992) pp. 283-284.

49. M. E. Bush and P. M. Kelly, "Strengthening Mechanisms in Bainitic Steels," *Acta Metall.*, (1971) **19**:1363-1371.

50. D. V. Edmonds, "The Relationship between Structure and Properties in Bainitic Steels," *Iron & Steelmaker*, (1990) **17**:75-84.

51. G. Thomas and M. Sarikaya, "Lath Martensite in Carbon Steels--Are They Bainitic?" *Proc. Int. Conf. on Solid --> Solid Phase Transformations*, Pittsburgh, PA, USA, ASM, (1981) pp. 999-1003.

52. M. Sarikaya, H. Tokushige and G. Thomas, "Lath Martensite and Bainite in Low Alloy Steels," *Proc. Int. Conf. on Martensitic Transformations*, Jpn. Inst. of Metals, (1986) pp. 613-618.

53. A. Hultgren, "Isothermal Transformation of Austenite," *Trans. AIME*, (1947) **39**:915-1005.

54. M. Hillert, "The Formation of Pearlite," *Decomposition of Austenite by Diffusional Processes [Conf. Proc.]*, V.F. Zackay and H.I. Aaronson eds. Philadelphia, PA, USA, Metallurgical, Soc. of AIME, (1960) pp. 197-237.

55. R.F. Hehemann, "The Bainite Transformation," *Phase Transformations*, ASM, (1970) pp. 397-432.

56. G.R. Speich, "Growth Kinetics of Bainite in a Three Per Cent Chromium Steel," *Decomposition of Austenite by Diffusional Processes, [Conf. Proc.]*, Pheladelphia, PA, USA, (1960) pp. 353-370.

57. H.I. Aaronson, "Mechanisms of Diffusional Growth," *Phase Transformations, [Conf. Proc.]*, London, Inst. Metall., (1979) pp. II.1-II.18.

58. K.R. Kinsman and H.I. Aaronson, "Discussion of "Structure and Growth of Widmanstätten Ferrite and Bainite"," *Transformation and Hardenability in Steels [Symposium]*, Ann Arbor, Michigan, USA, Climax Molybdenum Co., (1967) pp. 33-38.

59. H.I. Aaronson, C. Laird and K.R. Kinsman, "Mechanisms of Diffusional Growth of Precipitate Crystals," *Phase Transformations*, Metals Park, OH, USA, ASM, (1970) pp. 313-396.

60. F. Wever, "über die Umwandlungen bei der Stahlärtung," *Z. Metallkde.*, (1932) **24**:270.

61. F. Wever and W. Jellinghaus, "The Kinetics of the Transformations of Austenite -- II. Dilatometric Investigation of the Decomposition of Austenite," *Mitt. Kaiser-Wilhelm-Inst. Eisenforsch*, (1932) **14**:85-89.

62. A. Portevin and H. Jolivet, "Les Transformations Au Refroidissement Dans Les Aciers," *Annales de l'Academie des Sciences Techniques à Varsorie*, (1937) **4**:177-195.

63. A. Portevin and P. Chevenard, "Sur un mode de décomposition de l'austénite," *Compt. Rend.*, (1938) **207**:1412-1414.

64. A. Portevin and P. Chevenard, "Les transformations au refroidissement des aciers," *Compt. Rend.*, (1937) **204**:772-774.

65. J. R. Vilella, G. E. Guellich and E. C. Bain, "On Naming the Aggregate Constituents in Steel," *Trans. ASM*, (1936) **24**:225-261.

66. E. P. Klier and T. Lyman, "The Bainite Reaction in Hypoeutectoid Steels," *Trans. AIME*, (1944) **158**:394-422.

67. J.M. Oblak and R.F. Hehemann, "Structure and Growth of Widmanstätten Ferrite and Bainite," *Transformation and Hardenability in Steels*, Ann Arbor, MI, USA, Climax Molybdenum Co., (1967) pp. 15-30.

68. K. Tsuya, "Observation of Bainite Transformation by Hot Stage Microscope," *J. Mech. Lab Japan*, (1955) **1**:1-9.

69. J. W. Spretnak and R. Speiser, "A Hypothesis for the Boron Hardenability Mechanism," *Trans. ASM*, (1954) **46**:1089-1135.

70. H. Yada and T. Ooka, "Investigation of the Growth of Bainite in Fe-Ni-C Alloys by Hot Stage Microscopy," *J. Met. Soc. Japan*, (1967) **31**:766-771.

71. J.W. Christian and D.V. Edmonds, "The Bainite Transformation," *Phase Trasnsformations in Ferrous Alloys [Proc. Int. Conf.]*, Philadelphia, PA, USA, Metallugical Society of AIME, (1984) pp. 293-326.

72. H. K. D. H. Bhadeshia and A. R. Waugh, "Bainite: An Atom-probe Study of the Incomplete Reaction Phenomenon," *Acta Metall.*, (1982) **30**:775-784.

73. I. Stark, G.D.W. Smith and H.K.D.H. Bhadeshia, "The Element Redistrubution Associated with 'the Incomplete-Reaction Phenomenon' in Bainitic Steels: An Atom Probe Investigation," *Phase Transformations '87, [Conf. Proc.]*, London, Inst. of Metals, (1988) pp. 211-215.

74. G. V. Smith and R. F. Mehl, "Lattice Relationships in Decomposition of Austenite to Pearlite, Bainite and Martensite," *Trans. AIME*, (1942) **150**:211-226.

75. A.T. Davenport, "The Crystallography of Upper Bainite," *Republic Steel Research Report on Project 12051*, Cleveland, OH, USA, Republic Steel Corp., Research Center, (1974)

76. B. P. J. Sandvik, "The Bainite Reaction in Fe-Si-C Alloys: The Primary Stage," *Metall. Trans. A*, (1982) **13A**:777-787.

77. H. K. D. H. Bhadeshia and J. W. Christian, "Bainite in Steels," *Metall. Trans. A*, (1990) **21A**:767-797.

78. A.E. Austin and C.M. Schwartz, "Electron-Diffraction Study of Iron Carbides in Bainite and Tempered Martensite," *Proc. ASTM*, (1952) pp. 592-596.

79. B. P. J. Sandvik, "The Bainite Reaction in Fe-Si-C Alloys: The Secondary Stage," *Metall. Trans. A*, (1982) **13A**:789-800.

80. G. Y. Lai, "On the Precipitation of Epsilon-Carbide in Lower Bainite," *Metall. Trans. A*, (1975) **6A**:1469-1471.

81. D. Kalish and M. Cohen, "Structural Changes and Strengthening in the Strain Tempering of Martensite," *Mater. Sci. Eng.*, (1970) **6**:156-166.

82. J. Deliry, "Nouveau carbure de fer. Transformation bainitique dans les aciers au carbone silicium," *Mém. Sci. Rev. Mét.*, (1965) **62**:527-550.

83. J. Pomey, "Revenu de la martensite et réaction bainitique inférieure. Cas des aciers au carbone-silicium et des aciers au carbone," *Mém. Sci. Rev. Mét.*, (1966) **63**:507-532.

84. V. Franetovic, A. K. Sachdev and E. F. Ryntz, "A Transmission Electron Microscopy Study of Austempered Lower Bainitic Nodular Cast Iron," *Metallography*, (1987) **20**:15-36.

85. V. Franetovic, M. M. Shea and E. F. Ryntz, "Transmission Electron Microscopy Study of Austempered Nodular Iron: influence of silicon content, austenitizing time and austempering temperature," *Mater. Sci. Eng.*, (1987) **96**:231-245.

86. D.N. Shackleton and P.M. Kelly, "Morphology of Bainite," *Physical Properties of Martensite and Bainite*, London, Special Report 93, Iron and Steel Inst., (1965) pp. 126-134.

87. T. Kunitake, "On the Yield Strength of Quenched and Tempered Structures of Low-Carbon Low-Alloy Steel," *Trans. ISIJ*, (1967) **7**:254-262.

88. M. J. Roberts, "Effect of Transformation Substructure on the Strength and Toughness of Fe-Mn Alloys," *Metall. Trans.*, (1970) **1**:3287-3294.

89. L. . Norström, "On the Yield Strength of Quenched Low-Carbon Lath Martensite," *Scand. J. Metall.*, (1976) **5**:159-165.

90. D. Lonsdale and P. E. J. Flewitt, "The Role of Grain Size on the Ductile-Brittle Transition of a 2.25 Pct Cr-1 Pct Mo Steel," *Metall. Trans. A*, (1978) **9A**:1619-1623.

91. F.B. Pickering, "High-Strength, Low-Alloy Steels —— A Decade of Progress," *Microalloying '75, [Proc. Int. Symp.]*, Washington, D.C., USA, Union Carbide Corp., (1975) pp. 9-31.

92. F.B. Pickering, "The Structure and Properties of Bainite in Steels," *Transformation and Hardenability in Steels*, Ann Arbor, MI, USA, Climax Molybdenum Co., (1967) pp. 109-132.

93. R. W. K. Honeycombe and F. B. Pickering, "Ferrite and Bainite in Alloy Steels," *Metall. Trans.*, (1972) **3**:1099-1112.

94. T. Gladman, B. Holmes and I.D. McIvor, "Effects of Second-Phase Particles on Strength, Toughness and Ductility," *The Effects of Second Phase Particles on the Mechanical Properties of Steels, [Conf. Proc.]*, Scarborough, England, Iron and Steel Institute, (1971) pp. 68-78.

95. T. Gladman, D. Dulieu and I.D. McIvor, "Structure-Property Relationships in High-Strength Microallyed Steels," *Microalloying '75, [Proc. Int. Symp.]*, Washingtion,D.C., USA, Union Carbide Corp., (1975) pp. 32-55.

96. T. Gladman and F.B. Pickering, "The Effect of Grain Size on the Mechanical Properties of Ferrous Materials," *Yield, Flow and Fracture of Polycrystals*, T.N. Baker ed. Essex, UK, Applied Science Publishers, (1983) pp. 141-198.

97. J.A. Whiteman, "The Contribution of Physical Metallurgy to the Development of Low Carbon Steels," *Low Carbon Structural Steels for the Eighties*, Plymouth, UK, Inst. of Metallurgists, (1977) pp. I1-I7.

98. P. Brozzo, G. Buzzichelli, A. Mascanzoni and M. Mirabile, "Microstructure and Cleavage Resistance of Low-Carbon Bainitic Steels," *Metal Sci.*, (1977) **11**:123-129.

99. G. Langford and M. Cohen, "Strain Hardening of Iron by Severe Plastic Deformation," *Trans. ASM*, (1969) **62**:623-638.

100. D. V. Edmonds and R. C. Cochrane, "Structure-Property Relationships in Bainitic Steels," *Metall. Trans. A*, (1990) **21A**:1527-1540.

101. J. P. Naylor, "The Influence of the Lath Morphology on the Yield Stress and Transition Temperature of Martenitic-Bainitic Steels," *Metall. Trans. A*, (1979) **10A**:861-873.

102. H.K.D.H. Bhadeshia, *Bainite in Steels*, The Institute of Materials, (1992) pp. 297.

103. A.J. McEvily and C.L. Magee, "Transformation-Structure-Property Characteristics of Low-Carbon Alloy Steels," *Low Alloy Steels*, London, Iron and Steel Institute, (1968) pp. 111-117.

104. J.R. Yang, "Development of Microstructure in High-Strength Weld Deposits," *Ph.D Dissertation*, Cambridge, UK, Unvi. of Cambridge, (1987)

105. V. I. Izotov, "Transformation of Retained Austenite Layers Separating Martensite and Bainite Crystals on Tempering and Straining," *Phy. of Metals and Metall.*, (1993) **75(1)**:70-73.

106. J.J. Irani, "The Application of Thermomechanical Treatments to Steels," *BISRA Open Report, No. MG/A/60/67, ISMET 3814, FM558*, London, The British Iron and Steel Research Association, (1967)

107. R. H. Edwards and N. F. Kennon, "The Morphology and Mechanical Properties of Bainite Formed from Deformed Austenite," *Metall. Trans. A*, (1978) **9A**:1801-1809.

108. I. Stark, "An Atom-Probe Study of the Chemical Redistribution Accompanying Phase Transformation in Steels," *Ph.D. Dissertation*, UK, Univ. of Oxford, (1988)

109. P. Vasudevan, L. W. Graham and H. J. Axon, "The Kinetics of Bainite Formation in a Plain Carbon Steel," *J. Iron Steel Inst.*, (1958) **190**:386-391.

110. W. T. Reynolds, S. S. Brenner and H. I. Aaronson, "An Fim/Ap Study of the Mo Concentration within Ferrite/Austenite Interfaces in an Fe-0.88at%C-1.06at%Mo Alloy," *Scripta Metall.*, (1988) **22**:1343-1348.

111. R.W.K. Honeycombe, *Steels - Microstructure and Properties*, ASM, (1981)

112. K. J. Irvine and F. B. Pickering, "The Metallography of Low-Carbon Bainitic Steels," *J. Iron Steel Inst.*, (1958) **188**:101-112.

113. F.B. Pickering, "The Structure and Properties of Bainite in Steels (discussion)," *Transformation and Hardenability in Steels*, Ann Arbor, MI, USA, Climax Molybdenum Co., (1967) pp. 130-132.

114. I.D. McIvor, *British Steel Research Report, No.PROD/PM/6498/-/72/A*, London, British Steel, (1972)

115. K. J. Irvine and F. B. Pickering, "The Impact Properties of Low Carbon Bainitic Steels," *J. Iron Steel Inst.*, (1963) **201**:518-531.

116. J.R. Low,Jr., "A Review of the Microstructural Aspects of Cleavage Fracture," *Fracture, [Proc. Int. Conf.]*, Cambridge, MA, USA, (1959) pp. 68-90.

117. A. M. Turkalo, "The Morphology of Brittle Fracture in Pearlite, Bainite and Martensite," *Trans. Met. Soc. AIME*, (1960) **218**:24-30.

118. A. Kamada, N. Koshizuka and T. Funakoshi, "Effect of Austenite Grain Size and C Content on the Substructure and Toughness of Tempered Martensite and Bainite," *Trans. ISIJ*, (1976) **16**:407-416.

119. J. P. Naylor and P. R. Krahe, "The Effect of the Bainite Packet Size on Toughness," *Metall. Trans.*, (1974) **5**:1699-1701.

120. H. Ohtani, F. Terasaki and T. Kunitake, "The Microstructure and Toughness of High Tensile Strength Steels," *Trans. ISIJ*, (1972) **12**:118-127.

121. S. Matsuda, T. Inoue, H. Mimura and Y. Okamura, "Toughness and Effective Grain Size in Heat-Treated Low-Alloy High Strength Steels," *Trans. ISIJ*, (1972) **12**:325-333.

122. Y. Ohmori, H. Ohtani and T. Kunitake, "Tempering of the Bainite and the Bainite/Martensite Duplex Structure in a Low-Carbon Low-Alloy Steel," *Metal Sci.*, (1974) **8**:357-366.

123. J. Tanaka, S. Tani and C. Ouchi, "Low Temperature Toughness of Water-Cooled and Tempered Low Carbon Manganese Steel," *Trans. ISIJ*, (1975) **15**:19-26.

124. A.S. Tetelman and A.J. McEvily, "Fracture of Steel," *Fracture of Structural Materials*, John Wiley&Sons, Inc., (1967)

125. F.B. Pickering, *Physical Metallurgy and the Design of Steels*, London, Applied Science, (1978)

126. R. Ramesh, N. J. Kim and G. Thomas, "Improvement in Toughness of Fe-Cr-Mn-C Steels by Thermal-Mechanical Treatments," *Metall. Trans. A*, (1990) **21A**:683-695.

127. Y. Tomita, "Low-Temperature Improvement of Mechanical Properties of AISI 4340 Steel through High Temperature Thermomechanical Treatment," *Metall. Trans. A*, (1991) **22A**:1093-1102.

128. M. Sarikaya, Steinberg.B.G. and G. Thomas, "Optimization of Fe/Cr/C Base Structural Steels for Improved Strength and Toughness," *Metall. Trans. A*, (1982) **13A**:2227-2237.

129. B. V. N. Rao and G. Thomas, "Structure-Property Relations and the Design of Fe-4Cr-C Base Structural Steels for High Strength and Toughness," *Metall. Trans. A*, (1980) **11A**:441-457.

130. P. Bowen, S. G. Druce and J. F. Knott, "Effects of Microstructure on Cleavage Fracture in Pressure Vessel Steel," *Acta Metall.*, (1986) **34**:1121-1131.

131. H. K. D. H. Bhadeshia and D. V. Edmonds, "Bainite in Silicon Steels: new composition-property approach --Part 1," *Metal Sci.*, (1983) **17**:411-419.

132. M. Sarikaya, A. K. Jhingan and G. Thomas, "Retained Austenite and Tempered Martensite Embrittlement in Medium Carbon Steels," *Metall. Trans. A*, (1983) **14A**:1121-1133.

133. G. Thomas, "Retained Austenite and Tempered Martensite Embrittlement," *Metall. Trans. A*, (1978) **9A**:439-450.

134. J.E. King, R.F. Smith and J.F. Knott, "Toughness Variations during the Tempering of a Plain Carbon, Martensitic Steel," *Advances in Research on the Strength and Fracture of Materials, Fracture 1977, [Conf. Proc.]*, Waterloo, Canada, Univ. of Waterloo, (1977) pp. 279-286.

135. H. K. D. H. Bhadeshia and D. V. Edmonds, "Tempered Martensite Embrittlement: Role of Retained Austenite and Cementite," *Metal Sci.*, (1979) **13**:324-334.

136. J. E. King, R. F. Smith and J. F. Knott, "ICF4 Response: Discussion of 'Toughness Variations of a Plain Carbon, Martensitic Steel' by B. N. V. Rao and G. Thomas," *Int. J. of Fracture*, (1977) **13**:877-878.

137. R. M. Horn and R. O. Ritchie, "Mechanisms of Tempered Martensite Embrittlement in Low Alloy Steels," *Metall. Trans. A*, (1978) **9A**:1039-1053.

138. H. Nakajima and T. Araki, "Impact Toughness of Martensite and Bainite in Medium Carbon Ni-Cr-Mo Steels," *Tetsu-to-Hagané*, (1972) **58**:1993-2004.

139. C. W. Marschall, R. F. Hehemann and A. R. Troiano, "The Characteristics of 9% Nickel Low Carbon Steel," *Trans. ASM*, (1962) **55**:135-148.

140. D. Webster, "Increasing the Toughness of the Martensitic Stainless Steel AFC 77 by Control of Retained Austenite Content, Ausforming and Strain Aging," *Trans. ASM*, (1968) **61**:816-828.

141. H. W. Hayden and S. Floreen, "The Deformation and Fracture of Stainless Steels Having Microduplex Structures," *Trans. ASM*, (1968) **61**:474-488.

142. S. Floreen and H. W. Hayden, "The Influence of Austenite and Ferrite on the Mechanical Properties of Two-Phase Stainless Steels Having Microduplex Structures," *Trans. ASM*, (1968) **61**:489-499.

143. J.A. McMahon and G. Thomas, "Development of Economical, Tough, Ultra-High-Strength Fe-Cr-C Steels," *The Microstructure and Design of Alloys, [Proc. 3rd Int. Conf.]*, Cambridge, England, vol.1, Inst. Metals and Iron & Steel Inst., (1973) pp. 180-184.

144. G. Thomas, "Utilization and Limitations of Phase Transformations and Microstructures in Alloy Design for Strength and Toughness," *Fundamental Aspects of Structural Alloy Design, [Conf. Proc.]*, R.I. Jaffee and B.A. Wilcox eds. Plenum Publishing Co., (1977) pp. 331-361.

145. G. Y. Lai, W. E. Wood, R. A. Clark, V. F. Zackay and E. R. Parker, "The Effect of Austenitizing Temperature on the Microstructure and Mechanical Properties of As-Quenched 4340 Steel," *Metall. Trans.*, (1974) **5**:1663-1670.

146. R.H. Horn, "The Inflence of Retained Austenite on the Thick Section Mechanical Properties of a Commercial Low Alloy Ultra-High Strength Steel," *Ph.D. Thesis, LBL Report No.5787*, Berkeley, CA, USA, Univ. of California, (1976)

147. V.F. Zackay, E.R. Parker and W.E. Wood, "Influence of Some Microstructural Features on the Fracture Toughness of High Strength Steels," *Proc. 3rd Int. Conf. on Strength of Metals and Alloys*, Cambridge, UK, (1973) pp. 175-179.

148. V. T. T. Miihkinen and D. V. Edmonds, "Fracture Toughness of Two Experimental High-strength Bainitic Low-alloy Steels Containing Silicon," *Mater. Sci. Tech.*, (1987) **3**:441-449.

149. Y. Sakuma, O. Matsumura and H. Takechi, "Mechanical Properties and Retained Austenite in Intercritically Heat-Treated Bainite-Transformed Steel and Their Variation with Si and Mn Additions," *Metall. Trans. A*, (1991) **22A**:489-498.

150. H. K. D. H. Bhadeshia and D. V. Edmonds, "Bainite in Silicon Steels: new composition-property approach --Part 2," *Metal Sci.*, (1983) **17**:420-424.

151. Y. Sakuma, D. K. Matlock and G. Grauss, "Mechanical Behavior of an Intercritically Annealed and Isothermally Transformed Low C Alloy Steel with Ferrite-Bainite-Austenite Microstructures," *J. Heat Treat.*, (1990) **8**:109-120.

152. K. W. Burns and F. B. Pickering, "Deformation and Fracture of Ferrite-Pearlite Structures," *J. Iron Steel Inst.*, (1964) **202**:899-906.

153. V.K. Sharma, G.H. Walter and D.H. Breen, "The Effect of Alloying Elements on Case Toughness of Automotive Gear Steels," *Carburizing: Processing and Performance [Conf. Proc.]*, (1989) pp. 291-301.

154. N. P. Allen, W. P. Rees, B. E. Hopkins and H. R. Tipler, "Tensile and Impact Properties of High-Purity Iron-Carbon and Iron-Carbon-Manganese Alloys of Low Carbon Content," *J. Iron Steel Inst.*, (1953) **174**:108-120.

155. C. Maldonado and B. Hernández-Reyes, "Developments in Low-carbon Microalloyed Steels for Plates," *Metallurgy of Vacuum-Degassed Steel Products, [Conf. Proc.]*, The Minerals, Metals & Materials Society, (1990) pp. 485-506.

156. G.J. Roe and B.L. Bramfitt, "Notch Toughness of Steels," *Metals Handbook*, 10th ed., vol. 1, (1993) pp. 737-754.

157. G.E. Dieter, *Mechanical Metallurgy*, 3rd ed., (1986) pp. 479.

158. J. V. Bee, "Improved Wear- and Corrosion-Resistant Steels," *J. S. Afr. Inst. Min. Metall.*, (1987) **87(1)**:1-6.

159. P.E. Grobler and R.J. Mostert, "Experience in the Laboratory and Commercial Development of Abrasion-Corrosion Resistant Steels for the Mining Industry," *Wear of Materials 1989 [Int. Conf. Proc.]*, Denver,Colorado,U.S.A., (1989) pp. 289-295.

160. W.R. Callender, "Bainitic Steels for Railway Applications," *Ph.D Thesis*, England, Univ. of Sheffield, (1983)

161. P. Maitrepierre, J. Rofes-Vernis and D. Thivellier, "Structure-Properties Relationships in Boron Steels," *Boron in Steel, [Proc. Int. Symp.]*, S.K. Banerji and J.E. Morral eds. Milwaukee, WI, USA, Metallurgical Society of AIME, (1979) pp. 1-18.

162. R. Wilcock, "Effect of Boron on the Mechanical Properties of Low-Alloy Steels," *J. Iron Steel Inst.*, (1953) **173**:406-419.

163. D. T. Llewellyn and W. T. Cook, "Metallurgy of Boron-Treated Low-Alloy Steels," *Met. Tech.*, (1974) **1(12)**:517-529.

164. P. Maitrepierre, J. Rofes-Vernis, D. Thivellier and R. Tricot, "Influence of M23(B,C)6 Precipitation on the Properties of Low-Alloy Boron-Containing Steels," *Heat Treatment '76, [Int. Conf. Proc.]*, London, UK, Metal Society, (1976) pp. 177-187.

165. G. F. Melloy, P. R. Slimmon and P. P. Podgursky, "Optimizing the Boron Effect," *Metall. Trans.*, (1973) **4**:2279-2289.

166. G. Thomas and Y-L Chen, "Structure and Mechanical Properties of Fe-Cr-Mo-C Alloys with and without Boron," *Metall. Trans. A*, (1981) **12A**:933-950.

167. G. Thomas, J.K. Kim, D. Manojlovic and R. Milovic, "Development of High Strength and Toughness Microcomposite HSLA Fe/Cr/Mn/C Steel with and without Nb," *Processing, Microstructure and Properties of HSLA Steels*, A.J. Deardo ed. The Minerals, Metals & Materials Society, (1988) pp. 399-414.

168. N. J. Kim and G. Thomas, "Effects of the Constituents on the Mechanical Behavior of Low Carbon Steels," *Scripta Metall.*, (1984) **18**:817-820.

169. V. T. T. Miihkinen and D. V. Edmonds, "Microstructural Examination of Two Experimental High-Strength Bainitic Low-Alloy Steels Containing Silicon," *Mater. Sci. Tech.*, (1987) **3**:422-431.

170. H.P. Jost, *Lubrication (Tribology) Education and Research*, London, H. M. Stationary Office, (1966)

171. *Webster's New World Dictionary*, 3rd college ed., (1988)

172. F.T. Barwell, "Theories of Wear and Their Significance for Engineering Practice," *Treatise on Materials Science and Technology*, D. Scott ed. 13th ed., New York, Academic Press, (1979) pp. 1-83.

173. P. Clayton, M.P.B. Allery and P.J. Bolton, "Surface Damage Phenomena in Rails," *Contact Mechanics and Wear of Rail/Wheel Systems*, (1982) pp. 419-443.

174. A. F. Bower and K. L. Johnson, "Plastic Flow and Shakedown of the Rail Surface in Repeated Wheel-Rail Contact," *Wear*, (1991) **144**:1-18.

175. H. G. Feller and K. Walf, "Surface Analysis of Corrugated Rail Treads," *Wear*, (1991) **144**:153-161.

176. K. Hempelmann, F. Hiss, K. Knothe and B. Ripke, "The Formation of Wear Patterns on Rail Tread," *Wear*, (1991) **144**:179-195.

177. W. F. Hayes and H. G. Tucker, "Wheelset-Track Resonance as a Possible Source of Corrugation Wear," *Wear*, (1991) **144**:211-226.

178. D. R. Ahlbeck and L. E. Daniels, "Investigation of Rail Corrugations on the Baltimore Metro," *Wear*, (1991) **144**:197-210.

179. N. P. Suh, N. Saka and S. Jahanmir, "Implications of the Delamination Theory on Wear Minimization," *Wear*, (1977) **44**:127-134.

180. N. P. Suh, "An Overview of the Delamination Theory of Wear," *Wear*, (1977) **44**:1-16.

181. V. Dikshit, P. Clayton and D. Christensen, "Investigation of Rolling Contact Fatigue in a Head-Hardened Rail," *Wear*, (1991) **144**:89-102.

182. V.A. Dikshit, "Rolling Contact Fatigue Behavior of Pearlitic Rail Steels," *Ph.D. thesis*, Beaverton, OR, USA, Oregon Graduate Institute of Science & Technology, (1992)

183. S. B. Newcomb and W. M. Stobbs, "A Transmission Electron Microscopy Study of the White-Etching Layer on a Rail Head," *Mater. Sci. Eng.*, (1984) **66**:195-204.

184. B. J. Griffiths, "Mechanisms of White Layer Generation with Reference to Machining and Deformation Processes," *J. Tribol.*, (1987) **109**:525-530.

185. A.W. Worth, J.R. Hornaday and P.R. Richards, "Prolonging Rail Life through Rail Grinding," *Proc. 3rd Int. Heavy Haul Railway Conf*, Vancouver, Canada, Assoc. American Railroads, (1986) pp. IB-9-1.

186. P. Clayton and M. B. Allery, "Metallurgical Aspects of Surface Damage Problems in Rails," *Can. Metall. Q.*, (1982) **21**:31-46.

187. L. Q. Xu and N. F. Kennon, "A Study of the Abrasive Wear of Carbon Steels," *Wear*, (1991) **148**:101-112.

188. M. M. Khrushchov and M. A. Babichev, "The Effect of Heat Treatment and Work Hardening on the Resistance to Abrasive Wear of Some Alloy Steels," *Friction and Wear in Machinery*, (1965) **19**:1-15.

189. N. M. Serpik and M. M. Kantor, "Investigation on the Wear of Steel during Rubbing against a Loose Powder Abrasive," *Friction and Wear in Machinery*, (1965) **19**:28-50.

190. N. M. Serpik and M. M. Kantor, "Effect of Heat Treatment on Abrasive Resistance of Steels for Earth Moving Equipment," *Metalloved. Obrab. Met.*, (1958) **7**:46-50.

191. K.H. Zum Gahr, "Relation between Abrasive Wear Rate and the Microstructure of Metals," *Wear of Materials 1979, [Proc. Int. Conf.]*, (1979) pp. 266-274.

192. J. Larsen-Basse and K. G. Mathew, "Influence of Structure of the Abrasion Resistance of a 1040 Steel," *Wear*, (1969) **14**:199-205.

193. K.H. Zum Gahr, *Microstructure and Wear of Materials, Tribology Series 10*, (1987)

194. N.J. Kar, "Investigation of the Role of Microstructures on the Two-Body Abrasive Wear Resistance of Steels," *Wear of Materials, [Proc. Int. Conf.]*, (1993) pp. 415-425.

195. P. L. Hurricks, "Some Metallurgical Factors Controlling the Adhesive and Abrasive Wear Resistance of Steels, A Review," *Wear*, (1973) **26**:285-304.

196. K. H. Zum Gahr, "The Influence of Thermal Treatments on Abrasive Wear Resistance of Tool Steels," *Z. Metallkde.*, (1977) **68**:783-792.

197. K. H. Zum Gahr, "How Microstructure Affects Abrasive Wear Resistance," *Met. Prog.*, (1979) **116**:46-52.

198. T. Chandrasekaran, K. A. Natarajan and Kishore, "Influence of Microstructure on the Wear of Grinding Media," *Wear*, (1991) **147**:267-274.

199. J.F. Archard and W. Hirst, "The Wear of Metals under Unlubricated Conditions," *Proc. R. Soc. London, Ser. A*, (1956) pp. 397.

200. P. Liu, S. Bahadur and J. D. Verhoeven, "Friction and Wear Behavior of High Silicon Bainitic Structures in Austempered Cast Iron and Steel," *Wear*, (1990) **138**:269-284.

201. J. Larsen-Basse, "The Abrasion Resistance of Some Hardened and Tempered Carbon Steels," *Trans. Met. Soc. AIME*, (1966) **236**:1461-1466.

202. B. W. E. Avient, J. Goddard and H. Wilman, "An Experimental Study of Friction and Wear during Abrasion of Metals", *Roy. Soc. Proc., Ser. A*, (1960) **258**:159-180.

203. J. Larsen-Basse, "Abrasion Resistance of Some S.A.P.-Type Alloys at Room Temperature," *Wear*, (1968) **12**:357-368.

204. R. C. D. Richardson, "The Maximum Hardness of Strained Surfaces and the Abrasive Wear of Metals and Alloys," *Wear*, (1967) **10**:353-382.

205. K. Hirakawa, K. Toyama, S. Suzuki and A. Hamazaki, "Effects of Chemical Composition and Microstructure on Wear Properties of Steels for Railroad Wheel," *The Second International Heavy Haul Railway Conference, Pre-Conference Proceedings*, Colorado Springs, CO, USA, (1982) pp. 82-HH-59.

206. D.K. Subramanyam, A.E. Swansiger and H.S. Avery, "Austenitic Manganese Steels," *Metals Handbook, Volume 1*, 10th ed., Materials Park, OH, USA, ASM, (1993) pp. 822-840.

207. ASTM, "Standard Test Methods for Determining Average Grain Size," E112-88, *Annual Book of ASTM Standards*, vol. 03.01, (1989) pp. 284-308.

208. S.P. Timoshenko and J.N. Goodier, *Theory of Elasticity*, New York, McGraw-Hill, (1970) pp. 419.

209. ASTM, "Standard Test Methods of Tension Testing of Metallic Materials," E8-91, *Annual Book of ASTM Standards*, vol. 03.01, (1992) pp. 130-149.

210. ASTM, "Standard Test Methods for Notched Bar Impact Testing of Metallic Materials," E23-92, *Annual Book of ASTM Standards*, vol. 03.01, (1994) pp. 205-224.

211. B.V. Narasimha Rao, R.W. Miller and G. Thomas, "Heat Treatment, Microstructure and Mechanical Properties of Experimental High Strength Fe-4Cr-0.4C Steels," *Heat Treatment '76, Proceedings of the 16th International Heat Treatment Conference*, The Metals Society, (1976) pp. 75-85.

212. D. Singh, *Thesis work*, Oregon Graduate Institute (1994)

213. K. W. Andrews, "Empirical Formulae for the Calculation of Some Transformation Temperatures," *J. Iron Steel Inst.*, (1965) **203**:721-727.

214. D. Danks, "Wear and Microstructure of Eutectoid Steels," *Ph.D Thesis*, Beaverton, OR, USA, Oregon Graduate Institute (former Oregon Graduate Center), (1989)

215. N. Yurioka, "Weldability of Modern High Strength Steels," *Seminar at the Oregon Graduate Institute*, (1994)

216. J.F. Lancaster, *Metallurgy of Welding*, 4th ed., Boston, Allen & Unwin, (1987) pp. 178.

217. N. Yurioka, H. Suzuki, S. Ohshita and S. Saito, "Determination of Necessary Preheating Temperature in Steel Welding," *Weld. J.*, (1983) **62**:147-s-153-s.

218. R.M. Dighde, *Private Communication*, (1994)

219. M.E. Ashton and R.S. Johnson, "Developments in Steels and Their Welding in Railway Engineering," *Select Conference -- Hardenability of Steels*, Derby, England, Welding Institute, (1990) pp. 7-24.

220. W. Steven and A. G. Haynes, "The Temperature of Formation of Martensite and Bainite in Low-Alloy Steels -- Some Effects of Chemical Composition," *JISI*, (1956) **183**:349-359.

221. R. L. Bodnar and K. A. Taylor, "Structure/Property Relationships in Medium Carbon Bainitic Steels for Thick Sections," *Iron & Steelmaker*, (1990) **17**:47-63.

222. R. L. Bodnar, T. Ohhashi and R. I. Jaffee, "Effects of Mn, Si, and Purity on the Design of 3.5NiCrMoV, 1CrMoV, and 2.25Cr-1Mo Bainitic Alloy Steels," *Metall. Trans. A*, (1989) **20A**:1445-1460.

223. G. J. P. Buchi, J. H. R. Page and M. P. Sidey, "Creep Properties and Precipitation Characteristics of 1%Cr-Mo-V Steels," *JISI*, (1965) **203**:291-298.

224. H. Ohtani, S. Okaguchi, Y. Fujishiro and Y. Ohmori, "Morphology and Properties of Low-Carbon Bainite," *Metall. Trans. A*, (1990) **21A**:877-888.

225. B. Josefsson and H. O. Andrén, "Microstructure of Granular Bainite," *J. Physique*, (1988) **49**:C6.293-C6.298.

226. B. A. Leont'yev and G. V. Kovalevskaya, "On the Bainitic Transformation Mechanism of Austenite," *Fiz. Metall. Metalloved.*, (1974) **38**:1050-1055.

227. S. W. Thompson, D. J. Colvin and G. Krauss, "Continuous Cooling Transformations and Microstructures in a Low-Carbon, High-Strength Low-Alloy Plate Steel," *Metall. Trans. A*, (1990) **21A**:1493-1507.

228. D.S. Sarma and F.H. Samuel, "On the Formation of Granular Bainite and the Martensite-Austenite Constituent in Low Alloy Steels," *Proc. Int. Conf. on Solid --> Solid Phase Transformations*, Pittsburgh, PA, USA, ASM, (1981) pp. 1035-1039.

229. J. L. Lee, M. H. Hon and G. H. Cheng, "The Structure of Microphases in a Bainitic Transformation Product of Mn-Mo-Nb Steel," *Scripta Metall.*, (1987) **21**:293-298.

230. S. Zhang, H. Zhang and Y. Yuan, "Deformation and Fracture of a Microalloyed 12SiMoVNb Steel with Granular Bainite Structure," *HSLA Steels: Metallurgy and Applications, [Proc. Int. Conf.]*, Beijing, China, ASM, (1985) pp. 113-120.

231. Y. B. Xu, G. J. Liu and T. Y. Zhang, "Granular Product in a High Strength, Low Alloy Containg Molybdenum and Niobium," *Metall. Trans. A*, (1987) **18A**:1923-1927.

232. G. Thomas, M. Sarikaya, G.D.W. Smith and S.J. Barnard, "Microstructure, Retained Austenite and Mechanical Properties of Experimental 0.3%C Steels," *Advance in the Physical Metallurgy and Applications of Steels, [Conf. Proc.]*, Liverpool, UK, (1981) pp. 259-265.

233. W. S. Owen, "The Effect of Silicon on the Kinetics of Tempering," *Trans. ASM*, (1954) **46**:812-829.

234. M. Katsumata, O. Ishiyama, T. Inoue and T. Tanaka, "Microstructure and Mechanical Properties of Bainite Containing Martensite and Retained Austenite in Low Carbon HSLA Steels," *Mater. Trans. JIM*, (1991) **32**:715-728.

235. C. P. Luo, G. C. Weatherly and Z-Y Liu, "The Crystallography of Bainite in a Medium-Carbon Steel Containing Si, Mn, and Mo," *Metall. Trans. A*, (1992) **23A**:1403-1411.

236. W.C. Leslie, *The Physical Metallurgy of Steels*, New York, McGraw-Hill Book Co., (1981) pp. 189.

237. W.C. Leslie, *The Physical Metallurgy of Steels*, New York, McGraw-Hill Book Company, (1981) pp. 201.

238. C.I. Garcia, A.K. Lis and A.J. DeArdo, "The Physical Metallurgy of Ultra-Low Carbon Bainitic Plate Steels," *Metallurgy of Vacuum-Degassed Steel Products*, R. Pradhan ed. TMS, (1990) pp. 451-467.

239. F.B. Pickering, "The Optimisation of Microstructures in Steel and Their Relationship to Mechanical Properties," *Hardenability Concepts with Applications to Steel, [Conf. Proc.]*, D.V. Doane and J.S. Kirkaldy eds. Metallurgical Soc. of AIME, (1977) pp. 179-227.

240. K. J. Irvine and F. B. Pickering, "Low-Carbon Steels with Ferrite-Pearlite Structures," *JISI*, (1963) **201**:944-959.

241. K.-E. Thelning, "Evaluation and Practical Application of the Hardenability of Boron Steel," *Boron in Steel*, S.K. Banerji and J.E. Morral eds. Milwaukee, WI, USA, Metallurgical Society of AIME, (1979) pp. 127-146.

242. J. P. Snyder,II and A. W. Pense, "The Effects of Titanium on Submerged Arc Weld Metal," *Weld. J.*, (1982) **62**(7):201s-211s.

243. C. Thaulow, "Structural Changes in Submerged-Arc Weld Metals of CMn Steels Containing Small Amounts of Titanium," *Weld Pool Chemistry and Metallurgy, [Proc. Int. Conf.]*, London, UK, The Welding Institute, (1980) pp. 17-29.

244. K.J. Sawley, J.A. Benyon and E.G. Jones, "Bainitic Steels for Railway Wheels," *Wheel Set Congress [Conf. Proc.]*, Montreal, Canada, (1988)

245. K.J. Irvine and F.B. Pickering, "High-Carbon Bainitic Steels," *Physical Properties of Martensite and Bainite, [Conf. Proc.]*, London, Special Report 93, Iron and Steel Inst., (1965) pp. 110-125.

246. Stout and Doty, "Weldability of Steels," *WRC Bulletin*, New York, (1953)

247. P. Clayton, *Private communication*, (1994)

248. W.J. Salesky and G. Thomas, "Design of Medium Carbon Steels for Wear Applications," *Wear of Materials 1983*, San Francisco, CA, USA, ASME, (1981) pp. 298-305.

249. D. L. Holt, "Dislocation Cell Formation in Metals," *J. App. Phys.*, (1970) **41**:3197-3201.

250. C. M. Young, L. J. Anderson and O. D. Sherby, "On the Steady State Flow Stress of Iron at Low Temperature and Large Strains," *Metall. Trans. A*, (1974) **5A**:519-520.

251. E. Ganin, Y. Komen and B. Z. Weiss, "The Structure of Joint Zone in an Explosively Bonded Cu/Cu-2Be System," *Acta Metall.*, (1986) **34**:147-158.

252. A.W. Ruff, L.K. Ives and G.A. Glaeser, "Characterization of Wear Surfaces and Wear Debris," *Fundamentals of Friction and Wear of Materials*, Metal Park, Ohio, USA, ASM, (1981) pp. 235-289.

253. K. Kato, T. Kayaba and Y. Ono, "Dislocation Density and Cell Structure Produced in the Subsurface Layer of Aluminum during Sliding Wear," *Wear of Materials [Int. Conf. Proc.]*, ASM, (1985) pp. 463-470.

254. R. Devanathan and P. Clayton, "Rolling-Sliding Wear Behavior of Three Bainitic Steels," *Wear*, (1991) **151**:255-267.

255. P. Clayton and D. Danks, "AAR-OGI Research Program," *Progress Report 1990*, (1990)

VITA

Nong Jin was born in Beijing, China on October 18, 1963. He entered Tsinghua University in 1981 and graduated in 1986 with a Bachelor's degree in the Department of Mechanical Engineering. In 1989, he received a Master's degree in Materials Science and Engineering in the Central Iron & Steel Research Institute. One year after working with the Star New Technology Development Center, Nong Jin came to the United States and joined the Oregon Graduate Institute pursing a Ph.D. degree in the Department of Materials Science and Engineering.